BIOIMPEDANCE SPECTROSCOPY IN PREDICTION OF TYPE I OSTEOPOROSIS IN MENOPAUSED WOMEN

by

Fırat Matur

B.S., in Electrical and Electronics Engineering, Boğaziçi University, 1991

M.S., in Biomedical Engineering, Boğaziçi University, 1995

Submitted to the Institute of Biomedical Engineering

in partial fulfillment of the requirements

for the degree of

Doctor

of

Philosophy

Boğaziçi University

2021

ACKNOWLEDGMENTS

I want to thank my wife Nevcihan and my daughter Ece for their patience and support during my thesis writing period.

I also thank Prof. Dr. Yekta Ülgen for his guidance and supervision during my data collection and analysis period.

I want to thank Prof. Dr. Ülkü Akarırmak and to medical staff in the Radiology Department of İstanbul University, Cerrahpaşa Medical School, for their kind support and hospitality during the Impedimed study. I also thank John Hopkins Ozel Anadolu Sağlık Merkezi Radiology department and Dr. Kezban Berberoğlu for their kind support and hospitality.

This study is not funded by any organization or a company.

In all procedures performed involving human participants in this study, the ethical standards of the institutional and/or national research committee and the 1964 Helsinki declaration and its later amendments or comparable ethical standards are followed. All subjects have signed an informed consent form before participating in this study.

I, Fırat Matur, declare that I do not have any competing interest.

ACADEMIC ETHICS AND INTEGRITY STATEMENT

I, Fırat Matur, hereby certify that I am aware of the Academic Ethics and Integrity Policy issued by the Council of Higher Education (YÖK) and I fully acknowledge all the consequences due to its violation by plagiarism or any other way.

Name :

Signature:

Date:

ABSTRACT

BIOIMPEDANCE SPECTROSCOPY IN PREDICTION OF TYPE I OSTEOPOROSIS IN MENOPAUSED WOMEN

Bone mineral density (BMD) is a measure of survival for men and women, and it is used to diagnose Osteoporosis that can be diagnosed and treated with an effective screening. We measured bioimpedance spectroscopy (BIS) parameters of 129 menopaused women and compared them with their DEXA reference measurements. We observed a region specificity for the central BMD assessment using BIS. When sensing electrodes are on the dominant hand and infraclavicular fossa, dominant arm f_c correlates with the hip BMD ($r = -0.412, P < 0.05$), and f_{cut} for Osteoporosis is 49.565 kHz. When sensing electrodes are over the hands, f_c correlates with lumbar BMD ($r = 0.580, P < 0.05$), and f_{cut} is 32.4 kHz. BMI also affects BIS measurements, and if BMI < 30 kg/m^2, the correlation of f_c with the hip BMD is improved ($r = -0.456, P < 0.05$). f_c may be alternatively calculated using the proposed original 3P-Nyquist method. Both f_c and the phase angle of the impedance measured at a single frequency are a function of the same impedance model parameters, and measurement at a single frequency is less complicated than BIS. Phase angle of the measured impedance at 5 kHz has correlations with both lumbar ($r = 0.403, P < 0.05$) and hip ($r = 0.559, P < 0.05$) BMDs. When DEXA devices are not available or inaccessible, with its high mobility, non-invasive and cost-effective nature, BIS can be a good substitute in screening for BMD; however, clinical studies should be continued over a larger population to obtain the normative BIS cutoff frequency or phase angle values. A practical 2D-ROC method for combining two discrete markers in a 2-way classifier is also proposed: both for simulated and clinical data, the $AVERAGE$ function combining markers has higher correct classification rates than the individual markers.

Keywords: Osteoporosis, Bone Mineral Density, Bioimpedance Spectroscopy, 3-Point Nyquist, Single Frequency Phase Angle, Characteristic Frequency, 2D-ROC.

ÖZET

MENOPOZ SONRASI KADINLARDA TİP I OSTEOPOROZUN TESPİTİNDE BIOEMPEDANS SPEKTROSKOPİSİ

Kemik yoğunluğu (BMD) kadın ve erkek için hayati bir konudur ve etkin bir tarama ile tespit ve tedavi edilebilen Osteoporoz tanısında kullanılır. 129 menopoz sonrası kadının biyoempedans spektroskopi (BIS) parametrelerini ölçtük ve referans DEXA değerleri ile karşılaştırdık. BIS yöntemi ile merkezi kemik yoğunluğu tespitinde bölgesel ayırt edicilik gözlemledik: algılama elektrotları el ve infraklavikular fossa üzerindeyken baskın kol f_c ile hip BMD korole ($r = -0.412, P < 0.05$) ve Osteoporoz için sınır frekansı f_{cut} 49.565 kHz'dir. Algılama elektrotları eller üzerinde olduğunda ise f_c ile lomber BMD korole ($r = 0.580, P < 0.05$), ve Osteoporoz için f_{cut} 32.4 kHz'dir. BMI ayrıca BIS ölçümlerini etkiler ve < 30 kg/m^2 olduğunda f_c ile hip BMD arasında korelasyon iyileşmektedir ($r = -0.456, P < 0.05$). f_c alternatif olarak önerilen 3P-Nyquist metoduyla da hesaplanabilir. f_c ve tek frekansta ölçülen empedansın açısı aynı empedans model parametrelerine bağlıdır ve tek frekansta ölçüm BIS'nden daha kolaydır. 5 kHZ'te ölçülen empedans açısı lomber ($r = 0.403, P < 0.05$) ve hip BMD ile ($r = 0.559, P < 0.05$) koroledir. DEXA cihazlarına erişim olmadığında, yüksek mobilite, non-invazif ve maliyet avantajı nedeniyle, BMD taraması için BIS iyi bir alternatif olabilir; ancak, öncesinde yüksek sayıda örnekle klinik çalışmalar tekrarlanarak normatif BIS frekans ve tek faz açısı sınır değerleri bulunmalıdır. Ayrıca, 2 yönlü sınıflandırıcı için çoklu markörleri birleştirmek için orijinal ve pratik bir 2D-ROC yöntemi önerilmiştir: simülasyon ve klinik data için ayrık markörlerlerin $AVERAGE$ fonksiyonu ile birleştirilmesi, her bir marköre göre daha iyi bir doğru sınıflandırma oranı vermiştir.

Anahtar Kelimeler: Osteoporoz, Kemik Mineral Yoğunluğu, Biyoempedans Spektroskopisi, 3-Nokta Nyquist, Tek Frekans Faz Açısı, Karakteristik Frekans, 2D-ROC.

TABLE OF CONTENTS

LIST OF FIGURES

LIST OF TABLES

LIST OF SYMBOLS

a,b	Radii of terminated cone
f	Frequency (Hertz)
f_c	Characteristic frequency (Hz)
f_{cut}	Cutoff frequency (Hz)
j	Imaginary unit number
ln	Natural logarithm function
r	Pearson correlation coefficient
w	Frequency (radian)
z^*	Tissue specific impedance (Ohm)
A	Measured segment area (m^2)
C	Cell membrane capacitance (Farad)
$Circ_a$	Circumferences of terminated cone one end
$Circ_b$	Circumferences of terminated cone at the other end
I	Current
I^o	Attenuated photon intensity
J	Youden Index
L	Measured segment length
P	Statistical significance criterion
R	Resistance (Ohm)
R_e	BIS Extracellular resistance
R_i	Intracellular resistance
R_0	Resistance when signal frequency is ZERO
R_∞	Resistance when signal frequency is infinite
V	Voltage
Z^*	Complex impedance
Z_{CPA}	Constant phase element, the lumped capacitance of the tissue
Z_m^*	Measured complex impedance

α	Depression constant
κ	Level of kurtosis
δ	Partial derivative
μ	Mean
μ_m	Linear attenuation factor for material
μ_w	Linear attenuation factor of water
μ_a	Linear attenuation factor of air
σ	Standard deviation
ϕ	Phase angle
ρ	Specific impedance
τ	Characteristic time constant

LIST OF ABBREVIATIONS

2D-ROC	2 Dimensional Receiver Operating Characteristic
AD-SoS	Amplitude Dependent Speed of Sound
AUC	Area Under Curve
BIS	Bioimpedance Spectroscopy
BMC	Bone Mineral Content
BMD	Bone Mineral Density
CA	Cortical Area
CCR	Correct classification rate
CI	Cortical Index
CV	Coefficient of Variation
D	Diseased
DA	Dominant arm
DEXA	Dual Energy X-ray Absorptiometry
DPA	Dual Photon Absorptiometry
ECW	Extracellular Water
FAT%	Total body fat percentage estimate
FFB	Fat free body
FFM	Fat-free mass
FM	Fat Mass
FN	False Negative
FP	False Positive
HBMD	Total Hip Bone Mineral Density
HU	Hounsfield Unit
LA	Left Arm
LBMD	Total Lumbar Bone Mineral Density
LF	Left Foot
LH	Left Hand
LL	Left Leg

MCR	Mis-classification rate
MRI	Magnetic Resonance Imaging
MUS	Muscle
N	Number of Subjects
NCT	Non-conducting Tissue
NHANES	National Health and Nutrition Examination Survey
NPV	Negative Predictive Value
NS	Not Significant
PDXA	Peripheral Dual Energy X-ray Absorptiometry
PPV	Positive Predictive Value
QCT	Quantitative Computed Tomography
QSEG	Segment Fat Quotient
QUS	Quantitative Ultrasound
RA	Right Arm
RF	Right Foot
RGA	Radiographic Absorptiometry
RH	Right Hand
RL	Right Leg
ROC	Receiver Operating Characteristic
ROS	Multidimensional Receiver Operating Characteristics Surface
RU	Repeatability Uncertainty
SD	Standard Deviation
SEG	Segment
SNR	Signal to Noise Ratio
SoS	Speed of Sound
SPA	Single Photon Absorptiometry
SXA	Single Energy X-ray Absorptiometry
T score	Standard deviation from young normal
TN	True Negative
TP	True Positive
WHO	World Health Organization

Z score	Standard deviation from the same age group

1. INTRODUCTION

Osteoporosis is a skeletal disorder causing low bone density and low bone density is an essential factor in fracture risk [1, 2]. Osteopenia is the less severe deficit in bone mass [3].

According to the *World Heath Organization* (WHO), osteoporosis is characterized by bone tissue reduction per unit volume of bone, and it is a major but not the unique cause of fractures in elderly or postmenopausal women [4].

Regardless of gender or race, Osteoporosis is a disease that builds up in time in every individual. For women in the premenopausal state, bone mineral density stays reasonably stable, but there is a significant bone mineral density loss in the postmenopausal state, that may reach up to 0.47 to 1.07%, annually. For men, there is a gradual bone density drop throughout the life starting at the age the bone mass peak is reached, and it is between 0.22 to 0.33% annually at lumbar and for women upto 0.42% [5].

Although osteoporosis is always considered as the white women's disease, Hispanics and Asians can not be excluded from fracture risks [6].

Some researchers also claim that obesity may help to retain bone mineral density by stimulating bone formation and by forcing cortical bones to carry more weight, similarly to physical exercise [7]. However, some researches like Sharma *et al.* put some reserves to this hypothesis: although both BMD increases to obesity, the fracture risk is increased with obesity and can not be considered as protective [8, 9].

Besides the age or hormonal changes after the end of menopause, medications and other underlying disorders may also cause bone loss. Osteoporosis is classified into two broad groups: if built naturally, it is called *Primary osteoporosis*, and if there is

an underlying disorder, it is called *Secondary osteoporosis*. The primary osteoporosis is further divided in two subgroups: *Type I* is the osteoporosis developed due to menopause in women only, and *Type II* is the osteoporosis developed by age in both genders [10].

Osteoporosis has a significant economic burden on society, and with the increased average age this burden is globally increasing [11]. In every 3 seconds, an osteoporosis related fracture is happening, corresponding to 9 million fractures annually [12]. Economic burden only to US society is calculated as 12 to 18 billion USD [13]. For Europe, by 2010 already 22 million women and 5.5 million men have already developed osteoporosis, and with a 28% increase in number from 2010 to 2025, the number of annual osteoporosis linked fractures is expected to reach 4.5 million, by 2025 [14, 15].

Although the number of studies are less in less developed countries, it also effects the developing or less developed countries, including Turkey [16, 17]. Sozen *et al.* hav shown that, similar to developed countries, osteoporosis is an increasing problem for Turkish society due to increased average age of the society [16]. Tuzun *et al.* have shown that, the hip fracture rate for Turkish society is increasing exponentially by increased age, and for women and men at age 50, the probability of having a hip fracture in their rest of life is 14.6% for women and 3.5% for men [17]. In 2019, with over 455 million USD economic burden on the society, over 255 thousand osteoporosis related fractures occurred in Turkey; and, the total estimated economic burden to society between years 2019 and 2023 will be over 2.4 billion USD [18].

There are several bone mineral assessment techniques involving x-ray and ultrasound. *Dual Energy X-ray Absorptiometry* (DEXA) is widely used to measure *Bone Mineral Density* (BMD) in grams/cm^2 (g/cm^2) from the hip and lumbar is the gold standard in diagnosing the osteoporosis non-invasively [19].

Osteoporosis is a silent disease until it results in a fracture. With an efficient screening, osteoporosis can be diagnosed, and with more effective treatments fractures

can be prevented [16]. However, the screening is not at desired levels [20]. Nayak *et al.* have studied 1268 patients and shown that 88.2% of the elder people with osteoporosis are believing that they are perfectly healthy, and doctors are not suggesting more screening to elders then they do to young population either [20]. Altin *et al.* have shown that the osteoporosis awareness for pre-menopausal and post-menopausal women in Turkey is the same, supporting Nayak's study, and even having a family history of osteoporosis in the family does not increase this awareness level [21]. The awareness of men is even lower than women [21].

DEXA devices are not mobile and risk groups should be visiting a hospital. Although there is no statistical number about the number of DEXA devices and their distribution across the country, there are 1538 hospitals in 2019 [22], with the average of 2 DEXA devices in each, the DEXA device capacity may be estimated to be less than 4 thousand units. Therefore, it is unlikely to have elder people go to an hospital, to go under an osteoporosis screening examination using DEXA. Instead, like the best practices in dental care, the bone mineral assessments should have mobility for an effective screening [23].

Bioimpedance spectroscopy (BIS) is a non-invasive technique used in tissue characterization [24]. Each body tissue has its own impedance characteristics, which can be used for tissue characterization [25].

Three compartment model of body composition consists of fat mass (FM), fat-free mass (FFM), and non-conducting tissues (NCT). The non-conducting tissues in the arms and legs are mostly bones, and regardless of their measurement axis, the specific capacitance of both trabecular and cortical bones have statistically significant correlation to their mineral densities. The same correlation exists at wet, dry or ash forms [26]. Therefore, as a non-invasive, highly portable, safe and economical solution, segmental BIS is worth to be investigated to find if segmental BIS results may be used for osteoporosis screening.

With two separate BIS measurement systems, i.e., HP4284A LCR meter and

Impedimed SFB7, a total of 139 women have gone BIS examination, following the bone mineral density measurements with the gold standard DEXA to investigate the diagnostic potential of BIS in osteoporosis.

In BIS measurements, to model the body segment as an equivalent electrical circuit, the Fricke's model is used. Fricke's model is widely used to model micro-organisms in a liquid environment [27]. In this model, the frequency dependent tissue impedance Z is modeled as a parallel combination of R_e, the extracellular fluid resistance with the serial combination of R_i, the intracellular fluid resistance and C representing the cell membrane capacitance.

The equivalent impedance for the model is:

$$Z^* = \frac{R_e.(R_i + \frac{1}{j2\pi fC})}{R_e + (R_i + \frac{1}{j2\pi fC})} \tag{1.1}$$

However, due to dispersion of the cell membrane capacitive behavior; the complex impedance is generalized with a dimensionless α constant between 0 and 1 [28, 29]. Single cell membrane capacitance is replaced with a Z_{CPE} constant phase element, i.e., the lumped capacitance of the tissue [30]

$$Z_{CPE} = \frac{1}{(jwC)^{\alpha}} = (jwC)^{-\alpha} \tag{1.2}$$

BIS parameters of interest in this study are the *Intracellular and Extracellular fluid resistances*, and the *Characteristic frequency* at (f_c) the imaginary component of the model impedance is maximized. The characteristic frequency (f_c) can be calculated by using the traditional Cole-clot plot method or by the proposed innovative 3 point Nyquist algorithm.

And finally, with the proposed innovative 2D-Receiver operating characteristic surface method, how paired independent tests can be combined to increase a two-way classifiers' *Sensitivity* (S_e), i.e., the ability to diagnose the disease when disease exists, and *Specificity* (S_p) , i.e., the ability to diagnose normal when disease does not exist.

The superiority of both BIS over DEXA is the portability. This study can be repeated with a larger population with a more standardized protocol to obtain a normative cutoff frequency for the population, and this method can be an option if DEXA devices are not available or not accessible.

BIS characteristic frequency which is a function of BIS model capacitance, correlates with bone mineral density. The measured complex impedance is a function of model capacitance, and other BIS model parameters do not have a statistically significant correlation to the bone mineral densities ($P < 0.05$). Since model capacitance only affects the BIS model complex impedance's imaginary component, the impedance phase angle at a given frequency should also be a function of the bone mineral density. This assumption may dramatically reduce the complexity of the bone mineral screening measurements: instead of having a multi-frequency BIS measurement device with complex BIS model calculation algorithms, a single frequency, high precision, and well-calibrated impedance phase measurement device might be a cheaper and a reliable solution for screening the population.

2. BONE

Bone is a vital complex organ with essential functions: provisioning the body's mechanical integrity and locomotion, protecting vital organs and enabling a metabolic pathway for the minerals. Furthermore, bone is the primary hematopoiesis site that interplays a critical role in the immune system [31, 32, 33]. Bone plays a major role in phosphate and calcium balance and plays a vital role in the detoxification of heavy metals [34].

Bone can grow and can change the shape and size that suits best external stress factors, including mechanical forces [34].

As a normal skeletal function, proposed in the well known Wolff's Law and others, the principal stress direction determines the trabecular bone alignment [35, 36].

Bone tissue is a combination of an extracellular protein-rich matrix with apatite crystals. With this structure, it is similar to engineering composite materials [37]. However, bone is a living tissue constantly undergoing the bone remodeling process to quickly respond to mechanical and structural needs.

By their shapes, bones are categorized as long, short, flat, and irregular bones. Long bones are clavicles, humeri, radii, ulnae, metacarpals, femurs, tibiae, fibulae, metatarsals, and phalanges. Short bones are the carpal and tarsal bones, patellae, and sesamoid bones. Flat bones are the skull, mandible, scapulae, sternum, and ribs. Irregular bones are the vertebrae, sacrum, coccyx, and hyoid bone. Flat bones are formed by membranous bone formation, whereas long bones are formed by a combination of endochondral and membranous bone formation [38].

By their physical formation, there are two types of bones, trabecular and cortical bone. Trabecular bone is the spongy bone which is also known as the cancellous bone.

Cortical bone is the dense bone which is also known as the compact bone.

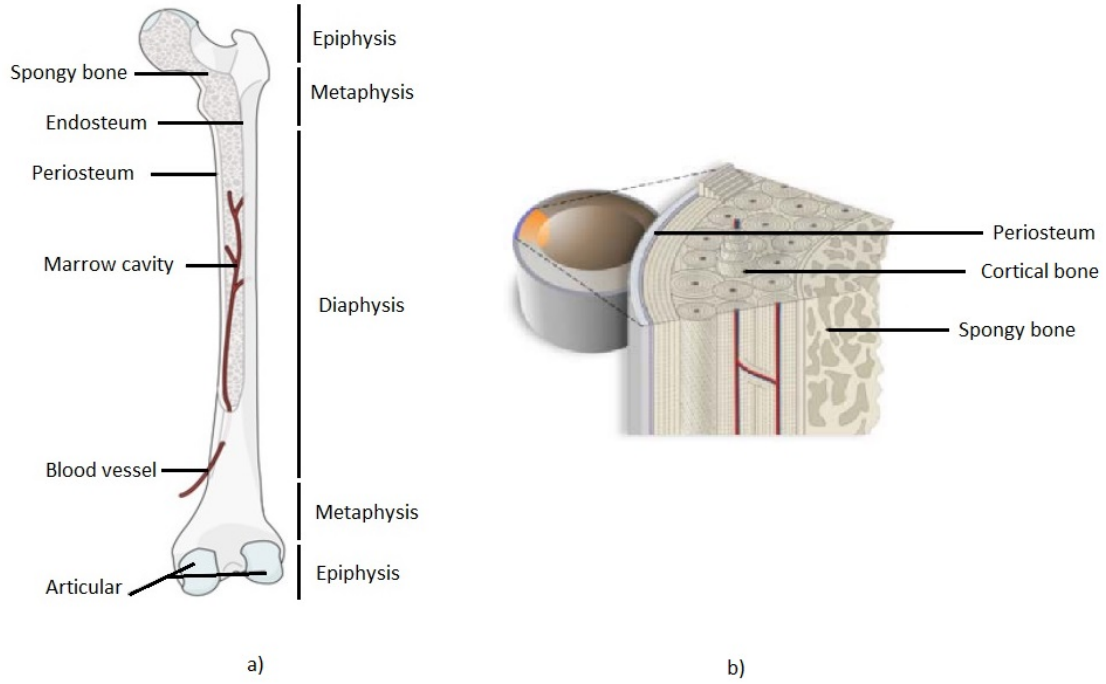

Figure 2.1 Long bone a) parts and b) the anatomy. Adapted from [39].

Trabecular bone is primarily seen in metaphyses and epiphyses of the long bones constituting the axial skeleton (Figure 2.1) [40, 39]. Trabecular bone is a highly porous networked structured rod and plate-shaped trabeculae, which also surrounds an interconnected space filled with bone marrow (Figure 2.2).

Approximately 20% of trabecular bone is skeletal mass, and for cortical bone, this ratio is 80% [3]. Cortical and trabecular bones have different porosity. While trabecular bone has a porosity due to marrow space ranging from 40% at the femoral neck up to 95% in an elderly spine, the porosity of cortical bone is due to Haversian and Volkmann's canals, lacunar, and canalicular spaces ranging between 5% to 20% of volume (Figure 2.3). Porosity is the primary determinant of the stiffness and strength of the trabecular bone [41, 42].

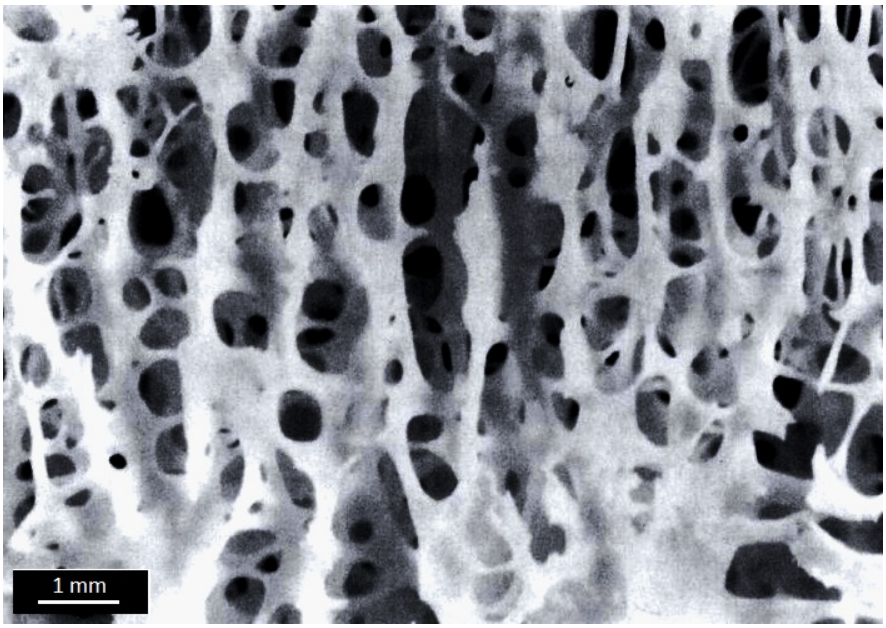

Figure 2.2 Spongy structure of trabecular bones. Adapted from [3].

2.1 Bone remodeling

Bone remodeling is a regulated process for replacing the old bone with the new bone for ensuring the repair of micro-damage. The process is a sequential process of osteoclastic resorption and osteoblastic bone formation [43, 44, 45].

Bone remodeling occurs on the bone surface at the Haversian canal, endosteal, periosteal, and trabecular surfaces. The rate of cortical bone remodeling depends on the age: in the first two years, it may be up to 50% per year, declining down to 2 to 5% per year in the elder ages. The annual rate of remodeling also dependent on the bone type, and the trabecular bone modeling rate is 5 to 10 fold higher than the cortical bone remodeling rate [44].

Under normal conditions, the remodeling process is a strongly coupled repetitive sequence of the resorption followed by the formation, and bone mass stays stable with no net change. However, several stimuli affect bone turnover, including cytokines, hormones, and mechanical stimuli. All of these factors affect the amount and the quality of the tissue produced. Mechanical loading mainly stimulates bone cells, improving bone strength and inhibiting bone loss with age [46].

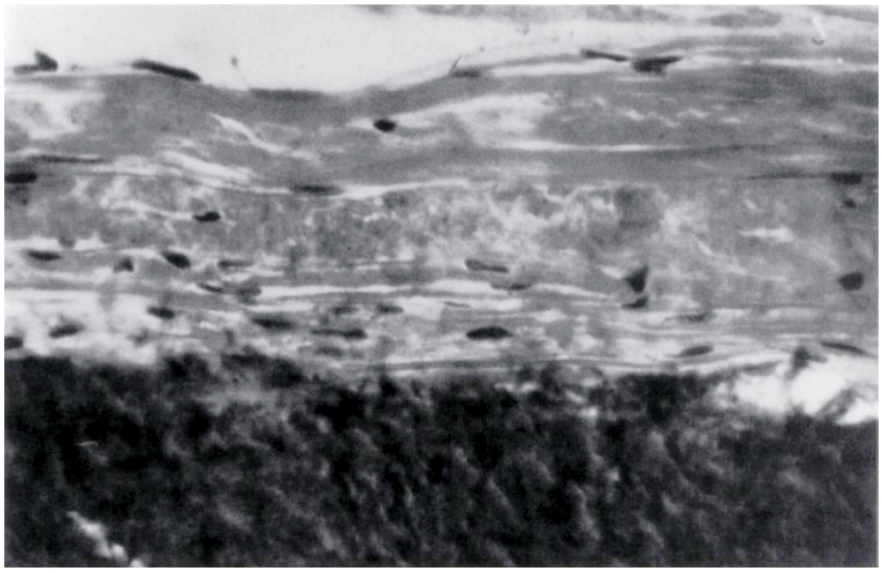

Figure 2.3 Magnified view of the periosteum of a long bone. The darker tissue at the lower portion of the picture is the cortical bone and above this is the periosteum. Adapted from [3].

However, bone metabolism is regulated by environmental signals, too, including chemical, electrical or magnetic. Bone responds to these environmental signals by modulating the balance between the new bone formation and the resorption of older bone [47, 48, 49].

The bone coupling concept is based on the idea that osteoblasts influence osteoclast formation, and similarly, osteoclasts influence osteoblast differentiation formation and activity, as sketched in Figure 2.4 [50].

Defects in remodeling result in a range of metabolic and congenital bone diseases in humans, including osteoporosis, Paget's disease of bone, and osteopetrosis [51]. *Osteoporosis* is a skeletal disease that is characterized by low bone density and micro-architectural deterioration of bony tissue, leading to fracture risk [1, 52]. Paget's disease of bone is a chronic focal high turnover bone disorder that is primarily present in middle-aged or older adults [53]. Osteopetrosis is also named *stone bone*, a heritable disorder that leads to failure of osteoclasts to resorb bone [54].

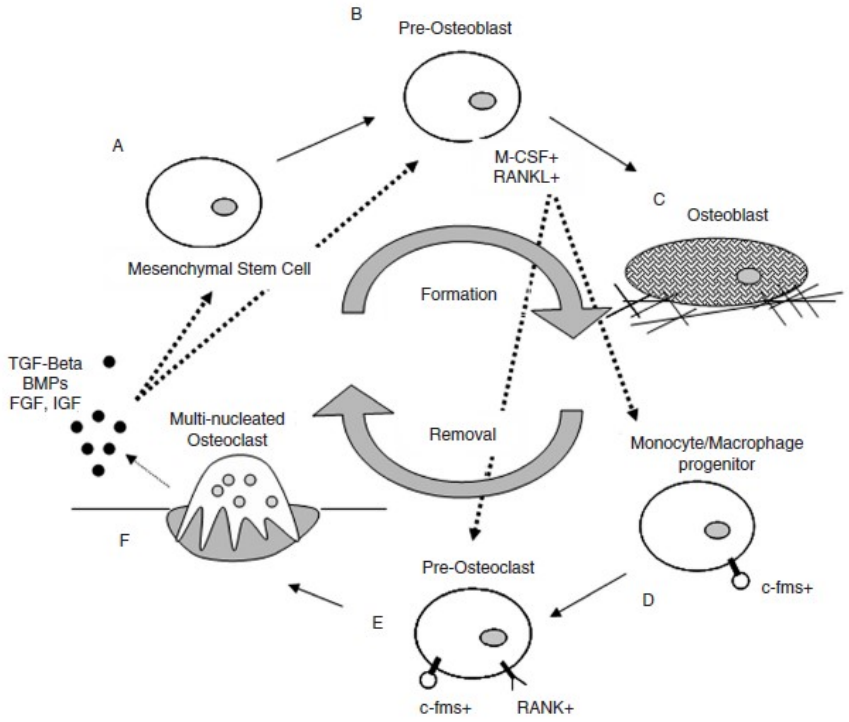

Figure 2.4 Graphic representation of the cellular interactions between osteoblast lineage cells (A–C) and osteoclast lineage cells (D–F). Dashed lines indicate cell signaling events important in the coupled differentiation of the respective lineages. Pre-osteoclasts (B) express the majority of M-CSF and RANKL that induces osteoclast differentiation (dashed lines are indicating effects on progenitor cells and pre-osteoclast). Conversely, morphogens released from bone during osteoclast-mediated removal (F) influence the differentiation of the mesenchymal stem cell and pre-osteoblast (indicated with dashed line). Adapted from [3].

2.2 Bone mineral density

Bone mineral density (BMD) is the parameter the measures the bone quality. Since BMD is a non-invasive and reliable parameter, it is a standard and essential factor in bone quality assessment [55].

BMD is the most critical factor for skeletal fragility, and it plays a vital role in the diagnosis of osteoporosis [56].

The deposition of calcium and phosphorus as hydroxyapatite during the bone mineralization process results in bone tissue rigidity. 70% of the bone composition is minerals, and the remaining 30% is mainly organic matter, including collagen. Bone tissue rigidity results from the deposition of calcium and phosphorus as hydroxyapatite

during the bone mineralization process, and minerals are 70% of the bone composition; the remaining 30% is mainly organic matter, including collagen. Since hydroxyapatite and aluminum have similar densities, many authors conducted radiological studies to relate bone mineralization degree with the aluminum density in pre-determined scales (Figure 2.5). This technique is later called "Optical Densitometry in Radiographic Images" [57].

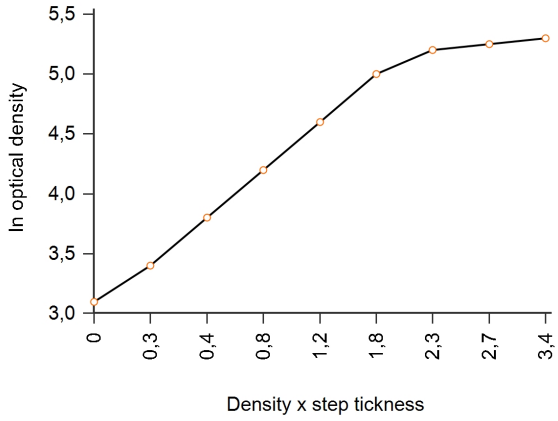

Figure 2.5 The correlation between the natural logarithm of optical density and the aluminum slab thickness is typically better than 0.99. Adapted from [58].

Bone mineral density can also be measured invasive as measuring bone-breaking strength, bone mineral composition or by using Seedor index [55].

Bone breaking strength, also known as bone strength, is not a function of bone ash percentage but is a function of bone volume [59].

$$Seedor\ index = bone\ weight / bone\ length \tag{2.1}$$

The Seedor index is the bone weight to the bone length ratio, and it is an indicator for bone density [60].

Shapurian *et al.* has calculated the fracture threshold for the bone density as

100-110 mg/cm^2. Fracture threshold is the threshold for the osteoporotic fracture prevalence: if BMD is above, the osteoporotic fracture is rarely seen. However, most patients experience spinal fractures if their BMD is less than 50 mg/cm^2, [61].

Bone mineral density is a measure of survival [62]. Johansson *et al.* have shown that both for men and women, the correlation between bone mineral density and mortality is more substantial than many well-known morbidity risk factors, including cholesterol and blood pressure. The predictors of survivals are tabulated in Table 2.1 [62].

Table 2.1
Age-adjusted statistics of various predictors for those who died and survived after seven years. Adapted from [62].

Variable	Mortality within 7 years	Alive after 7 years	P-value
Men (N = 463)			
Bone mineral density (g/cm^2)	0.423 ± 0.124	0.466 ± 0.124	0.0001
Height (cm)	172.4 ± 6.6	173.1 ± 6.4	NS
Weight (cm)	75.9 ± 12.9	77.6 ± 11.6	0.05
Body mass index (kg/cm^2)	25.5 ± 3.7	25.9 ± 3.6	NS
Serum cholestrol (mmol/liter)	5.54 ± 1.07	5.70 ± 1.06	0.02
Serum tryglycerides (mmol/liter)	1.55 ± 0.95	1.39 ± 0.73	0.01
Systolic blood pressure (mm Hg)	159.9 ± 22.8	159.2 ± 22.8	NS
Diastolic blood pressure (mm Hg)	84.5 ± 11.4	85.3 ± 11.2	NS
Women (N = 815)			
Bone mineral density (g/cm^2)	0.265 ± 0.250	0.286 ± 0.279	0.007
Height (cm)	159.0 ± 6.7	159.6 ± 5.7	NS
Weight (cm)	64.5 ± 11.7	65.9 ± 10.8	0.04
Body mass index (kg/cm^2)	25.5 ± 4.1	25.9 ± 4.1	NS
Serum cholestrol (mmol/liter)	6.37 ± 1.33	6.35 ± 1.16	NS
Serum cholestrol (mmol/liter)	1.62 ± 0.94	1.44 ± 0.69	NS
Serum cholestrol (mmol/liter)	163.4 ± 24.1	166.7 ± 22.6	NS
Diastolic blood pressure (mm Hg)	84.5 ± 11.0	86.5 ± 11.3	0.05

3. OSTEOPOROSIS

In 1987, European Foundation for Osteoporosis and Bone Disease had sponsored a conference held in Aalborg. A consensus statement is declared to the public at a press conference: *Osteoporosis* is a disorder characterized by bone tissue reduction per unit volume of bone. It is a major but not the sole cause of fractures in postmenopausal women and the elderly [4].

Osteoporosis is a skeletal disorder causing low bone density [1]. Low bone density is an essential factor in fracture risk [2]. Osteopenia is the less severe deficit in bone mass [3].

Shapurian *et al.* has calculated the fracture threshold for the bone density as 100-110 mg/cm^2. Fracture threshold is the threshold for the osteoporotic fracture prevalence: if BMD is above, the osteoporotic fracture is rarely seen. However, If BMD is less than 50 mg/cm^2, most patients experience spinal fractures [61].

Bone mass is considered as a strong predictor for bone fracture, and Dual Energy X-ray Absorptiometry (DEXA) is widely used for measuring the Bone Mineral Density (BMD) [3]. World Health Organization (WHO) has set the diagnostic criteria for osteoporosis and osteopenia using BMD only [63]. Measurements of BMD in grams/cm^2 (g/cm^2) from the hip and lumbar are the gold standard for non-invasive diagnostic measurement [19].

Bone mineral density is calculated as

$$BMD = \frac{BMC(grams)}{Area(cm^2)} \tag{3.1}$$

where BMC is the bone mineral content.

Rizzoli *et al.* say that the peak accumulated bone mass achieved at the end of

the skeletal growth is the predictor for future bone fracture risk and suggest that the bone mass measurements are for calculating the bone loss from this peak accumulated bone mass [64]. Although there is not any consensus on the age, for most bone sites, the peak accumulated bone mass is achieved between ages 20 and 30 [65, 66].

For young adult women, the peak bone mineral density has approximately Gaussian normal distribution, and the BMD of individuals can be expressed with the standard deviation units of the distribution. This measurement is referred to as the T scores (Figure 3.1) and calculated as [2]:

$$T = \frac{x - \mu_y}{\sigma_y} \tag{3.2}$$

where x is the measured BMD, μ_y is the mean BMD for the young population, and σ_y is the standard deviation for the young population.

On the contrary, Z-scores define the deviation from a demographically similar population, and they may assist in decision-making [34, 67, 68]. Z-scores are expected to be more *normal* with advancing age than the T scores, and low BMD Z scores suggest unusual bone mineral density loss possible due to secondary conditions other than usual aging or natural menopause [69]. Z-score is calculated as

$$Z = \frac{x - \mu_a}{\sigma_a} \tag{3.3}$$

where x is the measured BMD, μ_a and σ_a are the mean and standard deviation of BMD for a similar age population [70].

With a normal distribution, 0.5% of young adult women are expected to be in the osteoporotic range with T $<$ -2.5. With an increased age population in the osteoporotic range (Figure 3.2), i.e., the fracture risk also increases [71].

Based on their measured BMD T-scores using DEXA, the WHO and the International Osteoporosis Foundation have proposed four categories for women: Normal, Low bone mass (Osteopenia), Osteoporosis, and Severe Osteoporosis (Established Os-

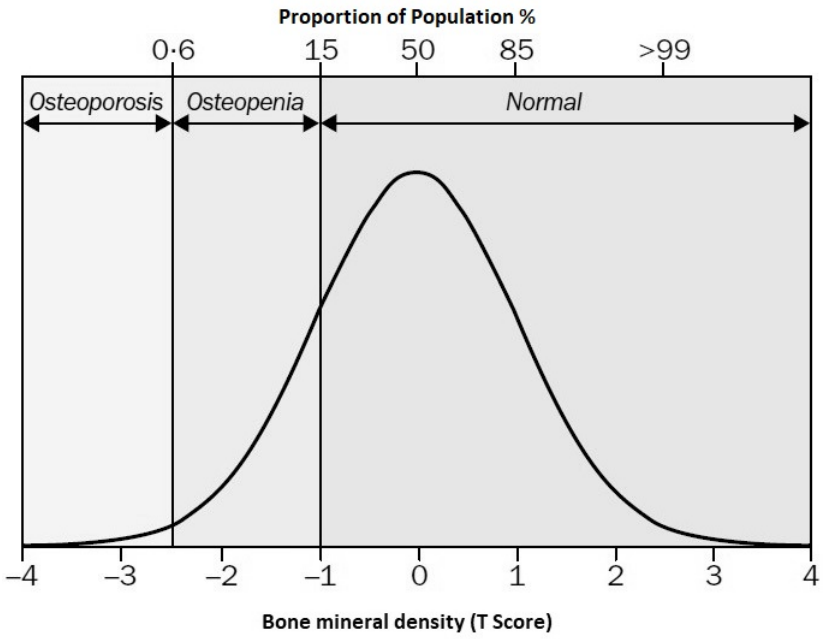

Figure 3.1 Distribution of bone mineral density in healthy women aged in the range of 30-40 years. Adapted from [2].

teoporosis) compared to their bone mineral density with young adult female reference values tabulated in Table 3.1 [63, 72].

Table 3.1
Descriptive Statistics of Bone Density Measurements. Adapted from [63].

Classification	T Score
Normal	T > -1
Low bone mass (osteopenia)	-2.5 < T < -1
Osteoporosis	T < -2.5
Severe osteoporosis (established osteoporosis)	T < -2.5 with one or more fractures

In Osteoporosis, without having any chemical composition change, the bone mass is reduced in cubic unit volume. Osteoporosis can be *nonfocal*, where bone mass reduction occurs at the entire skeletal system, or it can be *regional*, where bone mass is lost locally because of disuse or immobilization [34].

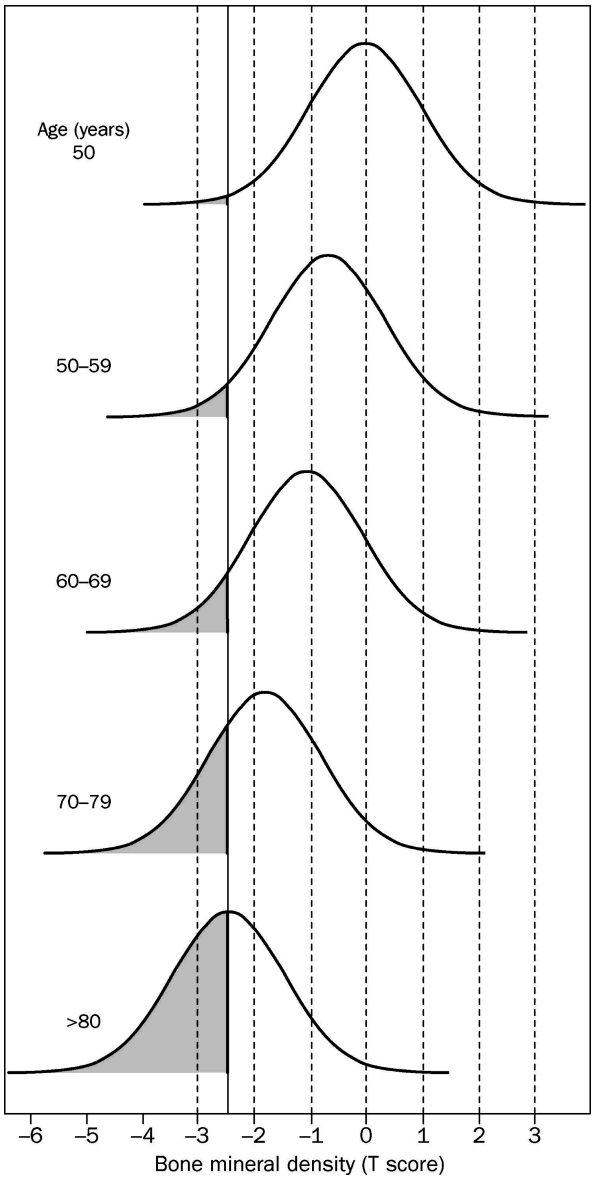

Figure 3.2 Bone mineral density distribution and the prevalence of osteoporosis (shaded area) for different age groups. Adapted from [71].

3.1 Types of osteoporosis

Osteoporosis is mainly observed in elders, especially older women, rare in children or young people. Children or adolescents can also rarely develop osteoporosis without any known underlying disorder, and this is called Juvenile osteoporosis. Juvenile osteoporosis can be very painful and can lead to prolonged or short-term disability [73]. If osteoporosis is observed in young, there is mostly an underlying medical disorder or side-effect of medications used to treat those disorders [10]. Osteoporosis is classified into two broad groups: If osteoporosis is built naturally, it is called *Primary*, and if

there is an underlying disorder, it is called *Secondary*. Table 3.2 tabulates disorders related to osteoporosis [10].

Melton and Riggs have shown that common osteoporosis starts in the middle ages in life, and it is more frequent with the increased age. They also proposed that there are two distinct types for this phenomenon: type I ("postmenopausal") and type II ("senile"). Melton and Riggs claim that type I osteoporosis develops only in women during the postmenopausal phase with rapid trabecular bone loss due to estrogen deficiency, and this bone loss causes vertebral fractures. They also claim there is also a *senile*, slow and steady bone loss (type II) at both trabecular and cortical bone in older women and men, and this type of osteoporosis causes proximal femur and vertebral fractures [74]. Later, Gallagher has named secondary type osteoporosis as type III [75].

Trabeculae bone becomes thinner with disuse and increasing age, and it can be even perforated at resorption cavities (Figure 3.3). This phenomenon can create anisotropy in trabecular structure at specific sites like the vertebral body or proximal tibia [76, 77].

3.2 Factors affecting bone mineral density

Many factors affect the bone mineral density: gender, ethnicity, aging, menopause age, duration of menopause, weight, inadequate physical exercise, metabolic and endocrine diseases, smoking, thyroid function, vitamin D deficiency, and several others [78].

Demir *et al.* has shown that the age at which menopause has started and the duration of menopause are essential BMD determinants: menopausal years is positively correlated with the prevalence of osteoporosis, and menopause start age is inversely correlated [79].

Researchers claim that obesity help to retain bone mineral density by stimulating

Table 3.2
Disorders associated with types of osteoporosis. Adapted from [10].

Disorders	
Primary osteoporosis	Secondary osteoporosis
Postmenopausal (Type I)	Endocrine related
Senile (Type II)	Adrenal cortex (Cushing's disease)
Juvenile osteoporosis	Gonadal disorders (hypogonadism)
	Pituitary (hypopituitarism)
	Pancreas (diabetes)
	Thyroid (hyperthyroidism)
	Parathyroid (hyperparathyroidism)
	Marrow replacement and expansion related
	Myeloma
	Leukemia
	Metastatic disease
	Gaucher's disease
	Anemias (sickle cell disease, thalassemia)
	Drugs and substances related
	Corticosteroids
	Heparin
	Anticonvulsants
	Immunosuppressants
	Alcohol (in combination with malnutrition)
	Chronic disease related
	Chronic renal disease
	Hepatic insufficiency
	Gastrointestinal malabsorption
	Chronic inflammatory polyarthropathies
	Chronic immobilization
	Deficiency related
	Vitamin D
	Vitamin C (scurvy)
	Calcium
	Malnutrition
	Inborn errors of metabolism related
	Osteogenesis imperfecta
	Homocystinuria

Table 3.3
Classification of osteoporosis according to Albright, Riggs and Melton, and Gallagher. Adapted from [75].

	Primary		Secondary
Type	Type I	Type II	Type III
Acronym	Postmenopausal	Senile	Secondary
Age	*55-70*	*75-90*	*Any age*
Years past menopause	5-15	25-40	
Sex ratio (female:male)	20:1	2:1	1:1
Fracture site	Spine	Hip, spine, pelvis, humerus	Spine, hip, peripheral skeleton
Bone loss			
Trabecular	High	Medium	High
Cortical	Low	Medium	High
Contributing factor			
Menopause	High	Medium	Medium
Age	Low	High	Medium

bone formation and by forcing cortical bones to carry more weight similar to physical exercise [7]. However, Sharma *et al.* put some reserves to this hypothesis, saying that, both for men and women, the fracture risk is increased with obesity despite the increased BMD due to obesity, and obesity can not be considered as protective [8, 9].

While some researchers are claiming that smoking decrease the bone mineral density both for men and women, even in young [80, 81, 82] and some others are claiming that there is no correlation between [83], smoking is a significant risk factor of hip fracture, increases hip fracture over 50% at old age, and among women, one in eight in total hip fractures is correlated to smoking [84].

Yu *et al.* have shown that physical exercise in aerobic dance could improve femoral neck BMD in 6 months but has no effect on spine BMD, suggesting that exercise affects trabecular bone than the cancellous bone [85]. Whereas, Huuskonen *et al.* say that with the exercise with aerobic exercise, bone mineral density does not change in men even after a long period of exercise; the only effect observed is

the decrease in Ward's triangle, suggesting that exercise has redistributed bone from trabecular to cortical bone [86].

3.2.1 Gender and age

While the prevalence of decreased BMD in the population at age 50 is five percent, at age 85, the prevalence increases to 50%. However, for women above 60 years of age, more than 75% of the population has decreased BMD: i.e., females develop osteoporosis four times more than males, and women are known to be at a greater risk than males [87, 88]. While the osteoporosis in women is mostly type I or type II, in men, osteoporosis is primarily type III or secondary type (Figure 3.4).

Due to lower prevalence, it has been found that men are mostly not screened and even rarely treated, even the ones using corticosteroids for extended periods [89]. Martinis *et al.* have shown that BMD for men is higher than women, but T scores for the osteoporotic population are similar for both gender, i.e., bone loss for men is higher, and also for similar BMD, the number of osteoporosis-related fractures in men is significantly higher than women [88].

Due to high prevalence, postmenopausal women have a higher risk; however, the response of older men to fracture treatment is not predictable. Recovery is notably difficult for femur fractures; therefore mortality rate due to osteoporotic fractures is higher in males [90, 91].

Age is an important determinant of bone mineral density both for women and men. For women in the premenopausal state, both lumbar and hip bone mineral density stays reasonably stable. However, there is a significant bone mineral density drop at all body sites in the postmenopausal state, and the bone loss is up to 0.47 to 1.07% annually. For men, there is a gradual bone density drop throughout the life starting the age the bone mass peak is reached, and it is between 0.22 to 0.33% annually at lumbar and 0.42% for hip (Figure 3.5). For men, the peak bone volume is around 25%

Table 3.4
Bone mineral density across the age groups. Adapted from [5].

Age (years)	N	BMD (g/cm^2) ± SD			
		Spine	Hip		Total body
			Femoral neck	Total	
Women					
20–29	39	1.05 ± 0.13	0.86 ± 0.13	0.95 ± 0.12	1.12 ± 0.08
30–39	65	1.07 ± 0.11	0.83 ± 0.10	0.94 ± 0.10	1.14 ± 0.08
40–49	90	1.06 ± 0.14	0.82 ± 0.12	0.94 ± 0.13	1.13 ± 0.09
50–59	106	0.96 ± 0.14	0.74 ± 0.11	0.86 ± 0.13	1.05 ± 0.10
60–69	61	0.88 ± 0.15	0.69 ± 0.11	0.82 ± 0.12	0.97 ± 0.09
70–89	37	0.83 ± 0.15	0.61 ± 0.13	0.72 ± 0.16	0.93 ± 0.11
Men					
20–29	21	1.12 ± 0.14	0.98 ± 0.15	1.10 ± 0.13	1.26 ± 0.10
30–39	40	1.11 ± 0.16	0.92 ± 0.15	1.06 ± 0.15	1.24 ± 0.11
40–49	48	1.04 ± 0.17	0.87 ± 0.13	1.03 ± 0.14	1.20 ± 0.10
50–59	50	1.01 ± 0.15	0.83 ± 0.13	0.99 ± 0.17	1.19 ± 0.12
60–69	37	1.03 ± 0.16	0.79 ± 0.12	0.96 ± 0.13	1.16 ± 0.10
70–89	26	0.99 ± 0.17	0.73 ± 0.09	0.88 ± 0.11	1.10 ± 0.09

higher than the women [5].

For the same age group, increased age increases the fracture risk (Figure 3.6) [92].

3.2.2 Genetic and ethnicity

Bone mass is higher for the black population compared to the white population [93], and Hispanics have similar bone mass with whites [94], and Asians have the least bone mass, although by correcting their body size, the difference is negligible [95, 96]. T scores show variations with ethnicity as well, and the black population has the highest, and Asians have the least T scores at all age groups (Figure 3.7), although osteoporosis is always considered the white women's disease [6].

Although Asian women have the lowest and black people have the highest bone mineral density, they have similar risk fracture risk, which is the least among ethnic groups: other musculoskeletal factors may affect fracture risk more than BMD [97].

A few bone mineral density normative data study is conducted for Turkish population [98, 99, 100]. From published literature, for Turkish men and women, the bone mineral density decreases with increased age.

For women between age 20-49, lumbar BMD is lower than European women's scores, which also gets closer to European values after the fifth decade. Similarly young Turkish women's hip BMD is lower compared to American Caucasian population scores [98].

Bone mineral density scores for Turkish men are lower at lumbar and hip than European and US men scores [100, 98].

Bone mineral densities of Danish and Turkish population is tabulated in Table 3.5 for comparison [98, 5].

Lower BMD scores do not always mean the highest bone fracture risk: Mediterranean Osteoporosis Study (MEDOS) shows that number of hip fractures reported from Turkey is lower than in Europe [101].

3.3 Economic burden of osteoporosis

As a skeletal disease, osteoporosis has a significant economic burden on societies, and with the increased average age of the global population, this burden is also increasing [11]. Osteoporosis is causing mortality or morbidity due to bone fractures, and negatively impacts patient's life quality [102]. Johnell *et al.* estimate an osteoporosis-related bone fracture happens every 3 seconds globally, causing more than 8.9 million fractures annually [12]. Only in 2010, in the European Union, over 22 million women

Table 3.5
Comparison of bone mineral densities of Turkish and Danish populations. Adapted from [98, 5].

Age (years)	BMD (g/cm^2) ± SD					
	Turkish			Danish		
	Spine	Femoral neck	Total hip	Spine	Femoral neck	Total hip
Women						
20–29	0.96 ± 0.10	0.79 ± 0.09	0.89 ± 0.11	1.05 ± 0.13	0.86 ± 0.13	0.95 ± 0.12
30–39	0.96 ± 0.14	0.80 ± 0.15	0.88 ± 0.12	1.07 ± 0.11	0.83 ± 0.10	0.94 ± 0.10
40–49	0.93 ± 0.11	0.79 ± 0.11	0.89 ± 0.11	1.06 ± 0.14	0.82 ± 0.12	0.94 ± 0.13
50–59	0.88 ± 0.12	0.74 ± 0.09	0.85 ± 0.10	0.96 ± 0.14	0.74 ± 0.11	0.86 ± 0.13
60–69	0.81 ± 0.14	0.69 ± 0.12	0.80 ± 0.15	0.88 ± 0.15	0.69 ± 0.11	0.82 ± 0.12
70–79	0.76 ± 0.15	0.63 ± 0.10	0.73 ± 0.13	0.83 ± 0.15	0.61 ± 0.13	0.72 ± 0.16
Men						
20–29	0.97 ± 0.10	0.88 ± 0.12	1.02 ± 0.13	1.12 ± 0.14	0.98 ± 0.15	1.10 ± 0.13
30–39	1.00 ± 0.11	0.88 ± 0.07	1.04 ± 0.10	1.11 ± 0.16	0.92 ± 0.15	1.06 ± 0.15
40–49	0.93 ± 0.14	0.80 ± 0.15	0.99 ± 0.15	1.04 ± 0.17	0.87 ± 0.13	1.03 ± 0.14
50–59	0.91 ± 0.12	0.78 ± 0.12	0.96 ± 0.12	1.01 ± 0.15	0.83 ± 0.13	0.99 ± 0.17
60–69	0.86 ± 0.15	0.71 ± 0.10	0.91 ± 0.12	1.03 ± 0.16	0.79 ± 0.12	0.96 ± 0.13
70–79	0.77 ± 0.09	0.60 ± 0.07	0.77 ± 0.12	0.99 ± 0.17	0.73 ± 0.09	0.88 ± 0.11

and over 5.5 million men have developed osteoporosis, and more than 3.5 million bone fractures occurred. With the change in demography, the number of fractures will rise 28% to 4.5 million in 2025 [14, 15]. Only in the USA, with a minimum of 1.5 million annual fractures, the economic burden to US society is between 12 to 18 billion US dollars annually [13].

Turkey is not exempt from the osteoporosis problem, and it is also an increasing problem in Turkey due to the increase in the average age of the population [16]. The FRACTURK study shows that similar to all other countries, in Turkey, the hip fracture rate is also increasing exponentially by age [17]. Tuzun *et al.* have shown that for the Turkish population at the age of 50, the probability of having a hip fracture in their remaining life is 14.6% for women and 3.5% for men [17].

Unless it is screened for, osteoporosis is a silent disease until it results in a fracture. With an efficient screening, osteoporosis can be prevented, diagnosed, and later with effective treatments, fractures can be prevented [16].

Aziziyeh *et al.* show that osteoporosis is under-treated in Turkey. In 2019 over 255 thousand osteoporosis-related fractures occurred with over 455 million USD economic burden on the Turkish economy. From 2019 to 2023, the total burden is expected to be over 2.4 billion USD [18].

Unfortunately, despite the increased osteoporosis rates, the studies show that the osteoporosis treatment rates did not increase in the last decade either because of the missing public awareness limiting the early diagnosis or the other factors limiting the treatment rates after the diagnosis. After diagnosis, the factors limiting the treatment rates are lack of motivation, and patient education, medication costs, or concerns about the side effects [103]. Cipriani *et al.* show that even the misleading information in media is also a significant cause of low treatment rates [104].

Altın *et al.* have shown that the osteoporosis awareness for pre-menopausal and post-menopausal women in Turkey is the same. Furthermore, the women who had an osteoporosis diagnosis are not higher than women who did not have any, and having a family history of osteoporosis does not increase this awareness level either [21]. The awareness of men is even lower than women [21]. A study conducted among young nurses shows that, even among healthcare personnel, osteoporosis awareness is low, and specific education is needed to improve the awareness [105].

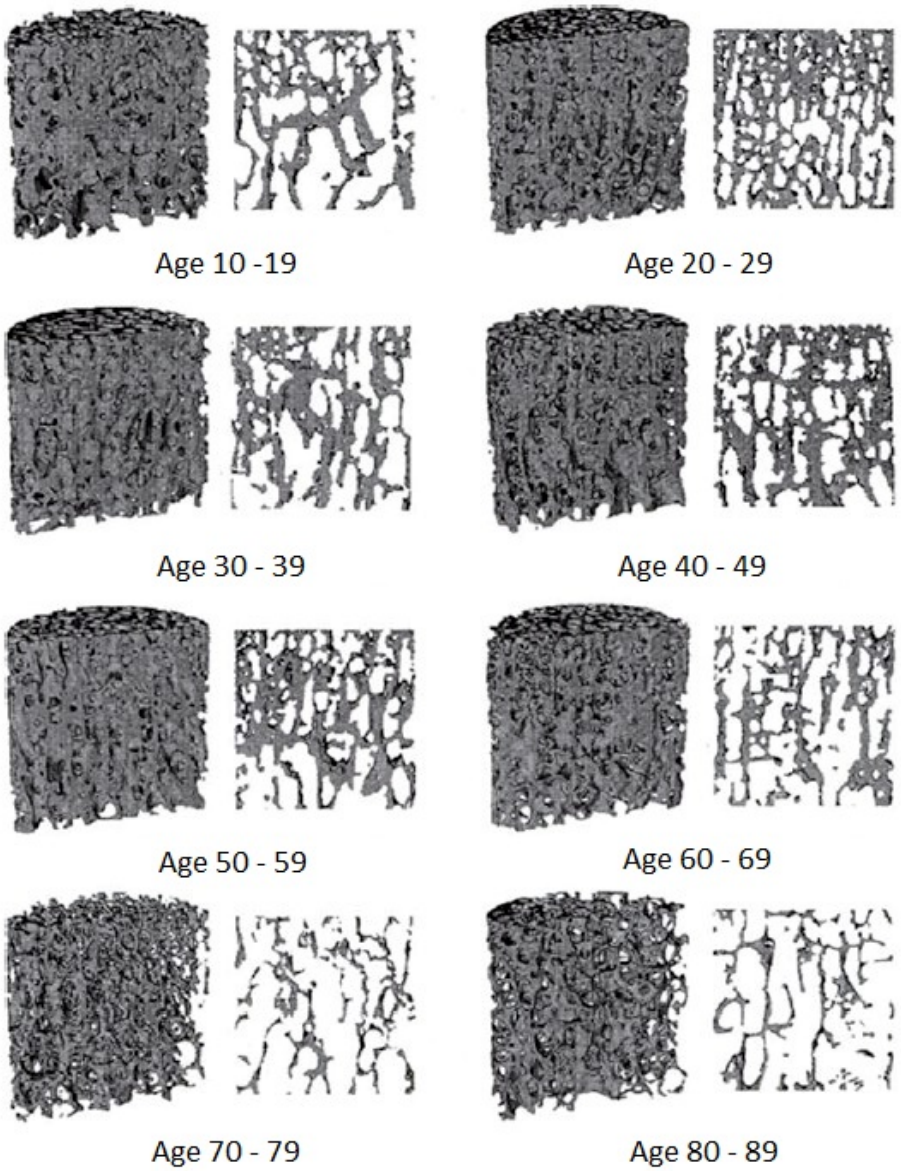

Figure 3.3 High-resolution, three-dimensional renderings and two-dimensional cross-sections of trabecular bone from the human proximal tibia in the 2nd–9th decades of life. Adapted from [77].

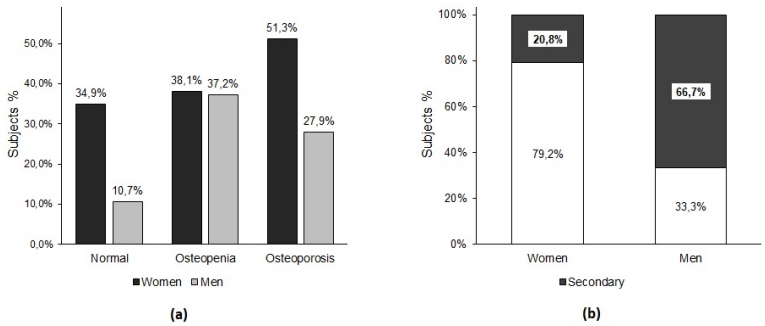

Figure 3.4 Gender differences in a) osteoporosis prevalence and b) ratio of secondary type osteoporosis in osteoporotic population. Adapted from [88].

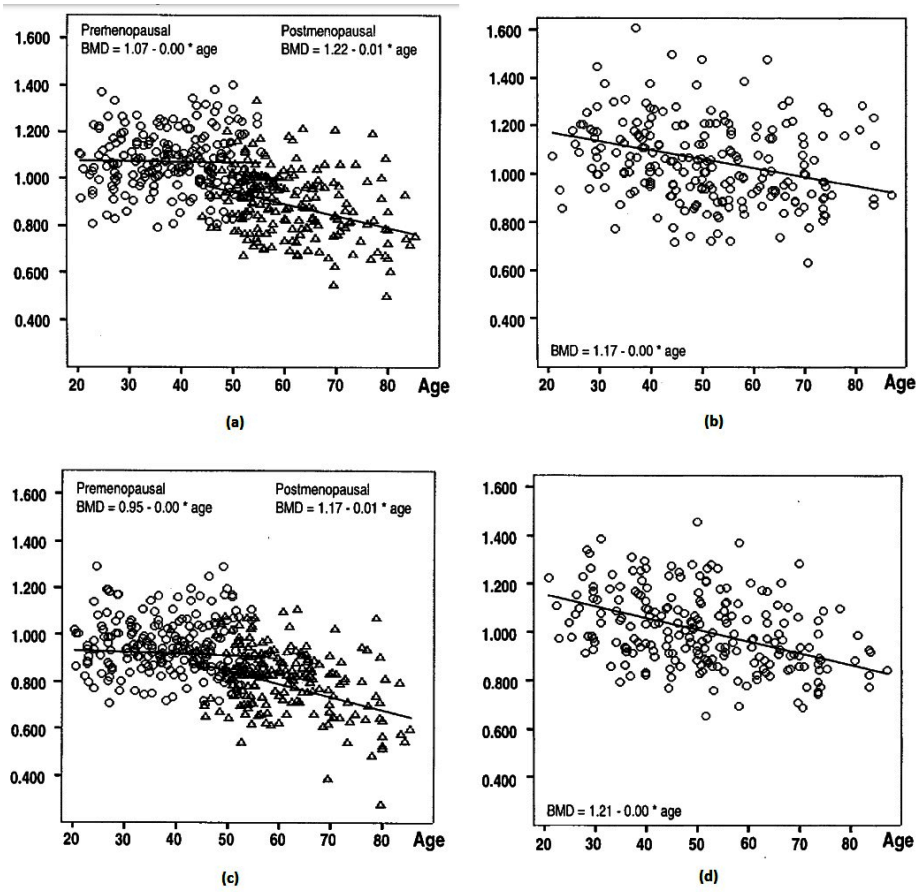

Figure 3.5 Bone mineral density changes with the age and gender a) for women at lumbar and b) for men at lumbar c) for women at hip and d) for men at hip. Adapted from [5].

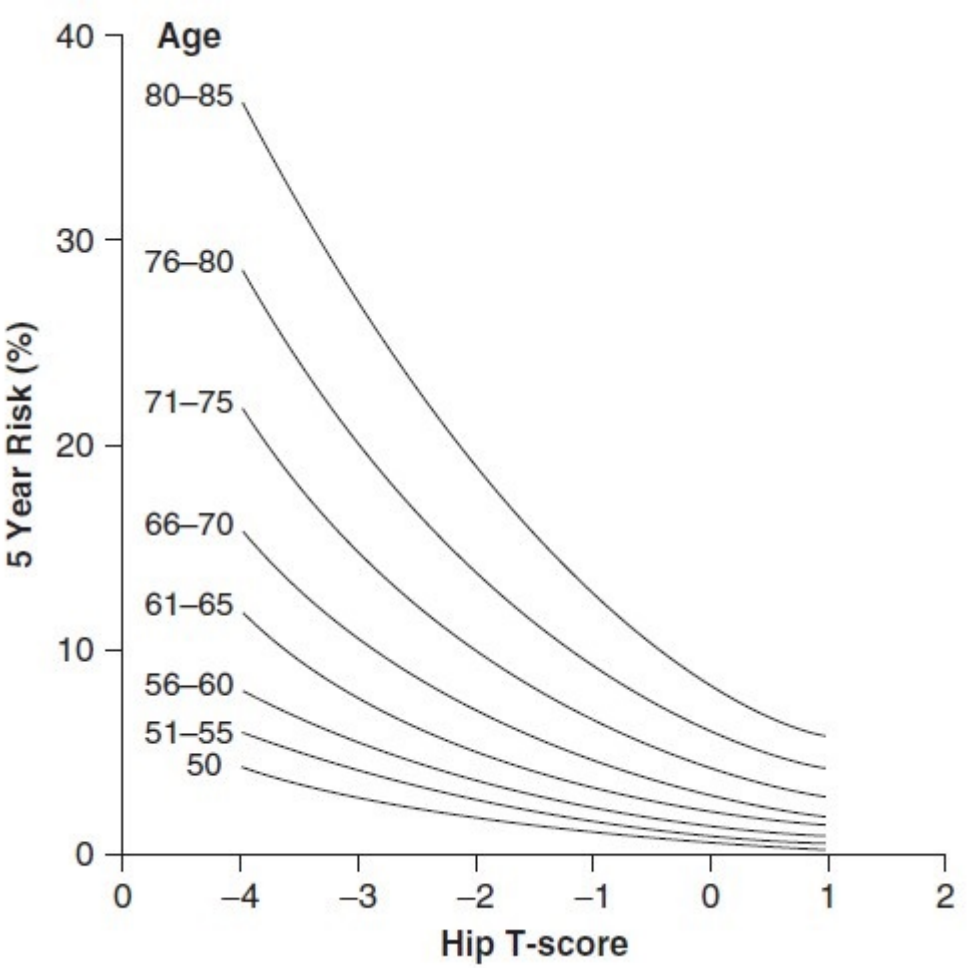

Figure 3.6 Risk of fracture in 5 years as a function of hip. Adapted from [3].

.

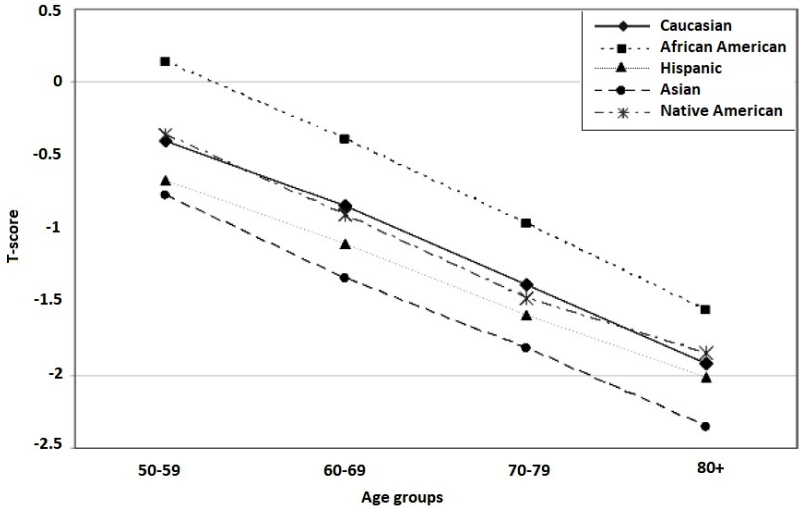

Figure 3.7 Mean hip T scores of different ethnic groups at different ages. Adapted from [6].

4. BONE DENSITOMETRY

Diagnosis of bone mineral density changes is critical for the early treatment of underlying diseases. Physicians can visualize the bone structure with conventional radiographic imaging techniques, but they can not measure bone mineral density directly. On the other hand, with bone densitometry physicians can accurately measure bone mineral density [106]. Before bone densitometry, physicians were calculation the Singh index to predict bone strength [107]. In conventional radiography, the trabeculae

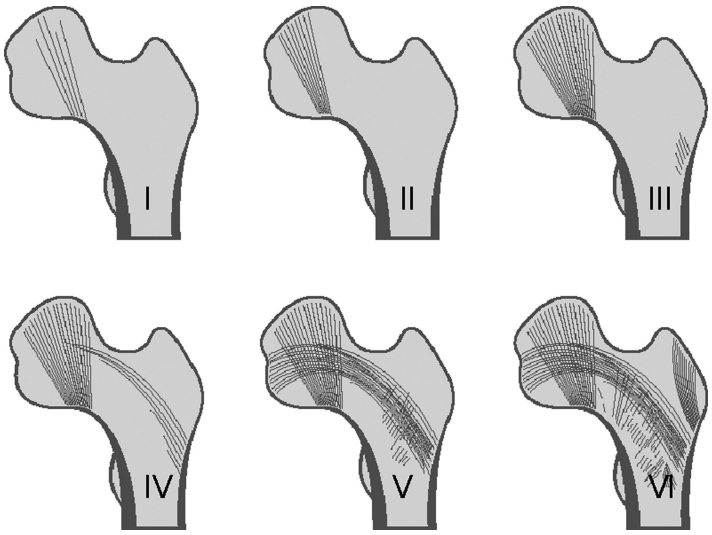

Figure 4.1 Scheme of changes in trabecular pattern of the proximal femur (Singh index values from I to VI). Adapted from [107].

in the proximal femur are assumed to be disappearing in the radiological images; the reduction in the original thickness is used to calculate the Singh Index as in Figure 4.1. The degree of bone loss is classified from grade VI (normal, all trabecular groups visible) to grade I (even the principal compressive trabeculae is invisible). Later a grade VII is added to scale for dense bones [108]. Griffith *et al.*, Peacock *et al.*, and Koot *et al.* have shown the relationship of the Singh Index with the bone mass in their studies [109, 110, 107]. The Singh index is a subjective grading since it is strongly dependent on the observer's experience, and it is also affected by the quality of the radiological image [10].

In Radiogrammetry, metacarpal bones are measured to calculate the Cortical

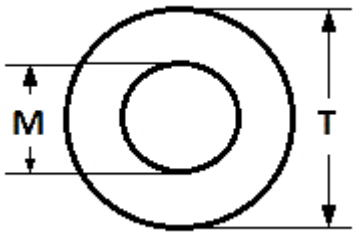

Figure 4.2 Cortical model.

Index (CI) and Cortical Area (CA) parameters using the model in Figure 4.2.

$$CI = (T - M)/T \tag{4.1}$$

$$CA = (T^2 - M^2) * \pi/4 \tag{4.2}$$

Kalla *et al.* have shown that the cortical area is more closely parallel to the actual physical bone mass [111]. Due to radiographic geometry and soft tissue thickness, cortical area measurement precision is moderate, and cortical measurements are more useful in clinical research but less likely to be used for individual patient management [10]. Digital X-ray radiogrammetry (DXR) also uses cortical thickness to calculate bone density and with computer-aided image processing algorithms, this time with adequate precision. Bouxsein *et al.* have shown that digital radiogrammetry can be used as predictive measurements for hip, spine, and wrist fractures [112].

4.1 Dual Energy X-ray Absorptiometry (DEXA)

The amount of the x-ray shadow cast on a radiological film is a function of the x-ray absorbed by a tissue through which the x-ray beam passes. The absorbed amount depends on the quality of the x-ray beam, the density, the thickness, and the character of the atoms composing the penetrated tissue [10]. X-ray absorption is positively correlated with the third power of the atomic number. Calcium has a higher atomic number; therefore, the X-ray absorption of bone tissue is primarily determined by its calcium content [113]. The calcium content of a mineralized bone is constant at

about 35% [114]. Therefore decrease in the mineralized bone volume is equivalent to a decrease of bone calcium content and a decrease in x-ray beam absorption, and this phenomenon is called increased radiolucency [10].

However, Heucks and Schmidt summarize the factors affecting the radiographic appearance in four major groups: radiation source, the object under inspection, film, and screen, and finally, the film processing [115].

In central DEXA measurements, the lumbar spine and hip are measured, and in bone densitometry, these scans form the gold standard for osteoporosis diagnosis [10].

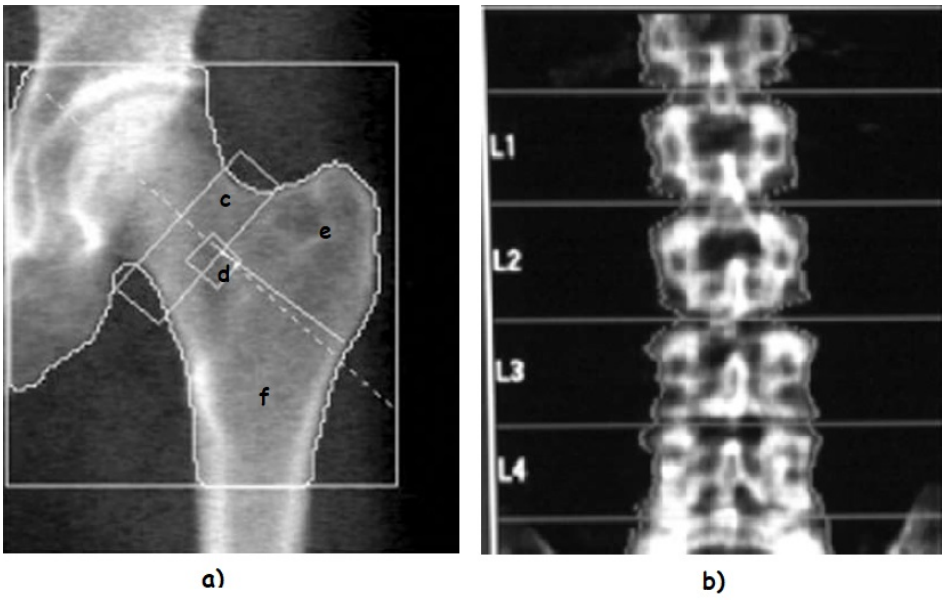

Figure 4.3 In central DEXA scan both a) left hip and b) lumbar spine from L1 to L4 are measured. Hip measurement areas are c) the femoral neck shown as inclined rectangle, d) the Ward's area shown as a square, e) the trochanter area and f) the inter-trochanter area.

For lumbar spine measurement, L1, L2, L3, and L4 bone mineral densities are separately measured and summed up to find the total lumbar spine data, whereas, for hip measurement, femoral neck, Ward's area, trochanter area, and inter-trochanter area of the femur bone is measured (Figure 4.3).

For finding bone mineral density, first, the bone mineral content is measured in grams from the area of the inspection and divided to the area in cm^2. Later BMD is compared with the age, gender, and ethnicity-specific National Health and Nutrition

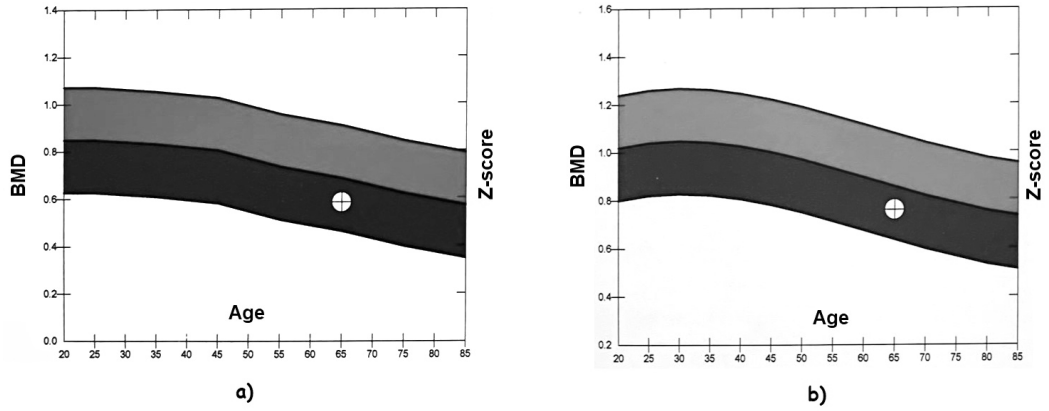

Figure 4.4 To find the Z scores, measured DEXA results are compared with the US National Health and Nutrition Examination Survey (NHANES) gender and ethnicity specific reference data. a) is the femoral neck Z score reference chart and b) is the total lumbar spine reference chart for the white women.

Examination Survey (NHANES) reference data of US in Figure 4.4 to find its Z score. Finally, BMD is compared with NHANES "young normal" population reference data to find the T score; T score is the standard deviation from the mean bone mineral density of the "young normal" population, and Z score is the standard deviation from the mean bone mineral density of the same age population [116].

To measure how bone mineral density is changing in time, either the precision of the bone densitometer should be better than the random measurement error or the amount of BMD change in time should be comparably high; therefore, the precision of the measurement system is crucial [117]. However, the annual change of bone mineral density for an individual is in the order of 1%, which is comparable to random errors [118]. The precision of the measurement is also dependent on the technician's expertise: patient positioning error, spinal scoliosis, and excessive or too much weight of the patient can change the measurement results [10]. DEXA can also produce false-negative results if there is an unsuspected lumbar compression fracture [119].

Hui *et al.* have compared the measurement results of Hologic, Lunar, and Norland model devices by using phantoms, and they have found that Hologic and Norland devices overestimate BMD while Lunar devices underestimate due to their manufacturer dependent systematic errors. In order to normalize the DEXA measurements, Hui *et al.* also propose the use of model-dependent conversion factor as in Table 4.1

Table 4.1
Manufacturer dependent sBMD conversion formula. Adapted from [56].

Manufacturer	sBMD formula
Hologic	sBMD = 1.0755 BMD
Lunar	sBMD = 0.9522 BMD
Norland	sBMD = 1.0761 BMD

to find a standard bone mineral density (sBMD) [56].

4.2 Peripheral Dual Energy X-ray Absorptiometry (PDXA)

Peripheral dual-energy X-ray absorptiometry devices use the same measurement technology with DEXA; however, they are designed to measure BMD at peripheral skeletal sites such as the forearm, finger phalanges and, calcaneus. Therefore, their instruments are less expensive, smaller, and more portable compared to DEXA [120].

PDXA measurements are performed at less radiation-sensitive organs with a significantly lower radiation dose even compared to DEXA. Their primary purpose is to measure the global fracture risk of post-menopausal women [119]. The use of PDXA in clinical practice is not well defined, and the success rate in predicting fracture risk is lower than DEXA [120].

4.3 Single Energy X-ray Absorptiometry (SXA)

In this technique, a single energy X-ray beam is used for the bone mineral density assessment. Bone mineral density is computed using the increased absorption rates of the beam as it passes through a constant thickness of soft tissue or water bag into the bone. The measurement area is the wrist or heel, and measurement location is usually defined by external landmarks [119]. SXA is easier to use and shows good measurement precision at the forearm [121]. Nevertheless, SXA does not consider the

X-ray absorption of soft tissues, and it can be performed at peripheral sites only like the forearm, where there is less soft tissue [118]. Hence, SXA is considered an inferior measurement technique compared to DEXA [122].

4.4 Radiographic Absorptiometry (RGA)

In radiographic absorptiometry, an X-ray image of the hand is captured together with an aluminum wedge. The image is captured with a high-resolution video camera then compared with the wedge readings for calibration. Images are analyzed centrally. Calculated bone density in the middle phalanges is then used to assess the bone status [123, 124].

Due to its inexpensive nature, RGA is a preferred bone mass measurement method [125, 119]. The measurement devices are portable and accessible, also their ease of use making this technique attractive [126, 124, 127].

The time delay in analyzing images centrally, using single x-ray energy in measurement, and the difficulties in the calibration of aluminum wedges are the limitations of RGA [128].

Gulam *et al.* have shown that RGA can be used to separate young from postmenopausal women in terms of their phalangeal bone mineral density measurements (Table 4.2). They have also formulated the bone mineral density conversion formula as

$$BMD_{RGA} = 419 * BMD_{PDXA} - 15 \tag{4.3}$$

,and demonstrated the strong correlation ($r^2 = 0.811, P < 0.001$) between RGA and the Peripheral Dual Energy X-ray Absorptiometry (PDXA), and have shown that they are comparable methods [128].

Table 4.2
Descriptive statistics of RGA and PDXA bone density measurements in women. Adapted from [128].

	Young women		Postmenopausal	
Hand Data	Mean	SD	Mean	SD
RGA_{BMD} index	109.8	9.8	84.6	11.9
$PDXA_{BMD}$ (g/cm^2)	0.289	0.025	0.245	0.032

4.5 Single Photon Absorptiometry (SPA)

Single-photon absorptiometry (SPA) can quantitatively measure the BMD [129]. As a gamma-ray source, ^{125}I (Iodine-125) is used, which emits 27.3 keV average energy, which is not sufficient for central skeletal bone measurements [130]. Therefore, the measurement area is limited to peripheral bones, and measurements are limited to the wrist [119, 106]. The SPA method solved the non-uniformity of film sensitivity and polychromatic X-rays problems in the radiographic photo-densitometric measurements; however, the scanning time was up to 30 minutes due to the low photon flux. Patients generally occasionally could not stay still during the measurement period, which was leading to poor image quality with limited reproducibility [106]

4.6 Dual Photon Absorptiometry (DPA)

Dual Photon Absorptiometry (DPA) is based on the same principle as SPA. In DPA, ^{153}Gd (Gadolinium-l53) with two photon energies of 44 keV and 100 keV is used (Figure 4.5) [131]. Using two different photon energies allows the exclusion of the contribution of soft tissue in the measured attenuation. Therefore, DPA can scan deeper structures like the spine, hip, or even total body [106, 119]. However, the technique cannot calculate the true volumetric calcium density but measures as in two dimensions as grams per square centimeter [132, 133]. For two distinct photon energies of 44 keV and 100 keV, the equations for calculating the bone mineral density (BMD)

are formulated as

$$M_{Bone}(x,y) = \frac{ln(I^o_{44}/I_{44}) - RST * ln(I^o_{100}/I_{100})}{\mu_{Bone:44} - RST * \mu_{Bone:100}} \tag{4.4}$$

$$RST = \mu_{ST:44}/\mu_{ST:100} \tag{4.5}$$

where $M_{Bone}(x,y)$ is the BMD (g/cm^2) at point location (x, y) in the BMD image, and I_{100} and I_{44} are the measured photon intensities at that point, I^o_{100} and I^o_{44} are the attenuated photon intensities, RST is the ratio of attenuation of the two photon energies in soft tissue, $\mu_{Bone:44}$, $\mu_{Bone:100}$, $\mu_{ST:44}$ and $\mu_{ST:100}$ are the mass attenuation coefficients for bone mineral and soft tissue at low and high energies, respectively [134].

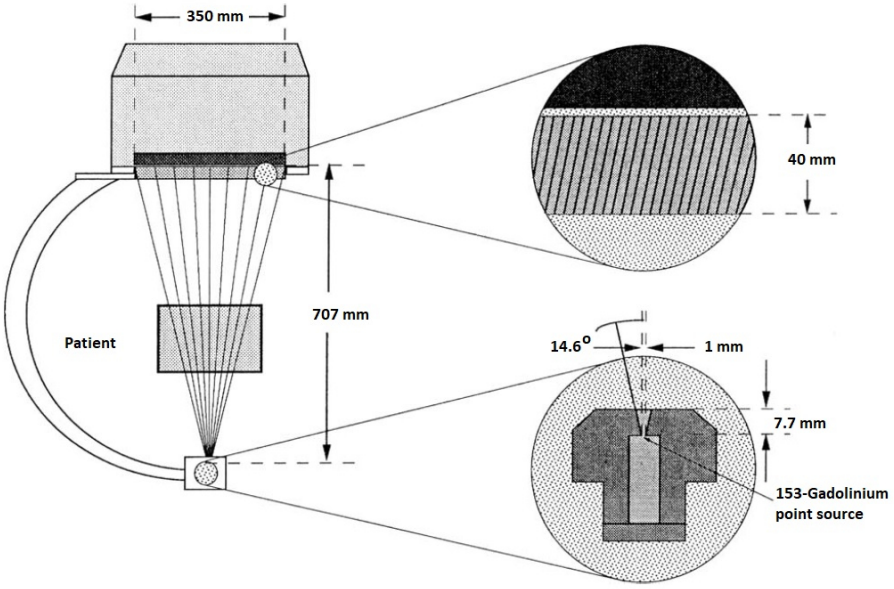

Figure 4.5 Schematic view of the Gamma Camera detector with C-arm attached (left). Details of converging collimator (right, top) and source holder (right, bottom). The patient is pictured in the beam, with different path lengths for photons passing through the center and through peripheral parts. Adapted from [131].

4.7 Quantitative Ultrasound (QUS)

The quantitative ultrasound (QUS) technique is a safe, non-invasive, easy to use, and cost-effective radiation-free technique. Therefore, this technique is used with patients that radiological imaging is not appropriate, especially for children, or radiation-free technique is needed [135].

QUS does not measure bone mineral density directly. The traveling speed of sound in the bone is used to predict bone mineral density. Nevertheless, QUS also gives structural information, which may be necessary to determine the fracture risk [126, 136, 137].

Speed of Sound (SoS) is calculated by dividing the distance by the time; taken by the impulse to travel the distance between the probes. Amplitude dependent speed of sound (AD-SoS) reflects the amplitude-dependent velocity with a threshold of 2 mV; Bone transmission time (BTT) is the time difference between the first peak received and maximum peak received; Broadband ultrasound attenuation (BUA) is the slope of the attenuation against frequency plot (Figure 4.6).

$$BUA = \nabla db / \nabla MHz \tag{4.6}$$

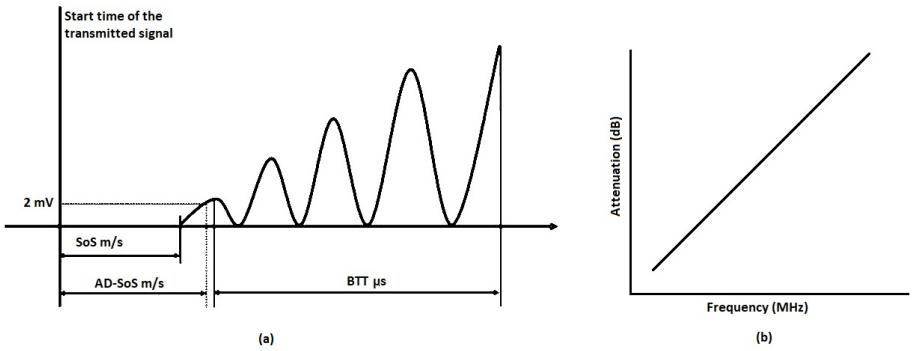

Figure 4.6 QUS variables calculated by a) ultrasound velocity and b) ultrasound attenuation. Adapted from [135].

Depending on the measurement site QUS is named as Phalangeal, Tibial or Calcaneal QUS, where measurements are performed at hand proximal phalanges of the hand, at tibia mid-shaft radius distal third or heel, respectively.

A decrease in QUS velocity and attenuation-based variables are indicators for reduced bone mineral density in children, with disturbances of growth or disorders affecting bone health [138, 139].

The disturbances or disorders versus QUS parameters are tabulated in Table

4.3.

Table 4.3
Summary of some QUS studies in children with disturbances of growth or disorders affecting bone health. Adapted from [135].

Disease/disorder	N	Skeletal site of measurement	QUS variables	Obs.
Bone and mineral disorders	135	Proximal phalanges of the hand	AD-SoS	↓
Genetic disorders	50	Proximal phalanges of the hand	AD-SoS	↓
Chronic rheumatic diseases	53	Heel	BUA	↓
Chronic rheumatic diseases	40	Tibia midshaft, Radius distal third	SoS	↓
Juvenile idiopathic arthritis	70	Heel	SoS, BUA	↓
Chronic diseases and/or fragility fractures	42	Heel	SoS, BUA	↓
Inflammatory bowel disease	10	Heel	SoS	↓
Crohn disease	35	Tibia midshaft, Radius distal third	SoS	↓
Celiac disease	41	Tibia midshaft, Radius distal third	SoS	↓
End-stage renal failure	30	Proximal phalanges of the hand	AD-SoS	↓
Severely handicapped institutionalized	87	Tibia midshaft, Radius distal third	SoS	↓
Severe cerebral palsy	67	Heel	QUI	↓
Acute lymphoblastic leukemia	54	Proximal phalanges of the hand	AD-SoS	↕
Acute lymphoblastic leukemia	37	Tibia midshaft	SoS	↓
Acute lymphoblastic leukemia	42	Heel	BUA	↓
Sickle cell disease	80	Heel	SoS	↓
HIV-infected	44	Heel	BUA	↓
HIV-infected	44	Proximal phalanges of the hand	AD-SoS, BTT	↓
Central precocious puberty, idiopathic short stature after Gn-RH agonist treatment	25	Heel	BUA	↓*
Delayed puberty	45	Tibia midshaft, Radius distal third	SoS	↓
Isolated growth hormone deficiency	68	Proximal phalanges of the hand	AD-SoS, BTT	↓
Insulin-dependent diabetes mellitus	30	Tibia midshaft, Radius distal third	SoS	↓
Insulin-dependent diabetes mellitus	86	Proximal phalanges of the hand	AD-SoS	↓

* Only in children with idiopathic short stature.

4.8 Quantitative Computed Tomography (QCT)

In Quantitative Computed Tomography (QCT) measurements, the Hounsfield Unit (HU) is used, which is introduced by Sir Godfrey Hounsfield, who has also received Nobel Prize in Physiology or Medicine in 1979 [140]. HU is the relative radio-density in interpreting the image in computed tomography (CT). The HU varies with the tissue

density and proportional to particle numbers and atomic weights at the scan area [119]. The HU measurement scale is calibrated so that HU is -1000 for air and 0 for water. The more the tissue scanned is denser, the higher the HU number is [141].

Hounsfield Unit value is defined as

$$HU = \frac{\mu_m - \mu_w}{\mu_w - \mu_a} * 1000 \tag{4.7}$$

where μ_m, μ_w and μ_a are the linear attenuation factors of material, water and air, respectively [119].

For QCT, Shapurian *et al.* has calculated the fracture threshold for the bone density as 100-110 mg/cm^3. Fracture threshold is the threshold for the osteoporotic fracture prevalence: if BMD is above, the osteoporotic fracture is rarely seen. If BMD is less than 50 mg/cm^3, most patients experience spinal fractures. A BMD of 90 mg/cm^3, equivalent to 130 HU, is the 100% sensitivity for osteoporosis [61].

While other bone densitometry methods measure the trabecular bone and the overlying compact bone, Quantitative Computed Tomography (QCT) is a 3-dimensional measurement technique that can measure trabecular bone 100% isolated; [119]. Trabecular bone is more than eightfold active than cortical bone, and metabolic changes such as estrogen deficiency triggered by menopause affect trabecular bone much faster than the cortical bone. Therefore, QCT is very sensitive to bone density changes [142]. Celenk *et al.* propose that, with its high sensitivity, instead of DEXA, QCT should be the *gold standard* for diagnosing osteoporosis in fracture risk calculations [119].

4.9 Magnetic Resonance Imaging (MRI)

With this method, any site can be measured, but typically, spine, hip, or total body is measured. MRI is a non-invasive, radiation-free method to assess the bone structures, including trabecular bone, which has at least eight-fold turnover speed

[119]. Compared to other BMD assessment methods, MRI is the most costly one, with the lowest accessibility.

By comparing their RMI images and DEXA results of 139 subjects, Wehrli *et al.* have shown that there is a moderate correlation between RF-reversible spin dephasing (R_2') parameter of RMI and BMD, and also tabulated in Table 4.4 that R_2' can be used as a discriminator factor for normal, osteopenic and osteoporotic subjects [143].

Table 4.4
Descriptive Statistics of Bone Density Measurements with RF-reversible spin dephasing (R_2'). Adapted from [143].

Category		L2-4	Femoral Neck	Greater Trochanter
Normal (NO)		52.0±0.9	65.0±1.3	44.3±0.7
Osteopenic (OPE)		47.3±1.2	42.2±1.0	39.7±0.9
Osteoporotic (OPO)		43.4±1.9	37.4±1.6	36.6±1.4
	NO/OPE	< 0.01	< 0.01	< 0.01
P value	NO/OPO	< 0.01	< 0.01	< 0.01
	OPE/OPO	NS	NS	NS

5. BIS - BIOIMPEDANCE SPECTROSCOPY

Bioimpedance spectroscopy (BIS) is a non-invasive technique used in tissue characterization [24]. Each living tissue has its own impedance characteristics, which can be used for tissue identification [25].

For a cylindrical object, the resistance R of the material is calculated from

$$R = \rho \frac{L}{A} \tag{5.1}$$

where L is the object's length, A is the cross sectional area, and ρ is the specific resistance of the material.

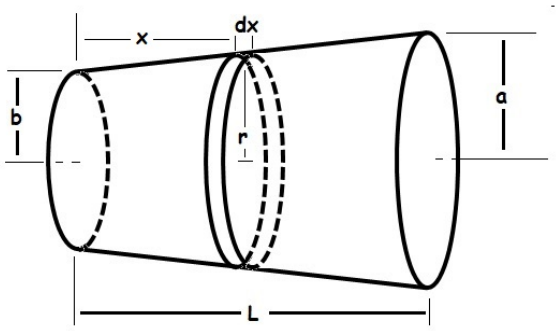

Figure 5.1 Truncated cone resistance.

For the truncated cone object shown in Figure 5.1, with $(b - a) << L$, the current is assumed to be flowing perpendicular to the axis, even at the boundaries [144] and the incremental resistance dR of the slab is

$$dR = \rho \frac{dx}{\pi r^2} \tag{5.2}$$

where r is the radius of the cross-section at a position x. If the radius of the truncated cone at both ends are a and b, and length is L, then with simple geometry

$$\frac{dx}{dr} = \frac{L}{b - a} \tag{5.3}$$

and dR can be formulated as

$$dR = \rho \frac{L}{b-a} \frac{dr}{\pi r^2} \tag{5.4}$$

and finally, R is calculated as follows:

$$\begin{aligned} R &= \int dR \\ R &= \rho \frac{L}{b-a} \int_a^b \frac{dr}{\pi r^2} \\ R &= \rho \frac{L}{\pi ab} \end{aligned} \tag{5.5}$$

The current flow in a living tissue is ionic, and the impedance is affected by relaxation phenomena caused by the dipolar rotation, rotation of macro-molecules, and interface polarization [28]. As shown in Figure 5.2, Schwan defines three frequency bands for dispersion: α, β, and γ dispersion [145].

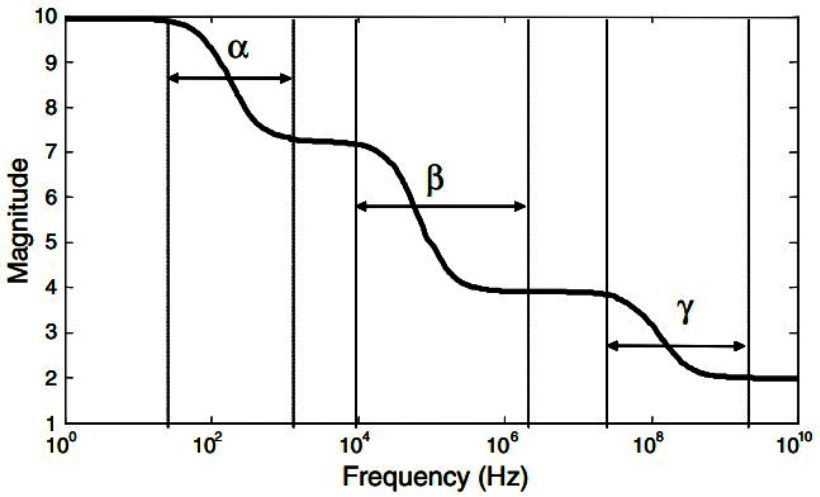

Figure 5.2 Frequency dependent impedance of biological tissues. Adapted from [28].

In Table 5.1, the conductivities of biological tissues are tabulated [25].

The α dispersion band is between a few Hertz to a few kilo Hertz. It is created by the relaxation of the non-permanent dipoles generated because of the ionic flow over the cell surfaces or large bio-molecules [146].

Table 5.1
Frequency dependence of electrical conductivity of tissues. Adapted from [25].

Tissue	σ (S/m) 10kHz	σ (S/m) 1MHz	$\phi_{max} < 10$MHz	anisotropy
Human skin, dry	10^{-7}	10^{-4}	80^o	?
Human skin, wet	10^{-5}	10^{-4}	30^o	?
Bone	0.005-0.06		20^o	Strong
Fat	0.02-0.05	0.02-0.05	3^o	Small
Lung	0.05-0.4	0.1-0.6	15^o	Local
Brain (gray matter)	0.03-0.4	0.15	15^o	Small
Brain (white matter)	0.03-0.3			Strong
Liver	0.2	0.3	5^o	?
Muscle	0.05-0.4	0.6	30^o	Strong
Whole blood	0.7	0.7	20^o	Flow dependent
Urine	0.5-2.6	0.5-2.6	0^o	0
CSF	1.6	1.6	0^o	0
Saline 0.9%,20^{o}C	1.3	1.3	0^o	0
Saline 0.9%,37^{o}C	2	2	0^o	0
Seawater	5	5	0^o	0

The β dispersion is sample dependent, and it is the intermediate relaxation band between few kilo Hertz to few tens of mega Hertz frequencies. The β dispersion is due to the interface polarization of cell membranes suspended in the extracellular fluid [147].

The γ dispersion band is the high-frequency band starting from a hundred mega Hertz frequency, and it is caused by the permanent dipole relaxation of small biological molecules or water molecules in the tissues [28].

There are different electrical models proposed to approximate tissues, but one of the well-known models is Fricke's model, which is widely used to model micro-organisms in a liquid environment [27]. Although Fricke's model is highly elementary, it simulates biological tissue components such as cells, their intracellular fluids and membranes, and the extracellular fluid surrounding [28].

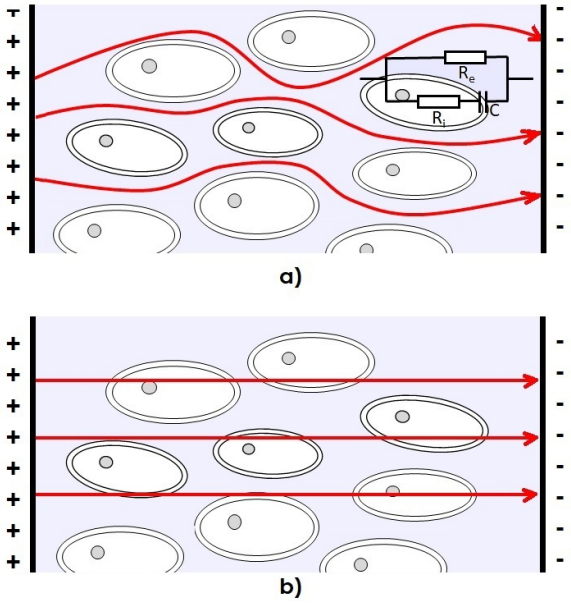

Figure 5.3 Fricke's impedance model for a biological tissues. Adapted from [27]. At low frequency currency passes through extracellular fluid, b) at high frequency currency passes though both intracellular and extracellular fluid.

In Fricke's model, the frequency f dependent tissue impedance Z is modeled as a parallel combination of R_e representing the extracellular fluid resistance with the serial combination of R_i representing the intracellular fluid resistance in series with the C representing the cell membrane capacitance as in Figure 5.3, and the equivalent impedance for the model is as:

$$Z^* = \frac{R_e.(R_i + \frac{1}{j2\pi fC})}{R_e + (R_i + \frac{1}{j2\pi fC})} \tag{5.6}$$

When the signal frequency approaches *zero*, the model capacitor C in the model is open-circuited, and the equivalent impedance is $R_0 = R_e$. When the frequency is very large, the model capacitor is short-circuited, and the equivalent impedance R_∞ is the parallel combination of R_i and R_e.

$$\lim_{f \to 0} Z^* = R_0 = R_e + j0 \tag{5.7}$$

$$\lim_{f \to \infty} Z^* = R_\infty = \frac{R_i R_e}{R_i + R_e} + j0 \tag{5.8}$$

The *specific impedance* Z of the tissue is a complex impedance and is usually represented as z^*.

z^* is the *specific impedance* of a unit volume in $(ohm.cm)$, and it is calculated by normalizing the measured impedance $Z_m^* = Z^*$ by the anthropometric dimensions of the object. For a cylindrical object, z^* is defined as

$$z^* = \frac{Z_m^* A}{L} \tag{5.9}$$

where A is the cross-sectional area, and L is the length of the cylinder.

If the object is a truncated cone, the specific impedance z^* of the tissue is

$$z^* = \frac{Z_m^* 2\pi ab}{L} \tag{5.10}$$

where the radius of the truncated cone at both ends are a and b, and length is L.

Each dispersion band can be fitted into a separate depressed Cole-Cole plots [148]. Depression of the plot is due to distribution in the dispersion of the cell membrane capacitive behavior; it is represented by a dimensionless α constant between 0 and 1 [28, 29].

Argand plane is a plot where coordinates are for real and imaginary components of an impedance, in which the complex impedance is plotted for changing frequencies (Figure 5.4). The projection of the impedance onto the Argand plane can be used to find Cole-Cole parameters used for tissue characterization [149].

The frequency at which the Cole-Cole plot has the maximum absolute imaginary component is called the *characteristic frequency*, and it is represented with f_c (Figure 5.5). The Cole-Cole plot intersects the apses at R_0 and R_∞; Z_{CPE} is the constant phase element, the lumped capacitance of the tissue [30]. Introducing the Constant Phase Element (CPE) instead of a single capacitance is the outcome of the observations of depressed loci in the complex plane, and impedance Z_{CPE} helps to model the cell

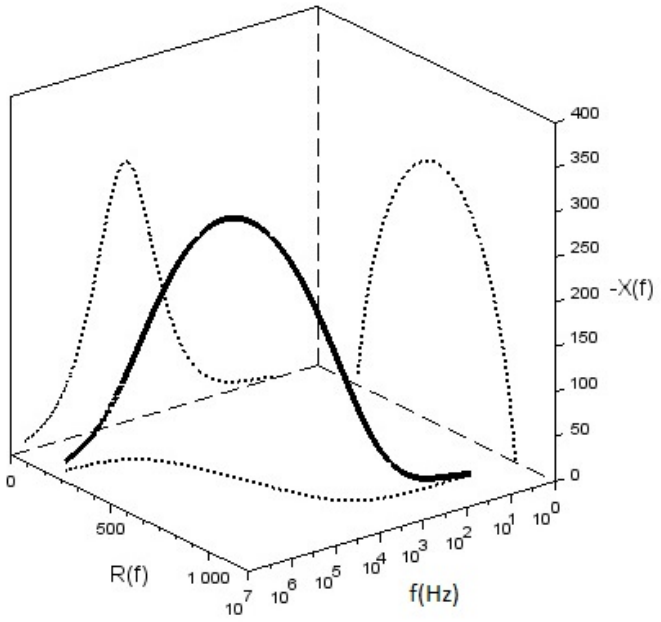

Figure 5.4 The projections of the complex impedance on Argand plane and its impedance spectroscopy plots.

suspensions and tissue better [150, 151].

$$Z_{CPE} = \frac{1}{(jwC)^{\alpha}} = (jwC)^{-\alpha} \tag{5.11}$$

$$Z^* = \frac{(R_i + Z_{CPE})R_e}{(R_i + Z_{CPE}) + R_e} \tag{5.12}$$

$$Z^* = \frac{R_i R_e + Z_{CPE} R_e}{(R_i + Z_{CPE}) + R_e} \tag{5.13}$$

By dividing the nominator and denominator of the equation with $R_i + R_e$,

$$Z^* = \frac{\frac{R_i R_e}{R_i + R_e} + \frac{Z_{CPE} R_e}{R_i + R_e}}{1 + \frac{Z_{CPE}}{R_i + R_e}} \tag{5.14}$$

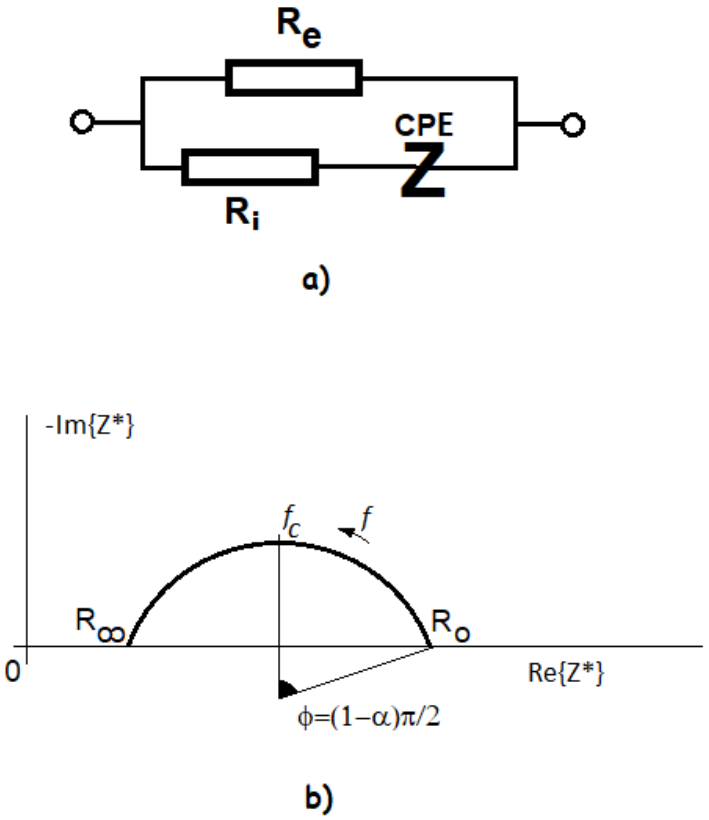

Figure 5.5 For biological tissues a) electrical circuit model is the parallel combination of extracellular fluid resistance to the serial combination if intracellular fluid resistance and the cell membrane capacitance, and b) the Cole-Cole plot of the model is a depressed circle.

and substituting $R_i R_e/(R_i + R_e)$ by R_∞, R_e by R_0, and $Z_{CPE}/(R_i + R_e)$ by a,

$$Z^* = \frac{R_\infty + aR_0}{1 + a} \tag{5.15}$$

and by adding and subtracting aR_∞,

$$Z^* = \frac{R_\infty + aR_\infty - aR_\infty + aR_0}{1 + a} \tag{5.16}$$

$$Z^* = \frac{R_\infty(1 + a)}{1 + a} + \frac{a(R_0 - R_\infty)}{1 + a} \tag{5.17}$$

After simplifications,

$$Z^* = R_\infty + \frac{R_0 - R_\infty}{1 + \frac{1}{a}} \tag{5.18}$$

Substituting a again with $(jwC)^{-\alpha}/(R_i + R_e)$,

$$Z^* = R_\infty + \frac{R_0 - R_\infty}{1 + \frac{1}{(R_i+R_e)(jwC)^\alpha}} \tag{5.19}$$

$$Z^* = R_\infty + \frac{R_0 - R_\infty}{1 + (jwC(R_i + R_e)^{1/\alpha})^\alpha} \tag{5.20}$$

and replacing $C(R_i + R_e)^{1/\alpha}$ with τ, Z^* can be simplified as

$$Z^* = R_\infty + \frac{R_0 - R_\infty}{1 + (jw\tau)^\alpha} \tag{5.21}$$

Characteristic frequency w_c of a tissue is $1/\tau$ and $w_c = 2\pi f_c$. For tissue characterization (R_0, R_∞, α , and f_c or τ) are used.

$$w_c\tau = 1 \tag{5.22}$$

$$\tau = [(R_i + R_e)^{1/\alpha}C] \tag{5.23}$$

$$Z(w)^* = R_\infty + \frac{(R_0 - R_\infty)}{1 + (jw\tau)^\alpha} \tag{5.24}$$

$$w = 2\pi f_c \tag{5.25}$$

Normalization of measured impedance Z_m by the anthropometric dimensions is a scaling and it changes where the Cole-Cole plot intersects the real impedance axis. Therefore normalization changes R_0 and R_∞, but it does not change the f_c , τ or the depression constant α.

5.1 Calculation of Cole-cole model parameters

The result of the Cole equation has a complex value

$$Z(w) = R_\infty + \frac{(R_0 - R_\infty)}{1 + (jw\tau)^\alpha} \tag{5.26}$$

where w is the frequency, $Z(w)$ is the frequency dependent impedance, R_0 is the intersection resistance of the the plot at frequency $w = 0$, R_∞ is the intersection resistance of the the plot at frequency $w = \infty$, τ is the characteristic time period and it is the inverse of the characteristic frequency w_c, α is the dimensionless factor and j is the imaginary unit. Similarly,

$$Z(w) = R(w) + jX(w) \tag{5.27}$$

where $R(w)$ and $X(w)$ are the frequency dependent resistance and reactance respectively. By replacing j^α with

$$j^\alpha = cos(\alpha\pi/2) + jsin(\alpha\pi/2) \tag{5.28}$$

and multiplying nominator and denominator by $1 + (jw\tau)^\alpha$,

$$R(w) = R_\infty + \frac{(R_0 - R_\infty)(1 + (w\tau)^\alpha cos(\alpha\pi/2))}{1 + 2(w\tau)^\alpha cos(\alpha\pi/2) + (w\tau)^{2\alpha}} \tag{5.29}$$

$$X(w) = -j\frac{(R_0 - R_\infty)(w\tau)^\alpha sin(\alpha\pi/2)}{1 + 2(w\tau)^\alpha cos(\alpha\pi/2) + (w\tau)^{2\alpha}} \tag{5.30}$$

The paramaters can be calculated by later by using the non-linear regression methods [152, 153].

The best fit curve can also be calculated using linear regression methods [154, 153]. The parameters can be estimated by curve fitting a circle to the measured points, and the best curve is found by minimizing the distances of each data point to the circle using the least square errors method [155, 154].

For the best fit circle to N points shown in Figure 5.6, the mean square radius

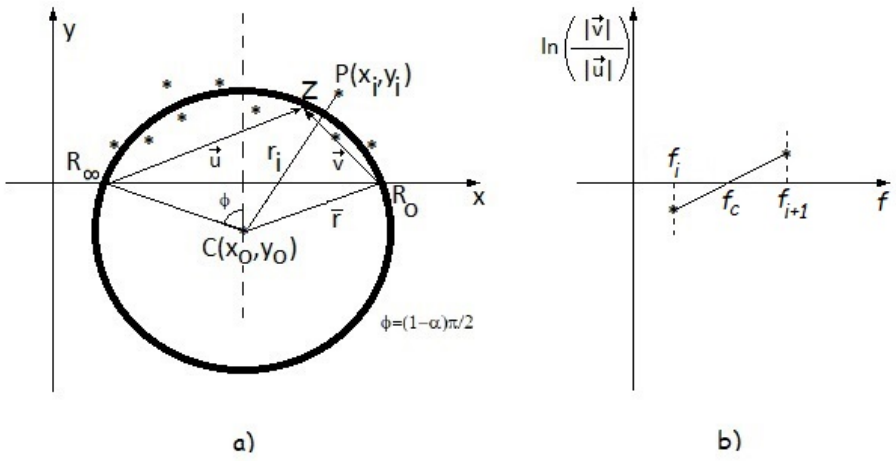

Figure 5.6 Calculation of Cole-cole parameters a) the center and the radius of best fit circle b) and $ln(\vec{u}/\vec{v})$ versus the frequency f is used for calculating the characteristic frequency. Adapted from [29].

is

$$\bar{r}^2 = \frac{1}{N}\sum_{i=1}^{N}(r_i)^2 \tag{5.31}$$

where r_i is the distance of point P_i to the center of the circle C. Using simple trigonometry,

$$\bar{r}^2 = \frac{1}{N}\sum_{i=1}^{N}((x_i - x_0)^2 + (y_i - y_0)^2) \tag{5.32}$$

$$\bar{r}^2 = \frac{1}{N}\sum_{i=1}^{N}(x_i^2 + x_0^2 - 2x_i x_0 + y_i^2 + y_0^2 - 2y_i y_0) \tag{5.33}$$

$$\bar{r}^2 = x_0^2 + y_0^2 + \frac{1}{N}\sum_{i=1}^{N}(x_i^2 - 2x_i x_0 + y_i^2 - 2y_i y_0) \tag{5.34}$$

The mean square error MSE is

$$MSE = \frac{1}{N}\sum_{i=1}^{N}(r_i^2 - \bar{r}^2)^2 \tag{5.35}$$

For best fit, the partial derivatives of MSE with respect to x and y should be zero:

$$\frac{\partial MSE}{\partial x} = \frac{4}{N}\sum_{i=1}^{N}((r_i^2 - \bar{r}^2)(-x_i + \frac{1}{N}\sum_{k=1}^{N}x_k)) = 0 \tag{5.36}$$

$$\frac{\partial MSE}{\partial y} = \frac{4}{N}\sum_{i=1}^{N}((r_i^2 - \bar{r}^2)(-y_i + \frac{1}{N}\sum_{k=1}^{N} y_k)) = 0 \tag{5.37}$$

By substituting

$$\begin{aligned} A_i &= x_i - \frac{1}{N}\sum_{i=1}^{N} x_i \\ B_i &= y_i - \frac{1}{N}\sum_{i=1}^{N} y_i \\ C_i &= x_i^2 - \frac{1}{N}\sum_{i=1}^{N} x_i^2 \\ D_i &= y_i^2 - \frac{1}{N}\sum_{i=1}^{N} y_i^2 \end{aligned} \tag{5.38}$$

and by simplifying the equation set is

$$\begin{bmatrix} 2\sum_{i=1}^{N} A_i^2 & 2\sum_{i=1}^{N} A_i B_i \\ 2\sum_{i=1}^{N} A_i B_i & 2\sum_{i=1}^{N} B_i^2 \end{bmatrix} \begin{bmatrix} x \\ y \end{bmatrix} = \begin{bmatrix} \sum_{i=1}^{N}(C_i + D_i)A_i \\ \sum_{i=1}^{N}(C_i + D_i)B_i \end{bmatrix} \tag{5.39}$$

And solution set for x and y is as

$$\begin{bmatrix} x \\ y \end{bmatrix} = \begin{bmatrix} 2\sum_{i=1}^{N} A_i^2 & 2\sum_{i=1}^{N} A_i B_i \\ 2\sum_{i=1}^{N} A_i B_i & 2\sum_{i=1}^{N} B_i^2 \end{bmatrix}^{-1} \times \begin{bmatrix} \sum_{i=1}^{N}(C_i + D_i)A_i \\ \sum_{i=1}^{N}(C_i + D_i)B_i \end{bmatrix} \tag{5.40}$$

After finding the center of the circle $C(x_0, y_0)$, R_0 and R_∞ are the intersection points of the $y = 0$ and the circle and they can be found by solving the quadratic equation:

$$\bar{r}^2 = (x - x_0)^2 + (0 - y_0)^2 \tag{5.41}$$

The quadratic equation will have 2 solutions, R_0 will be the bigger one and the R_∞ is the smaller, and they are symmetric around the vertical line passing through the center point $C(x_0, y_0)$, i.e.,

$$R_0 + R_\infty = 2x_0 \tag{5.42}$$

The depression constant α is calculated using trigonometry and it is found as

$$\alpha\pi/2 = \arctan \frac{|y_0|}{|R_0 - (R_0 + R_\infty)/2|} \tag{5.43}$$

and

$$\alpha = \arctan \left(\frac{2y_0}{R_0 - R_\infty} \right) 2/\pi \tag{5.44}$$

and f_c can be calculated by inserting R_0 , R_∞ and α into Cole equation [155].

For any point Z on the circle in Figure 5.6, if the phasor connecting the R_∞ to this point on the circle is $\vec{u}$ and the vector connecting the R_0 to the same point is $\vec{v}$ then

$$\frac{|\vec{v}|}{|\vec{u}|} = \left(\frac{f}{f_c} \right)^{1-\alpha} \tag{5.45}$$

and $ln\left(\frac{|\vec{v}|}{|\vec{u}|}\right)$ versus the frequency f graph crosses the frequency axis at the characteristic frequency f_c [29].

For measurement point i, measured at impedance Z_i at the frequency f_i is

$$Z = Z_{re} + jZ_{im} \tag{5.46}$$

where Z_{re} and Z_{im} are the real and the imaginary components of the measured complex impedance, and

$$|\vec{u}| = \sqrt{Z_{im}^2 + (Z_{re} - R_\infty)^2} \tag{5.47}$$

and

$$|\vec{v}| = \sqrt{Z_{im}^2 + (R_0 - Z_{re})^2} \tag{5.48}$$

5.1.1 A Novel approach for calculating BIS Characteristic frequency using Nyquist plot

The measured complex impedance $Z^*(f)$ at a frequency f has both real $R(f)$ and imaginary $X(f)$ components and expressed as:

$$Z^*(f) = R(f) + jX(f) \tag{5.49}$$

The frequency at which X versus the $ln(f)$ plot is maximized, is the characteristic frequency f_c.

$$\frac{\partial X}{\partial ln(f_c)} = 0 \tag{5.50}$$

When $-X$ versus $ln(f)$ is plot, the slope at the tangent at the maximum point ,i.e., at the characteristic frequency f_c is zero. Renaming X as y, and $ln(f_c)$ as x, the plot can be modeled as a second order polynomial around the characteristic frequency, and characteristic frequency f_c can be calculated using the following formula set:

$$\begin{aligned} y &= X \\ x &= ln(f_c) \\ y &= ax^2 + bx + c \\ \partial y/\partial x &= 0 = 2ax + b \\ x &= -b/2a \\ f_c &= e^{-b/2a} \end{aligned} \tag{5.51}$$

For a quadratic regression only 3 measurements near the characteristic frequency is enough (Figure 5.7). When S is the signum function which returns "1" if positive and "0" if negative, the selector function is defined as follows:

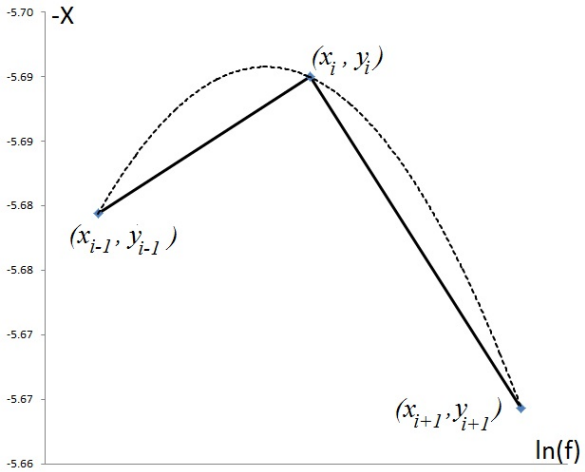

Figure 5.7 Selection function allows to select the closest 3 points to the characteristic frequency.

$$\begin{aligned} &\forall(x_i, y_i), S(y_i - y_{i-1}) * S(y_i - y_{i-1}) = 1 \Longrightarrow \\ &\qquad \text{include}(x_{i-1}, y_{i-1}) \\ &\qquad \text{include}(x_i, y_i) \text{ and} \\ &\qquad \text{include}(x_{i+1}, y_{i+1}) \\ &\text{else} \Longrightarrow \text{exclude} \end{aligned} \tag{5.52}$$

With 3 unknown and 3 equation, calculation of the parameters a, b, c and f_c is straightforward:

$$\begin{bmatrix} x_1^2 & x_1 & 1 \\ x_2^2 & x_2 & 1 \\ x_3^2 & x_3 & 1 \end{bmatrix} \begin{bmatrix} a \\ b \\ c \end{bmatrix} = \begin{bmatrix} y_1 \\ y_2 \\ y_3 \end{bmatrix} \tag{5.53}$$

5.2 Selecting Measurement Frequencies for bioimpedance spectroscopy

The range of frequencies used in bioimpedance spectroscopy can be equidistant in linear frequency space, equidistant in logarithmic frequency space, or equidistant in the Nyquist plot. The selected frequency set affects the estimation quality of Cole-cole parameters differently [156]. Kun *et al.* have shown that for the best estimation of R_0, the measurement frequency set should include frequencies in the range of 100 Hz to 1 kHz, for a better estimation of R_∞, the measurement frequency set should not include frequencies below 1 kHz, and for characteristic frequency f_c and depression constant α estimation, the measurement frequency set should be equidistant in the Nyquist plot [156]. The coefficient of variations (CV), for different measurement frequency sets, are tabulated in Table 5.2.

Table 5.2
The coefficient of variation (CV) for *in vivo* parameter extraction, in the 1 kHz to 300 kHz frequency band. Adapted from [156].

Frequency set	CV			
	R_0	R_∞	α	f_c
linear set	0.31	0.46	0.47	0.77
logarithmic set	0.36	0.56	0.62	0.92
equidistant set	0.32	0.35	0.39	0.27

For patient safety, the amplitude of the current injected during the bioimpedance spectroscopy should be below the permitted limits at all frequencies (Figure 5.8). The current limits are defined by EN60601 standards [157]. These limits are far below the minimum current that can induce a hearth fibrillation [158].

5.3 Electrodes in measurement systems

In BIS, measurements can be performed using two electrodes, three electrodes or four electrodes. When four electrodes are used, the measurement setup is called a

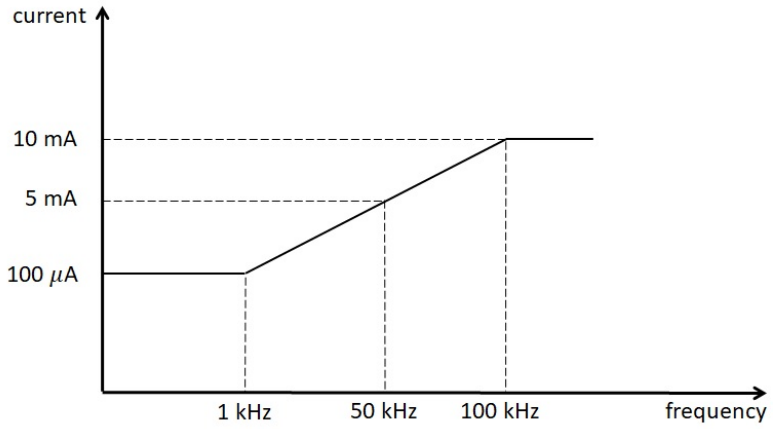

Figure 5.8 The EN60601 standards defines the safe limits for the electrical currents through the body. Adapted from [157].

tetrapolar measurement setup. WE: working electrode, CE: Counter electrode, and RE: Voltage reference electrode [24]. Figure 5.9 shows the 2, 3, and 4 electrode measurement

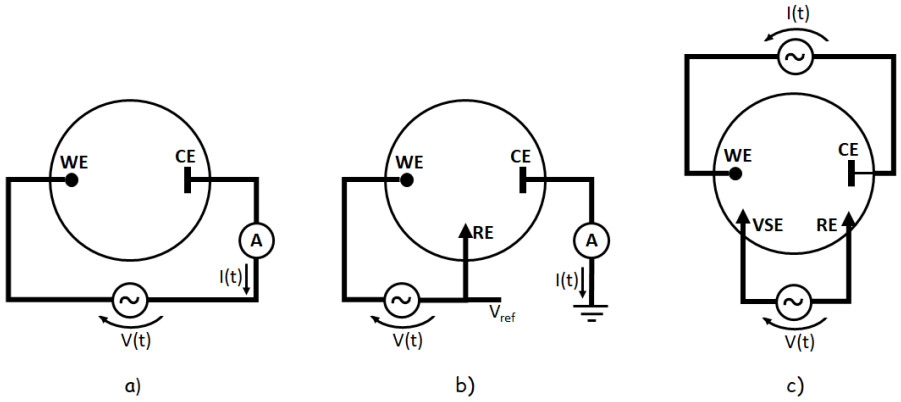

Figure 5.9 BIS Electrode configuration for (a) two electrodes, (b) three electrodes and (c) four electrodes. Adapted from [24].

systems. In the two electrode measurement system, the same WE and CE electrode pair is used to apply an alternating current and to sense voltage. The electrodes used in this setup are named the working electrode (WE) and the counter electrode (CE). Since applied current also passes through the voltage sense electrodes, the electrode polarization impedance of both electrodes contributes to the sensed voltage.

One of the popular measurement systems in electrochemical measurements is the three-electrode measurement system, where the 3rd electrode is introduced as a voltage reference electrode (RE). In this measurement setup, the voltage signal is ap-

plied between the WE and RE electrodes, and the current is measured from the CE electrode. Since no current will be flowing through the RE electrode, only the electrode polarization impedance of the WE electrode will contribute to the measured current.

In a tetrapolar measurement system, four electrodes are used. The current is applied between WE and CE electrodes, and the voltage sensed between the working sensing electrode (WSE) and the RE. Since the applied currency does not pass through the WSE or RE electrodes, their junction impedance also does not contribute to the sensed voltage [24]. Introducing more electrodes into the measurement system improves the measurement precision, but it also makes the measurement system more complex. Furthermore, electrochemical systems mostly behave semi-linear with the sensed voltage level, i.e., linear at low voltages and non-linear at higher voltages, therefore to operate in a relatively linear region, sensed voltages should be in the order of 10 to 100 mV [159]. Tetra polar measurement systems are considered to be immune to electrode polarization errors [160]. However, Sverre *et al* have shown that this is not always true: Sverre *et al.* named the possible source of errors as the *common-mode voltage* at the sense electrodes, the *negative sensitivity* of the voltage sensing electrodes, and possible surface shunt paths [161]. In a tetrapolar measurement setup, voltage sensing electrodes are placed between current signal electrodes, and voltage measured between the sensing electrodes are assumed to be due to tissue between voltage electrodes only. However, the tissue between current and voltage electrodes also contributes to the measured voltage, and this phenomenon is named the negative sensitivity. Surface shunt paths also occur when the skin is too damp, or the voltage electrodes are placed too close to the current electrodes [161].

5.4 Factors affecting body impedance measurement

Some researchers have shown that the subject's skin hydration level affects the impedance of skin [162]. Some other researchers have shown that by increasing the capacitance and the intracellular resistance of the skin cells, skin temperature also affects the skin impedance [163, 164]. Cornish *et al.* have shown that the ambient

temperature and hydration level of skin only affect the skin impedance and, as long as measured with the tetra-polar model, they do not statistically change body impedance measurement values [165].

The total intracellular (ICV) and extracellular fluid volumes (ECV) do not change by the body position [166]. Although segmental intracellular fluid volumes and total body impedance does not change with the body position; body position may change ECV regional distribution and may change impedance for body segments: therefore, during bioimpedance studies, it is suggested to keep the same posture for all subjects, i.e., all standing, all sitting, or all laid in the supine position [167].

5.5 Body compartment model

Assessment of body composition is very fundamental to many aspects of patient care and can be performed by bioelectrical impedance spectroscopy and bone densitometry. Among numerous factors effecting Bone Mineral Density (BMD), the body weight is known to have a positive correlation with (BMD), especially at hip, regardless the age group [168]. Some of the early studies also showed that fat is an independent predictor for (BMD). In 68 healthy premenopausal women, (BMD) was correlated with fat mass ($r = 0.60, P < 0.05$), and fat-free mass ($r = 0.55, P < 0.05$) [169, 170]. Being safe, inexpensive and portable, bioelectric impedance analysis is a very commonly used technique for body composition assessment including bone minerals. Biggs *et al.* has studied the body in 5 segments as forearm, upper arm, trunk, upper leg and calf; and shown that arm and leg segmental bioelectrical impedance measurements yield better results in whole body fat estimation [171, 172, 173]. The segmental resistance measured at 50 kHz were used for compartmental analysis and compared his calculations with the body fat percentage calculated by underwater weighing [174].

Since arm impedance can be used to determine body fat quotient which is an important determinant of body weight and body mass index, and body weight has a correlation with bone mineral density, it is worth to investigate the correlation of

segmental bioimpedance measurement results with reference bone mineral density to see if bioimpedance measurements can be used in predicting bone mineral deficiency.

The three compartment model of body composition consists of fat mass (FM), fat-free mass (FFM), and non-conducting tissues (NCT). The non-conducting tissues in the arms and legs are mostly bones, and regardless of their measurement axis, the specific capacitance of both trabecular and cortical bones have statistically significant correlation to their mineral densities. The same correlation exists at wet, dry or ash forms [26]. WB Thomas *et al* has shown that bone impedance measured in vivo has a high correlation with bone density and bone can be modeled as a resistance in series with constant phase element [175]. The (FFM) can be further divided into extracellular water (ECW) and a functional cellular compartment: predominantly composed of muscle, the body cell mass. By measuring the (ECW), the muscle can be assessed. The electrical equivalent circuit for the body segment can be represented in terms of Cole model: lumped extracellular fluid resistance R_e, in parallel with the serial combination of total intracellular fluid resistance of the tissues composing the body segment R_i and the lumped membrane capacitances of all tissues including bones C.

Total mass for the arm segment consists of fat, muscle and non-conducting tissue masses. In the compartmental model, when A represent the area of a tissue, the non-conducting tissue area A_{NCT} is proportional to the square of the segment length:

$$A_{NCT} = k_2 L_{SEG}^2 \tag{5.54}$$

and

$$A_{TOTAL} = A_{FAT} + A_{MUSCLE} + A_{NCT} \tag{5.55}$$

formulates the total base area of the conducting material [173].

By using the specific impedance ρ, the area A and the length of the segment

L, the resistance of fat, muscle or the total segment impedance can be calculated from the general formula:

$$R = \rho \frac{L}{A} \tag{5.56}$$

From the arm measurement, the fat percentage of the total body (%FAT) can be estimated as:

$$\%FAT = \frac{100\delta_{FAT} QSEG}{\delta_{FAT} QSEG + \delta_{MUS}(1 - QSEG)} *$$

$$(1 - \frac{k_1 H^3}{M_{TOT}}) \tag{5.57}$$

by taking , k_1 = 3.9 (kg.m^{-3}), k_2 =0.0025, ρ_{MUS}=1.37 (Ωm), δ_{MUS}=1340 (kg.m^{-3}) and δ_{FAT}=900 (kg.m^{-3}) [173]. H (m) is the height and M_{TOT} (kg) is the weight of the subject. The fat quotient (QSEG) is calculated as:

$$QSEG = \frac{V_{FAT}}{V_{FAT} + V_{MUS}} \tag{5.58}$$

$$\frac{V_{FAT}}{V_{FAT} + V_{MUS}} = \frac{\rho_{FAT}}{\rho_{MUS} - \rho_{FAT}} (\frac{\rho_{MUS} L_{SEG}}{R_{SEG} A_{CON}} - 1) \tag{5.59}$$

where R_{SEG} is the R_{ARM} measured impedance at 50kHz. In the calculations, the arm is assumed to be closer to a truncated cone. If the upper and lower radii and circumferences of the truncated cone are r_a, r_b, $Circ_a$ and $Circ_b$ respectively, the radius and the area of the equivalent perfect cylinder can be calculated using following formula set:

$$r_a = \frac{Circ_a}{2\pi}; r_b = \frac{Circ_b}{2\pi} \tag{5.60}$$

$$r_{eq} = \sqrt{\frac{{r_a}^2 + r_a r_b + {r_b}^2}{3}} \tag{5.61}$$

$$A_{eq} = \pi {r_{eq}}^2 \tag{5.62}$$

In the Cole model, the magnitude of the imaginary component of the arm complex impedance of body segment is maximized at the arm characteristic frequency and it is defined as:

$$Fc = \frac{1}{2\pi C(R_i + R_e)^{1/\alpha}} \tag{5.63}$$

where C is the equivalent capacitance, R_e is the extracellular fluid resistance, R_i is the intracellular fluid resistance and α defines the depressed angle of the best fit circle obtained when real component of the complex impedance is plotted against the imaginary component at varying frequencies. Calculated f_c is independent of the arm dimensions. Impedance at 50 kHz is a function of characteristics frequency which is also a function of the Cole model equivalent capacitance. Davidovic *et al* has shown that mineral content calculated using whole body impedance parameters has a correlation with the bone mineral density when hip is the area of interest [176].

In this study, arm bioimpedance measurement is used to calculate arm (QSEG) and whole body (%FAT) estimate, and their correlation with the subject's bone mineral density is analyzed. Using ANOVA tests, (QSEG) and (%FAT) are tested to see if they are different for normal and lowered bone mineral density population.

5.6 Effect of lean body mass

With foot-to-foot bioimpedance measurements, Heidi H. Y. Ngai *et al.* have shown that bioimpedance is correlated to BMD, with a higher correlation in men [177]. In his study, the gender difference is explained by the fact that women have less lean muscle mass and lower electrolyte content, making women potentially more susceptible to the factors that can induce errors in BI measurements [177, 178, 179]. Fat mass is also considered to be an important determinant of bone mass [180]. Any incremental weight gain is reflected arms only as 102±10 g, with 288±14g to legs and 466±14g to trunk [181]. The average density of the fat, fat-free body, soft tissue, and bone is 0.901 g.cm-3, 1.100 g.cm^{-3}, 1.066 g.cm^{-3} and 1.43 g.cm^{-3} [182, 183]. The average density of

protein and mineral are 1.34 g.cm^{-3} and 3.04 g.cm^{-3} [184, 174, 183]. Average density for arms, a trunk without shoulders and legs is 1.080 g.cm^{-3}, 1.009 g.cm^{-3}, and 1.052 g.cm^{-3} respectively [185]. With compartmental body composition analysis, the average fat mass of a healthy person is 20.0±10.8 kg for subjects of weight 76.7±12.7 kg, which resembles 29.8% of volume as fat [186]. With an average density of 1.041 g.cm^{-3}, and with the assumption of soft tissue and water volume are equal at a body segment, using Eq. 5.64 to 5.69, 15.2% of the total volume of the arm is estimated to be bone tissue while this ratio is reduced to 12.8% for leg and 9.2% for trunk respectively. In Equations 5.64 to 5.69, d refers to density, s segment, V volume, FFB fat-free body, w water, m soft tissue, f fat, and b bone.

Bioimpedance measurements are taken from all extremities of subjects to incorporate the effect of bone mass into measurements. The right arm is the dominant arm for a right-handed person. Correlation between the dominant arm Cole-Cole model parameters and DEXA reference results is expected to be higher compared to other extremities.

$$V_s = V_f + V_{FFB} \tag{5.64}$$

and

$$d_s.V_s = d_f.V_f + d_{FFB}.V_{FFB} \tag{5.65}$$

Rearranging formula, fat free body volume V_{FFB} is

$$V_{FFB} = \frac{d_s - d_f}{d_{FFB} - d_f} \tag{5.66}$$

Since

$$V_{FFB} = V_m + V_b + V_w \tag{5.67}$$

the density of fat free body is

$$d_{FFB} = \frac{d_m.V_m + d_b.V_b + 1.V_w}{V_{FFB}} \tag{5.68}$$

Finally, when volume for water is assumed to be same as soft tissue, the bone volume is estimated as

$$V_b|_{V_m=V_w} = \frac{2d_s - d_m - d_w + V_{FFB}(d_m + d_w - 2d_f)}{2d_b - d_m - d_f} \tag{5.69}$$

6. STATISTICS

All statistical analysis are performed by using MedCalc v18.2.1 application by MedCalc Software, Belgium [187]. For all statistical analysis, a significance criterion P equal to or smaller than 0.05 is used to determine the statistical significance.

6.1 F-test

The variance ratio test, which is also known as the F-test, is used for assessing two groups to find if they are statistically different from each other by looking into their variance ratios [188].

For sample groups of 1 and 2, with the sample size of n_1 and n_2, and the average of $\bar{x}_1$ and $\bar{x}_2$, respectively, the variance ratio F is calculated as

$$F = \frac{\sigma_1^2}{\sigma_2^2} \tag{6.1}$$

where

$$\sigma_1^2 = \frac{\sum(x_1 - \bar{x}_1)^2}{n_1 - 1} \tag{6.2}$$

and

$$\sigma_2^2 = \frac{\sum(x_2 - \bar{x}_2)^2}{n_2 - 1} \tag{6.3}$$

The null hypothesis H_0 is, the populations are equal. For 95% statistical confidence, the $F_{0.05} = 3.18$. And if $F > 3.18$, then the null hypothesis fails, i.e., the sample groups are statistically different [189].

6.2 Receiver operating characteristic (ROC) curve

In healthcare, sensitivity and specificity are the primary measures to quantify the quality of a diagnostic system. *Sensitivity* (Se) is the ability to diagnose the disease when disease exists, and *Specificity* (Sp) is the ability to diagnose normal when disease does not exist [190]. Sensitivity and specificity are also called *Positive Predictive Value* (PPV) and *Negative Predictive Value* (NPV) [191].

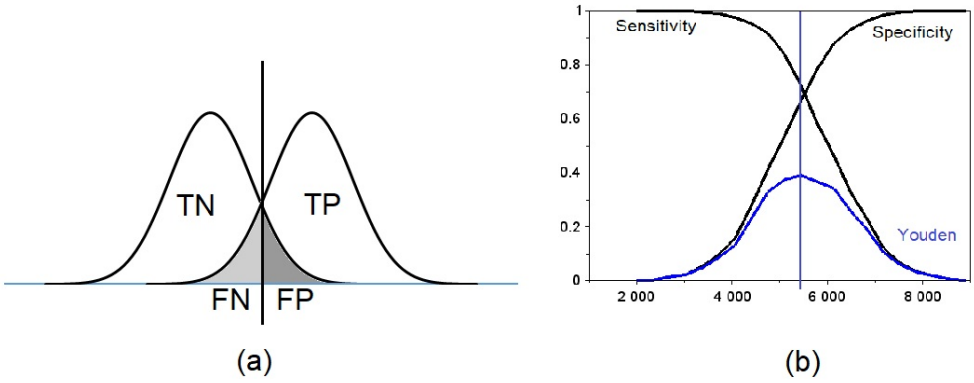

Figure 6.1 In ROC analysis, a) the sum of False Negative (FN) and False Positive (FP) predictions were minimized by selecting the optimal cutoff point and b) Youden index is a popular method for this selection.

If true positive is TR, true negative is TN, false positive is FP and false negative is FN then

$$PPV = Sensitivity = \frac{TP}{TP + FN} \tag{6.4}$$

and

$$NPV = Specificity = \frac{TN}{TN + FP} \tag{6.5}$$

and *False Positive Rate* (FPR) is

$$FPR = \frac{FP}{TN + FP} = 1 - Specificity \tag{6.6}$$

Correct Classification Rate (CCR) is

$$CCR = \frac{TN + TP}{TN + TP + FN + FP} \tag{6.7}$$

and since *Mis-Classification Rate* (MCR) and CCR always adds up to 1,

$$MCR = 1 - CCR. \tag{6.8}$$

For a binary, i.e., two-way classifier, the *Receiver Operating Characteristic* (ROC) curve can be constructed by plotting the PPV versus FPR values by selecting the different cutoff points as the diagnostic threshold [190]. In other words, the ROC curve will be similar to Figure 6.2, and it is the plot of sensitivity versus the 1-specificity. The better the classifier is, the larger the *Area Under the Curve* (AUC). For a perfect classifier, AUC is 1.0, and for a blind guess classifier, AUC is 0.5. As shown in Figure 6.1, the Youden index (J) is the summary measure of the ROC curve, and it serves to select of the optimal threshold value (the cutoff point) of the marker [192].

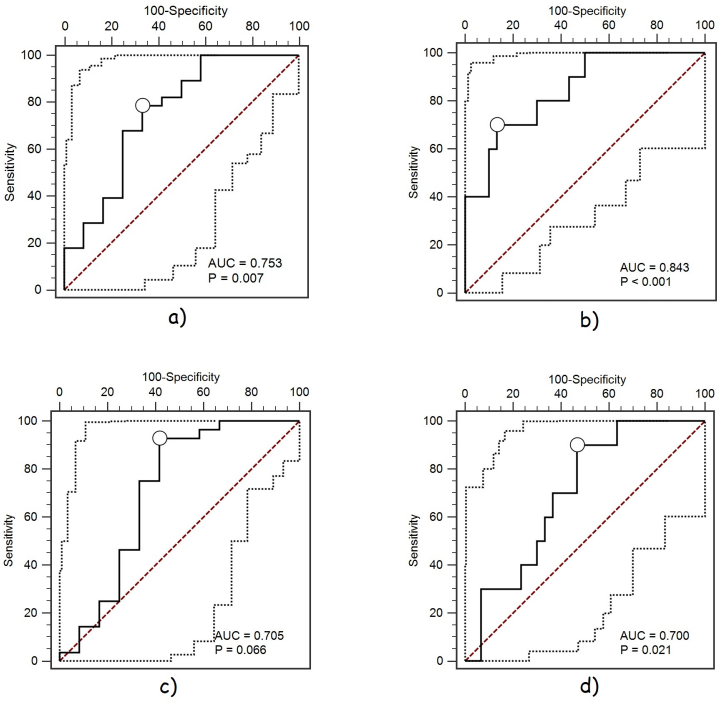

Figure 6.2 The receiver operating characteristic curve is the plot of Sensitivity versus the 1-Specificity for different cutoff threshold points. The diagonal line is the blind guess line, and the area under the curve is 0.5. For a perfect two-way classifier, the area under the curve is 1. Youden Index (J) is the summary measure of the ROC, and it enables the selection of the optimal threshold value (the cutoff point) for the marker.

6.3 Pearson correlation coefficient strength categorization

Pearson correlation coefficient (r) is the measure of the linear correlations of two variables. It is calculated as the covariance of two variables divided by the standard deviations of the variables, and it is calculated as

$$r = \frac{\sum_i (x_i - \bar{x})(y_i - \bar{y})}{\sqrt{\sum_i (x_i - \bar{x})^2} \sqrt{\sum_i (y_i - \bar{y})^2}} \tag{6.9}$$

where r is the Pearson correlation coefficient, x_i and y_i are the paired sample points and $\bar{x}$ and $\bar{y}$ are the means of the individual sample sets [193]. For correlation coefficient strength categorization, Dancey and Reidy's categorization is used, where 0.1 to 0.3 is weak, 0.4 to 0.6 is moderate, 0.7 to 0.9 strong, and 1 is a perfect correlation [193].

7. A NOVEL APPROACH: 2D RECEIVER OPERATING CHARACTERISTIC SURFACE FOR PAIRED TESTS

When there is a single test, the receiver operating characteristic curve is a two-way classifier, and it is useful for binary classification. The area under the curve (AUC) measures the classifier's success, and the decision boundary to maximize the area is determined by the Youden index [190]. In literature, some researchers tried to combine the results of multiple independent tests to form a multidimensional receiver operating characteristics surface (ROS) for grouping patients into linearly ordered multiple groups. With two independent tests, the multidimensional receiver operating characteristics surface reduces to a three-way classifier to classify patients into three different orderly patient groups [194]. In analogy to ROC, the volume under to ROS surface is used for classification [195]. However, this approach does not answer how paired test results can be combined to have a two-way classifier [196]. With a single test, the selection of cutoff point will change the *False Negative* (FN) or *False Positive* (FP) rates, and as in Figure 6.1; When the sensitivity and specificity are plotted, their intersection will be a single point. However, when there are paired tests, the sensitivity and specificity plots will be a surface, their intersection will be a curve, and the projection of the curve in 2 dimension will form the decision surface (Figure 7.1).

The sensitivity (Se) of the classifier is ratio of correctly identified positives (TP) to the total positives:

$$Se = \frac{TP}{TP + FN} \tag{7.1}$$

where TP is true positives and FN is false negatives.

The specificity (Sp) of the classifier is the ratio of correctly identified negatives to total negatives:

$$Sp = \frac{TN}{TN + FP} \tag{7.2}$$

where TN is true negatives and FP is false positives.

Correct Classification Rate (CCR) is the the ratio of correctly classifieds to total:

$$CCR = \frac{TP + TN}{TP + FN + TN + FP}. \tag{7.3}$$

Since mis-classification rate (MCR) and correct classification rate (CCR) adds up to 1,

$$MCR = 1 - CCR = \frac{FN + FP}{TP + FN + TN + FP}. \tag{7.4}$$

To create the optimal threshold, first, data is distributed into predefined number of bins (N:0,1,2,..N-1) by looking at their values compared to all data values. For the i^{th} data point with the value of x_i, the bin number n_i is found as

$$n_i = int\left(N\frac{x_i - x_{min}}{x_{max} - x_{min} + \epsilon}\right) \tag{7.5}$$

where x_{min} is the minimum value in the data set, x_{max} is the maximum value in the data set, int is the integer function and ϵ is a negligibly small number to ensure the maximum data point x_{max} is not left out of the calculations.

In ROC curve analysis, iterating through each bin with the assumption of that bin is the optimal cutoff bin, the FN and FP are calculated to find the MCR for the selection. The bin with the minimum MCR is selected as the optimal cutoff point. Youden index is one of the popular selection method in which (Se+Sp-1) is used for cutoff boundary selection [197]. For one test the boundary is a point, for two tests it is a curve, and for M tests it has M-1 dimensions [196].

To create a paired simulation data set for hypothetical tests A and B, i.e., $P(A, B)$, for test A, 500 random data points with standard normal distribution are generated to represent the healthy (H) and 500 random data points to represent dis-

eased (D) population. Relative to the mean of healthy population data μ_H, the mean of diseased data μ_D is offset to simulate different overlap rates of healthy and diseased population, ranging from 5% to 60% (Figure 7.2).

The data is later normalized to fall into a predefined number of bins ranging from 1 to N, where the minimum data falls into the first bin, and the largest data falls into the bin N. Using Eq. 7.5, the bin number n_i for the data point i with the value of x_i is calculated.

The same process is repeated for creating the pairing reference data set (R), and its data points are created in a way that, when paired with the data set A, the correlation is zero both for healthy and diseased sets.

To investigate the effect of correlation strength between the tests, a data set for B is created as

$$B_i = R_i + a.A_i \tag{7.6}$$

where i represent the index of the data pair, and a is the blending factor to adjust the correlation between the tests A and B. Keeping test data A unchanged and by changing the blending factor, separate B data sets with the correlation strength of 0.2, 0.4, 0.6 and 0.8 with the data set A are calculated. Later data bin number for B_i is calculated using the same equation given Eq. 7.5. Also, to analyze the kurtosis effect, both for A and B, leptokurtic data is prepared ($\kappa = 2$, P$<$0.0001) and used for the diseased population. Having M bins for the test A and M bins for the test B, there are MxN possible threshold combinations of the bins to iterate for finding the true positive (TP), true negative (TN), false positive (FP), and false negative (FN) values. Assuming that the bin, $bin(m, n)$, is the optimal boundary point, all test pairs falling into other bins $bin(i : 0..M-1, j : 0..N-1)$ should be classified as Healthy or Diseased to find the CCR and MCR of the selected $bin(m, n)$. The decision function for the

paired test data in $bin(i,j)$ can be as simple as follows

$$\begin{aligned} AND\text{: } (i > m \wedge j > n) &\implies (+), else(-) \\ OR\text{: } (i > m \vee j > n) &\implies (+), else(-) \\ AVERAGE\text{: } (i + j \geq m + n) &\implies (+), else(-) \end{aligned} \tag{7.7}$$

, where AND means, for paired test point, both bin number of test A and test B are greater than the iterated cell index, OR means, the bin number of test A or test B is greater than the iterated cell index, and $AVERAGE$ means, the average of the bin numbers for the tests A and B is greater than the sum of indexes defining the selected bin.

Figure 7.3 shows the Youden plots for different paired test decision functions, and their projection to the NxM matrix show the classifier decision matrix.

As shown in Table 7.1 and Table 7.2, for the normal distributed simulation data, when the pairing function is AND individual test mis-classification rates are always better than the paired test. When the pairing function is OR and there is a weak correlation or less overlap, then the success is better than the individuals. Finally, the $AVERAGE$ function always performed better then the other pairing functions and the individual tests at every overlap and correlation strength conditions. When data is leptokurtic unless correlation is medium or more ($r > 0.4, P = 0.0001$) while diseased and healthy population data are overlapping more than 50% then the performance of the $AVERAGE$ function is less than the individual tests. Therefore, before applying the 2D-ROC classification, testing data normality is needed. If data is right skewed logarithmic transformation, if data is left skewed exponentiation may help to reduce skewness [198].

Metabolic syndrome (MeS) data collected by Babai *et al.* from 5533 individuals between the age of 20 to 65, during their Shiraz heart study [199] are used in 2D-ROC surface analysis. All pairwise 2D-ROC studies with the $AVERAGE$ function have improved correct classification rates compared to using the parameters alone [196].

The study results are tabulated in Table 7.3.

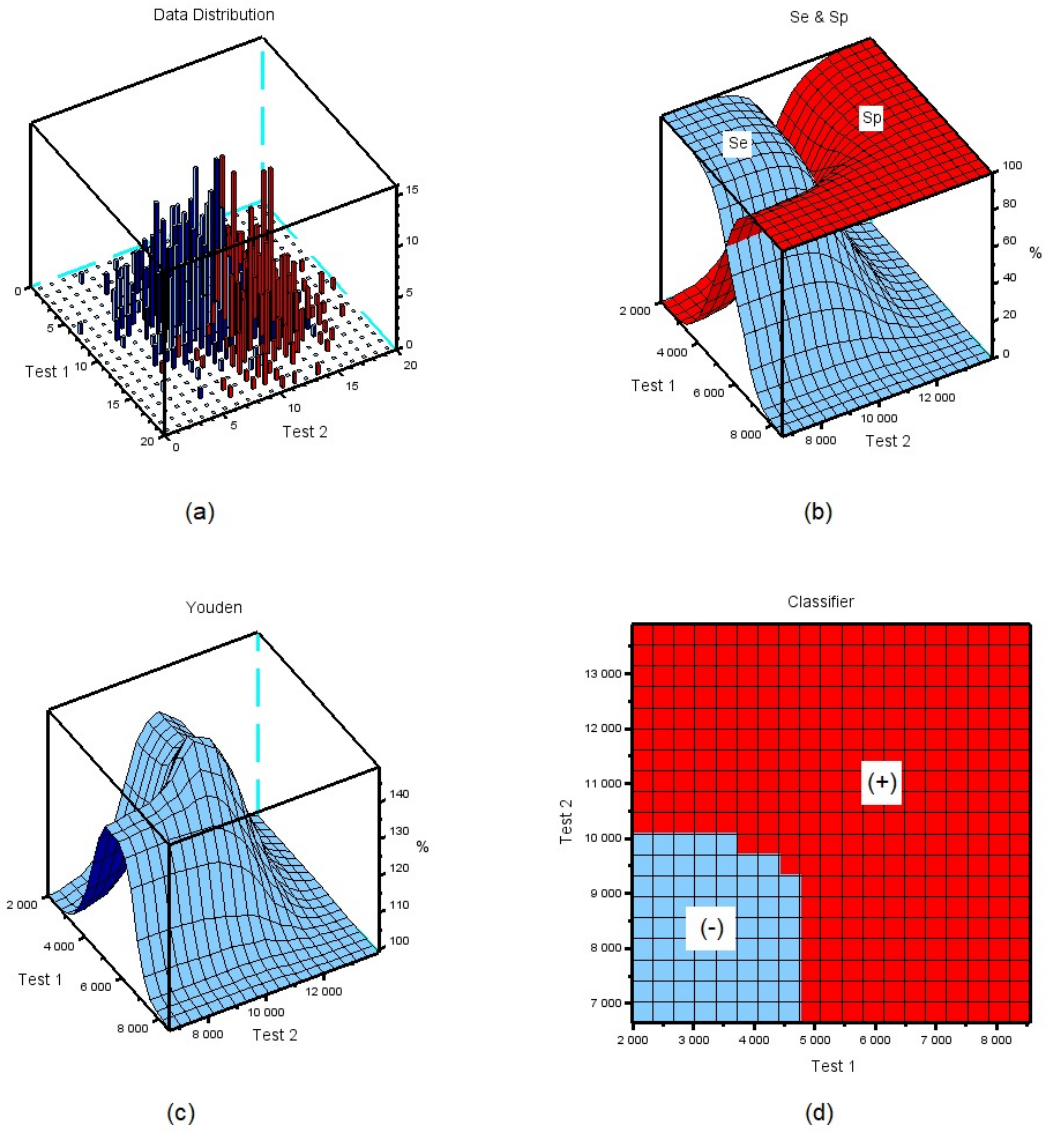

Figure 7.1 For a paired test simulation a) distribution of simulated data b) Specificity (Sp) and Sensitivity (Se) surfaces c) will intersect as a curve and d) the projection of the curve in 2 dimension will form the decision surface.

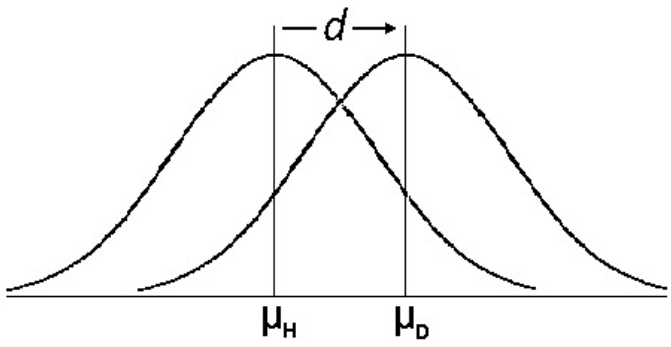

Figure 7.2 The mean of diseased data is offset by different d values to simulate different overlap ratio for healthy and diseased population.

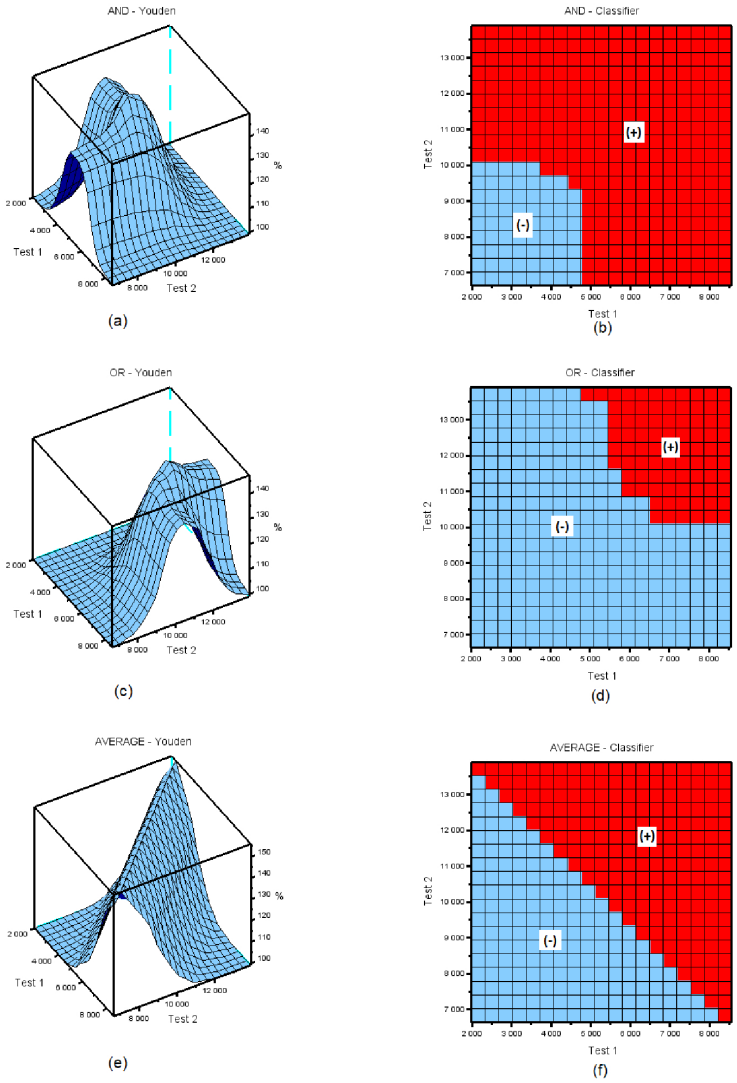

Figure 7.3 With different combination of the decision criteria of the paired tests, the Youden curve and the decision matrix changes: a) is the Youden plot for the AND function, b) is the classifier decision matrix for the AND function, c) is the Youden plot for the OR function, d) is the classifier decision matrix for the OR function, e) is the Youden plot for the $AVERAGE$ function and f) is the classifier decision matrix for the $AVERAGE$ function.

Table 7.1
For the normal distribution data, mis-classification rates of the simulation data for different correlation strengths between the paired tests, and for different overlap ratios of the healthy and diseased population.

Correlation[1]	Combination	Overlap[2]				
$(r, P < 0.0001)$	Function	5%	15%	30%	45%	60%
0.0						
	Test 1 only	15.0%	22.3%	29.9%	34.5%	39.6%
	Test 2 only	16.2%	22.6%	29.7%	34.1%	38.1%
	AND	29.7%	34.5%	39.2%	41.2%	44.7%
	OR	13.8%	21.6%	28.6%	33.0%	38.8%
	AVERAGE	8.5%	16.6%	23.7%	28.9%	35.5%
0.2						
	Test 1 only	15.0%	22.3%	29.9%	34.5%	39.6%
	Test 2 only	16.3%	22.9%	29.4%	34.8%	38.9%
	AND	27.5%	32.7%	39.5%	40.2%	44.7%
	OR	14.8%	21.8%	28.9%	33.6%	38.1%
	AVERAGE	11.1%	18.5%	25.2%	30.7%	35.8%
0.4						
	Test 1 only	15.0%	22.3%	29.9%	34.5%	39.6%
	Test 2 only	16.0%	22.9%	31.0%	34.6%	39.6%
	AND	23.0%	32.5%	36.5%	41.2%	44.3%
	OR	14.3%	22.2%	29.8%	34.9%	40.6%
	AVERAGE	13.0%	19.8%	26.9%	32.2%	36.4%
0.6						
	Test 1 only	15.0%	22.3%	29.9%	34.5%	39.6%
	Test 2 only	16.9%	23.2%	30.0%	34.1%	38.5%
	AND	22.3%	30.1%	34.9%	38.7%	43.7%
	OR	15.6%	23.1%	29.9%	35.2%	40.0%
	AVERAGE	14.3%	21.8%	27.9%	34.0%	38.2%

[1] Pearson correlation coefficient.

[2] Healthy and diseased population overlap percentage.

Table 7.2
Mis-classification rates of simulation data for various correlation strengths between paired tests and for various overlap ratios of healthy and diseased population: When healthy population is normal and diseased population is leprokurtic ($\kappa = 2$, P<0.0001).

Correlation[1]	Combination	Overlap[2]				
$(r, P < 0.0001)$	Function	5%	15%	30%	45%	60%
0.0						
	Test 1 only	13.7%	20.5%	26.1%	31.1%	35.3%
	Test 2 only	13.3%	19.3%	26.0%	30.7%	34.8%
	BOTH	25.9%	31.2%	35.7%	39.2%	44.4%
	ANY	11.6%	18.1%	25.9%	30.1%	34.6%
	AVERAGE	8.0%	15.6%	22.6%	28.0%	33.5%
0.2						
	Test 1 only	13.7%	20.5%	26.1%	31.1%	35.3%
	Test 2 only	13.1%	20.2%	27.0%	32.4%	36.6%
	BOTH	23.3%	30.6%	35.1%	38.1%	41.7%
	ANY	13.3%	19.7%	26.7%	32.2%	35.6%
	AVERAGE	10.3%	16.8%	24.1%	30.1%	34.7%
0.4						
	Test 1 only	13.7%	20.5%	26.1%	31.1%	35.3%
	Test 2 only	14.3%	21.5%	27.6%	32.5%	37.7%
	BOTH	23.4%	29.3%	32.0%	38.1%	42.9%
	ANY	13.5%	20.5%	27.3%	32.9%	35.6%
	AVERAGE	11.8%	19.3%	24.8%	31.2%	35.5%
0.6						
	Test 1 only	13.7%	20.5%	26.1%	31.1%	35.3%
	Test 2 only	15.8%	22.6%	28.3%	33.2%	37.8%
	BOTH	19.9%	29.7%	33.9%	37.6%	41.4%
	ANY	13.9%	20.4%	27.9%	32.2%	36.0%
	AVERAGE	12.9%	20.0%	26.9%	31.7%	36.5%

[1] Pearson correlation coefficient.

[2] Overlap of healthy and diseased population data.

Table 7.3
Metabolic syndrome analysis using ROC and 2D-ROC.

Parameters	CCR†				
	BMI	WC	TG	HDL	FBS
ROC	66.2%	66.5%	67.3%	67.2%	69.6%
2D-ROC‡					
Body mass index (BMI)		68.1%	71.0%	68.2%	71.1%
Waist circumference (WC)	68.1%		72.1%	69.9%	72.6%
Triglyceride (TG)	71.0%	72.1%		67.1%	70.3%
High density lipoprotein cholesterol (HDL)	68.2%	69.9%	67.1%		67.9%
Abnormal fasting blood sugar (FBS)	71.1%	72.6%	70.3%	67.9%	

† CCR, Correct classification rate.

‡ 2D-ROC, Parameters are combined using $AVERAGE$ function.

8. NOVEL APPROACH: SINGLE FREQUENCY METHOD FOR BONE MINERAL DENSITY ASSESSMENT

For the Frick impedance model, where tissues are modeled as a serial combination of intracellular resistance (R_i) with the membrane capacitance (C) is parallel to the extracellular fluid resistance (R_e), the impedance is

$$Z^* = |R| + j|X| \tag{8.1}$$

where $|R|$ is the real and $|X|$ is the imaginary component of the impedance. When the impedance is shown in phasor format

$$Z^* = |Z| \angle \Phi \tag{8.2}$$

and

$$|Z| = \sqrt{R^2 + X^2} \tag{8.3}$$

and

$$\Phi = arctan(|X|/|R|) \tag{8.4}$$

where Φ is the phase angle of the measured impedance between the impedance vector and the real part of the impedance, and Φ is maximized at the BIS model characteristic frequency (Figure 8.1).

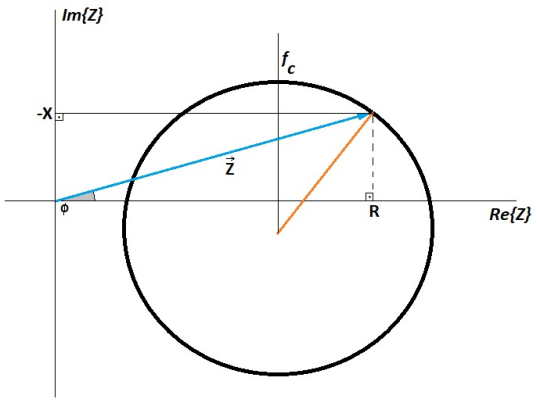

Figure 8.1 The phase angle Φ of the measured impedance vector is maximized at the characteristic frequency.

9. CLINICAL STUDY and MEASUREMENT RESULTS

Clinical studies are performed in 3 subsections:

- HP4284A Clinical BIS study, in which HP4284A Electrical impedance spectroscopy (BIS) measurements of both arms, legs, and trunk are performed and compared with the reference DEXA scans. The study is performed for women but some men also measured,
- Long-term medical treatment monitoring with HP428A BIS measurements,
- Impedimed SFB7 Clinical BIS study of the dominant arm of women to compare the BIS results with their DEXA scans.

9.1 Subjects in scope

Since type I (postmenopausal) osteoporosis develops rapidly after menopause and type II (senile) osteoporosis develops slowly, in this study, as the focus group, women subjects are selected among menopaused women with no arm or hip fracture history, no metabolic bone disease due to Paget's disease, osteomalacia, renal osteodystrophy or osteogenesis imperfecta. When a woman has no menstruation for at least 12 months, she is classified as postmenopausal [177].

9.2 Research ethics

The measurements are conducted in line with the Helsinki Declaration; before participating in this study, all subjects have signed an informed consent [200]. The names of the subjects are not exposed, and the faces of subjects are masked to ensure they are not identified.

The human research approval was obtained from the Boğaziçi University on March 03, 2016. The Application id is 2016/26, and the decision meeting id is 2016/03, as shown in Figure 9.1.

T.C.
BOĞAZİÇİ ÜNİVERSİTESİ
İnsan Araştırmaları Kurumsal Değerlendirme Kurulu (İNAREK) Toplantı Tutanağı

2016/03

14.03.2016

Fırat Matur
Boğaziçi Üniversitesi, Biyomedikal Mühendisliği Enstitüsü,
Rasathane Caddesi, Kandilli Rasathanesi Kampüsü, Kandilli - İstanbul
firat.matur@xerox.com

Sayın Araştırmacı,

"Baskın kol biyo-empedans karakteristik özelliklerinin DEXA kemik yoğunluk ölçümleri ile karşılaştırılması ve biyo-empedans karakteristik özelliklerinin Osteoporoz ön-tanısında kullanılabilirliğinin incelenmesi" başlıklı projeniz ile yaptığınız Boğaziçi Üniversitesi İnsan Araştırmaları Kurumsal Değerlendirme Kurulu (İNAREK) 2016/26 kayıt numaralı başvuru 14.03.2016 tarihli ve 2016/03 sayılı kurul toplantısında incelenerek etik onay verilmesi uygun bulunmuştur.

Bilgilerinize rica ederim.

Saygılarımızla,

Doç. Dr. Arzu Çelik Fuss (Başkan)
Fen-Edebiyat Fakültesi
Moleküler Biyoloji ve Genetik Bölümü
Boğaziçi Üniversitesi, İstanbul

Yrd. Doç. Dr. Özgür Kocatürk (Üye)
Biyo-Medikal Mühendisliği
Boğaziçi Üniversitesi, İstanbul

Doç. Dr. Özlem Hesapçı (Üye)
İktisadi ve İdari Bilimler Fakültesi
İşletme Bölümü
Boğaziçi Üniversitesi, İstanbul

Prof. Dr. Fatoş Gökşen (Üye)
Fen Edebiyat Fakültesi
Sosyoloji Bölümü
Koç Üniversitesi, İstanbul

Dr. Gülüstü Kaptanoğlu (Üye)
Serbest Hekim
Etiler, İstanbul

Yrd. Doç.Dr. Mine Göl Güven (Üye)
Eğitim Fakültesi, İlköğretim Bölümü
Boğaziçi Üniversitesi, İstanbul

Figure 9.1 Boğaziçi University İnsan Araştırmaları Kurumsal Değerlendirme Kurulu (INAREK) - Research Approval.

Before participating in the clinical study, each patient has read and signed a two-page informed consent shown in Figure 9.2. Patients rejected to participate in the study are not measured, and measurement data of patients who have previously consented are excluded from the study if they revoke their consents. One patient data is excluded from the study due to consent revoke.

9.3 Patient measurement card

For each patient, a measurement card is created, as in Figure 9.3. This card is used to capture the patient's living standards, including used medications.

9.4 Anthropological measurements

In this study, some anthropometric data of the subjects are collected. Collected data are gender, age, height, weight, arm length, hand wrist circumference, biceps circumference, body height, leg length, ankle circumference, and thigh circumference. The subjects' heights are measured with a wall-mount stadiometer of 0.1 cm precision, weights are measured with a 0.1 kg precision electronic scale while subjects are wearing indoor clothes, and all other lengths and circumferences are measured with a soft fabric tape measure where measurements are rounded to nearest 0.1 cm.

9.5 Reference bone mineral density measurements using DEXA

The reference DEXA measurements for the HP4284A study are performed at Anadolu Saglik Merkezi, and Cerrahpasa Medical Faculty is used for the Impedimed SFB7 study. The DEXA device used in Anadolu Saglik Merkezi was a Hologic Explorer with serial number 90409, and the DEXA device used in Cerrahpasa Medical Faculty was Hologic QDR 4500W model with 48329 serial number. Both devices used had a measurement precision of 1.14% or better. The DEXA measurements of subjects were performed by accredited technicians a maximum of 30 minutes before their BIS measurements, and radiologists verified the DEXA results. Since central DEXA measurements, i.e., the lumbar spine and hip measurements form the gold standard for osteoporosis diagnosis, this study's DEXA reference scan sites are selected as lumbar and hip [10].

9.6 BIS Measurement

BIS measurement rooms were selected as private rooms to ensure patient privacy. Patients were able to undress heavy coats if needed privately. The rooms were well ventilated with controlled temperature in the range of $21 - 23^0$C. Body impedance measurements are performed when subjects are in a sitting position; always the same room and the same armchair are used for the measurements while wearing indoor clothes.

For impedance measurements with HP4284A, standard Ag/AgCl Arbo Kendall electrodes (48x34mm) are used. For the HP4284A study, eight electrodes were used for each subject: 2 electrodes were placed over each hand and foot, along with their third metacarpal bones with a five cm distance in between. Before applying electrodes, the contact points are cleared with alcohol swabs with 70% isopropyl alcohol. As shown in Figure 9.5, the electrodes closer to the wrist or ankle are used for voltage measurements, and electrodes towards the fingers are used for applying current. By connecting measurement ports to 4 electrodes only, it is possible to measure arm, leg, or trunk impedances separately [201]. Trunk impedance measurements are excluded from the study to avoid the overnight fasting effect on the BI measurements.

In the HP4284A study, 20 frequencies between 10 kHz to 800 kHz are used as the measurement frequencies, and at each frequency, measurement is repeated 20 times and averaged to find the final measurement result. The Cole-Cole parameters are later calculated by using in-house developed software where its code listing is available in the Appendix.

For the Impedimed SFB7 study, 132 different frequencies between 10 kHz and 200 kHz are used. Four Skintact RT38 electrodes are used for the bioimpedance spectroscopy measurements, and always a new electrode pack is opened before the measurements. Two electrodes are placed over the hand of the dominant arm. Two electrodes are placed at the infraclavicular fossa of the patient. The electrodes are placed 1 cm distance; outer electrodes are used to apply current, and the inner ones as voltage sens-

ing electrodes [196]. Before applying electrodes, the contact points are cleared with alcohol swabs with 70% isopropyl alcohol. For Cole-Cole parameter calculations, the manufacturer propriety software ImpediMed SFB7 Multi-Frequency Analysis is used [202]. Each subject is measured 20 times, and the BIS model parameters found for each measurement are averaged to find their final values.

9.7 HP4284A Clinical BIS study

Clinical study is conducted at John Hopkins Ozel Anadolu Saglik Merkezi, Gebze Kocaeli, under the supervision of Dr. Kezban Berberoglu. 40 postmenopausal women subjects are measured.

9.7.1 Body segment measurement

For measuring the body segments, the body is approximated as five conical impedance excluding the head, i.e., four of them are for the limbs, and the fifth is for the trunk, as in Figure 9.5. With the assumption that no current will flow through the voltage sensing electrodes, using eight measurement ports combined in proper tetrapolar combinations as in Table 9.1, the impedance of each limb and the trunk can be measured separately. By connecting measurement ports to four electrodes simultaneously, it is possible to measure arm, leg, or trunk impedances separately [201]. As in Figure 9.4, when current is injected between the right hand and right foot, and voltage is measured between hands, the system measures the right arm impedance. On the other hand, for right leg impedance measurement, the current is applied between the right hand and right foot, while voltage is measured between feet. If the right and left side ports are swapped, the measured impedances are the left arm and the left leg impedances, respectively.

Each body segment is considered to be a conical resistance as in Figure 9.5, and assuming limb symmetry around the vertebral axis, body segment characteristic

Table 9.1
Port combinations for measuring body segments.

Body segment	Current source port	Current sink port	Voltage electrode	Ground port
Right arm	1	3	5	6
Right leg	1	3	8	7
Trunk	1	3	6	8
Left arm	2	4	6	5
Left leg	2	4	7	8

impedance is calculated with anthropometric normalization as

$$Z_{segment} = \frac{Z_{measured}.\pi.r_1.r_2}{L_{segment}} \tag{9.1}$$

where $L_{segment}$ is the right arm length L_{RA} measured from wrist to shoulder tip for the left and right arms, L_{RL} measured from ankle to hip for the right and left legs, and L_T measured from hip to clavicle for the trunk. The radius at each end of the truncated cone body segment are r_1 and r_2, and they are right wrist and right biceps radius r_w and r_{bi}, for the right and left arms, they are right ankle radius r_a and right tight radius r_t for right and left legs, and they are r_{br} and r_{be} that are body circumference around breast and belly for the trunk.

The radius of each body segment at the edges are calculated as

$$radius = \frac{Circumference}{2\pi} \tag{9.2}$$

with the assumption of perfect circular shape.

9.7.2 HP4284A front end

Since the HP4284A LCR meter is not offering a true tetra-polar electrode measurement system, a front-end amplifier has become necessary, as in Figure 9.6. The circuitry is designed to actively shield the voltage terminal electrodes for reducing capacitive cable loads [203].

9.7.3 BIS Measurement protocol

The measurement protocol with HP4284A is as follows:

1. Preparation of patient to the measurement

   - Participating in the study is on voluntary basis. The patient should read and sign the consent form.
   - Patients with a cardiac pacemaker or pregnant individuals can not participate. The status will be confirmed before the measurement.
   - For each patient, a patient card, as in Figure 9.3, is created.
   - The questions on the measurement card will be filled and signed by the patient.
   - The patient will be instructed to undress the thick coats and stay with indoor dresses only.
   - The patient will be tutored to remove all metallic objects, including wristwatches and wristbands: rings can stay since they are out of the measurement area.
   - The patient will be instructed to remove shoes and socks.
   - The patient's height will be measured with the wall-mounted stadiometer in centimeters, and the patient's weight will be measured using a precision electronic scale in kilograms, both with 0.1 unit precision, rounding to the nearest 0.1 value.
   - Dominant arm information will be captured. The arm that the patient is using for writing will be named the dominant arm.
   - Dominant arm information will be captured.
   - The anthropometric measurements of the patient will be measured using a soft fabric tape measure and recorded. For the limb measurements, the patients' dominant side will be used. Assuming the body is symmetrical around the vertebral axis, the same data will also be used for the opposite side. The measurements will be:

  - Whole arm length: stretch arm distance from wrist to shoulder tip
  - Biceps circumference: measured around biceps when the the arm is loose,
  - Wrist circumference: measured over the hand wrist
  - Body length: from hip to clavicle
  - Upper body circumference: above the breasts
  - Lower body circumference: around the belly
  - Leg length: from ankle to hip
  - Leg upper circumference: circumference of the leg at the thigh
  - Leg lower circumference: circumference of leg around the ankle
- The patient will sit in the armchair keeping legs untouched and keeping arms separated from the body

2. Preparation for BIS measurement
   - The electrode placement points (over the hands and feet) will be cleaned with an alcohol swab
   - Eight electrodes will be placed: two electrodes over the third metacarpal bones of both hands, two electrodes over the wrists, two electrodes over the third metacarpal bone of both feet, and two electrodes over the leg and foot joints
   - Inform the patient that measurement will start shortly, and ask the patient to stay still. Also, tell the patient that if they feel a tingling, this is normal, but the measurement can be terminated if it is asked for
3. Start the "Anthropometrik Elektrik Empedans Spektroskopisi" application (Figure 9.7), and follow directions on screen
   - Connect the measurement leads to directed electrodes on the application
   - Check message on the application to move to the next electrode combination
   - Disconnect all electrodes when application directs so
4. Complete measurement

- Inform patient that measurement is completed
- Remove electrodes
- Ask patient not to forget belongings when leaving the measurement room
- Check measurement card is signed by the patient

9.7.4 Measurement frequencies

Although HP4284A can measure data at 8610 distinct frequencies between 20 Hz to 1 MHz, for operational purposes, 20 frequencies at the β dispersion region between 10 kHz and 800 kHz is selected for the measurements. The frequencies tabulated in Table 9.2 are selected as equidistant logarithmic frequencies. Later as shown in Figure 9.8, for calculating the Cole-Cole parameters, the number of frequencies in the set is reduced to 10 to convert the set into an equidistant frequency set as Kun *et al.* have suggested [156].

Table 9.2
Selection of measurement frequencies (kHz).

Frequency Band	Frequency (kHz)				
10 kHz - 100 kHz	10.0	12.5	16.0	20.0	25.0
	32.0	40.0	50.0	62.5	80.0
100 kHz - 1 MHz	100.0	125.0	160.0	200.0	250.0
	320.0	400.0	500.0	640.0	800.0

9.7.5 Measurement noise and repeatability of measurement

As with every biomedical measurement system, reducing the noise in the measured signal is important before further processing the data [204].

The coefficient of variation CV is the reciprocal of the signal to noise ratio SNR,

and it is measured as:

$$CV_1 = \frac{\sigma_1}{\upsilon_1} \tag{9.3}$$

where σ_1 is the standard deviation i.e., the measurement noise, and υ_1 is the measured value.

When the measured value υ is with a Gaussian noise

$$\upsilon = \upsilon_1 + \upsilon_{noise} \tag{9.4}$$

with υ_1 the noise free value and υ_{noise} the Gaussian noise, for sum of N measurements

$$N.\upsilon = N.\sum_{1}^{N} \upsilon_1 + N.\sum_{1}^{N} \upsilon_{noise} \tag{9.5}$$

Since the standard deviation for the sum of N points for a Gaussian distribution is

$$\sigma_N = \sqrt{N}\sigma_1 \tag{9.6}$$

then the coefficient of variation can be calculated as

$$CV_N = \frac{\sigma_N}{\upsilon_N} = \frac{\sqrt{N}\sigma_1}{N\upsilon_1} \tag{9.7}$$

which can be reduced to

$$CV_N = \frac{CV_1}{\sqrt{N}} \tag{9.8}$$

In other words, by averaging N measurements, the SNR of the measurement is improved by a factor of $\sqrt{N}$ [205].

During clinical measurements from subjects, the measurements are repeated 20 times giving a SNR improvement of 4.47 times.

Within day and between day measurement uncertainties are dominated by the Repeatability Uncertainty (RU) of the measurements.

For a 95% confidence interval, it is calculated as

$$RU = \frac{2\sigma}{\sqrt{N}} \tag{9.9}$$

A single subject is measured with the same observer under the same measurement conditions. For within-day measurements, measurements are performed in 1 hour, and for between-day calculations in consecutive two days. RU and c_v for impedance model parameters are tabulated in Table 9.3.

Table 9.3
Repeatability uncertainty (RU) and coefficient of variations ($c_v = \sigma/\mu$) of the BIS measurements.

Impedance model parameters	RU	$c_v^{\dagger}$	$c_v^{\ddagger}$
R_0 (Ω.cm)	0.8	0.9%	0.5%
R_∞ (Ω.cm)	0.6	0.8%	0.5%
α	0.002	1.2%	0.1%
f_c (Hz)	235	2.0%	1.7%

† Within day coefficient of variation

‡ Between day coefficient of variation

9.7.6 Error correction of the measurement system

The HP4284A LCR meter measures the impedance in amplitude and phase pairs, and due to parasitic stray and residual impedance effects, the measurement system transfer function $|F(L,f)|\underline{/\Phi(L,f)}$ are load (L) and frequency (f) dependent, where $F(L,f)$ and $\Phi(L,f)$ are gain and phase shift of the system [206].

The measured impedance $Z'\underline{/\Theta'}$ changes with the measured load and the measurement frequency as:

$$Z'\underline{/\Theta'} = (|F(L,f)|.|Z|)\underline{/\Theta + \Phi(L,f)} \tag{9.10}$$

where $Z\angle\Theta$ is the actual impedance, L is load and equals to $|Z|$ and f is the measurement frequency.

The measurement data can be normalized as follows:

$$|G| = |G(L,f)| = \frac{1}{|F(L,f)|} \tag{9.11}$$

$$\underline{/\Psi} = \underline{/\Psi(L,f)} = \underline{/-\Phi(L,f)} \tag{9.12}$$

$$|Z|\underline{/\Theta} = (|G|.|Z^{'}|)\underline{/\Theta^{'} - \Psi} \tag{9.13}$$

Following the short circuit and open circuit calibrations of the HP4284A [206], 8 calibrated resistors are directly connected to HP4284A with a special front-end circuity (Figure 9.9) to form a direct measurement reference loads.

The gain and phase correction factors for the measurement system are empirically calculated by measuring 21.57 Ω, 26.92 Ω, 100.53 Ω, 119.72 Ω, 148.05 Ω, 215.14 Ω, 267.20 Ω, and 547.10 Ω resistors at the measurement frequencies of 10 kHz, 12.5 kHz, 16.0 kHZ, 20 kHz, 25 kHz, 32 kHz, 40 kHz, 50 kHz, 62.5 kHz, 80 kHz, 100 kHz, 125 kHz, 160 kHz, 200 kHz, 250 kHz, 320 kHz, 400 kHz, 500 kHz, 640 kHz and 800 kHz. Results are shown in Figure 9.10.

For a load $|L_x|\underline{/\Theta_x^{'}}$ at a measurement frequency f_m, the correction factors $|G(L_x, f_m)|$ and $\Psi(L_x, f_m)$ are calculated by the interpolation of the correction factors of the nearest smaller and larger loads L_1 and L_2, or by using the nearest 2 loads if extrapolation is needed.

$$|G(L_x,f_m)| = G(L_1,f_m) + (G(L_2,f_m) - G(L_1,f_m)) \,.\, \frac{|L_x| - |L_1|}{|L_2| - |L_1|} \tag{9.14}$$

$$\underline{/\Psi(L_x,f_m)} = \underline{/\Psi(L_1,f_m)} + (\underline{/\Psi(L_2,f_m)} - \underline{/\Psi(L_1,f_m)}) \,.\, \frac{|L_x| - |L_1|}{|L_2| - |L_1|} \tag{9.15}$$

9.7.7 Measurement results

Total of 40 menopaused women between ages 47 to 77 have participated in the study. The average age is 60.2 years with a standard deviation of 8.37 years. Average body mass index is 32.3 kg.m^{-2} with a standard deviation of 5.6 kg.m^{-2}. As tabulated in Table 9.4, using D'Agustiono Pearson test that computes a single P value for the combination of the coefficients of Skewness and Kurtosis of measured data, the P values are found to be greater than 0.05, i.e., all measured anthropometric data are with normal distribution except the body mass index (BMI) [207]. Average height of the subject is 152.4 cm with a standard deviation of 6.6 cm, average weight of subjects is 74.9 kg with a standard deviation of 12.4 kg. Hence, the average body mass index is 32.4 kg.m^{-2} with a standard deviation of 5.9 kg.m^{-2}, therefore the subject population can be considered as obese.

Table 9.4
Demographic data of menopaused women.

Parameter	Mean	SD	Minimum	Maximum	Normal Dist. P
N=40					
Age (year)	60.2	8.4	47	77	0.0898
Age at menopause (year)	44.4	5.4	30	53	0.2934
Height (cm)	152.4	6.6	141.0	165.0	0.1584
Weight (kg)	74.9	12.4	55.0	109.0	0.1381
BMI (kg.m^{-2})	32.4	5.9	22.7	50.4	0.0148
Arm length (cm)	48.3	3.6	41.1	56.8	0.8357
Biceps perimeter (cm)	33.6	3.4	27.1	43.0	0.1902
Wrist perimeter (cm)	17.4	1.5	15.0	20.9	0.3813
Leg length (cm)	70.9	5.5	60.2	82.8	0.8192
Thigh perimeter (cm)	56.7	7.7	43.1	77.0	0.5393
Ankle perimeter (cm)	24.5	2.2	20.3	29.9	0.6390

The subjects also scanned with DEXA to find their central reference bone mineral densities, and later their bone mineral densities are marked in WHO groups with their T scores.

With respect to total lumbar spine measurement results, 12 women are classified as normal, 18 with osteopenia and 10 with osteoporosis (Table 9.5). With WHO groups defined by their LBMD, bone mineral densities of L1, L2, L3 and L4 for the normal, osteopenic and osteoporotic groups are 0.916±0.068, 1.056±0.119, 1.111±0.094 and 1.120±0.158 g.cm^{-2} respectively. For the osteopenic population, for L1, L2, L3 and L4 the bone mineral densities are 0.745±0.042, 0.824±0.076, 0.911±0.073 and 0.892±0.083 g.cm^{-2}, and for the subjects with osteoporosis, they are 0.587±0.082, 0.721±0.088, 0.757±0.057 and 0.781±0.051 g.cm^{-2} in the order; suggesting that the average bone mineral density at lumbar disks are decreasing with the lower T scores of LBMD and with all WHO groups, the bone mineral densities of L1 to L4 are increasing with their lumbar index regardless of their WHO groups (Figure 9.11).

With respect to hip measurements results, 21 women are classified as normal, 18 with osteopenia and only 1 with osteoporosis (Table 9.6). With WHO groups defined by their hip bone mineral densities, for normal, osteopenic and osteoporotic groups, the inter-trochanter BMD is 1.099±0.107, 0.107±0.917 and 0.917±0.047 g.cm^{-2} respectively. For trochanter 0.665±0.064, 0.064±0.546 and 0.546±0.053 g.cm^{-2}, for femoral neck 0.750±0.065, 0.065±0.632 and 0.632±0.059 g.cm^{-2}, and for Ward's area the bone mineral densities are 0.577±0.090, 0.090±0.476 and 0.476±0.084 g.cm^{-2}; suggesting that the average bone mineral density at all hip sites are decreasing with the lower T scores of total hip BMD (Figure 9.12).

Within the same study, 12 men are also measured. Their mean age for men is 58.7 year with 13.6 years standard deviation. The minimum and maximum ages observed are 40 and 82 respectively. The demographic data for the measured men are tabulated in Table 9.7.

With respect to their total lumbar spine DEXA scan results, 9 subjects are diagnosed as normal, 2 are with osteopenia and and only 1 with osteoporosis. Their bone mineral densities are 1.056±0.100 g.cm^{-2} and 0.888±0.010 g.cm^{-2}, and 0.760±0.000 g.cm^{-2} respectively (Table 9.8).

With respect to their total hip DEXA scans, 9 male subjects are diagnosed as normal and 3 are with osteopenia. There is no subject with osteoporosis. Their bone mineral densities are 1.045±0.146 g.cm^{-2} and 0.831±0.059 g.cm^{-2} respectively (Table 9.9).

Number of measured men are limited, therefore their further analysis are excluded from this study.

BIS model parameters for different WHO groups are examined using the statistical F-test to understand if BIS parameters vary with the limb site used for the measurement. For menopaused women, BIS model characteristic frequency f_c and extracellular fluid resistance R_e of upper limbs are statistically different from the lower limbs' model parameters, and for left and right side limbs, they are statistically not different. For the other BIS model parameters, i.e., intracellular fluid resistance R_i and the depression constant α, the parameters are statistically not different for arms and legs, and they are statistically not different for the right and left side limbs (Table 9.10). For menopaused women subjects, the multiple data comparison graph of the BIS model characteristic frequency of different limbs are sketched in Figure 9.13.

When the BIS model characteristic frequencies are calculated by the Cole-Cole diagram is compared with the frequencies calculated directly using the Nyquist diagram, the correlation between the results of two calculations found as near perfect ($r = 0.993, P < 0.001$). For the dominant arm measurement, the regression function in between those is

$$ln(f_c)|_C = 0.598 + 0.941 ln(f_c)|_N \tag{9.16}$$

where C stands for Cole-Cole calculation and N stands for calculation using the imaginary part of the Nyquist diagram. The standard error for the intercept is 0.1892 with $P = 0.0031$, and the standard error for the slope is 0.01809 with $P < 0.0001$. When F-test is conducted to compare the variance of both parameters, the variance ratio is found as 1.1137 ($P = 0.738$), i.e., accepting the null hypothesis and variances of both

parameters do not differ statistically. Figure 9.24 displays the regression line for the menopaused women, where the BIS measurement site is the dominant arm.

The correlation of the BIS model parameters with the subjects' anthropometric dimensions, i.e., age, menopause age, weight, height, and body mass index, is calculated. The arm extracellular fluid resistance R_e has a statistically significant weak positive correlation with the body mass index. The depression constant α of all limbs has a statistically significant negative moderate correlation with the body mass index. The extracellular fluid resistance R_e of legs have statistically significant weak positive correlations with age, and the characteristic frequency f_c of legs have statistically significant moderate positive correlations with the subjects' age (Table 9.11).

When the correlation of the BIS model parameters with the subjects' lumbar area DEXA bone mineral density scans, i.e., L1, L2, L3, L4 disk and the LBMD, are calculated, both right arm and left arm characteristic frequencies with has a moderate positive correlation with all lumbar disks BMD measurements; maximum between the right arm characteristic frequency f_c with the L1 disk BMD as $(r = 0.636, P < 0.001)$ and minimum between the left arm f_c and the L3 disk BMD as $(r = 0.425, P = 0.006)$. For LBMD, there is a moderate positive correlation with the right arm f_c is $(r = 0.580, P < 0.001)$, and also with the left arm f_c, there is a moderate positive correlation in between with $(r = 0.473, P = 0.002)$. For the left leg, the inter-cellular fluid resistance R_i has a weak negative correlation with the L1 disk BMD scores with $(r = -0.324, P = 0.041)$. None of the other BIS model parameters of the limbs has a statistically significant correlation with any of the lumbar BMD results (Table 9.12).

The correlation of the BIS model parameters with the subjects' hip area DEXA bone mineral density scans, i.e., inter-trochanter, trochanter, femur neck, Ward's area, and the HBMDs are tabulated in Table 9.13. Right leg and left leg BIS model characteristic frequencies f_c have statistically significant but negative weak correlations with Ward's area BMD, and they are $(r = -0.389, P = 0.013)$ and $(r = -0.349, P = 0.027)$ respectively. Both right arm and left arm inter-cellular resistances R_i have negative weak correlations with the femoral neck bone mineral densities, and they are

($r = -0.346, P = 0.029$) and ($r = -0.324, P = 0.042$) respectively. All other correlations between the BIS model parameters and the DEXA measurements are either statistically not significant or are weak enough to ignore.

The regression functions of the BIS model parameters of the menopaused women, that have moderate or higher statistically significant correlation with their lumbar region BMD measurements ($r > 0.4, P < 0.05$), are as follows:

$$BMD_{L1} = -9.1835 + 0.9522.ln(f_c)_{RA}, P_{intercept} = 0.0001, P_{slope} = 0.0001 \quad (9.17)$$

$$BMD_{L2} = -8.6742 + 0.9140.ln(f_c)_{RA}, P_{intercept} = 0.0014, P_{slope} = 0.0005 \quad (9.18)$$

$$BMD_{L3} = -9.3293 + 0.9829.ln(f_c)_{RA}, P_{intercept} = 0.0002, P_{slope} = 0.0001 \quad (9.19)$$

$$BMD_{L4} = -7.7723 + 0.8338.ln(f_c)_{RA}, P_{intercept} = 0.0074, P_{slope} = 0.0030 \quad (9.20)$$

$$BMD_{LT} = -8.6174 + 0.9098.ln(f_c)_{RA}, P_{intercept} = 0.0003, P_{slope} = 0.0001 \quad (9.21)$$

$$BMD_{L1} = -6.1019 + 0.6551.ln(f_c)_{LA}, P_{intercept} = 0.0121, P_{slope} = 0.0053 \quad (9.22)$$

$$BMD_{L2} = -7.9107 + 0.8385.ln(f_c)_{LA}, P_{intercept} = 0.0046, P_{slope} = 0.0019 \quad (9.23)$$

$$BMD_{L3} = -6.5805 + 0.7176.ln(f_c)_{LA}, P_{intercept} = 0.0154, P_{slope} = 0.0062 \quad (9.24)$$

$$BMD_{L4} = -7.2956 + 0.7859.ln(f_c)_{LA}, P_{intercept} = 0.0140, P_{slope} = 0.0061 \quad (9.25)$$

$$BMD_{LT} = -6.9668 + 0.7495.ln(f_c)_{LA}, P_{intercept} = 0.0056, P_{slope} = 0.0021 \quad (9.26)$$

where RA is right arm, LA is the left arm, L1 to L4 are the lumbar disks 1 to 4, and LT is the weighted average of lumbar disk BMDs to resemble lumbar total BMD. For the right and left arm BIS model parameter $ln(f_c)$, the scatter diagram, the corresponding regression line with BMD_{L1} to BMD_{LT}, the 95% confidence and 95% prediction intervals are illustrated in Figure 9.14.

With the *One way analysis of variances* (ANOVA) test, the BIS model characteristic frequency is inspected to find if this parameter varies for different WHO groups with respect to their DEXA scores. Since only the left arm ($r = 0.474, P = 0.002$) and right arm ($r = 0.580, P < 0.001$) characteristic frequencies have a moderate correlation

with the lumbar area bone mineral densities, this test is performed only for the BIS model characteristic frequencies for defining the lumbar and hip DEXA scans.

For menopaused women WHO subgroups based on their lumbar area DEXA scores, the mean and the standard deviation of the right arm BIS model (f_c) is 36489 $\pm$ 3433 Hz, 34413 $\pm$ 2219 Hz and 31634 $\pm$ 2310 Hz for the normal, osteopenic and osteoporotic WHO subgroups respectively. Since the ANOVA test has $P = 0.001$, the hypothesis, at least the means of the f_c of 2 or more WHO subgroups differ significantly, is accepted. By using the Student-Newman-Keuls test for all pairwise comparisons (P$<$0.05), the characteristic frequency is found to be a qualitative factor on the dependent data, i.e., the mean of f_c for each WHO subgroup differs from all others' mean significantly (Table 9.14).

For menopaused women WHO subgroups based on their lumbar area DEXA scores, the mean and the standard deviation of the left arm BIS model (f_c) is 37179 $\pm$ 4317 Hz, 35080 $\pm$ 2470 Hz and 33807 $\pm$ 2008 Hz for the normal, osteopenic and osteoporotic WHO subgroups respectively. Since the ANOVA test has $P = 0.041$, the hypothesis, at least the means of the f_c of 2 or more WHO subgroups differ significantly, is accepted. By using the Student-Newman-Keuls test for all pairwise comparison (P$<$0.05), the characteristic frequency f_c is found to be a qualitative factor on the dependent data, the means of f_c for normal and osteoporotic WHO subgroups significantly different from each other, but the mean of f_c for the osteopenic population is not significantly different from the normal or osteoporotic population (Table 9.14).

In summary, in terms of BIS characteristic frequency f_c, upper and lower limbs are different from each other, however, symmetrical limbs with respect to spine are similar. There is a moderate positive correlation between the f_c and lumbar BMD ($r = 0.580, P < 0.05$). Although there is a negative correlation between the femure neck ($r = -0.346, P < 0.05$) and the Ward's area ($r = -0.399, P < 0.05$), for total lumbar BMD a statistically significant correlation is not observed ($P > 0.05$). Using Student-Newman-Keuls test, f_c of different WHO T score groups are statistically different, and f_c may be used a marker for classification for LBMD deficiency. Finally, when

dominant arm f_c is used as a marker to identify the bone mineral deficiency (T<-1), cutoff frequency f_{cut} is 35.4 kHz. And when f_c is used to identify Osteoporosis only (T<-2.5), f_{cut} is 32.4 kHz.

9.7.8 Compartmental analysis

The segmental resistance measured at 50 kHz is used for the compartmental analysis to find the segment fat quotient (QSEG) and the percentage of the body fat (FAT%). QSEG is found as 0.646 ± 0.086 and the FAT% as 66.796 ± 8.989 %. Neither QSEG nor FAT% does not have any statistically significant correlation with LBMD or HBMD ($P > 0.05$).

9.8 Long term medical treatment monitoring with HP428A BIS measurements

For osteoporosis treatment monitoring, an osteoporosis patient, intaking Crestor 10mg, Actonel 35mg, and Calcimax D3 as medical treatment, is monitored for eight months. Reference DEXA measurements of the patient are performed twice, at the beginning and at the end of the follow-up period. BIS measurements are performed monthly, and only the dominant arm impedance measurements are performed.

For measurements, standard Ag/AgCl Arbo Kendall electrodes (48x34mm) are used. To minimize electrode aging and electrode type effect, always freshly purchased electrodes of the same brand are used.

Four electrodes are used in each measurement: two electrodes placed over the right hand, one electrode over the left hand, and one electrode over the right foot, along with their third metacarpal bones. The right-hand anterior electrode and right-foot electrode are for current injection, and others are for voltage measurement. Positive leads are connected to the right hand. In each measurement, 20 consecutive measure-

ments performed in less than 5 minutes are averaged to obtain the final reading.

Body impedance measurements are performed with the patient in a sitting position; always the same room and the same armchair are used for the measurements.

For BIS model based bone mineral density classification, the Youden index cutoff frequency found in the segmental HP4284A measurements is used: the frequency used is 35400 Hz for two-level classification as Normal or lowered bone mineral density (T< -1). For 3 level classification, the frequencies used as cutoff are 37775 Hz and 32359 Hz, where a patient is classified as Normal if the calculated dominant arm characteristic frequency f_c is above 37775 Hz, with osteoporosis if f_c is lower than 32359 Hz, and osteopenic otherwise.

The BIS results are Long term measurement results of the patient, and the classifications of the results are tabulated in Table 9.15.

For the patient, the average measured characteristic frequency during the study period was 31604 Hz, with a standard deviation of 3194 Hz. The coefficient of variance was 10.11%. Summary statistics for the measured characteristic frequency is tabulated in Table 9.16.

The characteristic frequency change during the medication is plot in Figure 9.15.

In summary, the characteristic frequency f_c always classified the patient as a low bone density patient (T<-1), 4 times with Osteoporosis and 4 times with Osteopenia. The BIS measurement period might be synchronized with the medication intake to avoid possible side effects of overshoots in calcium concentrations.

9.9 Impedimed SFB7 Clinical BIS study

The clinical study is conducted at Istanbul University Cerrahpasa Medical Faculty, Fatih Istanbul, with the supervision of Dr. Ulku Akarirmak. Ninety-one subjects are measured. The measurement are conducted in two parts: first 55 subjects are measured, and later 36 for verification of the study. Four subjects are removed from the first set since their BIS model characteristic frequency is found to be far-out using Tukey method. Far-out data has a value that falls out of the data range between lower quartile minus three times interquartile range and upper quartile plus three times the interquartile range [208].

9.9.1 Body segment measurement

The body segment used for BIS measurement is the dominant arm of the subject, and as in Figure 9.17, and it is measured while subjects are sitting [167]. If the subject is right-handed, dominant arm hence the measuring arm is the right arm. The arm is approximated to a truncated cone, where its two end circumferences are assumed to be the loose biceps and wrist circumferences.

9.9.2 BIS Measurement protocol

The measurement protocol with Impedimed SFB7 is as follows:

1. Preparation of patient to the measurement
    - Participating in the study is voluntary basis. The patient should read the consent form and sign it first.
    - Patients with a cardiac pacemaker or pregnant individuals can not be measured. The status will be confirmed before the measurement.
    - For each patient, a patient card, as in Figure 9.3, is created.

- The questions on the measurement card will be filled and signed by the patient.
- The patient will be instructed to undress the thick coats and stay with indoor dresses only.
- The patient will be tutored to remove all metallic objects, including wristwatches and wristbands: rings can stay since they are out of the measurement area.
- The patient will be instructed to remove shoes and socks.
- The patient's height will be measured with the wall-mounted stadiometer in centimeters, and the patient's weight will be measured using a precision electronic scale in kilograms, both with 0.1 unit precision, rounding to the nearest 0.1 value.
- Dominant arm information will be captured. The arm that the patient is using for writing will be named the dominant arm.
- Dominant arm information will be captured.
- The anthropometric measurements of the patient will be measured using a soft fabric tape measure and recorded. For the limb measurements, the patients' dominant side will be used.
  - Whole arm length: stretch arm distance from wrist to shoulder tip
  - Biceps circumference: measured around biceps when the the arm is loose,
  - Wrist circumference: measured over the hand wrist
- The patient will sit on the bed keeping measured arm separated from the body

2. Preparation for BIS measurement

- The electrode placement points (over the hands and infraclavicular fossa) will be cleaned with an alcohol swab
- Four electrodes will be placed: two electrodes over the third metacarpal bones of dominant hand, and two electrodes over the infraclavicular fossa.

- Inform the patient that measurement will start shortly, and ask the patient to stay still. Also, tell the patient that if they feel a tingling, this is normal, but the measurement can be terminated if it is asked for

3. Enter patient data into Impedimed SFB7.

   - Connect the measurement leads
   - Check message on the Impedimed SFB7
   - Disconnect all electrodes when measurement is completed

4. Complete measurement

   - Inform patient that measurement is completed
   - Remove electrodes
   - Ask patient not to forget belongings when leaving the measurement room
   - Check measurement card is signed by the patient

9.9.3 Repeatability

The same subject is measured with Impedimed 500 times to find the repeatability of the measurement device. The Repeatability Uncertainty (RU) of Impedimed SFB7 for same day measurement is found as 301 Hz for f_c, and coefficient of variation is 1.24%. Results are BIS model parameters are tabulated in Table 9.17, and Figure 9.18 shows the individual measurement data of the test measurement.

9.9.4 Measurement results

In the Impedimed clinical study 91 menopaused women are measured. Since their measurement results are detected as outliers, 3 subjects are excluded from the study.

For the 88 women subjects measured the demographics data is tabulated in Table 9.18. The mean age of the subject is 59.0 ± 9.3 years. Average body mass index (BMI) is 29.7 kg.m^{-2} with a standard deviation of 5.4 kg.m^{-2}; 18 subject is normal (BMI<25 kg.m^{-2}), 25 is overweight (BMI between 25.0 and 30.0 kg.m^{-2}), 31 subject is obese (BMI between 30.0 and 35.0 kg.m^{-2}), 8 is severely obese (BMI between 35.0 and 40.0 kg.m^{-2}), and 4 subject is morbid obese with BMI greater than 40.0 kg.m^{-2}.

All parameters except the menopause age are with normal distribution. The minimum menopause age observed is 24 years, and three subjects are lower than 35 years; the menopause age is negatively skewed, and coefficient of skewness is -0.969 ($P < 0.001$) and the coefficient of Kurtosis is 2.846 ($P < 0.001$), causing the data do not have a normal distribution with the D'Agostino-Pearson test ($P < 0.001$) [207].

With respect to their DEXA total lumbar spine reference measurement T sores, 1 subject is excluded from the study since DEXA scan is not available, and 28 women are classified as normal, 37 with osteopenia and 22 with osteoporosis (Table 9.19), and LBMD are 1.045 ± 0.085, 0.862 ± 0.045 and 0.721 ± 0.060, and HBMD are 0.917 ± 0.117, 0.813 ± 0.105 and 0.700 ± 0.085 respectively.

With respect to their DEXA total hip reference measurement T sores, 45 women are classified as normal, 36 with osteopenia and 7 with osteoporosis (Table 9.20), and LBMD are 0.959 ± 0.126, 0.824 ± 0.096 and 0.742 ± 0.156, and HBMD are 0.922 ± 0.092, 0.737 ± 0.045 and 0.591 ± 0.045 respectively.

For measured 88 post-menopausal women subjects, the mean of the measured BIS model Intracellular fluid R_i and Extracellular fluid resistance R_e are is 965.3 ± 212.3 and 319.4 ± 47.4 (Ω.m) respectively. The mean of the characteristic frequency f_c is 49015 ± 7815 Hz, and the mean of the Depression Constant α is 0.315 ± 0.023. With the D'Agostine-Pearson normality test, R_i and α do not have normal distribution ($P < 0.05$), but f_c and R_e are with normal distribution ($P > 0.05$).

The coefficient of skewness for the f_c is 0.612 ($P = 0.020$), and the natural

logarithm is used, the coefficient of skewness is improved to 0.274 ($P = 0.277$), i.e., $ln(f_c)$ has an improved normal distribution. Therefore, in correlation analysis tables, both f_c and $ln(f_c)$ are tabulated [198].

For the first measurement group with 55 subjects, excluding four subject with outlier characteristic frequency f_c, the BIS model parameters with the subjects' anthropometric dimensions i.e., age, menopause age, weight, height, and body mass index are calculated. The dominant arm extracellular fluid resistance R_e has a statistically significant positive moderate correlation with the subject weight ($r = 0.667, P < 0.001$) and the body mass index ($r = 0.689, P < 0.001$), the dominant arm intracellular fluid resistance has a statistically significant moderate positive correlation with the body weight ($r = 0.569, P < 0.001$) and with the body mass index ($r = 0.596, P < 0.001$). No other BMI model parameter has a statistically significant correlation with the anthropometric data. Correlations are tabulated in Table 9.21. For the second set of subjects, R_e and R_i have statistically significant correlation with the body weight ($r = 0.694, P < 0.001$) and ($r = 0.606, P < 0.001$) respectively, similarly with BMI, their correlation factors are ($r = 0.812, P < 0.001$) and ($r = 0.671, P < 0.001$) respectively. No other BMI model parameters has correlation with other anthropometric dimensions.

For group 1 data, when the correlation of BIS model parameters with the subjects lumbar DEXA bone mineral density scans are studied, extracellular fluid resistance R_e ($r = 0.326, P = 0.021$), intracellular fluid resistance R_i ($r = 0.313, P = 0.027$) and α ($r = 0.381, P = 0.006$) have positive weak correlations f_c ($P > 0.05$) does not have a statistically significant correlation with the LBMD. Only the correlations with statistical significance ($P < 0.05$) are tabulated in the Table 9.22. For group 2 data, none of the BIS model parameters has correlation with the LBMD ($P > 0.05$).

When the correlation of BIS model parameters with the subjects hip DEXA bone mineral density scans are studied, for group 1 subjects, the extracellular fluid resistance R_e has a moderate positive correlation ($r = 0.487, P = 0.001$), the intracellular fluid resistance R_i has a weak positive correlation ($r = 0.311, P = 0.028$) characteristic frequency has a moderate negative correlation ($r = -0.412, P < 0.003$), and α has also

a positive weak correlation ($r = 0.310, P = 0.028$) with the total HBMD. For the group 2, none of the BIS model parameters have correlations with HBMD. The correlations are tabulated in Table 9.23.

Characteristic frequency does not have any statistical correlation with LBMD. But for group 1, f_c and $ln(f_c)$has a negative correlation with HBMD. The regression functions are:

$$BMD_{HIP} = 5.4546 - 0.4272ln(f_c), P_{intercept} = 0.0005, P_{slope} = 0.0030 \qquad (9.27)$$

For the group 2, since there is not any statistically significant correlation with the HMBD, regression function is not calculated.

For the BIS model parameter $ln(f_c)$, the scatter diagram, the corresponding regression line with hip total BMD, the 95% confidence and 95% prediction intervals are illustrated in Figure 9.19.

With the *One way analysis of variances* (ANOVA) test, the BIS model characteristic frequency is inspected to find if this parameter varies for different WHO groups, i.e., with respect to their DEXA T scores. This test is performed only for the BIS model characteristic frequencies.

For group 1 data and WHO subgroups based on their hip area DEXA T scores, the mean and the standard deviation of the right arm BIS model (f_c) is 47157 $\pm$ 5776 Hz, 51701 $\pm$ 6907 Hz and 57435 $\pm$ 8649 Hz for the normal, osteopenic and osteoporotic WHO subgroups respectively. Since the ANOVA test has $P > 0.05$, with 95% confidence, the hypothesis, at least the means of the f_c of 2 or more WHO subgroups differ significantly, is accepted. Using the Student-Newman-Keuls test for all pairwise comparison ($P < 0.05$), the characteristic frequency f_c is found to be a qualitative factor on the dependent data, i.e., the mean of f_c for normal WHO subgroups is statistically different from the osteoporosis. Similarly, when $ln(f_c)$ is tested with ANOVA, the characteristic frequency $ln(f_c)$ is also found to be a qualitative

factor on the dependent data (Table 9.24).

9.9.5 Compartmental analysis

The segmental resistance measured at 50 kHz is used for the compartmental analysis to find the segment fat quotient (QSEG) and the percentage of the body fat (FAT%). For Impedimed study group 1, QSEG is found as 0.5453 ± 0.0796 % and the FAT% as 35.3302 ± 7.6900 %. QSEG does not have statistically significant correlation with the LBMD ($P > 0.05$) and moderate positive correlation with the HBMD ($r = 0.434, P = 0.002$). Similarly FAT% does not have statistically significant correlation with the LBMD ($P > 0.05$) and moderate correlation with the HBMD ($r = 0.474, P = 0.001$). This is in line with the study of Davidovic *et al.* [176].

ROC analysis is used to find the two-way classification capacity of the BIS measurements, when the subject who are obese or higher BMI (> 30) are excluded from the data set. Using the 43 subject data from the group 1 and group 2. With respect to their total lumbar spine DEXA scan results, 12 subjects are normal, 16 with osteopenia, and 15 with osteoporosis. When the grouping is based on the total hip DEXA scan results, 15 subjects are normal, 23 subjects with osteopenia and 5 with osteoporosis. For 43 subjects, there is no statistically significant correlation with the LBMD ($r = -0.239, P = 0.123$), and there is a statistically significant negative moderate correlation with the HBMD ($r = -0.456, P = 0.002$).

For the other 44 subjects with higher BMI (> 30) the characteristic frequency f_c does not have any statistically significant correlation with the LBMD ($r = 0.071, P = 0.652$) and with the HMBD ($r = 0.099, P = 0.524$).

9.9.6 Effects of electrode types on the measurements

Impedimed SFB7 is a commercial product sold with its propriety electrodes. Since the number of electrodes supplied with the device is limited, the Skintact RT38 electrodes are used in clinical measurements. The effect of the electrode type is assessed by measuring the same patient subsequently, first by the propriety Impedimed electrode, later by the Skintact RT38 electrode, and finally using the Ag/AgCl Arbo Kendall electrodes keeping all measurement parameters unchanged. Later, the measurements are compared with the HP4284A measurement results.

For Impedimed measurements, the Impedimed propriety software is used to calculate the model parameter results, and for HP4284A, a self-developed application is used. The parameters calculated are compared in Table 9.25 and illustrated in Figure 9.20.

In summary, there is a negative moderate correlation between the BIS characteristic frequency f_c with the hip BMD ($r = -0.412, P < 0.05$). Student-Newman-Keuls test shows that dominant arm characteristic frequency f_c of different T score groups (WHO) are statistically different, and f_c may be used as a marker for classification. Finally, when f_c is used to diagnose the reduced bone mineral density (T<-1), the cutoff frequency f_{cut} is 49.097 kHz and when f_c is used to diagnose the Osteoporosis (T<-2.5), the cutoff frequency f_{cut} is 49.565 kHz.

9.10 Impedimed study, Single frequency measurement results

87 Women subjects are split into two main groups concerning their body mass indexes (BMI). The first group consists of 43 women with $BMI < 30kg.m^{-2}$, including normal and over-weighted subjects, and later includes 44 subjects with $BMI > 30kg.m^{-2}$, including the obese, severely obese, and the morbidly obese subjects.

At six different frequencies of 5 kHz, 10 kHz, 15 kHz, 20 kHz, 25 kHz, and 30 kHz,

the dominant arm impedance of each subject is measured 20 times using the Impedimed SFB7, and results are averaged to find their final impedances. The impedance angle is calculated by the Impedimed SFB7 Multi-frequency analysis software [202]. During the calculations, the rejection parameter of the software is set as 1%, and the software automatically compensates for the measurement lead transmission delays (td).

For the first group with $BMI < 30kg.m^{-2}$, both for their LHBM DEXA groups (Table 9.26), and HBMD DEXA groups (Table 9.27), the impedance phase angle Φ decreases with the reduced bone mineral density.

When the correlation strengths of the impedance angle Φ with the bone mineral densities are inspected, with the HIP bone mineral density, the correlation strength is highest for the measurement frequency of 5 kHz ($r = 0.559, P < 0.001$). For Group 1, for every measurement frequency, the impedance angle Φ has a moderate positive correlation with the HBMD. Also, when the frequency is 5 kHz, the correlation to LBMD is statistically significant and has a moderate correlation with the LBMD ($r = 0.403, P = 0.014$). On the other hand, when the measurement frequency is 10 kHz or higher, there is no statistically significant correlation between the impedance angle Φ and the LBMD. For Group 2, where $BMI > 30kg.m^{-2}$, no significant correlation of Φ and HBMD or LBMD is observed. The correlation of impedance angle Φ with the bone mineral densities is tabulated in Table 9.28.

The regression function between the Φ and the HBMD is

$$HBMD = 0.2584 + 0.2321\Phi \tag{9.28}$$

and $P < 0.05$ both for intercept and the slope.

For LBMD, the regression function is

$$LBMD = 0.4418 + 0.1880\Phi \tag{9.29}$$

and $P < 0.05$ both for the intercept and the slope.

When Receiver Operating Characteristic Curve analysis is performed, at 5 kHz, the Area Under Curve is calculated as (AUC=0.059, $P = 0.006$) and at 10 kHz (AUC=0.784, $P = 0.001$). Specificity for 5 kHz is 70%, and sensitivity is 81.48%. At 10 kHz, sensitivity and specificity values are 80.0% and 67.74%, respectively. However, when WHO groups are based on lumbar DEXA scores, subjects are indifferent concerning their phase angle Φ values. When the subject group has $BMI > 30kg.m^{-2}$, phase angle does not have any statistically significant correlation with the LBMD or the HBMD ($P > 0.05$). The ANOVA test does not show that Φ is a differentiating factor between different WHO groups, i.e., when the subjects have a higher body mass index, the correlation between the impedance phase angle and the bone mineral densities decreases.

9.11 Receiver Operating Curve and 2D-ROC Analysis

9.11.1 Study with the HP4284A LCR meter

For lumbar spine DEXA results, *Receiver Operating Characteristic* (ROC) curve analysis is conducted only for the BIS model parameters, that have a moderate correlation with the DEXA reference bone mineral density of the total lumbar area, i.e., right arm characteristic frequency f_c ($r = 0.587, P < 0.001$) and the left arm characteristic frequency ($r = 0.495, P = 0.001$). The *area under curve* (AUC) parameter is calculated using Delong *et al.* method [209]. The optimal cutoff point for the criterion is found by calculating the Youden index J, and the confidence interval for the Youden index and the optimal cutoff point is calculated [210, 211].

To reduce the 3 level WHO subgroups into 2-level subgroups as *healthy* and *diseased*, subjects with $T < -1$ are initially assumed to be in the diseased group, i.e., both osteopenic and osteoporotic; and, later when $T < -2.5$, only osteoporotic subjects are considered as diseased. When the criterion is the RA BIS model characteristic frequency, the area under the curve is found ($AUC = 0.753, P = 0.007$) and ($AUC = 0.843, P < 0.001$) with $f_c < 35400$ Hz and < 32359 Hz respectively. When the criterion

is the LA BIS model characteristic frequency, the area under the curve is found ($AUC = 0.705, P = 0.066$) and ($AUC = 0.700, P < 0.021$) and f_c is < 37666 Hz and < 35422 Hz. Results of ROC curve analysis are shown in Table 9.29, and corresponding charts are illustrated in Figure 9.21.

The correlation of *body mass index* (BMI) and the lumbar spine bone mineral density is ($r = 0.071, P = 0.662$), and the correlation of body mass index with the RA BIS model characteristic frequency f_c is ($r = -0.012, P = 0.943$), i.e., BMI does not have a statistically significant correlation neither with the bone mineral density at lumbar area, nor with the RA f_c. For BMI, when ROC curve analysis is studied, where T<-2.5 is assumed as diseased, the ($AUC = 0.700, P = 0.021$) and the associated criterion is BMI≤ 32.9 (kg.m^{-2}). For the RA f_c, the associated criterion is $f_c < 32.359$ Hz and ($AUC = 0.843, P = 0.001$). The correct classification rate for f_c is 80%, and for BMI 55%. With the 2D-ROC test, the correct classification rate is improved from 80% to 83% and the sensitivity increased from 60% to 90%. Classification results are given in Table 9.30.

9.11.2 Study with the Impedimed SFB7 Body Analyzer

Using the group 1 data, for hip DEXA results, *Receiver Operating Characteristic* (ROC) curve analysis is conducted for the BIS model characteristic frequency f_c which correlates ($r = -0.408, P = 0.003$) with the total hip DEXA reference BMD. The *Area Under Curve* (AUC) parameter is calculated using Delong *et al.* method [209]. The optimal cutoff point for the criterion is found by calculating the Youden index J, and the confidence interval for the Youden index and the optimal cutoff point is calculated [210, 211].

To reduce the 3 level WHO subgroups into 2-level subgroups as *healthy* and *diseased*, subjects with $T < -1$ are initially assumed to be the diseased group, i.e., both osteopenic and osteoporotic subjects, and later $T < -2.5$, only osteoporotic subjects are considered as diseased, i.e., osteopenic group is belonging to the normal group.

While criterion is the DA BIS model characteristic frequency f_c, for $T < -1$ case, the area under the characteristic curve is ($AUC = 0.651, P = 0.0560$), the specificity is 57.69%, and sensitivity is 70.83%; For $T < -2.5$ case, the area under the curve is ($AUC = 0.748, P = 0.0041$), the specificity is 77.8%, and sensitivity is 65.9%. If the criterion is $ln(f_c)$, for $T < -1$ the area under the characteristic curve ($AUC = 0.651, P = 0.0560$), the specificity is 57.69%, and the sensitivity is 70.83%, and for $T < -1$ ($AUC = 0.748, P = 0.0041$), the specificity is 77.8%, and the sensitivity is 65.9%. The ROC curve analysis results are given in Table 9.31, and corresponding charts are illustrated in Figure 9.22.

When 2D-ROC analysis is performed in the 53 early engaged subjects of the Impedimed study, in which the correlation between the body mass index (BMI) with the characteristic frequency is ($r = 0.200, P < 0.05$) and both data are normal ($P < 0.05$), the mis-prediction rate (MPR) of BMI in diagnosing the existence of osteoporosis in hip area and the healthy individuals is 20.8%, and the for BIS model characteristic frequency the MPR is 34.0%. When both tests are combined with the 2D-ROC, the MPR is improved to 19.2%. Results are shown in Table 9.32.

For BMI<30 kg.m^{-2} subjects, when the ROC curve analysis is performed to analyze the diagnostic potential of f_c in reduced bone mineral density in HBMD, when subjects with $T < -1$ are assumed to have disease, the cutoff frequency is 49570 Hz, the AUC is 0.717 ($P = 0.006$), sensitivity is 62.07% and the specificity is 85.71% (Figure 9.23). When subjects with $T < -2.5$ are assumed to have disease, the cutoff frequency is 49570 Hz, the AUC is 0.839 ($P < 0.001$), the sensitivity is 90.00% and the specificity is 69.70%. When the analysis is repeated in BMI>30 kg.m^{-2} subjects, i.e., the obese population, AUC is 0.634 ($P = 0.5534$), the sensitivity is 100% but the specificity is 41.16% which suggest that, when disease does not exist, the ability to diagnose normal is very low in obese population.

In summary, although there are many alternative approaches and classifiers with complex calculations, the 2D-ROC method is a practical and easy to use method which can be extended to multiple dimensions, to include multiple test results combined for

a 2 way classifier. The $AVERAGE$ function can be modified by applying different weights for each individual tests, if test diagnostician wants to give more importance to a specific test. Measured data may be skewed or diseased and healthy population may have different kurtosis, however, if correlation between individual tests are low ($r < 0.4$), the $AVERAGE$ function still performs better than the individual markers. If correlation is higher ($r > 0.4$) to reduce the effect of non-normal data on the final success level of the 2D-ROC AVERAGE function, before applying the method, the normality of test data should be checked and necessary logarithmic or exponentiation transformations (or possible others) should be applied to reduce skewness or kurtosis of data.

9.12 Comparing the two methods in calculating the characteristic frequency

By using the HP4284A LCR meter measured data, the BIS characteristic frequencies calculated by the Cole-Cole plot are compared with the frequencies calculated according to the proposed approach by using the imaginary part of Nyquist plots.

Although calculation of f_{Nyq} is less complex compared to calculation of f_{CC}, the correlation between the two frequencies calculated with two different techniques is found almost perfect ($r = 0.993, P < 0.001$). For the regression line, the slope is 0.9193 ($P < 0.001$), and the line intercepts axis at 2151.7 Hz ($P = 0013$). The regression function is

$$f_{CC} = 2151.7 + 0.9193 f_{Nyq} \tag{9.30}$$

where f_{CC} and f_{Nyq} are the characteristic frequencies by the Cole-Cole plot and the novel 3-Point Nyquist plot approach. The regression function is illustrated in Figure 9.24.

The correlation of the characteristic frequencies with the total lumbar spine

DEXA reference bone mineral density is statistically significant and positive moderate; when the Cole-cole method is used to find the BIS characteristic frequency, it is ($r = 0.585, P < 0.001$) and with the 3-point Nyquist approach it is ($r = 0.572, P < 0.001$). When ($T < -2.5$) is the cutoff for disease prevalence, the area under the curve in ROC curve analysis is ($AUC = 0.843, P < 0.001$) and ($AUC = 0.807, P < 0.001$), with the Cole-cole method and the 3-point Nyquist method respectively. Statistical results are tabulated in Table 9.33 for comparison.

In summary, calculation of the characteristic frequency in 3-Point Nyquist plot is a direct method by solving 3 unknowns using 3 linear equations, and it is much simpler than Cole-Cole plot calculations. In Cole-Cole plot calculations multiple and complex circle fit calculations are involved, and characteristic frequency is calculated indirectly after circle parameters are found. The 3P-Nyquist characteristic frequency also has a moderate correlation with the LBMD ($r = 0.572, P < 0.05$) and it is comparable to the characteristic frequency found by the Cole-Cole plot ($r = 0.587, P < 0.05$). Furthermore capacity of 3P-Nyquist characteristic frequency for diagnosing Osteoporosis assessed by ROC curve (AUC=0.807) and it is comparable to the diagnostic capacity of the characteristic frequency found by the Cole-Cole plot (AUC=0843).

KATILIMCI BİLGİ ve ONAM FORMU

Araştırmayı destekleyen kurum: Boğaziçi Üniversitesi Biyomedikal Mühendisliği Enstitüsü

Araştırmanın adı: Baskın kol biyo-empedans ölçümlerinin Osteoporoz ön-tanısı için kullanılabilirliğinin araştırılması

Proje Yürütücüsü/Araştırmacının adı: Fırat Matur

Adresi: Boğaziçi Üniversitesi, Biyomedikal Mühendisliği Enstitüsü

E-mail adresi: firatmatur@hotmail.com

Telefonu: 0552 ■■ ■53

Proje konusu: Kemik erimesi (Osteoporoz), kemik sağlamlığını azaltan bir kemik hastalığı olmanın yanı sıra, sosyal maliyeti, ölüm oranı ve görülme sıklığı yüksek olan bir sorundur. Hasta yaşı osteporoz hastalığı için önemli bir etkendir ve özellikle ortalama yaşam süresinin uzadığı düşünülürse, bu hastalığın tedavisi için yapılan sağlık harcamalarının her geçen gün artması beklenmelidir. Düşük kemik yoğunluğu olan kişilerin tespiti, kırık riskini ve dolayısıyla hastalığın tedavi masraflarını da azaltacaktır. Toplumun yaygın olarak taranması ve osteoporoz hastalığının erken teşhisi için, maliyeti düşük ve etkin bir öntanı tekniğinin geliştirilmesi gerekmektedir.

Her organın kendine özgü bir biyo-empedansı bulunur. Vücutta bulunan her doku gibi kemik dokunun da kendine özgü bir biyo-empedans değeri bulunmaktadır. Bu nedenle, vücuttan ölçülen biyo-empedans değeri ile kemik yoğunluğu arasında bir ilişkili olması beklenir.

Bu çalışmada, vücuttan ölçülen biyo-empedans ile katılımcıların DEXA kemik yoğunluk ölçüm raporları karşılaştırılacak ve biyo-empedans ölçümü yöntemiyle osteoporoz hastalığının ön tanısının yapılabilme imkânı araştırılacaktır.

Onam:
Araştırmaya katılmayı kabul ettiğiniz takdirde derinize yapıştırılacak 4 elektrot ile vücudunuzun dışından, biyo-empedans ölçümünüz alınacak ve ölçüm sonuçlarınız önceden DEXA ile ölçülmüş kemik yoğunluğu test sonuçlarınızla karşılaştırılacaktır. Ayrıca, ölçüm kartında belirtilen anket sorularını cevaplamanızı da rica ediyoruz. İsminiz ve bu bilgiler tamamen gizli tutulacaktır.

Anket sonuçlarının cevaplanması dâhil, bu çalışma yalnızca 5 dakikanızı alacaktır.

Çalışmaya katılmanız tamamen isteğe bağlıdır. Sizden ücret talep etmiyoruz ve size herhangi bir ödeme yapmayacağız.

Bu araştırma bilimsel bir amaçla yapılmaktadır ve katılımcı bilgilerinin gizliliği esas tutulmaktadır. Sizden alınan ölçümler kimliğiniz belli edilmeden başka çalışmalar için de kullanılabilir. Seçilmiş ölçümler kimliği belirtilmeden bilimsel nitelikte sunumlarda kullanılabilir.

İstediğiniz zaman çalışmaya katılmaktan vazgeçebilirsiniz. Bu durumda sizden almış olduğumuz ölçümler imha edilecektir.

Yapmak istediğimiz araştırmanın ve biyo-empedans ölçümünün size risk getirmesi beklenmemektedir. Kalp pili yada, elektronik implant taşınması veya gebelik riski bulunduğunda, çalışılacak bölgelerde enfeksiyon olması ve elektrot malzemesine karşı bir allerji bulunması durumunda bu çalışma **kesinlikle** yapılmaz. Nadiren de olsa elektrik empedans ölçümü sırasında karıncalanma ya da ağrı hissedilebilir ve elektrot uygulama noktalarında elektrot jeline karşı hassasiyete bağlı geçici kızarıklık gözlenebilir. Biyo-empedans ölçümünün bunun dışında bilinen herhangi bir yan etkisi bulunmamaktadır. **Bu araştırmaya katılarak, ölçüm anında gebe olmadığınızı, kalp pili ya da elektronik implant taşımadığınızı ve kullanılacak tıbbi elektrot malzemesi ve solüsyonuna karşı bilinen bir allerjinizin olmadığını kabul ediyorsunuz.**

Araştırmanın ileride kemik erimesi riski taşıyan kişilerin erken teşhisine katkıda bulunarak insan sağlığına yarar sağlamasını beklemekteyiz.

Bu formu imzalamadan önce, çalışmayla ilgili sorularınız varsa lütfen sorun. Daha sonra sorunuz olursa, Fırat Matur (Telefon: 0552 ■■ ■53) sorabilirsiniz. Araştırmayla ilgili haklarınız konusunda yerel etik kurullarına da danışabilirsiniz.

Adres ve telefon numaranız değişirse, bize haber vermenizi rica ederiz.

Bana anlatılanları ve yukarıda yazılanları anladım. Bu formun bir kopyasını aldım.
Bu çalışmaya, hiçbir baskı ve zorlama olmaksızın kendi rızamla katılmayı kabul ediyorum.

Katılımcı Adı-Soyadı:……..
İmzası:……
Tarih (gün/ay/yıl):...../...../.....

Varsa Katılımcının Vasisinin Adı-Soyadı:.....

İmzası:.....

Tarih (gün/ay/yıl):...../...../.....

KALP PİLİ, ELEKTRONİK IMPLANT taşıyanlar ve HAMİLELER bu çalışmaya KATILAMAZ.

Araştırmacının Adı-Soyadı:……..
İmzası:.....

Tarih (gün/ay/yıl):...../...../.....

Figure 9.2 The informed consent form.

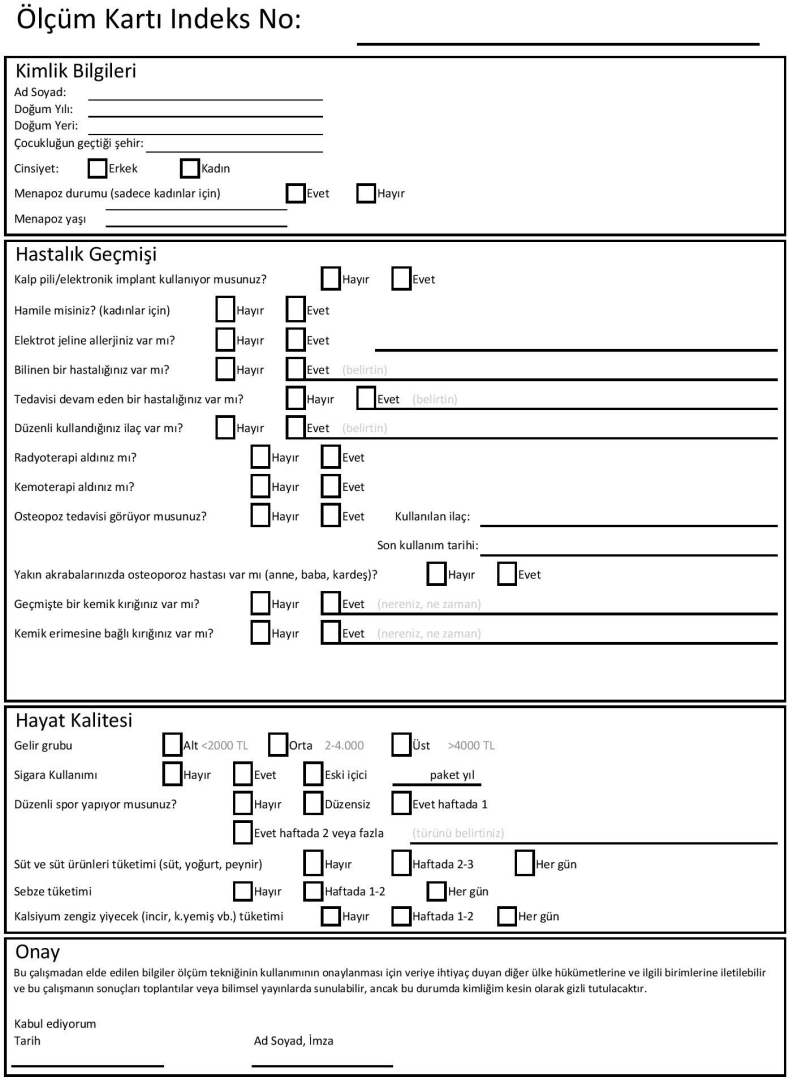

Ölçüm Kartı Indeks No: _____

Kimlik Bilgileri

Ad Soyad: _____
Doğum Yılı: _____
Doğum Yeri: _____
Çocukluğun geçtiği şehir: _____
Cinsiyet: ☐ Erkek ☐ Kadın
Menapoz durumu (sadece kadınlar için) ☐ Evet ☐ Hayır
Menapoz yaşı _____

Hastalık Geçmişi

Kalp pili/elektronik implant kullanıyor musunuz? ☐ Hayır ☐ Evet
Hamile misiniz? (kadınlar için) ☐ Hayır ☐ Evet
Elektrot jeline allerjiniz var mı? ☐ Hayır ☐ Evet _____
Bilinen bir hastalığınız var mı? ☐ Hayır ☐ Evet (belirtin) _____
Tedavisi devam eden bir hastalığınız var mı? ☐ Hayır ☐ Evet (belirtin) _____
Düzenli kullandığınız ilaç var mı? ☐ Hayır ☐ Evet (belirtin) _____
Radyoterapi aldınız mı? ☐ Hayır ☐ Evet
Kemoterapi aldınız mı? ☐ Hayır ☐ Evet
Osteopoz tedavisi görüyor musunuz? ☐ Hayır ☐ Evet Kullanılan ilaç: _____
Son kullanım tarihi: _____
Yakın akrabalarınızda osteoporoz hastası var mı (anne, baba, kardeş)? ☐ Hayır ☐ Evet
Geçmişte bir kemik kırığınız var mı? ☐ Hayır ☐ Evet (nereniz, ne zaman) _____
Kemik erimesine bağlı kırığınız var mı? ☐ Hayır ☐ Evet (nereniz, ne zaman) _____

Hayat Kalitesi

Gelir grubu ☐ Alt <2000 TL ☐ Orta 2-4.000 ☐ Üst >4000 TL
Sigara Kullanımı ☐ Hayır ☐ Evet ☐ Eski içici _____ paket yıl
Düzenli spor yapıyor musunuz? ☐ Hayır ☐ Düzensiz ☐ Evet haftada 1
☐ Evet haftada 2 veya fazla (türünü belirtiniz) _____
Süt ve süt ürünleri tüketimi (süt, yoğurt, peynir) ☐ Hayır ☐ Haftada 2-3 ☐ Her gün
Sebze tüketimi ☐ Hayır ☐ Haftada 1-2 ☐ Her gün
Kalsiyum zengiz yiyecek (incir, k.yemiş vb.) tüketimi ☐ Hayır ☐ Haftada 1-2 ☐ Her gün

Onay

Bu çalışmadan elde edilen bilgiler ölçüm tekniğinin kullanımının onaylanması için veriye ihtiyaç duyan diğer ülke hükümetlerine ve ilgili birimlerine iletilebilir ve bu çalışmanın sonuçları toplantılar veya bilimsel yayınlarda sunulabilir, ancak bu durumda kimliğim kesin olarak gizli tutulacaktır.

Kabul ediyorum
Tarih _____ Ad Soyad, İmza _____

Figure 9.3 The patient measurement card.

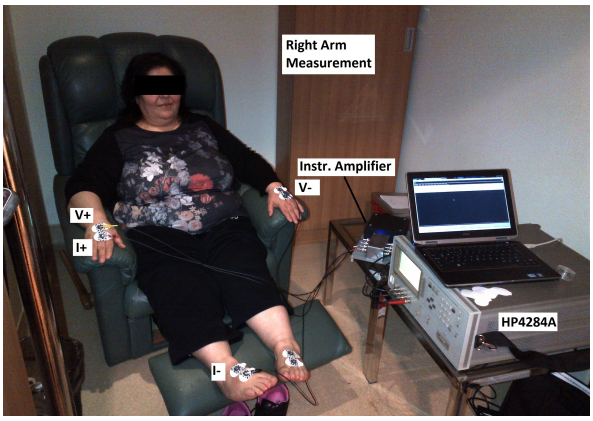

Figure 9.4 In RA impedance measurements, the current is injected between the right hand and right foot, and the voltage is measured between two hands.

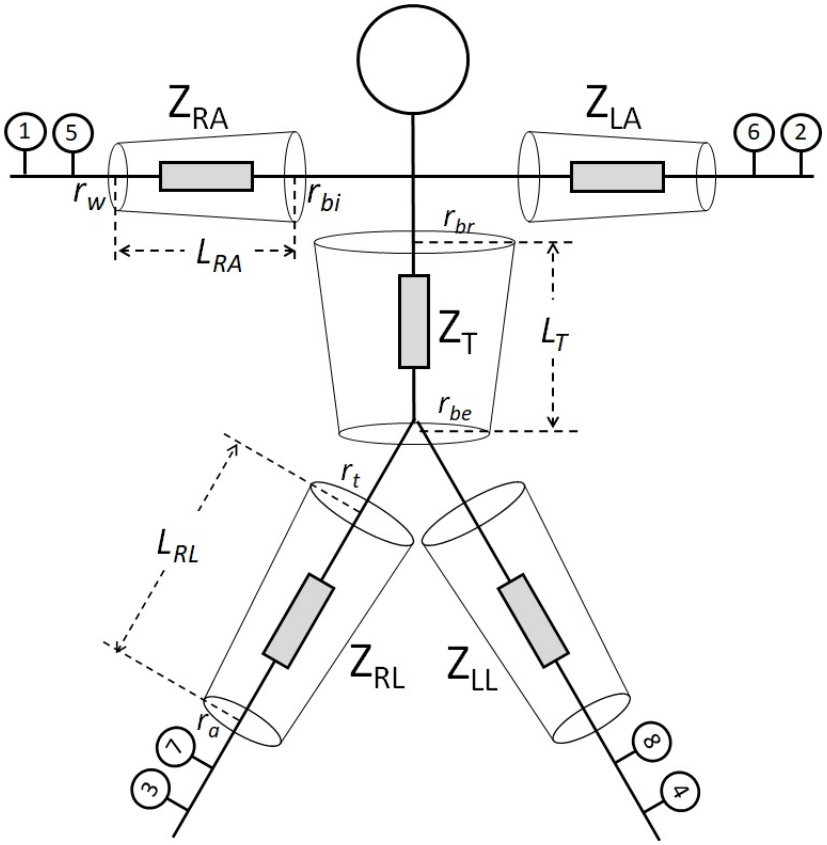

Figure 9.5 Body segmental impedances: r_w, r_{bi}, r_a, r_t, r_{br}, r_{be} refer to right wrist, right biceps, right ankle, right thigh, breast and belly radii calculated from their circumferences with the assumption of perfect circular shape at measurement points. L_{RA}, L_{RL} and L_T are the RA length from wrist to shoulder tip, RL length from ankle to hip, and from hip to clavicle respectively. Z_{RA}, Z_{LA}, Z_{RL}, Z_{RL} and Z_T are impedance of RA, LA, RL, LL and trunk respectively.

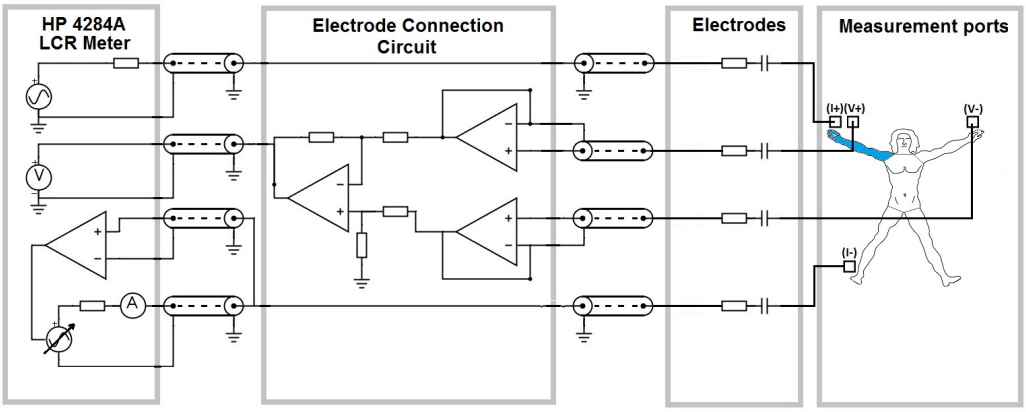

Figure 9.6 The front end designed to convert the LCR meter into a true tetra polar BI measurement system, with active electrode shielding. Electrodes are placed along the 3rd metacarpal bones of each hand and foot. To measure RA impedance, current ports are connected to RH and RF and voltage is measured between RH and LH.

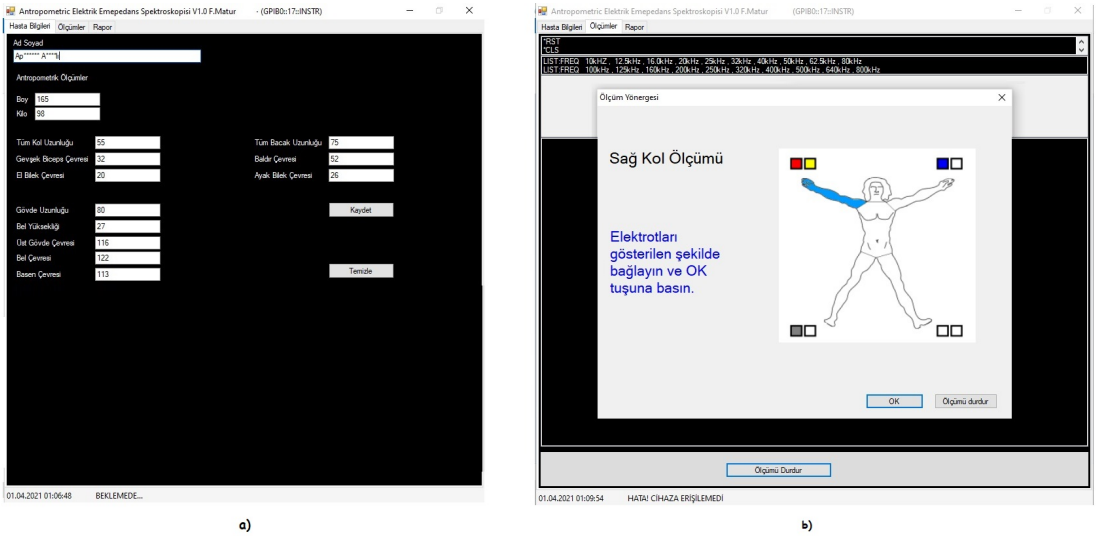

Figure 9.7 For performing the bioimpedance spectroscopy measurements with HP4284A, a special software is developed to ensure a) anthropometric data are captured correctly and b) electrodes are placed properly.

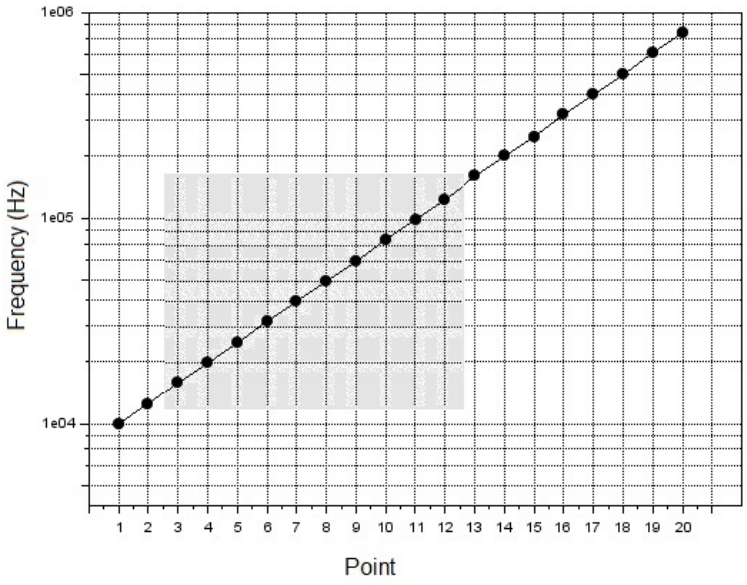

Figure 9.8 Logarithmic measurement frequency set. Shaded frequencies are the equidistant frequency set.

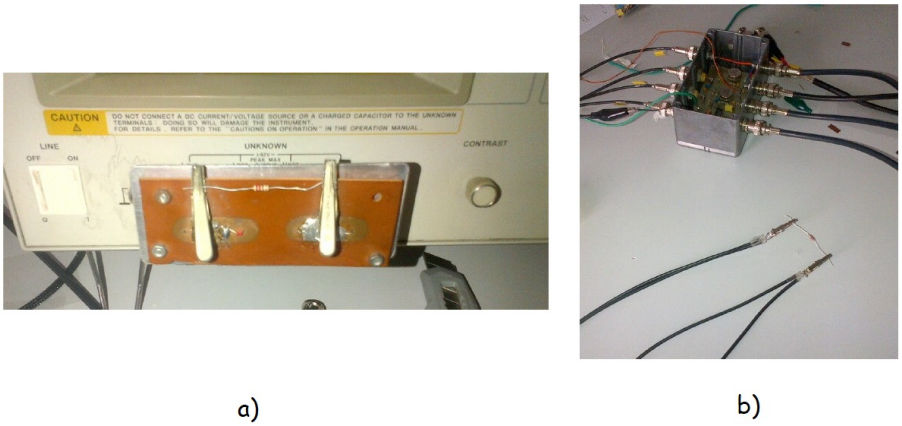

Figure 9.9 For finding transfer function of the HP4284 LCR meter measurement system a) resistive loads are directly connected to HP4284A as the reference load set, and then b) the same loads are connected with the front end amplifier included.

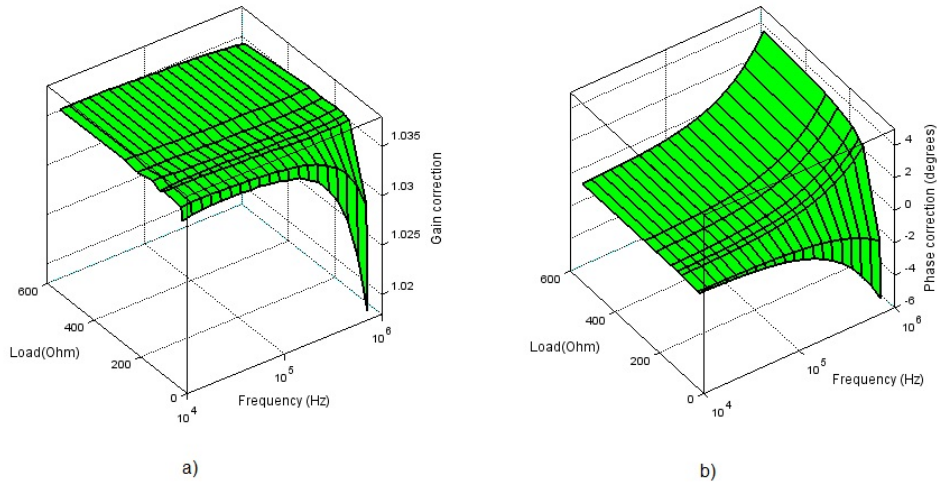

Figure 9.10 The HP4284A measurements normalized with the load dependent a) gain $|G(L, f)|$ and b) phase $\angle\Psi(L, f)$.

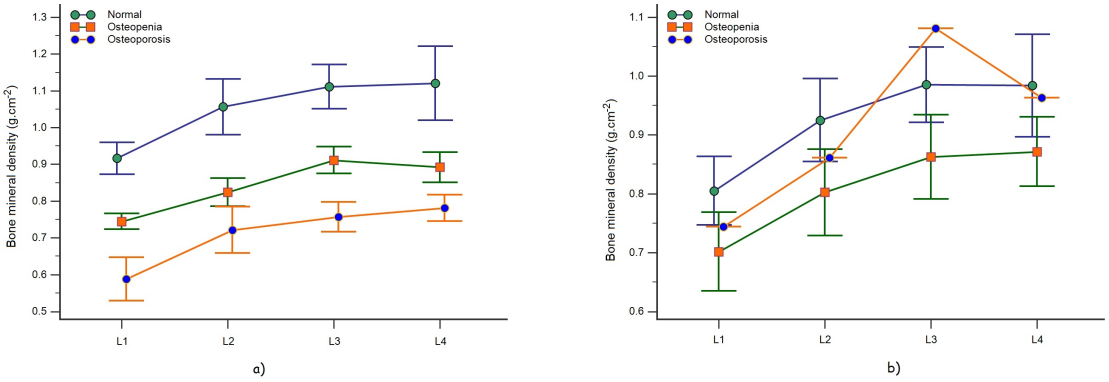

Figure 9.11 Bone mineral densities of L1 to L4 are increasing with the lumbar index, both for the subjects classified with a) their LBMD and b) their HBMD.

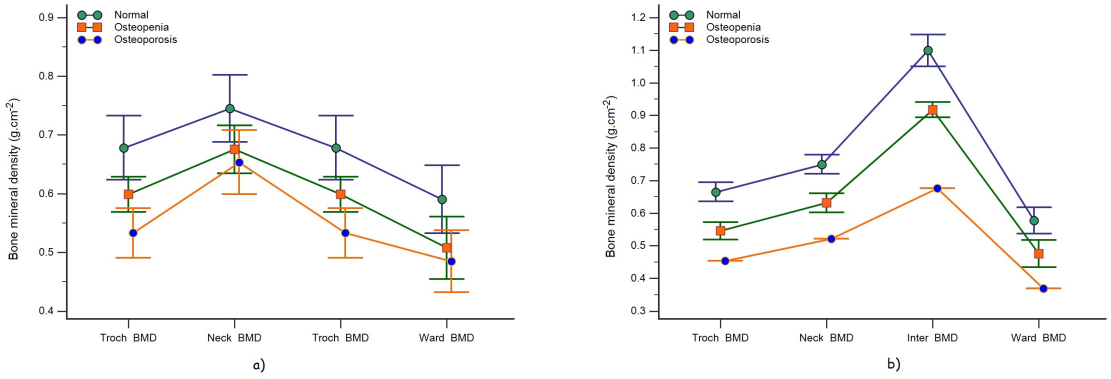

Figure 9.12 Bone mineral densities of Inter-trochanter, trochanter, femoral neck and Ward's area are decreasing with the lowered total bone mineral density both a) for WHO grouping with respect to their LBMD, and b) or WHO grouping with respect to their HBMD.

Table 9.5
Anthropometric dimensions and DEXA BMD scores of menopaused women with respect to their LBMD WHO classification (with the HP4284A).

	WHO class by LBMD					
	Normal		Osteopenia		Osteoporosis	
	Mean	SD	Mean	SD	Mean	SD
Number of subjects	12		18		10	
Age (year)	58.8	10.0	61.2	7.4	60.0	8.6
Age at menopause (year)	44.5	5.4	44.4	5.8	44.3	5.2
Height (cm)	152.3	8.5	150.8	4.5	155.1	7.1
Weight (kg)	74.8	13.4	76.4	13.9	72.3	8.6
BMI ($kg.m^{-2}$)	32.4	6.1	33.7	6.5	30.2	4.1
Arm length (cm)	47.9	3.9	48.9	3.3	47.8	4.0
Biceps perimeter (cm)	33.9	3.9	33.4	3.3	33.7	3.0
Wrist perimeter (cm)	17.3	1.3	17.7	1.8	16.9	1.2
Leg length (cm)	71.4	6.6	70.8	5.0	70.3	5.6
Thigh perimeter (cm)	58.9	4.9	55.0	9.1	57.1	7.4
Ankle perimeter (cm)	24.3	2.3	25.1	2.1	23.5	1.7
L1 BMD ($g.cm^{-2}$)	0.916	0.068	0.745	0.042	0.587	0.082
L2 BMD ($g.cm^{-2}$)	1.056	0.119	0.824	0.076	0.721	0.088
L3 BMD ($g.cm^{-2}$)	1.111	0.094	0.911	0.073	0.757	0.057
L4 BMD ($g.cm^{-2}$)	1.120	0.158	0.892	0.083	0.781	0.051
Total lumbar BMD ($g.cm^{-2}$)	1.059	0.102	0.850	0.041	0.721	0.040
Inter-trochanter BMD ($g.cm^{-2}$)	1.077	0.127	1.001	0.144	0.934	0.079
Trochanter BMD ($g.cm^{-2}$)	0.678	0.086	0.599	0.060	0.533	0.059
Femoral neck BMD ($g.cm^{-2}$)	0.745	0.090	0.675	0.082	0.654	0.076
Ward's area BMD ($g.cm^{-2}$)	0.590	0.091	0.508	0.107	0.485	0.073
Total hip BMD ($g.cm^{-2}$)	0.894	0.103	0.823	0.098	0.771	0.061

Table 9.6
Anthropometric dimensions and DEXA BMD scores of menopaused women with respect to their HBMD WHO classification.

	WHO class by total hip BMD					
	Normal		Osteopenia		Osteoporosis	
	Mean	SD	Mean	SD	Mean	SD
Number of subjects	21		18		1	
Age (year)	59.1	7.7	61.1	9.3	66.0	NA
Age at menopause (year)	42.5	5.4	46.3	4.8	49.0	NA
Height (cm)	152.6	6.7	152.0	6.9	153.0	NA
Weight (kg)	78.2	13.7	71.7	10.1	63.0	NA
BMI ($kg.m^{-2}$)	33.7	6.2	31.2	5.5	26.9	NA
Arm length (cm)	49.0	3.8	47.8	3.2	45.0	NA
Biceps perimeter (cm)	34.5	3.7	32.8	2.7	30.0	NA
Wrist perimeter (cm)	17.8	1.4	17.0	1.6	16.0	NA
Leg length (cm)	72.6	5.4	69.4	5.1	62.0	NA
Thigh perimeter (cm)	57.5	7.3	56.5	7.8	44.0	NA
Ankle perimeter (cm)	24.8	2.3	24.2	2.0	23.0	NA
L1 BMD ($g.cm^{-2}$)	0.805	0.128	0.702	0.134	0.744	NA
L2 BMD ($g.cm^{-2}$)	0.925	0.155	0.802	0.148	0.861	NA
L3 BMD ($g.cm^{-2}$)	0.985	0.141	0.863	0.144	1.081	NA
L4 BMD ($g.cm^{-2}$)	0.984	0.192	0.872	0.119	0.963	NA
Total lumbar BMD ($g.cm^{-2}$)	0.932	0.146	0.818	0.123	0.923	NA
Inter-trochanter BMD ($g.cm^{-2}$)	1.099	0.107	0.917	0.047	0.677	NA
Trochanter BMD ($g.cm^{-2}$)	0.665	0.064	0.546	0.053	0.454	NA
Femoral neck BMD ($g.cm^{-2}$)	0.750	0.065	0.632	0.059	0.521	NA
Ward's area BMD ($g.cm^{-2}$)	0.577	0.090	0.476	0.084	0.369	NA
Total hip BMD ($g.cm^{-2}$)	0.905	0.077	0.759	0.028	0.586	NA

Table 9.7
Demographic data of men.

Parameter	Mean	SD	Minimum	Maximum	Normal Distr. (P)
N=12					
Age (year)	58.7	13.6	40	82	0.632
Height (cm)	167.5	3.7	163.0	174.0	0.460
Weight (kg)	84.1	14.0	68.0	112.0	0.523
BMI ($kg.m^2$)	30.0	5.0	22.8	40.2	0.470
Arm length (cm)	54.9	3.4	50.1	62.9	0.162
Biceps perimeter (cm)	32.1	4.0	28.0	41.8	0.047
Wrist perimeter (cm)	18.9	1.4	17.0	21.3	0.893
Leg length (cm)	73.9	9.2	55.2	89.9	0.642
Thigh perimeter (cm)	55.7	12.0	46.1	88.8	0.000
Ankle perimeter (cm)	25.1	3.4	18.1	29.8	0.761

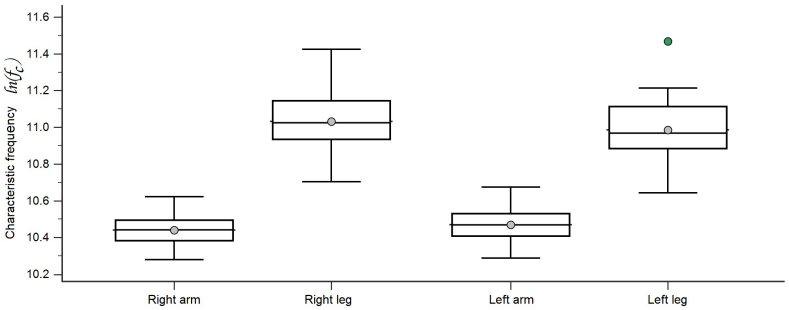

Figure 9.13 Box and Whisker diagrams for BIS model characteristic frequency for different limbs: using F-test, symmetrical limbs with respect to vertebra are similar to each other (P>0.05), and upper limbs are different from the lower limbs (P<0.05).

Table 9.8
Anthropometric dimensions and DEXA BMD scores of men with respect to their LBMD WHO classification.

	WHO classification by LBMD					
	Normal		Osteopenia		Osteoporosis	
	Mean	SD	Mean	SD	Mean	SD
N	9		2		1	
Age (year)	56.1	13.8	73.0	2.8	53.0	NA
Height (cm)	168.1	3.9	166.0	4.2	165.0	NA
Weight (kg)	83.9	15.3	78.0	4.2	98.0	NA
BMI (kg. m^{-2})	29.7	5.4	28.3	0.1	36.0	NA
Arm length (cm)	53.8	2.5	59.9	4.2	55.0	NA
Biceps perimeter (cm)	32.4	4.6	30.5	2.1	32.0	NA
Wrist perimeter (cm)	18.6	1.5	19.5	0.7	20.0	NA
Leg length (cm)	72.6	8.9	79.5	14.8	75.0	NA
Thigh perimeter (cm)	57.9	13.2	48.0	1.4	52.0	NA
Ankle perimeter (cm)	24.7	3.7	26.5	3.5	26.0	NA
L1 BMD (g.c m^{-2})	0.978	0.095	0.883	0.082	0.644	NA
L2 BMD (g.c m^{-2})	1.048	0.124	0.898	0.056	0.708	NA
L3 BMD (g.c m^{-2})	1.074	0.102	0.896	0.078	0.817	NA
L4 BMD (g.c m^{-2})	1.110	0.126	0.883	0.008	0.837	NA
Total lumbar BMD (g.c m^{-2})	1.056	0.100	0.888	0.010	0.760	NA
Inter-trochanter BMD (g.c m^{-2})	1.209	0.176	1.138	0.042	0.930	NA
Trochanter BMD (g.c m^{-2})	0.794	0.134	0.697	0.030	0.522	NA
Femoral neck BMD (g.c m^{-2})	0.853	0.128	0.730	0.107	0.679	NA
Ward's area BMD (g.c m^{-2})	0.688	0.186	0.471	0.139	0.384	NA
Total hip BMD (g.c m^{-2})	1.032	0.160	0.925	0.023	0.763	NA

Table 9.9
Anthropometric dimensions and DEXA BMD scores of men with respect to their total HBMD WHO classification.

	WHO class by total hip BMD					
	Normal		Osteopenia		Osteoporosis	
	Mean	SD	Mean	SD	Mean	SD
N	9		3		0	
Age (year)	61.0	14.1	51.7	11.1	NA	NA
Height (cm)	167.3	3.5	168.0	5.2	NA	NA
Weight (kg)	86.0	13.4	78.3	17.0	NA	NA
BMI ($kg.m^{-2}$)	30.7	4.5	27.9	7.1	NA	NA
Arm length (cm)	54.8	4.0	55.3	1.5	NA	NA
Biceps perimeter (cm)	33.0	4.2	29.4	2.3	NA	NA
Wrist perimeter (cm)	19.1	1.2	18.1	1.7	NA	NA
Leg length (cm)	76.0	8.2	67.7	10.9	NA	NA
Thigh perimeter (cm)	57.1	13.7	51.7	1.5	NA	NA
Ankle perimeter (cm)	26.0	2.9	22.4	4.0	NA	NA
L1 BMD ($g.cm^{-2}$)	0.969	0.105	0.830	0.166	NA	NA
L2 BMD ($g.cm^{-2}$)	1.015	0.141	0.932	0.197	NA	NA
L3 BMD ($g.cm^{-2}$)	1.034	0.130	0.989	0.156	NA	NA
L4 BMD ($g.cm^{-2}$)	1.087	0.156	0.937	0.087	NA	NA
Total lumbar BMD ($g.cm^{-2}$)	1.029	0.125	0.926	0.144	NA	NA
Inter-trochanter BMD ($g.cm^{-2}$)	1.238	0.145	0.983	0.057	NA	NA
Trochanter BMD ($g.cm^{-2}$)	0.795	0.134	0.636	0.101	NA	NA
Femoral neck BMD ($g.cm^{-2}$)	0.854	0.131	0.710	0.056	NA	NA
Ward's area BMD ($g.cm^{-2}$)	0.649	0.214	0.558	0.163	NA	NA
Total hip BMD ($g.cm^{-2}$)	0.905	0.077	0.759	0.028	NA	NA

Table 9.10
Comparison of BIS model parameters for all limb pairs, with HP4284A.

Limb pairs‡	Variance ratio ($P^{\dagger}$)			
	R_i $(\Omega.m)$	R_e $(\Omega.m)$	$ln(f_c)$ (Hz)	α
N	40	40	40	40
Vertical sym.				
RA and LA	1.0271 (0.934)	1.0127 (0.969)	1.0215 (0.947)	1.1069 (0.753)
RL and LL	1.2450 (0.497)	1.0814 (0.808)	1.0550 (0.868)	1.0436 (0.895)
Horizontal sym.				
RA and RL	1.1254 (0.714)	**8.5979 (<0.001)**	**2.9976 (0.001)**	1.1326 (0.699)
LA and LL	1.0771 (0.818)	**9.1808 (<0.001)**	**3.2302 (<0.001)**	1.0680 (0.838)
Cross sym.				
RA and LL	1.1063 (0.754)	**9.2976 (<0.001)**	**3.1624 (0.001)**	1.1821 (0.604)
LA and RL	1.1559 (0.653)	**8.4899 (<0.001)**	**3.0619 (0.001)**	1.0233 (0.943)

† When the associated two sided $P < 0.05$, the variances of the pairs are significantly different.

‡ RA: right arm, LA:left arm, RL: right leg, and LL: left leg.

Table 9.11
Correlation of Cole-cole parameters with anthropometric measurements.

Model parameters	Pearson coefficient $(r, P < 0.05)^{\dagger}$				
	Age	Menopause age	Height (cm)	Weight (kg)	BMI ($kg.m^{-2}$)
Right arm					
ECF[‡] $R_e(\Omega.m)$				0.275	0.361
Char. freq. $ln(f_c)(Hz)$		0.291			
Depression constant α				-0.392	-0.394
Left arm					
ECF $R_e(\Omega.m)$					0.294
Depression constant α				-0.528	-0.489
Right leg					
ECF $R_e(\Omega.m)$	-0.293				
Char. freq. $ln(f_c)(Hz)$	0.490				
Depression constant α					-0.529
Left leg					
ECF $R_e(\Omega.m)$	-0.276				
Char. freq. $ln(f_c)(Hz)$	0.457				
Depression constant α				-0.488	-0.447

[†] Only BIS model parameters with $P < 0.05$ are tabulated

[‡] ICF: Extracellular fluid resistance

Table 9.12
Correlation of Cole-cole parameters with the BMD results from the DEXA lumbar scans.

	Pearson coefficient $(r, P < 0.05)^{\dagger}$				
	L1	L2	L3	L4	Total Lumbar
Right arm					
Char. freq. $ln(f_c)(Hz)$	0.636	0.525	0.589	0.457	0.580
Left arm					
Char. freq. $ln(f_c)(Hz)$	0.433	0.476	0.425	0.426	0.473
Right leg					
NONE[§]					
Left leg					
ICF[‡] $R_i(\Omega.m)$	-0.324				
Char. freq. $ln(f_c)(Hz)$			0.277		

[†]Only BIS model parameters with $P < 0.05$ are tabulated

[‡]ICF: Intracellular fluid resistance

[§]NONE: BIS model parameter has no statistically meaningful correlation.

Table 9.13
Correlation of Cole-cole parameters with the BMD results from the DEXA hip scans.

	Pearson coefficient $(r, P < 0.05)^{\dagger}$				
	Inter-troch. BMD	Femure Neck BMD	Trochentar BMD	Wardś area BMD	Total hip BMD
Right arm					
ICF[‡] $R_i(\Omega.m)$		-0.346		-0.399	
Char. freq. $ln(f_c)(Hz)$	0.169				
Left arm					
ICF $R_i(\Omega.m)$		-0.324	-0.333		
Right leg					
Char. freq. $ln(f_c)(Hz)$				-0.389	
Left leg					
ICF $R_i(\Omega.m)$			-0.346		-0.329
Char. freq. $ln(f_c)(Hz)$				-0.349	

[†]Only BIS model parameters with $P < 0.05$ are tabulated

[‡]ICF: Intracellular fluid resistance

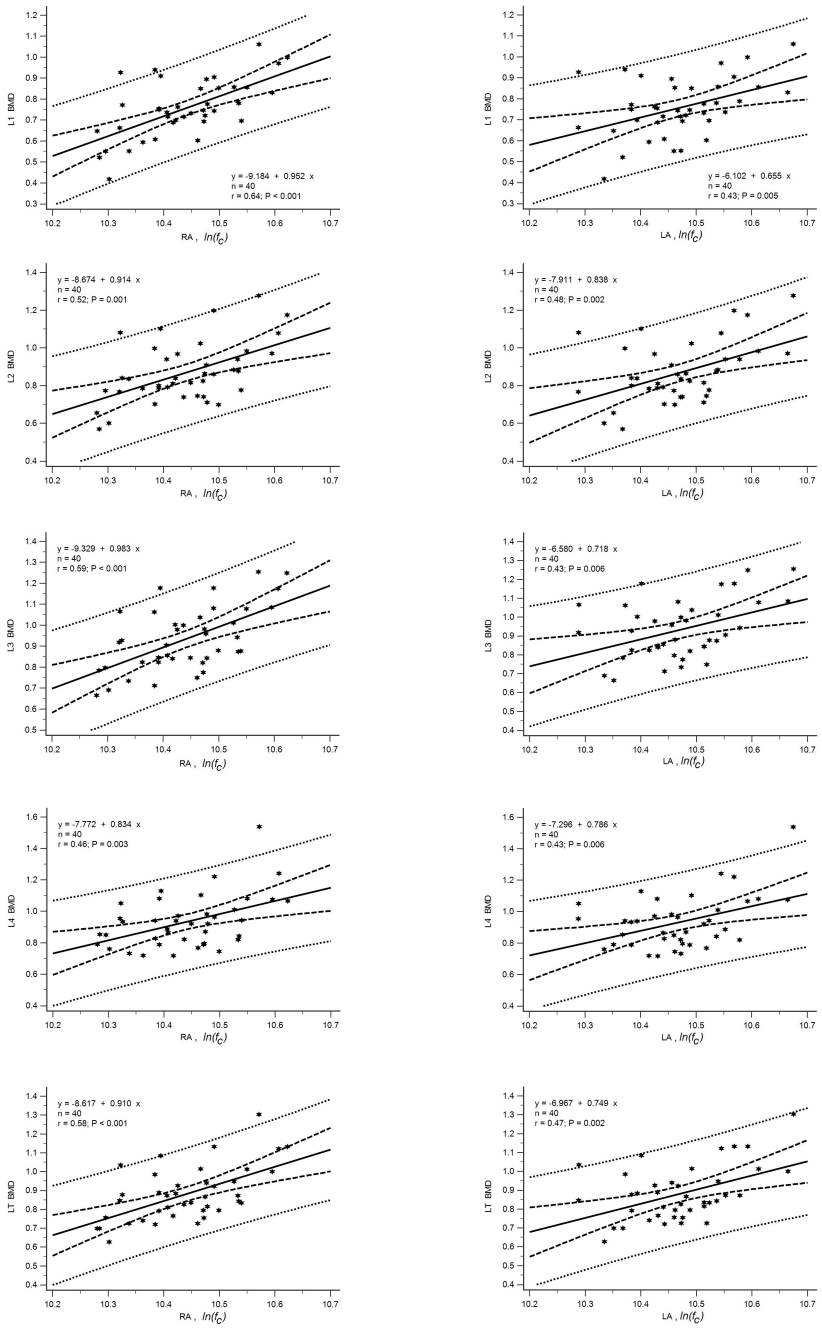

Figure 9.14 Characteristic frequencies versus the lumbar disk BMDs. The straight line shows the regression line, dashed lines show the 95% confidence interval, and dotted lines are the 95% prediction interval. Parameter x in the regression formula is the natural logarithm of the limb's BIS model characteristic frequency $ln(f_c)$ and y is the reference bone mineral density measured by DEXA.

Table 9.14
Pairwise comparison of f_c for the WHO subgroups of lumbar DEXA scan results, using Student-Newman-Keuls test.

Factor	N	Mean	SD	Different (P<0.05) from factor nr.
Right arm f_c				
(1) Normal	12	36489	3433	(2)(3)
(2) Osteopenia	18	34412	2219	(1)(3)
(3) Osteoporosis	10	31634	2310	(1)(2)
Left arm f_c				
(1) Normal	12	37179	4317	(3)
(2) Osteopenia	18	35080	2470	
(3) Osteoporosis	10	33807	2008	(1)

Table 9.15
Dominant arm f_c measurement and DEXA reference scores of followup patient.

Total Lumbar Spine Initial DEXA Meas. T: -2.7 (Osteoporosis) 21/02/17			
Measurement	f_c (kHz)	2 Level Classification[†]	3 Level Classification[‡]
1	33.057	Low BMD	Osteopenia
2	33.002	Low BMD	Osteopenia
3	28.285	Low BMD	Osteoporosis
4	34.531	Low BMD	Osteopenia
5	32.270	Low BMD	Osteoporosis
6	34.732	Low BMD	Osteopenia
7	25.478	Low BMD	Osteoporosis
8	31.478	Low BMD	Osteoporosis
Total Lumbar Spine Final DEXA Meas. T: -2.5 (Osteoporosis) 01/10/17			

[†] For total lumbar spine, f_c 35400 Hz is LOW BMD, otherwise Normal

[‡] For total lumbar spine, $f_c < 32359$ Hz is Osteoporosis,

and $f_c > 37775$ Hz is Normal, otherwise with Osteopenia

Table 9.16
Summary of statistics for the long term monitored characteristic frequency, f_c.

Name	Value
N	8
Lowest value	25478
Highest value	34732
Arithmetic mean	31604
95% Conf. Int. for the Arithmetic mean	28933 to 34274
Median	32636
95% Conf. Int. for the median	27753 to 34569
Standard deviation	3194
Coefficient of variance CV	0.1011 (10.11%)
Coefficient of Skewness	-1.1964 ($P = 0.1107$)
Coefficient of Kurtosis	0.7234 ($P = 0.5199$)

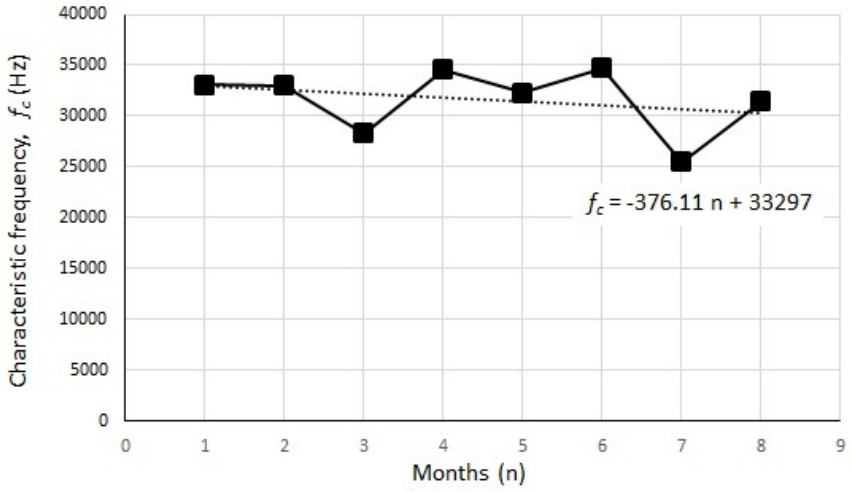

Figure 9.15 Characteristic frequency during long term monitoring.

Figure 9.16 BIS measurements room.

Figure 9.17 In Impedimed SFB7 clinical studies, the tetra-polar electrode measurement model is used. Two electrodes are placed on the 3^{rd} metacarpal bone of the DA, and two electrodes are placed at the infraclavicular fossa, 1 cm apart. The outer electrodes are used for applying current, and the inner electrodes are for sensing the voltage.

Table 9.17
Repeatability uncertainty (RU) and coefficient of variations ($c_v = \sigma/\mu$) of the Impedimed measurement system.

Impedance model parameters	RU	$c_v^{\dagger}$
R_i (Ω.cm)	5.108	1.37%
R_e (Ω.cm)	0.671	0.44%
α	0.002	1.13%
f_c (Hz)	301	1.24%

† Within day coefficient of variation

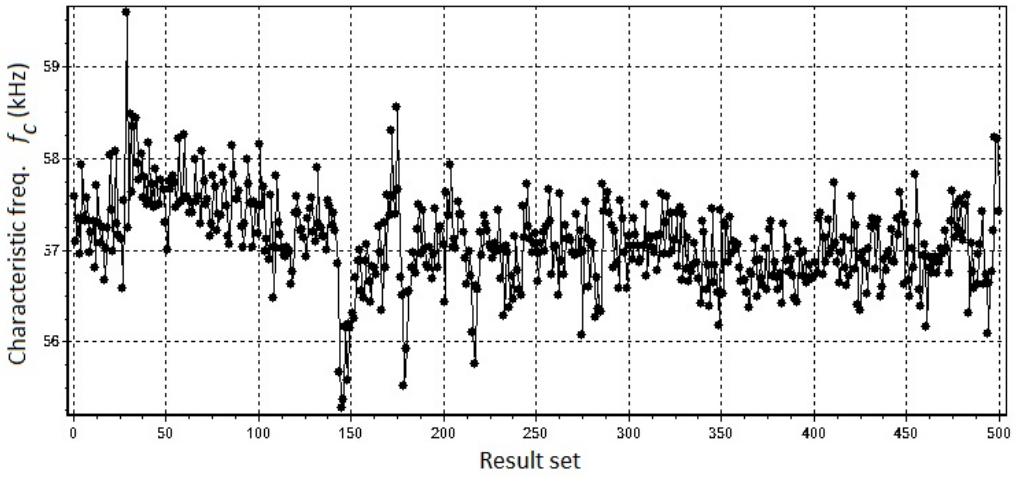

Figure 9.18 Impedimed measurement repeatability: the same subject measured 500 times in 5 minutes to find the Impedimed measurement repeatability.

Table 9.18
Demographic data of menopaused women.

Parameter	Mean	SD	Minimum	Maximum	Normal Dist. P
N=89					
Age (year)	59.0	9.3	32	80	0.7419
Age at menopause (year)	45.9	5.9	24	58	<0.0001
Height (cm)	156.0	6.9	143.0	175.0	0.0854
Weight (kg)	72.2	13.1	42.0	102.1	0.8756
BMI (kg.m2)	29.7	5.4	16.4	43.6	0.6315
Arm length (cm)	49.9	3.2	43.0	58.0	0.8993
Biceps perimeter (cm)	29.7	3.4	21.5	38.0	0.8562
Wrist perimeter (cm)	17.0	1.4	14.5	21.0	0.2411

Table 9.19
Anthropometric dimensions and BMD scores of menopaused women with respect to their LBMD WHO classification.

	WHO classification by LBMD					
	Normal		Osteopenia		Osteoporosis	
	Mean	SD	Mean	SD	Mean	SD
N	28		37		22	
Age (year)	59.5	9.9	58.3	9.1	59.7	9.4
Age at menopause (year)	46.8	6.0	46.3	4.0	44.1	7.9
Height (cm)	158.3	8.3	155.4	6.1	154.3	5.4
Weight (kg)	77.2	11.9	72.2	14.4	65.7	9.0
BMI ($kg.m^{-2}$)	31.0	5.1	30.0	6.2	27.7	4.0
Arm length (cm)	50.6	3.2	49.4	3.3	49.8	2.8
Biceps perimeter (cm)	30.6	3.0	30.0	3.6	27.9	2.9
Wrist perimeter (cm)	17.4	1.3	17.0	1.6	16.5	1.2
L1 BMD ($g.cm^{-2}$)	0.941	0.118	0.790	0.085	0.652	0.083
L2 BMD ($g.cm^{-2}$)	1.042	0.108	0.858	0.046	0.715	0.077
L3 BMD ($g.cm^{-2}$)	1.092	0.100	0.893	0.057	0.74	0.080
L4 BMD ($g.cm^{-2}$)	1.102	0.129	0.902	0.097	0.741	0.069
Total lumbar BMD ($g.cm^{-2}$)	1.045	0.085	0.862	0.045	0.721	0.060
Inter-trochanter BMD ($g.cm^{-2}$)	1.072	0.141	0.964	0.140	0.829	0.112
Trochanter BMD ($g.cm^{-2}$)	0.682	0.102	0.601	0.090	0.510	0.071
Femoral neck BMD ($g.cm^{-2}$)	0.833	0.187	0.694	0.103	0.627	0.068
Ward's area BMD ($g.cm^{-2}$)	0.708	0.264	0.543	0.140	0.449	0.109
Total hip BMD ($g.cm^{-2}$)	0.917	0.117	0.813	0.105	0.700	0.085

Table 9.20
Anthropometric dimensions and DEXA BMD scores of menopaused women with respect to their HBMD WHO classification.

	WHO class by total hip BMD					
	Normal		Osteopenia		Osteoporosis	
	Mean	SD	Mean	SD	Mean	SD
N	45		36		7	
Age (year)	59.6	9.7	58.3	9.1	59.7	9.4
Age at menopause (year)	46.8	5.9	46.3	4.0	44.1	7.9
Height (cm)	152.9	30.0	151.2	26.2	154.3	5.4
Weight (kg)	75.12	18.5	72.2	14.4	65.7	9.0
BMI ($kg.m^{-2}$)	31.2	5.2	30.0	6.2	27.7	4.0
Arm length (cm)	50.7	3.3	49.4	3.3	49.8	2.8
Biceps perimeter (cm)	30.8	3.1	30.0	3.6	27.9	2.9
Wrist perimeter (cm)	17.5	1.3	17.0	1.6	16.5	1.2
L1 BMD ($g.cm^{-2}$)	0.938	0.116	0.790	0.085	0.652	0.083
L2 BMD ($g.cm^{-2}$)	1.039	0.107	0.858	0.046	0.715	0.077
L3 BMD ($g.cm^{-2}$)	1.088	0.101	0.893	0.057	0.740	0.080
L4 BMD ($g.cm^{-2}$)	1.098	0.129	0.902	0.097	0.741	0.069
Total lumbar BMD ($g.cm^{-2}$)	1.041	0.086	0.862	0.045	0.721	0.060
Inter-trochanter BMD ($g.cm^{-2}$)	1.070	0.139	0.964	0.140	0.829	0.112
Trochanter BMD ($g.cm^{-2}$)	0.680	0.101	0.601	0.090	0.510	0.071
Femoral neck BMD ($g.cm^{-2}$)	0.829	0.185	0.694	0.103	0.627	0.068
Ward's area BMD ($g.cm^{-2}$)	0.701	0.262	0.543	0.140	0.449	0.109
Total hip BMD ($g.cm^{-2}$)	0.915	0.116	0.813	0.105	0.700	0.085

Table 9.21
Correlation of dominant arm BIS model parameters with the anthropometric measurements.

	Pearson coefficient $(r, P < 0.05)^{\dagger}$				
Model parameters	Age (years)	Meno.age age (years)	Height (cm)	Weight (kg)	BMI ($kg.m^{-2}$)
ICF§ R_i $(\Omega.m)$	NS	NS	NS	0.569	0.596
ECF‡ R_e $(\Omega.m)$	NS	NS	NS	0.667	0.689
Char. freq. f_c (Hz)	NS	NS	NS	NS	NS
Char. freq. $ln(f_c)$ (Hz)	NS	NS	NS	NS	NS
Depression constant α	NS	NS	NS	NS	NS

† NS:Statistically not significant if $P < 0.05$

§ ICF: Intracellular fluid resistance

‡ ECF: Extracellular fluid resistance

Table 9.22
Correlation of dominant arm BIS model parameters with lumbar BMD results.

	Pearson coefficient $(r, P < 0.05)^{\dagger}$				
	L1	L2	L3	L4	Total Lumbar
N=89					
ICF‡ $R_i(\Omega.m)$	0.326	NS	0.301	0.283	0.313
ECF△ $R_e(\Omega.m)$	0.330	NS	0.317	0.288	0.326
Char. freq. $f_c(Hz)$	NS	NS	NS	NS	NS
Char. freq. $ln(f_c)(Hz)$	NS	NS	NS	NS	NS
Depr. factor α	0.365	0.373	0.360	0.319	0.381

† Only BIS model parameters with $P < 0.05$ are tabulated

‡ ICF: Intracellular fluid resistance

△ ECF: Extracellular fluid resistance

§ NS: No statistically meaningful correlation $(P > 0.05)$.

Table 9.23
Correlation of dominant arm BIS model parameters with hip BMD results.

	Pearson coefficient $(r, P < 0.05)^{\dagger}$				
	Inter-trochanter BMD	Femure Neck BMD	Trochentar BMD	Wardś area BMD	Total hip BMD
ICF‡ $R_i(\Omega.m)$	NS	0.326	0326	NS	0.311
ECF$^{\triangle}$ $R_e(\Omega.m)$	0.448	0.408	0.464	NS	0.487
Char. freq. $f_c(Hz)$	-0.426	-0.228	-0.385	NS	-0.408
Char. freq. $ln(f_c)(Hz)$	-0.432	NS	-0.384	NS	-0.412
Depr. constant α	0.332	NS	NS	NS	0.310

† Only BIS model parameters with $P < 0.05$ are tabulated

‡ ICF: Intracellular fluid resistance

$^{\triangle}$ ECF: Extracellular fluid resistance

§ NS: No statistically meaningful correlation $(P > 0.05)$

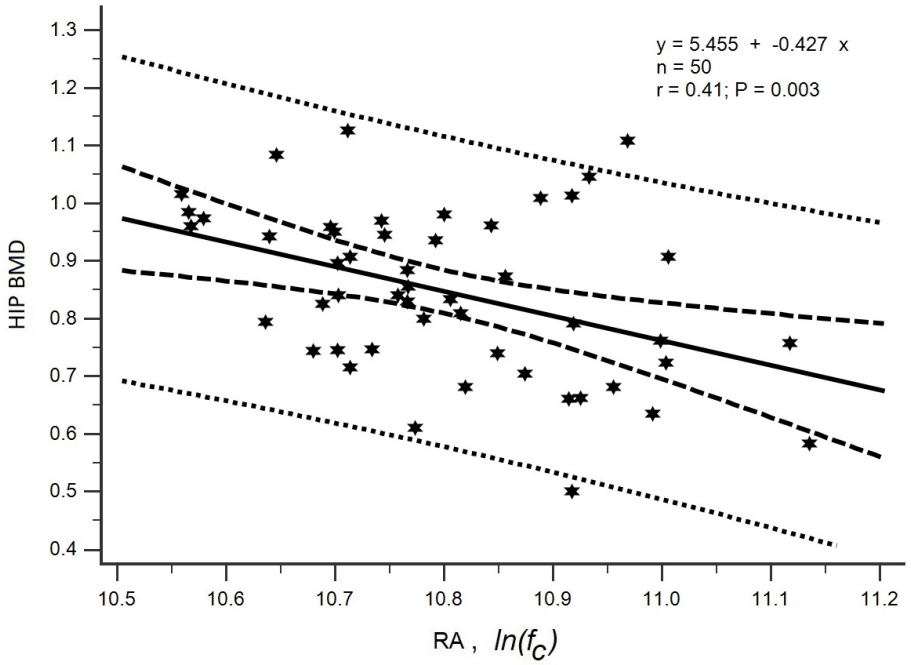

Figure 9.19 Regression line of the characteristic frequency and hip bone mineral density.

Table 9.24
Pairwise comparison of dominant arm f_c and $ln(f_c)$ for the WHO subgroups of hip DEXA scan results, using Student-Newman-Keuls test.

		$(P < 0.05)$					
		f_c			$ln(f_c)$		
Factor	N	Mean	SD	Diff.	Mean	SD	Diff.
(1) Normal	30	47157	5776	(3)	10.7541	0.1209	(2)(3)
(2) Osteopenia	17	51701	6907		10.8450	0.1320	(1)
(3) Osteoporosis	4	57435	8649	(1)	10.9499	0.1508	(1)

Table 9.25
BIS model parameters: comparison of different electrodes and instruments.

	Impedimed SFB7			HP4284A
Parameters†	Skintact RT38	Impedimed	Arbo Kendall	Arbo Kendall
R_e (Ω)	429.7	429.1	335.4	324.1
R_i (Ω)	1353.4	1355.2	918.8	1131.2
f_c (Hz)	53700	56400	63600	41693
Depression constant α	0.678	0.683	0.707	0.767

† Before anthropometric normalization.

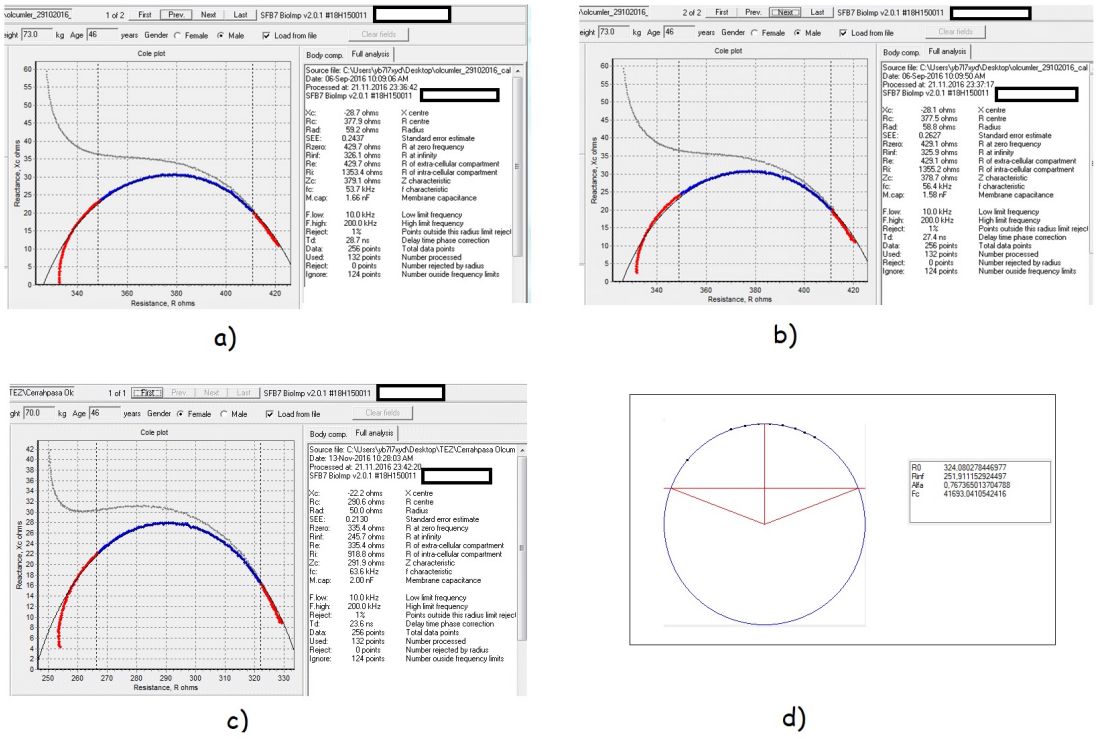

Figure 9.20 Effects of electrodes and the instruments on the measurements: with Impedimed SFB7 a) using Skintact RT38 electrodes, b) using Impedimed propriety electrodes, c) using Ag/AgCl Arbo Kendall electrodes, and d) with HP4284A using Ag/AgCl Arbo Kendall electrodes.

Table 9.26
Impedance angle Φ for different LHBM DEXA groups.

Frequency	Φ in degrees (mean ± SD)		
	Normal	Osteopenia	Osteoporosis
Group 1: BMI < 30 kg.m^{-2}			
5 kHz	2.360 ± 0.311	2.087 ± 0.262	2.109 ± 0.271
10 kHz	3.159 ± 0.430	3.027 ± 0.398	2.971 ± 0.369
15 kHz	3.771 ± 0.496	3.671 ± 0.476	3.595 ± 0.424
20 kHz	4.180 ± 0.531	4.107 ± 0.516	4.019 ± 0.445
25 kHz	4.448 ± 0.543	4.400 ± 0.535	4.307 ± 0.451
30 kHz	4.629 ± 0.550	4.603 ± 0.543	4.509 ± 0.449
Group 2: BMI > 30 kg.m^{-2}			
5 kHz	2.323 ± 0.201	2.473 ± 0.271	2.555 ± 0.148
10 kHz	3.123 ± 0.342	3.240 ± 0.434	3.218 ± 0.564
15 kHz	3.713 ± 0.391	3.873 ± 0.505	3.839 ± 0.663
20 kHz	4.108 ± 0.407	4.297 ± 0.545	4.253 ± 0.716
25 kHz	4.366 ± 0.405	4.573 ± 0.566	4.527 ± 0.743
30 kHz	4.545 ± 0.398	4.766 ± 0.581	4.707 ± 0.757

Table 9.27
Impedance angle Φ for different HBMD DEXA groups.

Frequency	Φ in degrees (mean ± SD)		
	Normal	Osteopenia	Osteoporosis
Group 1: BMI < 30 kg.m^{-2}			
5 kHz	2.325 ± 0.276	2.130 ± 0.266	1.871 ± 0.189
10 kHz	3.208 ± 0.384	3.040 ± 0.354	2.589 ± 0.249
15 kHz	3.850 ± 0.447	3.676 ± 0.412	3.141 ± 0.298
20 kHz	4.277 ± 0.481	4.104 ± 0.438	3.537 ± 0.336
25 kHz	4.559 ± 0.495	4.392 ± 0.446	3.815 ± 0.364
30 kHz	4.745 ± 0.505	4.592 ± 0.450	4.023 ± 0.387
Group 2: BMI > 30 kg.m^{-2}			
5 kHz	2.429 ± 0.252	2.356 ± 0.227	2.387 ± 0.170
10 kHz	3.264 ± 0.402	2.985 ± 0.413	3.433 ± 0.170
15 kHz	3.890 ± 0.467	3.572 ± 0.494	4.066 ± 0.110
20 kHz	4.308 ± 0.497	3.965 ± 0.539	4.491 ± 0.051
25 kHz	4.580 ± 0.508	4.225 ± 0.564	4.769 ± 0.007
30 kHz	4.769 ± 0.514	4.403 ± 0.578	4.953 ± 0.075

Table 9.28
Correlation of impedance angle Φ with the bone mineral densities.

	Impedance angle ($r, P < 0.05$)	
Frequency	LBMD	HBMD
Group 1: BMI < 30 kg.m^{-2}		
5 kHz	0.403	0.559
10 kHz	0.265 †	0.492
15 kHz	NS	0.472
20 kHz	NS	0.455
25 kHz	NS	0.442
30 kHz	NS	0.422
Group 2: BMI > 30 kg.m^{-2}		
5 kHz	-0.332†	-0.003†
10 kHz	NS	NS
15 kHz	NS	NS
20 kHz	NS	NS
25 kHz	NS	NS
30 kHz	NS	NS

NS: Statistically not significant

† $P < 0.1$

Table 9.29
Lumbar area ROC curve analysis summary, when the criterion is arm f_c.

Model parameter and	Right arm f_c		Left arm f_c	
criterion for diseased	T< −1	T< −2.5	T< −1	T< −2.5
Demographics				
Sample size	40	40	40	40
Positive group	28 (70.00%)	10 (25.00%)	28 (70.00%)	10 (25.00%)
Negative group	12 (30.00%)	30 (75.00%)	12 (30.00%)	30 (75.00%)
Area under the ROC curve (AUC)				
Area under the ROC curve (AUC)	0.753	0.843	0.705	0.7
Standard Error[§]	0.0944	0.0697	0.112	0.0863
95% Confidence interval[†]	0.591 to 0.875	0.694 to 0.939	0.540 to 0.839	0.535 to 0.834
z statistic	2.681	4.925	1.837	2.316
Significance level P (Area=0.5)	0.0073	0.0001	0.0662	0.0205
Youden index				
Youden index J	0.4524	0.5667	0.5119	0.4333
95% Confidence interval[‡]	0.1689 to 0.6429	0.2756 to 0.7667	0.2262 to 0.7619	0.2005 to 0.6208
Associated criterion	≤35400	≤32360	≤37663	≤35422
95% Confidence interval[‡]	≤30360 to ≤37775	≤29789 to ≤35312	≤37003 to ≤39274	≤34887 to ≤37003
Sensitivity	78.57	70	92.86	90
Specificity	66.67	86.67	58.33	53.33

[§] Using DeLong *et al.* method to find AUC [209].

[†] Binomial Confidence Interval is calculated exactly using the area under the curve

[‡] Bootstrap confidence interval [210, 211].

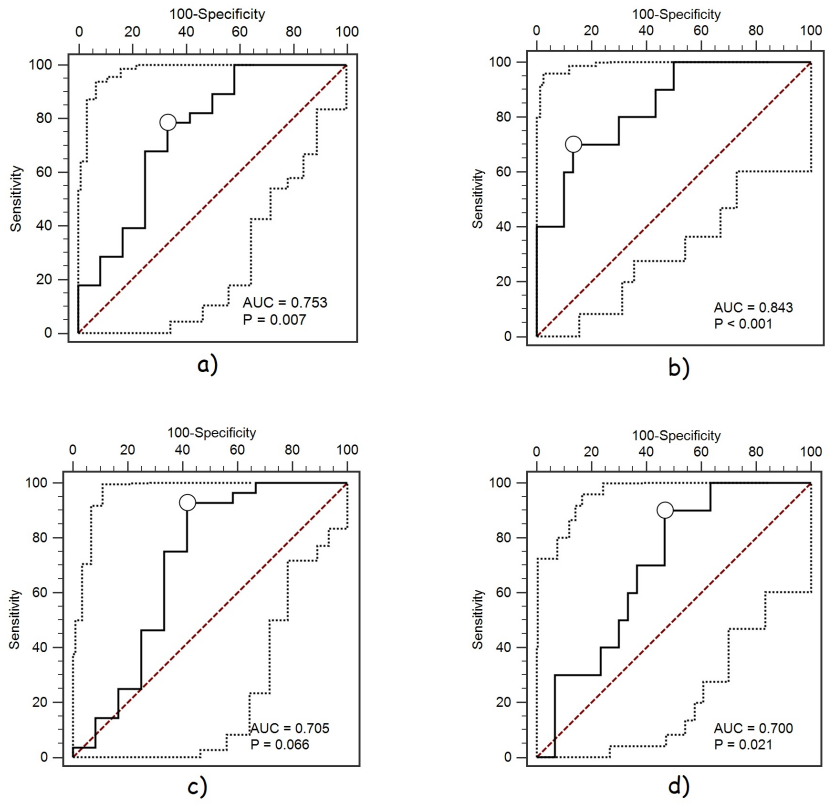

Figure 9.21 ROC curve analysis using arm f_c, when criterion is a) RA f_c and diseased if T< -1, b) RA f_c and diseased if T< -2.5, c) LA f_c and diseased if T< -1, and d) LA f_c and diseased if T< -2.5. Dotted lines show the confidence interval and dashed lines are the blind guess diagonal where AUC=0.5.

Table 9.30
By using the 2D-ROC for paired test, both the mis-classification rate and the accuracy are improved.

	ROC Curve		2D Roc
	f_c (Hz)	BMI (kg.m^{-2})	f_c and BMI
Associated criterion	≤32360	≤32.9	AVERAGE
TN	26	13	24
FP	4	17	6
TP	6	9	9
FN	4	1	1
Sensitivity	60.0%	90.0%	90.0%
Specificity	86.7%	43.3%	80.0%
Sensitivity x Specificity	52.0%	39.0%	72.0%
Mis-classification Rate	20.0%	45.0%	17.5%
Correct classification rate (accuracy)	80.0%	55.0%	82.5%

Table 9.31
Impedimed group 1 study: hip area ROC curve analysis summary, when the criterion is arm f_c and $ln(f_c)$ they have the same results.

Model parameter and criterion for diseased	f_c	
	T< −1	T< −2.5
Demographic		
Sample size	50	50
Positive group	26 (52.00%)	9 (18.00%)
Negative group	24 (48.00%)	41 (82.00%)
Area under the ROC curve (AUC)		
Area under the ROC curve (AUC)	0.651	0.748
Standard Error§	0.079	0.086
95% Confidence interval†	0.503 to 0.780	0.605 to 0.860
z statistic	1.911	2.871
Significance level P (Area=0.5)	0.056	0.004
Youden index		
Youden index J	0.2853	0.4363
95% Confidence interval‡	0.1314 to 0.4199	0.2033 to 0.6098
Associated criterion	>49097	>49565
95% Confidence interval‡	>41570 to >54947	>44247 to >57753
Sensitivity %	57.69	77.78
Specificity %	70.83	65.85

§ Using DeLong *et al.* method to find AUC [209].

† Binomial Confidence Interval is calculated exactly using the area under the curve

‡ Bootstrap confidence interval [210, 211].

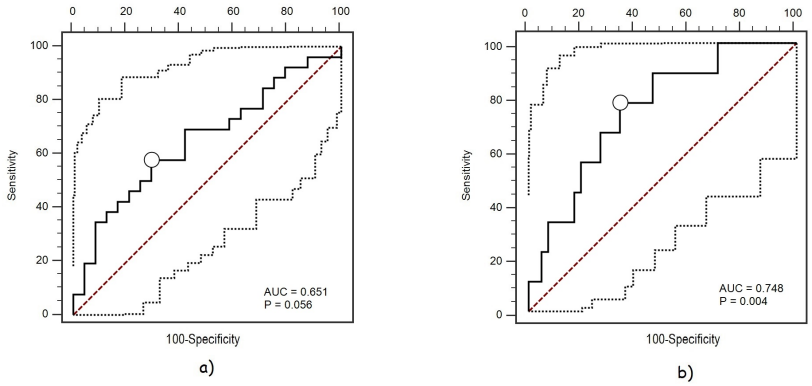

Figure 9.22 Study with the Impedimed, ROC curve analysis using arm f_c, when criterion is a) DA f_c and diseased if T< −1, and b) DA f_c and diseased if T< −2.5. Dotted lines show the confidence intervals and dashed lines are the blind guess diagonal where AUC=0.5. The graphics for $ln(f_c)$ are exactly same as f_c graphics.

Table 9.32
HIP bone mineral deficiency analysis using ROC and 2D-ROC.

	ROC		2D-ROC		
	BMI ($kg.m^{-2}$)	$\ln(f_c)$	BOTH	ANY	AVERAGE
True positive rate‡	71.4%	81.0%	95.2%	61.9%	76.2%
True negative rate§	84.4%	56.3%	28.1%	90.6%	83.9%
Correct classification rate	79.2%	66.0%	54.7%	79.2%	80.8%
Mis-classificaton rate	20.8%	34.0%	45.3%	20.8%	19.2%

‡ True positive rate, TPR = TP/(TP + FN)

§ True negative rate, TNR = TN/(TN + FP)

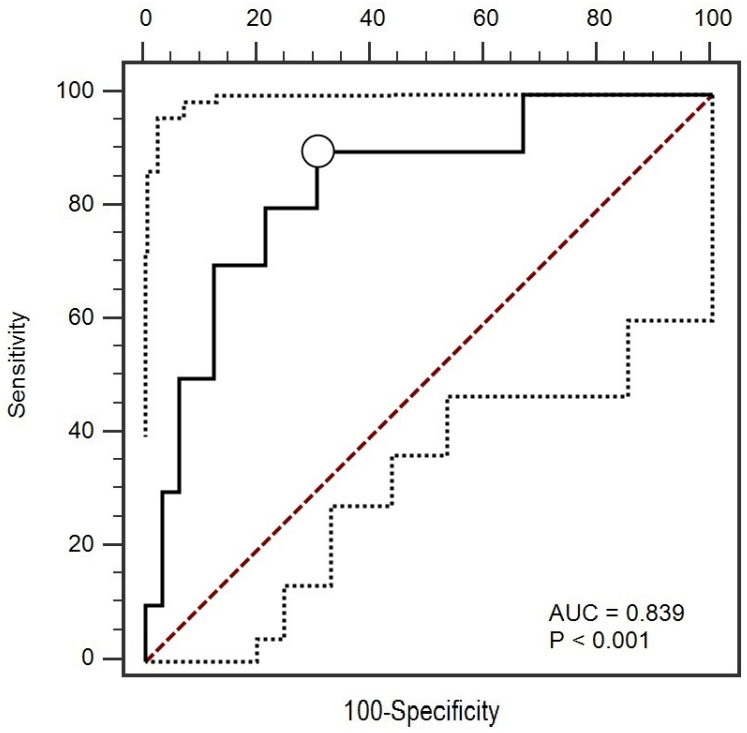

Figure 9.23 ROC curve analysis for normal weight subjects. AUC is the maximum observed AUC in this study ($0.839, P < 0.001$).

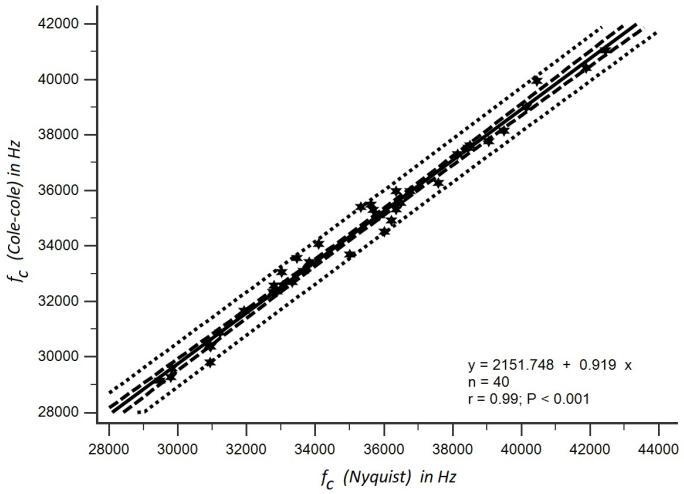

Figure 9.24 The BIS characteristic frequency by the 3-point Nyquist method and Cole-cole plot. Dotted lines are the 95% prediction zone, dashed lines are the 95% confidence zone and the straight line is the regression line.

Table 9.33
The statistical result comparison of Cole-cole and novel 3 point Nyquist method characteristic frequencies.

	Total lumbar BMD ($P < 0.05$)	
	Cole-cole f_c	3P-Nyquist f_c
N=40		
Correlation, r	0.587	0.572
AUC ($T < -1$)†	0.753	0.735
AUC ($T < -2.5$)	0.843	0.807

When T< -1, subjects with osteopenia are considered as diseased.

and when T< -2.5, they are considered as normal.

10. DISCUSSION

While measurements with the HP4284A LCR meter have shown positive correlations with the LBMD ($r = 0.580, P < 0.001$) and no statistically significant correlation with HBMD (P>0.05), Impedimed study group 1 have shown a moderate negative correlation with HBMD ($r = -0.408, P < 0.003$) no statistically significant correlation with the LBMD ($P > 0.05$), Impedimed study group 2 does not have a statistically significant neither with LBMD nor HBMD ($P > 0.05$). Results are tabulated in Table 10.1, the only moderate correlation observed between the BIS model parameters and DEXA reference bone mineral densities is between the characteristic frequency and the LBMD.

Multiple comparison graphs for the BIS model characteristic frequencies for HP4284A and SFB7 Impedimed studies are reversed in shape; however, and the frequency ranges for all WHO T score groups in the Impedimed study are higher than the ranges found in the HP4284A study. Side by side comparison of calculated characteristic frequencies is illustrated in Figure 10.1.

When BIS is used for central bone mineral density assessment, measurement has shown a region specificity based on the sense electrode placements. When the negative sense electrode is placed over the infraclavicular fossa, the observed correlation between the BIS characteristic frequency is negatively correlated with the hip BMD ($r = -0.412, P < 0.05$), and when negative sense electrode is placed on the inferior hand then the correlation is positive with the lumbar BMD ($r = 0.580, P < 0.05$).

When ROC cutoff frequencies are calculated to use for the optimal frequency in two-way classification; if subjects with osteopenia are considered as diseased, i.e., diseased if $T < -1$, the cutoff frequency for HP4284A study is 35400 Hz (between 30360 and 37775 Hz, with 95% confidence), whereas for Impedimed study it is 49310 Hz (between 48413 and 58533 Hz, with 95% confidence).

If the subjects with osteopenia are considered as normal, i.e., diseased if $T < -2.5$, the cutoff frequencies calculated for HP4284A and Impedimed are 32359 Hz (between 29789 and 35311 Hz, with 95% confidence) and 49097 Hz (between 41570 and 54947 Hz, with 95% confidence) respectively. However, for HP4284A frequencies below the cutoff frequency is the diseased range, but for Impedimed group 1 it is when higher than cutoff. For Impedimed group 2 study, the ($AUC = 0.562, P = 0.560$) and statistically not significant, cutoff frequency is not calculated.

If the disease prevalence criterion is $T < -1$, i.e. subjects with osteopenia are considered as diseased, then with 95% confidence, the cutoff frequencies calculated with HP4284A and Impedimed are 35340 Hz (between 30360 and 37775 Hz, with 95% confidence) and 49565 Hz (between 44247 and 57753 Hz, with 95% confidence) respectively. However, with HP4284A frequencies below the cutoff frequency is the diseased range, but with the Impedimed group 1, it is when higher than cutoff. For Impedimed group 2 study, the ($AUC = 0.677, P = 0.527$) and statistically not significant, therefore the cutoff frequency is not calculated.

The use of different electrodes may impact on the Impedimed measurements, in the range of 10 kHz as tabulated in Table 9.25. Differences in the measurements may be partially explained by the the fact that different electrodes are used. However, the polarization change for the cutoff frequencies and why different systems have sensitivities at different patient sites are not clear.

The subjects who participated in the HP4284A study are those who have visited the hospital for bone mineral density screening. However, the subjects in the Impedimed study are already and have their bone mineral regularly controlled. For the Impedimed study, the bone mineral density reduction might be due to secondary osteoporosis that patients are not aware of or reluctant to share their medical history.

Impedimed is a device designed for a whole-body analysis, and calculates the BIS model parameters using its own software. The device's internal structure is not known, and it has some built-in functions to compensate electrode lead transmission

delays, in which the underlying algorithm is not clear. The HP4284A front-end uses active electrode lead shielding; hence placing signal and sensing electrodes to separate limbs is not changing the measurement quality. However, in Impedimed measurements, the leads have injection plastic around as insulator, making it impossible to check if there is an active drive for the lead shielding. With Impedimed, to complete measurements successfully, it is mandatory to closely place signal and sense electrodes (1 cm separation) whereas for HP4284A this is not required. When the same lead connection scheme of HP4284A is attempted, i.e., signal and sense electrodes are placed on different limbs, Impedimed proprietary analysis software could not calculate BIS model parameters, suggesting the leads might not be adequately shielded.

During the measurements, the environment is maintained similar. However, the layout of the measurement rooms is entirely different. HP4284A measurement is performed in an injection room, in which there is no visible metal in the patient's vicinity. Whereas, Impedimed measurement is done in the DEXA measurement room, where the bed on which the subjects are sitting is metallic. There is 1.5 meters by 1.5 meters and a 5 cm thick lead panel approximately 100 cm away from the subject to protect the DEXA operator from the DEXA radiation, which may negatively impact on the measurement results. Furthermore, when Group 2 measurements are performed, the metallic shield is even closer, approximately 50 cm.

Both studies show that the BIS characteristic frequency from the arms has some statistically significant correlation with the lumbar area bone mineral density or hip bone mineral density depending on the measurement device, and HP4284A measurement from legs does not show any correlation. For women, anatomically, fat is primarily accumulated in the lower body. In line with the study of Heidi H. Y. Ngai *et al.* in which foot to foot bioimpedance is measured to analyze its correlation to bone mineral density, our study also did not show any statistically significant ($P > 0.05$) correlation when legs are used for the measurement either.

In order to analyze the effect of body mass index over the correlations, the subjects are divided into two subgroups as *Normal to Obese range, BMI* $< 30\ kg.m^{-2}$,

and *Severe to morbid obese range, BMI > 30 kg.m^{-2}.*

When the study is limited for BMI < 30 kg.m^{-2}, the correlation of the f_c with the lumbar spine BMD is statistically significant for both studies: for HP4284A ($r = 0.599, P < 0.001$) and for Impedimed ($r = -0.294, P = 0.10$). For total hip BMD, HP4284A study shows a correlation if confidence interval is extended ($r = 0.333, P = 0.064$), and Impedimed study has moderate negative correlation ($r = -0.541, P = 0.006$).

When $BMI > 30$ kg.m^{-2}, unless statistically significance boundary is extended to $P < 0.1$ there is no correlation between the f_c and the bone mineral densities in both studies. However, when the significance criterion is changed to ($P < 0.10$) then for HP4284A study the correlation of f_c with the LBMD is ($r = 0.610, P = 0.061$), and there is no statistically significant correlation with the HBMD. For Impedimed study group 1, when $BMI > 30$ kg.m^{-2} the correlation of f_c does not have any statistically significant correlation with the LBMD and the HBMD. QSEG or FAT% might be suppressing the correlation and the results are tabulated in the Table 10.2.

Although for different measurement devices the cutoff frequencies for two-way classifiers are found different and the selection direction is different, with the limited number of subjects in the studies, the success rate of correctly identifying the osteoporotic individuals (Sensitivity) is between 70% and 78%, and the success rate of correctly identifying non-osteoporotic individuals (Specificity) is between 66% and 87%. For both devices, the success rates are comparable to pDXA scanner success rates (50% to 60%) [120].

Similar to changes of DEXA results with changing bone densitometer models, BIS measurement with different devices have also lead to different results. Therefore, this study is not justifying the clinical use of BIS characteristic frequency in diagnosing osteoporosis and even initiating treatment. However, the study may be repeated with a larger population with a more standardized protocol to obtain a normative cutoff frequency for the population so that this method can be a solution in case DEXA

devices are not available or not accessible.

The superiority of both BIS and pDXA over the DEXA is the portability. By combining the characteristic frequency and BMI with our innovative 2D-ROC test algorithm proposed, the correct classification rate is improved from 80% to 83%, and sensitivity has increased from 59% to 90%. As a future study, combining the results of pDXA and BIS results in bone mineral density screening may worth checking if a higher success rate can be achieved.

The correlations of arm characteristic frequencies with the BMD are statistically meaningful and of the legs are not ($P < 0.05$). As Heidi H. Y. Ngai *et al.* have suggested, this may be due to lower lean body mass of legs: having less lean body mass is a cause for BIS measurement errors [177].

Depending BIS measurement device and measurement protocol, within the BIS model parameters, characteristic frequency is found to have the most statistically significant correlation with the reference DEXA bone mineral densities ($P < 0.05$). Characteristic frequency is the reciprocal of the BIS model period, which is the multiplication of the model membrane capacitance with the sum of intracellular (R_i) and extracellular fluid (R_e) model resistances times two pi (Eq. 5.23). When the bone mineral density increases, so the lumped model capacitance will increase, leading to an increase in the characteristic frequency. As expected, the correlation between the characteristic frequency and the LBMD is driven by the model capacitance, and model frequency is calculated higher for higher bone mineral densities. This is in line with the study of Williams *et al.*, i.e., regardless of their measurement axis, the specific capacitance of both trabecular and cortical bones have statistically significant correlations to their mineral densities [26]. However, in HP428A studies, the frequency decreases with the increased bone mineral density which can not be explained by the BIS model capacitance, but can be explained as: HP4284A is not a true tetra-polar measurement system, and its measurement results are severely affected from its nature.

BIS characteristic frequency which is a function of BIS model capacitance cor-

relates with bone mineral density. The measured complex impedance is a function of model capacitance ($P < 0.05$). Model capacitance affects the BIS model complex impedance's imaginary component, the impedance phase angle ϕ at a given frequency should also be a function of the bone mineral density. The novel single frequency method shows that the correlation of the impedance phase angle is higher when the subjects have less fat mass proportion and when the measured frequency is lower. On the other hand, reducing the measurement frequency also reduces the safely usable signal amplitude, which may further increase the complexity of the measurement system. However, using a single frequency and measuring only the phase angle may dramatically reduce the complexity of the bone mineral screening measurements: instead of having a multi-frequency BIS measurement device with complex BIS model calculation algorithms, a single frequency, high precision, and well-calibrated impedance phase measurement device might be a cheaper and a reliable solution for screening the population. The screening should always be limited to subjects with maximum of $30kg.m^{-2}$ body mass index.

In the osteoporosis treatment follow-up study, although medications might have some short-term effects in body electrolyte composition affecting the BIS measurement results, BIS measurements are always periodically performed irrespective of medication intervals. With the assumption that DEXA BMD scores are changing linearly in time with the medication, reference BMD DEXA measurements are taken at the beginning and at the end of the study only. However, in the long term treatment monitoring, DEXA reference measurements could have been repeated more frequently to obtain better DEXA reference measurements, or BIS measurements could have been repeated more frequently to investigate short term effects of the medication on the BIS results. Despite these facts, the characteristic frequency classifier always classified the patient successfully as a patient with a reduced bone mineral density, four times as with osteopenia, four times as with osteoporosis but never as normal. With the assumption that the bone mineral density will be increasing with the medical treatment, there should be a statistically meaningful negative correlation between the characteristic frequency and the measurement points resembling months elapsed with medical treatment. Although the correlation coefficient found between the time and

the characteristic frequency is negative ($r = -0.288, P = 0.489$), it is also statistically insignificant. During the treatment period of 8 months, the DEXA reference measurement T score has increased from -2.7 to -2.5, which was only 7.4%. DEXA devices used as reference measurements have a precision of 1.14% or better. The between-day measurement precision of the BIS measurement system is 1.7% or better. Also, the calcium intake with the medication is affecting the extracellular mineral concentration dramatically and might be affecting the measurement results as well. As a future study, for long term patient followup, to eliminate the effects of medication on the measurements, the monitoring BIS measurements might be performed after a specific time has passed over the medication intake.

When characteristic frequency f_c and body mass index BMI are used together, the 2D-ROC surface study has shown that, with the $AVERAGE$ function to combine the discrete markers, the mis-classification rate is improved compared to using each marker separately. The result is in line with the simulated data, explained in the *A novel approach: 2D receiver operating characteristic surface for paired test* section of this study. 2D-ROC study is also repeated for the Metabolic syndrome (MeS) data which is an important risk factor in heart disease [212]. By using the 5533 patient data set of Babai *et al.* of their Shiraz Heart study [199], the superiority of 2D-ROC $AVERAGE$ function over the single tests is again observed [196]. Measured data may be skewed or diseased and healthy population may have different kurtosis, which may affect the final success level of the 2D-ROC $AVERAGE$ function. Therefore, before applying the algorithm, the normality of test data should be checked and necessary logarithmic or exponentiation transformations should be applied to reduce skewness. The pairing algorithm may be further improved by weighted averaging of test results instead of simple averaging by emphasizing one test over the other by using its historical performance.

If more than 2 tests exists, then the algorithm can be extended for multiple dimensions. However, the success should be validated, and the correct classification rates should be measured before any generalization.

10.1 List of publications produced from the thesis

1. 2D-ROC: a receiver operating surface and its illustrative application in clinical diagnostics, F. Matur; Y. Ulgen, *Physiological measurement*, Vol. 40.7: 075004, 2019.

2. Prediction of Bone Mineral Density in Menopaused Women by Using Bioimpedance Parameters, F. Matur, N. Ozturk, Y. Ulgen In: *EMBEC & NBC 2017. Springer, Singapore*, pp: 807-810, 2017.

3. Screening Post-Menopausal Women for Osteoporosis by Complex Impedance Measurements of the Dominant Arm, F. Matur, Y. Ulgen, *International Journal of Biomedical and Biological Engineering*, Vol. 9.9: pp: 699-702, 2015.

Table 10.1
Comparison of the HP4284A and Impedimed SFB7 measured BIS model parameters.

	(Correlation r, Pearson Coeff. $P < 0.05$)					
	Total lumbar BMD			Total HIP BMD		
Parameter	HP4284	SFB7 Gr.1	SFB7 Gr.2	HP4284	SFB7 Gr.1	SFB7 Gr.2
N	40	52	36	40	52	36
ICF R_i (Ω.m)	NS	0.313	NS	NS	311	NS
ECF R_e (Ω.m)	NS	0.326	NS	NS	0.487	NS
Characteristic frequency f_c (Hz)	0.587	NS	NS	NS	-0.408	NS
Characteristic frequency $ln(f_c)$ (Hz)	0.580	NS	NS	NS	-0.412	NS
Depression constant α	NS	0.381	NS	0.310	NS	NS

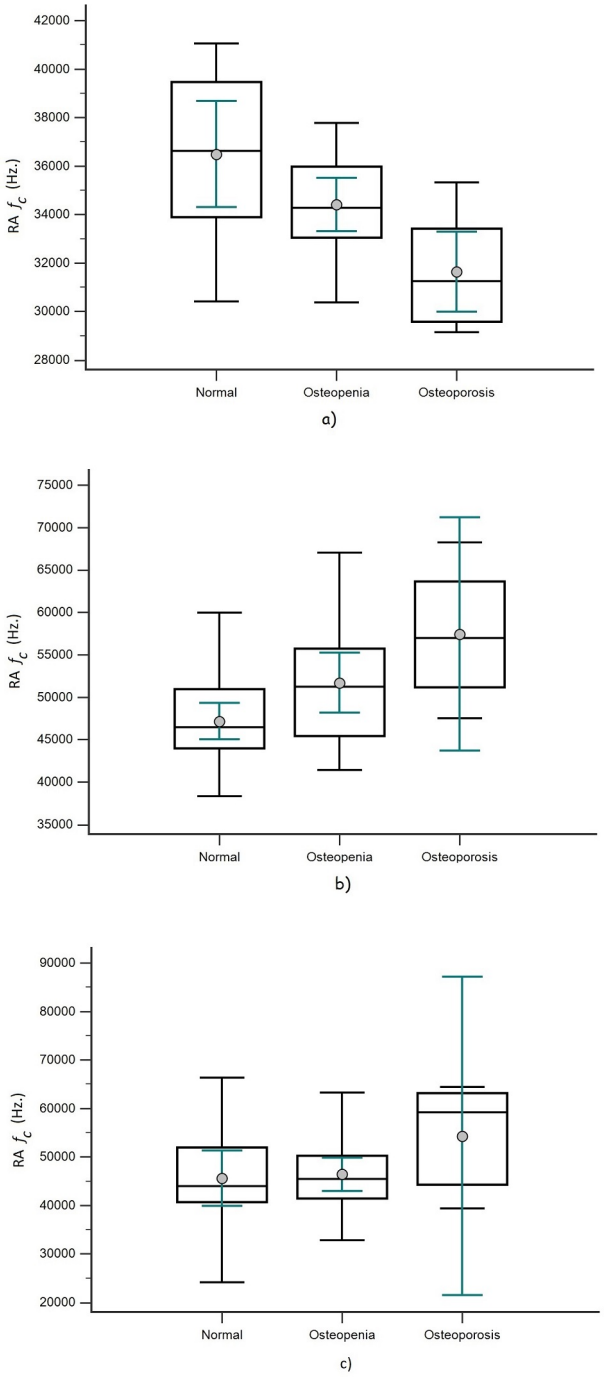

Figure 10.1 BIS model f_c comparison for different WHO groups with respect to their total lumbar spine T scores. With decreased T score, BIS f_c a) decreases for HP428A measurements, and increases for b) Impedimed group 1 measurements for HIP and c) Impedimed group 2 measurements for HIP.

Table 10.2
Correlation of characteristic frequency with the bone mineral density for different BMI groups.

	Total lumbar BMD		Total HIP BMD	
Subject group	HP2484A	SFB7	HP2484A	SFB7
Normal to Over-weight (BMI $< 30 \text{kg.m}^{-2}$)	0.599 †	-0.294 †	0.333 ‡	-0.541†
Obese to morbid obese (BMI $> 30 \text{kg.m}^{-2}$)	0.610 ‡	NS	NS	NS

† Significance level $P < 0.05$.

‡ Significance level $P < 0.10$.

NS: Significance level $P > 0.10$.

APPENDIX A. CODE LISTINGS

Applications coded for measurements and calculations.

A.1 Automation code listing for HP4284A

The setting of the application including the HP4284A timing parameters is passed to the application with a *settings.ini* file located in the folder where the application executable is saved. The settings file has 4 major parts marked with tags: CONSTR tag defines the connection parameter for the device, HEADER that defines the data to be sent to 4284 for device initialization, FREQUENCY defines the sweep frequency set, and CORRECTION is the gain and phase shift of the measurement system for known loads. The application compares the measured data with correction table to find the correction factor either by interpolating or extrapolating.

The settings file listing is as follows:

```
CONSTR=GPIB0::17::INSTR
HEADER=*RST
HEADER=*CLS
HEADER=ABORT
HEADER=TRIG:SOUR BUS
HEADER=COMP OFF
HEADER=CORR:OPEN:STAT 0
HEADER=CORR:SHOR:STAT 0
HEADER=CORR:LOAD:STAT 0
HEADER=FUNC:IMP:RANG AUTO
HEADER=FUNC:IMP ZTD
HEADER=CURR 1mA
HEADER=AMPL:ALC ON
HEADER=APER MED,4
HEADER=LIST:MODE SEQ
HEADER=DISP:PAGE LIST
HEADER=INIT:CONT OFF
FREQUENCY=LIST:FREQ  10kHz, 12.5kHz, 16.0kHz, 20kHz, 25kHz, 32kHz, 40kHz, 50kHz, 62.5kHz, 80kHz
FREQUENCY=LIST:FREQ  100kHz, 125kHz, 160kHz, 200kHz, 250kHz, 320kHz, 400kHz, 500kHz, 640kHz, 800kHz
CORRECTION=10000;20,847300;1,0351;-0,0803
CORRECTION=10000;25,980100;1,0364;-0,0309
CORRECTION=10000;96,978800;1,0366;0,0347
```

```
CORRECTION=10000;115,523000;1,0363;0,0386
CORRECTION=10000;142,793000;1,0368;0,0435
CORRECTION=10000;207,592000;1,0364;0,0444
CORRECTION=10000;257,751000;1,0367;0,0504
CORRECTION=10000;527,785000;1,0366;0,0486
CORRECTION=12500;20,847200;1,0353;-0,0960
CORRECTION=12500;25,982800;1,0365;-0,0378
CORRECTION=12500;96,995600;1,0366;0,0429
CORRECTION=12500;115,527000;1,0364;0,0478
CORRECTION=12500;142,814000;1,0368;0,0538
CORRECTION=12500;207,612000;1,0364;0,0580
CORRECTION=12500;257,770000;1,0367;0,0620
CORRECTION=12500;527,858000;1,0366;0,0656
CORRECTION=16000;20,848400;1,0354;-0,1212
CORRECTION=16000;25,986000;1,0365;-0,0484
CORRECTION=16000;97,014700;1,0366;0,0544
CORRECTION=16000;115,530000;1,0365;0,0616
CORRECTION=16000;142,832000;1,0367;0,0683
CORRECTION=16000;207,632000;1,0364;0,0745
CORRECTION=16000;257,792000;1,0366;0,0793
CORRECTION=16000;527,927000;1,0366;0,0864
CORRECTION=20000;20,847800;1,0355;-0,1524
CORRECTION=20000;25,987700;1,0365;-0,0602
CORRECTION=20000;97,030100;1,0366;0,0678
CORRECTION=20000;115,534000;1,0365;0,0760
CORRECTION=20000;142,847000;1,0366;0,0853
CORRECTION=20000;207,644000;1,0364;0,0928
CORRECTION=20000;257,805000;1,0366;0,0984
CORRECTION=20000;527,966000;1,0366;0,1069
CORRECTION=25000;20,847700;1,0355;-0,1909
CORRECTION=25000;25,988800;1,0364;-0,0738
CORRECTION=25000;97,043100;1,0366;0,0852
CORRECTION=25000;115,536000;1,0365;0,0951
CORRECTION=25000;142,856000;1,0366;0,1068
CORRECTION=25000;207,653000;1,0364;0,1163
CORRECTION=25000;257,818000;1,0366;0,1234
CORRECTION=25000;528,007000;1,0366;0,1332
CORRECTION=32000;20,848900;1,0355;-0,2411
CORRECTION=32000;25,990500;1,0364;-0,0935
CORRECTION=32000;97,053200;1,0365;0,1100
CORRECTION=32000;115,541000;1,0365;0,1223
CORRECTION=32000;142,863000;1,0366;0,1366
CORRECTION=32000;207,664000;1,0363;0,1499
CORRECTION=32000;257,832000;1,0365;0,1580
CORRECTION=32000;528,048000;1,0366;0,1713
CORRECTION=40000;20,850300;1,0355;-0,3001
CORRECTION=40000;25,992300;1,0363;-0,1151
CORRECTION=40000;97,071900;1,0365;0,1381
CORRECTION=40000;115,542000;1,0365;0,1530
CORRECTION=40000;142,871000;1,0365;0,1719
CORRECTION=40000;207,673000;1,0363;0,1882
CORRECTION=40000;257,842000;1,0365;0,1986
CORRECTION=40000;528,086000;1,0365;0,2147
CORRECTION=50000;20,851900;1,0354;-0,3717
CORRECTION=50000;25,994600;1,0363;-0,1414
CORRECTION=50000;97,086900;1,0364;0,1740
CORRECTION=50000;115,547000;1,0365;0,1921
```

```
CORRECTION=50000;142,878000;1,0365;0,2160
CORRECTION=50000;207,684000;1,0363;0,2368
CORRECTION=50000;257,855000;1,0365;0,2488
CORRECTION=50000;528,112000;1,0365;0,2693
CORRECTION=62500;20,854000;1,0354;-0,4610
CORRECTION=62500;25,996800;1,0362;-0,1740
CORRECTION=62500;97,094600;1,0364;0,2192
CORRECTION=62500;115,551000;1,0364;0,2420
CORRECTION=62500;142,885000;1,0365;0,2710
CORRECTION=62500;207,696000;1,0362;0,2972
CORRECTION=62500;257,863000;1,0364;0,3121
CORRECTION=62500;528,131000;1,0364;0,3381
CORRECTION=80000;20,857700;1,0352;-0,5837
CORRECTION=80000;26,000000;1,0361;-0,2185
CORRECTION=80000;97,111300;1,0364;0,2823
CORRECTION=80000;115,556000;1,0364;0,3113
CORRECTION=80000;142,892000;1,0364;0,3483
CORRECTION=80000;207,702000;1,0362;0,3820
CORRECTION=80000;257,875000;1,0364;0,4010
CORRECTION=80000;528,157000;1,0364;0,4349
CORRECTION=100000;20,860700;1,0351;-0,7254
CORRECTION=100000;26,003300;1,0360;-0,2684
CORRECTION=100000;97,124500;1,0363;0,3549
CORRECTION=100000;115,564000;1,0363;0,3903
CORRECTION=100000;142,900000;1,0364;0,4378
CORRECTION=100000;207,708000;1,0362;0,4790
CORRECTION=100000;257,883000;1,0364;0,5033
CORRECTION=100000;528,197000;1,0363;0,5456
CORRECTION=125000;20,866100;1,0348;-0,9016
CORRECTION=125000;26,007200;1,0358;-0,3333
CORRECTION=125000;97,130700;1,0363;0,4464
CORRECTION=125000;115,573000;1,0363;0,4898
CORRECTION=125000;142,905000;1,0364;0,5481
CORRECTION=125000;207,711000;1,0362;0,5997
CORRECTION=125000;257,892000;1,0364;0,6294
CORRECTION=125000;528,214000;1,0363;0,6843
CORRECTION=160000;20,872600;1,0346;-1,1422
CORRECTION=160000;26,012600;1,0357;-0,4169
CORRECTION=160000;97,147800;1,0362;0,5737
CORRECTION=160000;115,572000;1,0363;0,6289
CORRECTION=160000;142,909000;1,0363;0,7035
CORRECTION=160000;207,720000;1,0361;0,7701
CORRECTION=160000;257,895000;1,0364;0,8078
CORRECTION=160000;528,239000;1,0363;0,8783
CORRECTION=200000;20,883600;1,0340;-1,4224
CORRECTION=200000;26,019200;1,0354;-0,5173
CORRECTION=200000;97,159400;1,0361;0,7193
CORRECTION=200000;115,578000;1,0363;0,7879
CORRECTION=200000;142,911000;1,0363;0,8813
CORRECTION=200000;207,729000;1,0361;0,9621
CORRECTION=200000;257,904000;1,0364;1,0094
CORRECTION=200000;528,264000;1,0362;1,0995
CORRECTION=250000;20,898600;1,0334;-1,7670
CORRECTION=250000;26,028400;1,0351;-0,6413
CORRECTION=250000;97,169900;1,0361;0,9020
CORRECTION=250000;115,581000;1,0362;0,9877
CORRECTION=250000;142,916000;1,0363;1,1021
```

```
CORRECTION=250000;207,727000;1,0361;1,2063
CORRECTION=250000;257,913000;1,0363;1,2630
CORRECTION=250000;528,297000;1,0362;1,3774
CORRECTION=320000;20,924000;1,0321;-2,2458
CORRECTION=320000;26,043000;1,0345;-0,8107
CORRECTION=320000;97,190200;1,0360;1,1582
CORRECTION=320000;115,587000;1,0362;1,2678
CORRECTION=320000;142,926000;1,0362;1,4156
CORRECTION=320000;207,738000;1,0361;1,5473
CORRECTION=320000;257,922000;1,0363;1,6207
CORRECTION=320000;528,353000;1,0361;1,7651
CORRECTION=400000;20,956100;1,0306;-2,7918
CORRECTION=400000;26,059700;1,0339;-1,0028
CORRECTION=400000;97,195200;1,0361;1,4527
CORRECTION=400000;115,585000;1,0362;1,5879
CORRECTION=400000;142,924000;1,0363;1,7715
CORRECTION=400000;207,731000;1,0361;1,9373
CORRECTION=400000;257,916000;1,0363;2,0290
CORRECTION=400000;528,395000;1,0360;2,2101
CORRECTION=500000;21,005900;1,0283;-3,4685
CORRECTION=500000;26,084900;1,0330;-1,2449
CORRECTION=500000;97,201800;1,0361;1,8185
CORRECTION=500000;115,583000;1,0362;1,9876
CORRECTION=500000;142,918000;1,0363;2,2170
CORRECTION=500000;207,732000;1,0361;2,4232
CORRECTION=500000;257,915000;1,0363;2,5363
CORRECTION=500000;528,445000;1,0359;2,7663
CORRECTION=640000;21,092800;1,0241;-4,4035
CORRECTION=640000;26,127400;1,0313;-1,5804
CORRECTION=640000;97,206300;1,0361;2,3310
CORRECTION=640000;115,574000;1,0363;2,5461
CORRECTION=640000;142,908000;1,0364;2,8404
CORRECTION=640000;207,713000;1,0362;3,1054
CORRECTION=640000;257,900000;1,0364;3,2500
CORRECTION=640000;528,514000;1,0358;3,5452
CORRECTION=800000;21,214300;1,0183;-5,4533
CORRECTION=800000;26,187400;1,0290;-1,9571
CORRECTION=800000;97,209500;1,0362;2,9181
CORRECTION=800000;115,564000;1,0364;3,1856
CORRECTION=800000;142,895000;1,0365;3,5523
CORRECTION=800000;207,695000;1,0363;3,8845
CORRECTION=800000;257,898000;1,0364;4,0677
CORRECTION=800000;528,608000;1,0356;4,4390
```

The screens of the application is designed in a way that, the user can enter patient anthropometric data before the measurement. Also the application directs the user for correct electrode placement for measuring body segments in the correct order as shown in the Figure 9.7.

The code listing for performing a frequency sweep with HP4284A is as follows:

```
0010 '*************************************************************************
0020 '**** The following module connects to HP4284A  ***************************
0030 '**** send header data for device initialization ****************************
0040 '**** performs a frequency sweep      ****************************
0050 '**** records measurement results     ****************************
0060 '**** and disconnects from the device    ****************************
0070 '**** developed by Firat Matur       ****************************
0080 '*************************************************************************
0090
0100 Module GBIPFonksiyonlar
0110   Dim adimbeklemesuresi As Integer = 80
0120   Dim olcumbeklemesuresi As Integer = 400
0130   Dim maxsayac As Integer = 1000
0140   Dim maxiterasyon As Integer = 5
0150   Dim rm As Ivi.Visa.Interop.ResourceManager
0160   Dim ioobj As Ivi.Visa.Interop.FormattedIO488
0170   Dim cihazabagli As Boolean = False
0180   Dim STLabel As ToolStripStatusLabel
0190   Dim Gonderilen As ListBox
0200
0210   Public isMeasuring As Boolean = False
0220   Public outputdizin As String = ""
0230   Public inifilename As String = ""
0240   Public deviceaddress As String = ""
0250   Public isindebug As Boolean = True
0260   Public OlcumZamani As Date = Now()
0270   Public ismeasuresaved As Boolean = True
0280
0290   ' ********* Function to convert frequency to 4284A code ******************
0300   Public Function _frekansdonustur(ByVal afreq As String) As Double
0310    Dim res As String
0320    Dim r As Double = 0
0330    res = afreq.ToUpper
0340    res = res.Replace("HZ", "")
0350    Try
0360     If InStr(res, "K") Then
0370       res = res.Replace("K", "")
0380       res = res.Replace(" ", "")
0390       res = res.Replace(".", ",")
0400       r = res
0410       r = res * 1000
0420     ElseIf InStr(res, "M") Then
0430       res = res.Replace("M", "")
0440       res = res.Replace(" ", "")
0450       res = res.Replace(".", ",")
0460       r = res
0470       r = res * 1000000
0480     Else
0490       res = res.Replace(" ", "")
0500       res = res.Replace(".", ",")
0510       r = res
0520     End If
0530    Catch ex As Exception
0540     r = 0
0550    End Try
0560
0570    Return r
```

```
0580
0590  End Function
0600
0610  ' ********* Return code of 4284A needs decimal mark correction ***************
0620  ' ********* and scientific notation is converted to decimal numbers **********
0630  ' ********* before load dependent system gain correction *********************
0640  Public Function _rakamdonustur(ByVal arakam As String) As Double
0650   Dim res As String
0660   Dim r As Double = 0
0670   res = arakam.ToUpper
0680   Dim a As String = ""
0690   Dim b As String = ""
0700   Dim n As Integer
0710
0720   Dim aa As Double
0730   Dim bb As Double
0740   If InStr(res, "E") Then
0750    n = InStr(res, "E")
0760    a = Mid(res, 1, n - 1)
0770    b = Mid(res, n + 1, res.Length - n)
0780    a = a.Replace(".", ",")
0790    a = a.Replace("+", "")
0800    aa = a
0810    b = b.Replace(".", ",")
0820    b = b.Replace("+", "")
0830    bb = b
0840    r = aa * Math.Pow(10, bb)
0850   End If
0860   Return r
0870  End Function
0880
0890  '******** the function to convert data so that calculations can be performed with **********
0900  Public Function _KonsolideDonustur(ByVal giris As String) As String
0910   Dim res = ""
0920   Dim z As String = ""
0930   Dim alanlar() As String = giris.Split(";")
0940   For i = 0 To alanlar.Length - 2
0950    z = alanlar(i).ToUpper
0960    If InStr(z, "HZ") > 0 Then
0970      res = res & _frekansdonustur(z) & ";"
0980    ElseIf InStr(z, "E") > 0 Then
0990      res = res & _rakamdonustur(z) & ";"
1000    Else
1010      res = res & (z.Replace(" ", "").Replace(".", ",")) & ";"
1020    End If
1030   Next
1040   For i = alanlar.Length - 1 To alanlar.Length - 1
1050    z = alanlar(i).ToUpper
1060    If InStr(z, "HZ") > 0 Then
1070      res = res & _frekansdonustur(z)
1080    ElseIf InStr(z, "E") > 0 Then
1090      res = res & _rakamdonustur(z)
1100    Else
1110      res = res & (z.Replace(" ", "").Replace(".", ","))
1120    End If
1130   Next
1140   res.Replace(";;", ";")
```

```
1150    If res.Length > 0 And res(res.Length - 1) = ";" Then
1160     res = Mid(res, 1, res.Length - 1)
1170    End If
1180    Return res
1190   End Function
1200
1210
1220   '******** subroutine to send command to HP4284A ***************
1230   Sub IOWriteMyString(ByVal astr As String)
1240    Try
1250     ioobj.WriteString(astr)
1260    Catch ex As Exception
1270    End Try
1280    Gonderilen.Items.Add(astr)
1290    Application.DoEvents()
1300   End Sub
1310
1320  '******** function to read resut to HP4284A ***************
1330   Function IOReadMyString() As String
1340    Dim res As String = ""
1350    Try
1360     res = ioobj.ReadString()
1370    Catch ex As Exception
1380    End Try
1390    Return res
1400   End Function
1410
1420  '****** delay to get measurement result *************************
1430   Sub AdimBekle()
1440    System.Threading.Thread.Sleep(adimbeklemesuresi)
1450   End Sub
1460   Sub UzunAdimBekle()
1470    System.Threading.Thread.Sleep(olcumbeklemesuresi)
1480   End Sub
1490   Sub DurumGuncelle(ByVal astr As String)
1500    STLabel.Text = astr
1510   End Sub
1520
1530  '****** Function to connect to HF4284A ******************
1540   Function CihazaBaglan(ByVal constr As String, ByVal astatlabel As ToolStripStatusLabel, _
1550       ByVal gonderilenliste As ListBox) As Boolean
1560    STLabel = astatlabel
1570    Gonderilen = gonderilenliste
1580    Gonderilen.Items.Clear()
1590    Dim res As Boolean = True
1600    Try
1610     rm = New Ivi.Visa.Interop.ResourceManager
1620     ioobj = New Ivi.Visa.Interop.FormattedIO488
1630     ioobj.IO = rm.Open(constr)
1640     System.Threading.Thread.Sleep(adimbeklemesuresi)
1650     AdimBekle()
1660     DurumGuncelle("BAGLANDI")
1670
1680    Catch ex As Exception
1690     DurumGuncelle("HATA! CİHAZA ERİŞİLEMEDİ")
1700     res = False
1710    End Try
```

```
1720    Return res
1730   End Function
1740
1750   '****** Subroutine to send device initialization protocol ******************
1760   Sub ProtokolHeaderGonder(ByVal HeaderListe As ListBox)
1770    DurumGuncelle("PROTOKOL GÖNDERİLİYOR...")
1780    Try
1790     For i = 0 To HeaderListe.Items.Count - 1
1800       IOWriteMyString(HeaderListe.Items(i))
1810
1820       AdimBekle()
1830     Next
1840     DurumGuncelle("PROTOKOL GÖNDERİLDİ")
1850    Catch ex As Exception
1860     DurumGuncelle("PROTOKOL GÖNDERİMİ HATASI")
1870    End Try
1880   End Sub
1890
1900   '****** Function to do a frequency sweep ******************
1910   Function BirOlcumYap(ByVal frekanslar As String, ByVal adet As Integer, _
1915           ByVal iterasyon As Integer)
1920    Dim unbalancecheck As Boolean = iterasyon < maxiterasyon
1930    DurumGuncelle("OLÇÜM YAPILIYOR")
1940    IOWriteMyString("MEM:DIM DBUF," & adet.ToString)
1950    IOWriteMyString(frekanslar)
1960    AdimBekle()
1970    IOWriteMyString("MEM:FILL DBUF")
1980    AdimBekle()
1990    IOWriteMyString("TRIGGER")
2000    Dim sayac As Integer = 0
2010    Dim err As Double = 0
2020    Do
2030     AdimBekle()
2040     Try
2050       IOWriteMyString("*OPC?")
2060       err = ioobj.ReadNumber
2070     Catch ex As Exception
2080       err = 0
2090     End Try
2100     sayac = sayac + 1
2110    Loop While err <> 1 And sayac < maxsayac
2120    IOWriteMyString("MEM:READ? DBUF")
2130    AdimBekle()
2140    Dim sonuc As String = IOReadMyString.ToString
2150    If sonuc = "" Then
2160     For i = 1 To adet - 1
2170       sonuc = sonuc & "+0E+00,+0E+00,0,0,"
2180     Next
2190     sonuc = sonuc & "+0E+00,+0E+00,0,0"
2200    End If
2210    Dim eskifrekanslar As String = frekanslar.Replace("LIST:FREQ", "")
2220    eskifrekanslar = eskifrekanslar.Replace(" ", "")
2230    Dim eskifrekanslistesi() As String = eskifrekanslar.Split(",")
2240    Dim sonuclar() As String = sonuc.Split(",")
2250    Dim ensonsonuc As String = ""
2260
2270    Try
```

```
2280    For i = 0 To eskifrekanslistesi.Count - 2
2290     If unbalancecheck Then
2300       If sonuclar(i * 4) <> "+9.90000E+37" Then
2310        ensonsonuc = ensonsonuc & eskifrekanslistesi(i) & ";" & _
2320               sonuclar(i * 4) & ";" & _
2330               sonuclar(i * 4 + 1) & ";"
2340       End If
2350     Else
2360       ensonsonuc = ensonsonuc & eskifrekanslistesi(i) & ";" & _
2370        sonuclar(i * 4) & ";" & _
2380             sonuclar(i * 4 + 1) & ";"
2390     End If
2400     Next
2410    Catch ex As Exception
2420    End Try
2430
2440    Try
2450    For i = eskifrekanslistesi.Count - 1 To eskifrekanslistesi.Count - 1
2460     If unbalancecheck Then
2470       If sonuclar(i * 4) <> "+9.90000E+37" Then
2480        ensonsonuc = ensonsonuc & eskifrekanslistesi(i) & ";" & _
2490         sonuclar(i * 4) & ";" & _
2500               sonuclar(i * 4 + 1)
2510       End If
2520     Else
2530       ensonsonuc = ensonsonuc & eskifrekanslistesi(i) & ";" & _
2540        sonuclar(i * 4) & ";" & _
2550              sonuclar(i * 4 + 1)
2560     End If
2570    Next
2580    Catch ex As Exception
2590    End Try
2600
2610
2620    If unbalancecheck Then
2630     Dim yenifrek As String = ""
2640     Dim yeniadet As Integer = 0
2650
2660     For i = 0 To adet - 1
2670       If sonuclar(i * 4) = "+9.90000E+37" Then
2680        If yenifrek <> "" Then
2690         yenifrek = yenifrek & "," & eskifrekanslistesi(i)
2700        Else
2710         yenifrek = eskifrekanslistesi(i)
2720        End If
2730        yeniadet = yeniadet + 1
2740       End If
2750     Next
2760     If yeniadet > 0 Then
2770       yenifrek = "LIST:FREQ " & yenifrek
2780       Dim yenisonuc As String = BirOlcumYap(yenifrek, yeniadet, iterasyon + 1)
2790       ensonsonuc = ensonsonuc & ";" & yenisonuc
2800     End If
2810    End If
2820
2830    DurumGuncelle("ÖLÇÜM YAPILDI")
2840    While InStr(ensonsonuc, ";;", CompareMethod.Text) > 1
```

```
2850     ensonsonuc = ensonsonuc.Replace(";;", ";")
2860    End While
2870
2880    Return ensonsonuc
2890   End Function
2900
2910   '********* subroutine to disconnect from HP4284A ******************
2920   Sub CihaziKapat()
2930    Try
2940     ioobj.IO.Close()
2950    Catch ex As Exception
2960    End Try
2970    Try
2980     System.Runtime.InteropServices.Marshal.ReleaseComObject(ioobj)
2990    Catch ex As Exception
3000    End Try
3010    Try
3020     System.Runtime.InteropServices.Marshal.ReleaseComObject(rm)
3030    Catch ex As Exception
3040    End Try
3050    DurumGuncelle("BEKLEMEDE.")
3060    AdimBekle()
3070   End Sub
3080
3090 End Module
3100 '***************************** end module *****************************
```

The sample data collected for body segments are as follows:

```
Ad;Ap***** A******ı
Olcumtarihi;01.04.2021 01:06:59
Doğum Tarih;
Boy;165.0
Kilo;98.0
Tüm kol Uzunluğu;55.0
Biceps Çevresi;32.0
ElBilekcevre;20.0
Gövde Uzunluğu;80.0
Bel yüksekliği;27.0
Üst gövde çevresi;116.0
Bel çevresi;122.0
Basen çevresi;113.0
Bacak uzunluğu:75.0
Baldır çevresi:52.0
Ayakbilek çevresi:26.0
Frekanslar;  10kHZ ; 12,5kHz ; 16,0kHz ; 20kHz ; 25kHz ; 32kHz ; 40kHz ; 50kHz ; 62,5kHz ; 80kHz
Frekanslar;  100kHz ; 125kHz ; 160kHz ; 200kHz ; 250kHz ; 320kHz ; 400kHz ; 500kHz ; 640kHz ; 800kHz
Sonuc;RA;10000;217,315;-2,88088;225,237903535108;-2,83531693853546
Sonuc;RA;12500;214,132;-3,28902;221,934755256398;-3,23050004306392
Sonuc;RA;16000;210,174;-3,69339;217,826463832488;-3,61864674641148
Sonuc;RA;20000;208,524;-3,97447;216,115005248572;-3,88157175634457
Sonuc;RA;25000;205,306;-4,23373;212,780625670034;-4,11777409772057
Sonuc;RA;32000;200,952;-4,44025;208,252801900971;-4,29172759602475
```

```
Sonuc;RA;40000;199,006;-4,47363;206,235241046202;-4,28761005771427
Sonuc;RA;50000;195,26;-4,49283;202,355424684072;-4,26001758139678
Sonuc;RA;62500;192,366;-4,3687;199,343299525315;-4,07769718874882
Sonuc;RA;80000;189,421;-4,10285;196,288726221605;-3,7303557815152
Sonuc;RA;100000;186,589;-3,77245;193,355682561298;-3,30687585483274
Sonuc;RA;125000;184,234;-3,30056;190,916619136938;-2,71955291732247
Sonuc;RA;160000;181,258;-2,66243;187,81621514297;-1,91952243955501
Sonuc;RA;200000;179,75;-1,94302;186,254492989602;-1,01579770680984
Sonuc;RA;250000;177,396;-1,07537;183,816599565611;0,0821652810479703
Sonuc;RA;320000;175,569;0,113042;181,915755149153;1,59497359137197
Sonuc;RA;400000;175,264;1,4535;181,60859114587;3,30773754378385
Sonuc;RA;500000;175,233;2,94937;181,576484346771;5,26917731014904
Sonuc;RA;640000;177,906;4,03384;184,362562740134;7,01735349432914
Sonuc;RA;800000;174,246;5,4697;180,589118548315;9,18272225617284
Sonuc;T;10000;18,6693;1,42298;19,3245923812049;1,34267136447694
Sonuc;T;12500;18,7602;-0,0349617;19,4224350678307;-0,130961732766616
Sonuc;T;16000;18,5502;-0,59155;19,2068770842633;-0,712750057915905
Sonuc;T;20000;18,3007;-1,04434;18,9503748546615;-1,19674007947126
Sonuc;T;25000;18,2904;-1,40326;18,9397092;-1,5941600984582
Sonuc;T;32000;17,9114;-1,59372;18,5472547;-1,83482014746572
Sonuc;T;40000;17,6178;-1,58283;18,2432319;-1,88293019072167
Sonuc;T;50000;17,4068;-1,35263;18,0230007140031;-1,72433024667455
Sonuc;T;62500;17,1726;-0,931334;17,78051004;-1,3923343287562
Sonuc;T;80000;16,8789;-0,15223;17,4730372665682;-0,735930488209431
Sonuc;T;100000;16,6798;0,85899;17,2652609730262;0,133589407553519
Sonuc;T;125000;16,6631;2,16893;17,242975858989;1,26732925941521
Sonuc;T;160000;16,4259;4,08852;16,9942361253915;2,94631893010058
Sonuc;T;200000;16,2826;6,31006;16,8362083550493;4,88765871077159
Sonuc;T;250000;16,4667;8,87881;17,0166877362118;7,11180847273381
Sonuc;T;320000;16,4891;12,6871;17,0184000149322;10,4412978765233
Sonuc;T;400000;16,8478;16,8461;17,363342576174;14,0542977568189
Sonuc;T;500000;17,853;20,8842;18,3582397705331;17,4156978663856
Sonuc;T;640000;19,3364;23,5156;19,8024070973545;19,1120983577297
Sonuc;T;800000;19,4144;28,8137;19,7696833173204;23,360398110423
Sonuc;RL;10000;213,071;-2,91919;220,833766692364;-2,87413460415878
Sonuc;RL;12500;211,596;-3,30718;219,303136457881;-3,24886228398261
Sonuc;RL;16000;209,435;-3,70988;217,059939627213;-3,63520746411483
Sonuc;RL;20000;207,253;-4,06561;214,797259322453;-3,97285525672485
Sonuc;RL;25000;204,853;-4,41013;212,311419616532;-4,29424051283238
Sonuc;RL;32000;201,981;-4,73512;209,318224375507;-4,58638640020987
Sonuc;RL;40000;199,248;-4,98711;206,485883303059;-4,80102918613623
Sonuc;RL;50000;196,365;-5,17512;203,499908912508;-4,94195292287751
Sonuc;RL;62500;193,61;-5,315;200,631305738841;-5,0234942988073
Sonuc;RL;80000;190,635;-5,43259;197,546027325706;-5,05946452399321
Sonuc;RL;100000;188,066;-5,50369;194,885389003642;-5,03717689050734
Sonuc;RL;125000;185,657;-5,57552;192,390419512329;-4,99337989260254
Sonuc;RL;160000;183,283;-5,69108;189,913337678072;-4,94609154279366
Sonuc;RL;200000;181,314;-5,85906;187,874213422494;-4,92988807553457
Sonuc;RL;250000;179,575;-6,12069;186,073257924002;-4,95965142784404
Sonuc;RL;320000;177,867;-6,54684;184,29619635654;-5,06023880114794
Sonuc;RL;400000;176,469;-7,09345;182,856556140724;-5,23612962565772
Sonuc;RL;500000;175,3;-7,86204;181,645873523313;-5,54201953528559
Sonuc;RL;640000;174,137;-9,04866;180,458803760503;-6,08055866522645
Sonuc;RL;800000;173,324;-10,4313;179,634047987667;-6,72300441666667
Sonuc;LA;10000;209,793;-3,26062;217,432226944012;-3,21595671723918
Sonuc;LA;12500;208,341;-3,6239;215,925520812949;-3,56584186371067
Sonuc;LA;16000;205,604;-3,96597;213,089915993111;-3,89166403703704
```

```
Sonuc;LA;20000;203,518;-4,23601;210,928647033782;-4,14368756840595
Sonuc;LA;25000;200,529;-4,45913;207,832664966471;-4,34387446193497
Sonuc;LA;32000;197,225;-4,62691;204,393798981497;-4,47915253946698
Sonuc;LA;40000;194,593;-4,6815;201,664581449026;-4,49659008363939
Sonuc;LA;50000;191,378;-4,64498;198,334652019597;-4,41341354010431
Sonuc;LA;62500;188,438;-4,50951;195,27625339206;-4,22009509203685
Sonuc;LA;80000;185,564;-4,239;192,294093904867;-3,86851135010029
Sonuc;LA;100000;182,838;-3,9006;189,470768377003;-3,43741045549932
Sonuc;LA;125000;180,206;-3,45548;186,744753826948;-2,87768010184242
Sonuc;LA;160000;177,632;-2,84621;184,061008053423;-2,10702852926201
Sonuc;LA;200000;175,818;-2,1841;182,182341436268;-1,26177920947885
Sonuc;LA;250000;173,855;-1,38664;180,149337774953;-0,234797767971486
Sonuc;LA;320000;172,577;-0,311615;178,816392132724;1,16423675430476
Sonuc;LA;400000;171,465;0,929932;177,674076864282;2,77445031283658
Sonuc;LA;500000;171,791;2,30229;178,011707589681;4,6111468920295
Sonuc;LA;640000;174,64;3,15711;180,979793379893;6,12726819766993
Sonuc;LA;800000;169,653;4,40558;175,83132346613;8,09505604320988
Sonuc;LL;10000;211,715;-3,09196;219,426646803515;-3,04706680834945
Sonuc;LL;12500;210,124;-3,49845;217,775670612768;-3,44024967303322
Sonuc;LL;16000;207,835;-3,92897;215,400362223704;-3,85445057416268
Sonuc;LL;20000;205,516;-4,30203;212,998132271284;-4,20947630769943
Sonuc;LL;25000;202,976;-4,64703;210,367256531802;-4,53141570304181
Sonuc;LL;32000;199,839;-4,96942;207,100395126128;-4,82112603231432
Sonuc;LL;40000;196,954;-5,19828;204,109945893732;-5,01277620845036
Sonuc;LL;50000;193,988;-5,36316;201,037963824893;-5,13075583989137
Sonuc;LL;62500;191,096;-5,46873;198,028358788897;-5,17824058925182
Sonuc;LL;80000;188,032;-5,52808;194,850172038142;-5,15630803579695
Sonuc;LL;100000;185,381;-5,54501;192,104565319328;-5,08020380940625
Sonuc;LL;125000;183,032;-5,56517;189,671698611487;-4,985119976854
Sonuc;LL;160000;180,521;-5,59646;187,052959820168;-4,85430978321581
Sonuc;LL;200000;178,59;-5,69158;185,053156064427;-4,76580372489123
Sonuc;LL;250000;176,861;-5,88949;183,262527979946;-4,73281486614927
Sonuc;LL;320000;175,062;-6,21094;181,390564228995;-4,73003864839844
Sonuc;LL;400000;173,711;-6,66252;180,00020478488;-4,81225559800639
Sonuc;LL;500000;172,409;-7,29462;178,651757145833;-4,9837969957108
Sonuc;LL;640000;171,14;-8,25192;177,354584729326;-5,29607396960111
Sonuc;LL;800000;170,201;-9,44457;176,398992337944;-5,75228461111111
```

A.2 Cole-Cole analyzer code listing for HP4284A measurements

A Microsoft visual basic module is created for Cole-Cole parameter calculations. The code listing is as follows:

```
0010 '*********************************************************************************
0020 '********************** following subroutine calculates the cole parameters **************
0030 '********************** for measurement points are stored at Xmatris (nx1), **************
0040 '********************** Ymatris (nx1), and Fmatris (nx1) *********************************
0050 '********************** Firat Matur - Bogazici University ******************************
```

```
0060 '*************************************************************************************
0070
0080 Option Explicit On
0090 Module MYFunctions
0100 '***************************************************
0110 '************** Define Global variables ***************
0120 Dim Suu As Double, Suv As Double, Svv As Double, Suuu As Double
0130 Dim Svvv As Double, Suvv As Double, Suuv As Double
0140 Dim determinant As Double
0150 Dim xmean As Double
0160 Dim ymean As Double
0170 Public Xmatris() As Double
0180 Public Ymatris() As Double
0190 Public FMatris() As Double
0200 Dim Umatris() As Double
0210 Dim Vmatris() As Double
0220 Dim Ucenter As Double
0230 Dim Vcenter As Double
0240 Public xcenter As Double
0250 Public ycenter As Double
0260 Public radius As Double
0270 Public Rzero As Double
0280 Public Rinfinity As Double
0290 Public Alfa As Double
0300 Public Fcharacteristic1 As Double
0310 Public Fcharacteristic2 As Double
0320 Public Fcharacteristic As Double
0330 '****** End of definition ****************************
0340
0350
0360 '***************************************************
0370 '**** subroutine to initialize data ******************
0380 Public Sub Temizle()
0390 ReDim Xmatris(0)
0400 ReDim Ymatris(0)
0410 End Sub
0420 '************ End of initiazlization ******************
0430
0440
0450 '*********************************************************
0460 '**** Funcion NoktaEkle to add a data point P(R,X,f) ******
0470 Public Sub NoktaEkle(fi As Double, xi As Double, yi As Double)
0480 Dim n As Integer = Xmatris.Length
0490 ReDim Preserve FMatris(n)
0500 ReDim Preserve Xmatris(n)
0510 ReDim Preserve Ymatris(n)
0520 FMatris(n) = fi
0530 Xmatris(n) = xi
0540 Ymatris(n) = yi
0550 End Sub
0560 '*********** End of function *****************************
0570
0580
0590 '*************************************************************
0600 '************ Subroutine to find X and Y means *************
0610 Private Sub FindMeans()
0620 Dim sonuc As Double = 0
```

```
0630 Dim n As Integer = Xmatris.Length - 1
0640 For i = 1 To n
0650 sonuc = sonuc + Xmatris(i)
0660 Next
0670 xmean = sonuc / n
0680
0690 sonuc = 0
0700 For i = 1 To n
0710 sonuc = sonuc + Ymatris(i)
0720 Next
0730 ymean = sonuc / n
0740 End Sub
0750 '*********** End of sub routine ***************************
0760
0770
0780
0790 '*******************************************************
0800 '************ Subroutine matrix elements for calculation ***
0810 Private Sub FindUV()
0820 Dim n As Integer = Xmatris.Length - 1
0830 ReDim Umatris(n)
0840 ReDim Vmatris(n)
0850 For i = 1 To n
0860 Umatris(i) = Xmatris(i) - xmean
0870 Vmatris(i) = Ymatris(i) - ymean
0880 Next
0890 End Sub
0900
0910 Private Sub FindSValues()
0920 Suu = 0
0930 Suv = 0
0940 Svv = 0
0950 Suuu = 0
0960 Svvv = 0
0970 Suvv = 0
0980 Suuv = 0
0990 Dim n As Integer = Xmatris.Length - 1
1000 For i = 1 To n
1010 Suu = Suu + Umatris(i) * Umatris(i)
1020 Suv = Suv + Umatris(i) * Vmatris(i)
1030 Svv = Svv + Vmatris(i) * Vmatris(i)
1040 Suuu = Suuu + Umatris(i) * Umatris(i) * Umatris(i)
1050 Svvv = Svvv + Vmatris(i) * Vmatris(i) * Vmatris(i)
1060 Suvv = Suvv + Umatris(i) * Vmatris(i) * Vmatris(i)
1070 Suuv = Suuv + Umatris(i) * Umatris(i) * Vmatris(i)
1080 Next
1090 determinant = Suu * Svv - Suv * Suv
1100 End Sub
1110 '*********** End of sub routines ***************************
1120
1130
1140 '*****************************************************************************
1150 '********************** SolveCole subroutine calculates the cole parameters **************
1160 '********************** where measurement points are stored at Xmatris (nx1), ************
1170 '********************** Ymatris (nx1), and Fmatris (nx1) ********************************
1180 '*****************************************************************************
1190 Sub SolveCole()
```

```
1200 '********************** Define local variables **********************
1210 Dim u As Double
1220 Dim v As Double
1230 Dim VboluU1 As Double = 0.0001
1240 Dim n As Integer = 1
1250
1260
1270 '********************** Find matrix elements ************************
1280 FindMeans()
1290 FindUV()
1300 FindSValues()
1310
1320
1330 '********************** Find circle parameters, *********************
1340 Ucenter = Svv / determinant * 0.5 * (Suuu + Suvv) - Suv / determinant * 0.5 * (Svvv + Suuv)
1350 Vcenter = -Suv / determinant * 0.5 * (Suuu + Suvv) + Suu / determinant * 0.5 * (Svvv + Suuv)
1360 xcenter = Ucenter + xmean
1370 ycenter = Vcenter + ymean
1380 radius = Math.Sqrt(Ucenter * Ucenter + Vcenter * Vcenter + (Suu + Svv) / (Xmatris.Length - 1))
1390
1400
1410 '********************** Find cole parameters *************************
1420 Rzero = xcenter + Math.Sqrt(radius * radius - ycenter * ycenter)
1430 Rinfinity = xcenter - Math.Sqrt(radius * radius - ycenter * ycenter)
1440 Alfa = 1 - 2 / Math.PI * Math.Atan(ycenter / Math.Sqrt(radius * radius - ycenter * ycenter))
1450
1460
1470 '****** find the point right before the fc **********************
1480 For i = 1 To Xmatris.Count - 1
1490 v = Math.Sqrt((Xmatris(i) - Rzero) ^ 2 + (Ymatris(i) - 0) ^ 2)
1500 u = Math.Sqrt((Xmatris(i) - Rinfinity) ^ 2 + (Ymatris(i) - 0) ^ 2)
1510 If (v / u) <= 1 And (v / u) > VboluU1 Then
1520 VboluU1 = (v / u)
1530 n = i
1540 End If
1550 Next
1560
1570
1580 ' ******** calculate fc ***********************************************
1590 Dim VboluU2 As Double
1600 v = Math.Sqrt((Xmatris(n + 1) - Rzero) ^ 2 + (Ymatris(n + 1) - 0) ^ 2)
1610 u = Math.Sqrt((Xmatris(n + 1) - Rinfinity) ^ 2 + (Ymatris(n + 1) - 0) ^ 2)
1620 VboluU1 = Math.Log(VboluU1)
1630 VboluU2 = Math.Log(v / u)
1640
1650 Dim f_1 As Double = Math.Log(FMatris(n) * 2 * Math.PI)
1660 Dim f_2 As Double = Math.Log(FMatris(n + 1) * 2 * Math.PI)
1670
1680 ' y = ax + b
1690 Dim a As Double = (VboluU2 - VboluU1) / (f_2 - f_1)
1700 Dim b As Double = VboluU1 - a * f_1
1710 Dim lnf As Double = -1 * b / a
1720 Fcharacteristic = Math.Exp(lnf) / 2 / Math.PI
1730
1740 End Sub
1750 '************************** end of sub ********************************
1760
```

```
1770 End Module
1780 '****************************** End of module ******************************
```

A.3 2D-Calculator code listing

```
0001 '*******************************************************************************************
0002 '********************** following subroutine calculates 2d CCR     *******************
0003 '********************** copy and paste the clipboard for calculations   , **************
0004 '********************** Firat Matur - Bogazici University *******************************
0005 '*
0010 Public Class Form1
0020 Dim batchprocess As Boolean = False
0030 Dim TNData(,) As Double
0040 Dim FPData(,) As Double
0050 Dim TPData(,) As Double
0060 Dim FNData(,) As Double
0070 Dim SensitivityData(,) As Double
0080 Dim SpecificityData(,) As Double
0090 Dim YoudenData(,) As Double
0100 Dim Histogram(,) As Integer
0110 Dim HistogramH(,) As Integer
0120 Dim HistogramD(,) As Integer
0130 Dim ClassifierData(,) As Integer
0140 Dim ClassifierData1(,) As Integer
0150 Dim ClassifierData2(,) As Integer
0160 Dim ClassifierDataBaz(,) As Integer
0170 Dim DeltaData(,) As Integer
0180 Dim Param1Range() As Double
0190 Dim Param2Range() As Double
0200 Dim Param1Min As Double
0210 Dim Param2Min As Double
0220 Dim Param1Max As Double
0230 Dim Param2Max As Double
0240 Dim Param1AdimUzunlugu As Double
0250 Dim Param2AdimUzunlugu As Double
0260 Dim Param1() As Double
0270 Dim Param2() As Double
0280 Dim Param1Slot() As Integer
0290 Dim Param2Slot() As Integer
0300 Dim Observation() As Double
0310 Dim Prediction() As Double
0320 Dim SlotSayisi As Integer
0330 Dim DataSayisi As Integer
0340 Dim FPnew As Integer
0350 Dim TPNew As Integer
0360 Dim FNNew As Integer
0370 Dim TNNew As Integer
0380 Dim Excluded As Integer
0390 Dim TPR As Double
0400 Sub DataSifirla()
0410 Dim N As Integer = ComboBox1.Text
0420 '0.0001% sol ve sağda kalacak.
```

```
0430 SlotSayisi = N
0440 ReDim TNData(SlotSayisi - 1, SlotSayisi - 1)
0450 ReDim FNData(SlotSayisi - 1, SlotSayisi - 1)
0460 ReDim TPData(SlotSayisi - 1, SlotSayisi - 1)
0470 ReDim FPData(SlotSayisi - 1, SlotSayisi - 1)
0480 ReDim SensitivityData(SlotSayisi - 1, SlotSayisi - 1)
0490 ReDim SpecificityData(SlotSayisi - 1, SlotSayisi - 1)
0500 ReDim ClassifierData(SlotSayisi - 1, SlotSayisi - 1)
0510 ReDim ClassifierData1(SlotSayisi - 1, SlotSayisi - 1)
0520 ReDim ClassifierData2(SlotSayisi - 1, SlotSayisi - 1)
0530 ReDim ClassifierDataBaz(SlotSayisi - 1, SlotSayisi - 1)
0540 ReDim DeltaData(SlotSayisi - 1, SlotSayisi - 1)
0550 ReDim YoudenData(SlotSayisi - 1, SlotSayisi - 1)
0560 ReDim Param1Range(SlotSayisi - 1)
0570 ReDim Param2Range(SlotSayisi - 1)
0580 ReDim Histogram(SlotSayisi - 1, SlotSayisi - 1)
0590 ReDim HistogramH(SlotSayisi - 1, SlotSayisi - 1)
0600 ReDim HistogramD(SlotSayisi - 1, SlotSayisi - 1)
0610 End Sub
0620 Sub DataOku()
0630 Dim Param1Kolon As Integer
0640 Dim Param2Kolon As Integer
0650 Dim ObservationKolon As Integer
0660 Param1Kolon = ComboBox4.SelectedIndex
0670 Param2Kolon = ComboBox5.SelectedIndex
0680 ObservationKolon = ComboBox6.SelectedIndex
0690 Dim kontrol As Integer
0700 kontrol = Math.Max(Math.Max(Param1Kolon, Param2Kolon), ObservationKolon)
0710 Dim txt As String = RichTextBox1.Text
0720 txt = txt.Replace(vbCrLf, vbLf)
0730 txt = txt.Replace(vbCr, vbLf)
0740 Dim satirlar = txt.Split(vbLf)
0750 DataSayisi = 0
0760 ReDim Param1(satirlar.Count - 1)
0770 ReDim Param2(satirlar.Count - 1)
0780 ReDim Param1Slot(satirlar.Count - 1)
0790 ReDim Param2Slot(satirlar.Count - 1)
0800 ReDim Observation(satirlar.Count - 1)
0810 ReDim Prediction(satirlar.Count - 1)
0820 Param1Min = 99999999999
0830 Param2Min = 99999999999
0840 Param1Max = -999999999999
0850 Param2Max = -999999999999
0860 'ilk satır başlık atla
0870 For i = 1 To satirlar.Count - 1
0880 Dim kolonlar = satirlar(i).Split(vbTab)
0890 If kolonlar.Count >= kontrol + 1 Then
0900 Param1(DataSayisi) = kolonlar(Param1Kolon)
0910 Param2(DataSayisi) = kolonlar(Param2Kolon)
0920 Observation(DataSayisi) = kolonlar(ObservationKolon)
0930 If Param1(DataSayisi) < Param1Min Then
0940 Param1Min = Param1(DataSayisi)
0950 End If
0960 If Param2(DataSayisi) < Param2Min Then
0970 Param2Min = Param2(DataSayisi)
0980 End If
0990 If Param1(DataSayisi) > Param1Max Then
```

```
1000 Param1Max = Param1(DataSayisi)
1010 End If
1020 If Param2(DataSayisi) > Param2Max Then
1030 Param2Max = Param2(DataSayisi)
1040 End If
1050 DataSayisi = DataSayisi + 1
1060 End If
1070 Next
1080 Param1AdimUzunlugu = (Param1Max - Param1Min) / (SlotSayisi) * 1.000001
1090 Param2AdimUzunlugu = (Param2Max - Param2Min) / (SlotSayisi) * 1.000001
1100 'sağ ve solda 1.5 adet slot kalacak
1110 For i = 0 To SlotSayisi - 1
1120 Param1Range(i) = Param1Min + i * Param1AdimUzunlugu
1130 Param2Range(i) = Param2Min + i * Param2AdimUzunlugu
1140 Next
1150 For i = 0 To DataSayisi - 1
1160 Param1Slot(i) = Math.Truncate((Param1(i) - Param1Min) / Param1AdimUzunlugu)
1170 Param2Slot(i) = Math.Truncate((Param2(i) - Param2Min) / Param2AdimUzunlugu)
1180 Next
1190 End Sub
1200 Sub HesaplariYap()
1210 ProgressBar1.Maximum = SlotSayisi
1220 ProgressBar1.Value = 0
1230 Dim FN As Integer
1240 Dim FP As Integer
1250 Dim TP As Integer
1260 Dim TN As Integer
1270 Dim islemturu As String = ComboBox2.Text
1280 For i = 0 To SlotSayisi - 1
1290 For j = 0 To SlotSayisi - 1
1300 Histogram(i, j) = 0
1310 Next
1320 Next
1330 For i = 0 To DataSayisi - 1
1340 Histogram(Param1Slot(i), Param2Slot(i)) = Histogram(Param1Slot(i), Param2Slot(i)) + 1
1350 If Observation(i) = 0 Then
1360 HistogramH(Param1Slot(i), Param2Slot(i)) = HistogramH(Param1Slot(i), Param2Slot(i)) + 1
1370 Else
1380 HistogramD(Param1Slot(i), Param2Slot(i)) = HistogramD(Param1Slot(i), Param2Slot(i)) + 1
1390 End If
1400 Next
1410 For i = 0 To SlotSayisi - 1
1420 For j = 0 To SlotSayisi - 1
1430 FN = 0
1440 FP = 0
1450 TP = 0
1460 TN = 0
1470 For k = 0 To DataSayisi - 1
1480 If islemturu = "AND" Then
1490 If Param1Slot(k) >= i And Param2Slot(k) >= j Then
1500 If Observation(k) = 0 Then
1510 FP = FP + 1
1520 Else
1530 TP = TP + 1
1540 End If
1550 Else
1560 If Observation(k) = 0 Then
```

```
1570 TN = TN + 1
1580 Else
1590 FN = FN + 1
1600 End If
1610 End If
1620 ElseIf islemturu = "OR" Then
1630 If Param1Slot(k) >= i Or Param2Slot(k) >= j Then
1640 If Observation(k) = 0 Then
1650 FP = FP + 1
1660 Else
1670 TP = TP + 1
1680 End If
1690 Else
1700 If Observation(k) = 0 Then
1710 TN = TN + 1
1720 Else
1730 FN = FN + 1
1740 End If
1750 End If
1760 Else
1770 If Param1Slot(k) + Param2Slot(k) >= i + j Then
1780 If Observation(k) = 0 Then
1790 FP = FP + 1
1800 Else
1810 TP = TP + 1
1820 End If
1830 Else
1840 If Observation(k) = 0 Then
1850 TN = TN + 1
1860 Else
1870 FN = FN + 1
1880 End If
1890 End If
1900 End If
1910 Next
1920 FPData(i, j) = FP
1930 FNData(i, j) = FN
1940 TPData(i, j) = TP
1950 TNData(i, j) = TN
1960 SpecificityData(i, j) = TN / (TN + FP) * 100
1970 SensitivityData(i, j) = TP / (TP + FN) * 100
1980 Next
1990 ProgressBar1.Value = i + 1
2000 Next
2010 'YoudenBul
2020 For i = 0 To SlotSayisi - 1
2030 For j = 0 To SlotSayisi - 1
2040 YoudenData(i, j) = SpecificityData(i, j) + SensitivityData(i, j) - 100
2050 Next
2060 Next
2070 For i = 0 To SlotSayisi - 1
2080 For j = 0 To SlotSayisi - 1
2090 ClassifierData(i, j) = 0
2100 ClassifierData1(i, j) = 0
2110 ClassifierData2(i, j) = 0
2120 ClassifierDataBaz(i, j) = 0.001
2130 Next
```

```
2140 Next
2150 'Classifier Bul
2160 Dim Slotmaxdeger As Double
2170 For i = 0 To SlotSayisi - 1
2180 Slotmaxdeger = -99999999
2190 For j = 0 To SlotSayisi - 1
2200 If YoudenData(i, j) > Slotmaxdeger Then
2210 Slotmaxdeger = YoudenData(i, j)
2220 End If
2230 Next
2240 For j = 0 To SlotSayisi - 1
2250 If YoudenData(i, j) = Slotmaxdeger Then
2260 For k = j To SlotSayisi - 1
2270 ClassifierData1(i, k) = 1
2280 Next
2290 Exit For
2300 End If
2310 Next
2320 Next
2330 For j = 0 To SlotSayisi - 1
2340 Slotmaxdeger = -99999999
2350 For i = 0 To SlotSayisi - 1
2360 If YoudenData(i, j) > Slotmaxdeger Then
2370 Slotmaxdeger = YoudenData(i, j)
2380 End If
2390 Next
2400 For i = 0 To SlotSayisi - 1
2410 If YoudenData(i, j) = Slotmaxdeger Then
2420 For k = i To SlotSayisi - 1
2430 ClassifierData2(k, j) = 1
2440 Next
2450 Exit For
2460 End If
2470 Next
2480 Next
2490 For i = 0 To SlotSayisi - 1
2500 For j = 0 To SlotSayisi - 1
2510 If ComboBox2.Text = "AND" Then
2520 If ClassifierData1(i, j) = 1 Or ClassifierData2(i, j) = 1 Then
2530 ClassifierData(i, j) = 1
2540 Else
2550 ClassifierData(i, j) = 0
2560 End If
2570 ElseIf ComboBox2.Text = "OR" Then
2580 If ClassifierData1(i, j) = 1 And ClassifierData2(i, j) = 1 Then
2590 ClassifierData(i, j) = 1
2600 Else
2610 ClassifierData(i, j) = 0
2620 End If
2630 ElseIf ComboBox2.Text = "AVERAGE" Then
2640 If ClassifierData1(i, j) = 1 And ClassifierData2(i, j) = 1 Then
2650 ClassifierData(i, j) = 1
2660 Else
2670 ClassifierData(i, j) = 0
2680 End If
2690 End If
2700 Next
```

```
2710 Next
2720 ClassifierData(0, 0) = 0
2730 'prediction bul
2740 FPnew = 0
2750 FNNew = 0
2760 TPNew = 0
2770 TNNew = 0
2780 Excluded = 0
2790 For i = 0 To DataSayisi - 1
2800 If Observation(i) = 0 Then
2810 If ClassifierData(Param1Slot(i), Param2Slot(i)) = 0 Then
2820 Prediction(i) = 0
2830 TNNew = TNNew + 1
2840 Else
2850 Prediction(i) = 1
2860 FPnew = FPnew + 1
2870 End If
2880 Else
2890 If ClassifierData(Param1Slot(i), Param2Slot(i)) = 0 Then
2900 Prediction(i) = 0
2910 FNNew = FNNew + 1
2920 Else
2930 Prediction(i) = 1
2940 TPNew = TPNew + 1
2950 End If
2960 End If
2970 Next
2980 TPR = (TNNew + TPNew) / (TPNew + TNNew + FNNew + FPnew)
2990 ProgressBar1.Value = 0
3000 End Sub
3010 Sub hesabi_goster()
3020 Dim s As String = ""
3030 If Not batchprocess Then
3040 RichTextBox2.Text = RichTextBox2.Text & "X=["
3050 For i = 0 To SlotSayisi - 1
3060 s = s & Param1Range(i) & vbTab
3070 Next
3080 RichTextBox2.Text = RichTextBox2.Text & s & "];" & vbCrLf
3090 s = ""
3100 RichTextBox2.Text = RichTextBox2.Text & "Y=["
3110 For i = 0 To SlotSayisi - 1
3120 s = s & Param2Range(i) & vbTab
3130 Next
3140 RichTextBox2.Text = RichTextBox2.Text & s & "];" & vbCrLf
3150 RichTextBox2.Text = RichTextBox2.Text & "Histogram=["
3160 For i = 0 To SlotSayisi - 1
3170 s = ""
3180 For j = 0 To SlotSayisi - 1
3190 s = s & Histogram(i, j) & vbTab
3200 Next
3210 RichTextBox2.Text = RichTextBox2.Text & s & ";" & vbCrLf
3220 Next
3230 RichTextBox2.Text = RichTextBox2.Text & "];" & vbCrLf
3240 RichTextBox2.Text = RichTextBox2.Text & "HistogramH=["
3250 For i = 0 To SlotSayisi - 1
3260 s = ""
3270 For j = 0 To SlotSayisi - 1
```

```
3280 s = s & HistogramH(i, j) & vbTab
3290 Next
3300 RichTextBox2.Text = RichTextBox2.Text & s & ";" & vbCrLf
3310 Next
3320 RichTextBox2.Text = RichTextBox2.Text & "];" & vbCrLf
3330 RichTextBox2.Text = RichTextBox2.Text & "HistogramD=["
3340 For i = 0 To SlotSayisi - 1
3350 s = ""
3360 For j = 0 To SlotSayisi - 1
3370 s = s & HistogramD(i, j) & vbTab
3380 Next
3390 RichTextBox2.Text = RichTextBox2.Text & s & ";" & vbCrLf
3400 Next
3410 RichTextBox2.Text = RichTextBox2.Text & "];" & vbCrLf
3420 RichTextBox2.Text = RichTextBox2.Text & "Sensitivity=["
3430 For i = 0 To SlotSayisi - 1
3440 s = ""
3450 For j = 0 To SlotSayisi - 1
3460 s = s & SensitivityData(i, j) & vbTab
3470 Next
3480 RichTextBox2.Text = RichTextBox2.Text & s & ";" & vbCrLf
3490 Next
3500 RichTextBox2.Text = RichTextBox2.Text & "];" & vbCrLf
3510 RichTextBox2.Text = RichTextBox2.Text & "Specificity=["
3520 For i = 0 To SlotSayisi - 1
3530 s = ""
3540 For j = 0 To SlotSayisi - 1
3550 s = s & SpecificityData(i, j) & vbTab
3560 Next
3570 RichTextBox2.Text = RichTextBox2.Text & s & ";" & vbCrLf
3580 Next
3590 RichTextBox2.Text = RichTextBox2.Text & "];" & vbCrLf
3600 RichTextBox2.Text = RichTextBox2.Text & "Youden=["
3610 For i = 0 To SlotSayisi - 1
3620 s = ""
3630 For j = 0 To SlotSayisi - 1
3640 s = s & YoudenData(i, j) & vbTab
3650 Next
3660 RichTextBox2.Text = RichTextBox2.Text & s & ";" & vbCrLf
3670 Next
3680 RichTextBox2.Text = RichTextBox2.Text & "];" & vbCrLf
3690 RichTextBox2.Text = RichTextBox2.Text & "ClassifierData=["
3700 For i = 0 To SlotSayisi - 1
3710 s = ""
3720 For j = 0 To SlotSayisi - 1
3730 s = s & ClassifierData(i, j) & vbTab
3740 Next
3750 RichTextBox2.Text = RichTextBox2.Text & s & ";" & vbCrLf
3760 Next
3770 RichTextBox2.Text = RichTextBox2.Text & "];" & vbCrLf
3780 RichTextBox2.Text = RichTextBox2.Text & "ClassifierDataBaz=["
3790 For i = 0 To SlotSayisi - 1
3800 s = ""
3810 For j = 0 To SlotSayisi - 1
3820 s = s & ClassifierDataBaz(i, j) & vbTab
3830 Next
3840 RichTextBox2.Text = RichTextBox2.Text & s & ";" & vbCrLf
```

```
3850 Next
3860 RichTextBox2.Text = RichTextBox2.Text & "];" & vbCrLf
3870 RichTextBox2.Text = RichTextBox2.Text & "ClassifierData1=["
3880 For i = 0 To SlotSayisi - 1
3890 s = ""
3900 For j = 0 To SlotSayisi - 1
3910 s = s & ClassifierData1(i, j) & vbTab
3920 Next
3930 RichTextBox2.Text = RichTextBox2.Text & s & ";" & vbCrLf
3940 Next
3950 RichTextBox2.Text = RichTextBox2.Text & "];" & vbCrLf
3960 RichTextBox2.Text = RichTextBox2.Text & "ClassifierData2=["
3970 For i = 0 To SlotSayisi - 1
3980 s = ""
3990 For j = 0 To SlotSayisi - 1
4000 s = s & ClassifierData2(i, j) & vbTab
4010 Next
4020 RichTextBox2.Text = RichTextBox2.Text & s & ";" & vbCrLf
4030 Next
4040 RichTextBox2.Text = RichTextBox2.Text & "];" & vbCrLf
4050 RichTextBox2.Text = RichTextBox2.Text & "Youden=["
4060 For i = 0 To SlotSayisi - 1
4070 s = ""
4080 For j = 0 To SlotSayisi - 1
4090 s = s & SensitivityData(i, j) + SpecificityData(i, j) - 1 & vbTab
4100 Next
4110 RichTextBox2.Text = RichTextBox2.Text & s & ";" & vbCrLf
4120 Next
4130 RichTextBox2.Text = RichTextBox2.Text & "];" & vbCrLf
4140 RichTextBox2.Text = RichTextBox2.Text & "TN=" & TNNew & ";" & vbCrLf
4150 RichTextBox2.Text = RichTextBox2.Text & "FN=" & FNNew & ";" & vbCrLf
4160 RichTextBox2.Text = RichTextBox2.Text & "TP=" & TPNew & ";" & vbCrLf
4170 RichTextBox2.Text = RichTextBox2.Text & "FP=" & FPnew & ";" & vbCrLf
4180 RichTextBox2.Text = RichTextBox2.Text & "TPR=" & TPR & ";" & vbCrLf
4190 RichTextBox2.Text = Replace(RichTextBox2.Text, ",", ".")
4200 ' 3D Histogram hazırlayalım
4210 RichTextBox2.Text = RichTextBox2.Text & "scf;" & vbCrLf
4220 RichTextBox2.Text = RichTextBox2.Text & " hist3d(HistogramD);" & vbCrLf
4230 RichTextBox2.Text = RichTextBox2.Text & " hist3d(HistogramH);" & vbCrLf
4240 RichTextBox2.Text = RichTextBox2.Text & "a = gca();" & vbCrLf
4250 RichTextBox2.Text = RichTextBox2.Text & "a.thickness = 3;" & vbCrLf
4260 RichTextBox2.Text = RichTextBox2.Text & "a.tight_limits = [^on^,^on^,^on^];" & vbCrLf
4270 RichTextBox2.Text = RichTextBox2.Text & "a.isoview =^on^;" & vbCrLf
4280 RichTextBox2.Text = RichTextBox2.Text & "a.axes_visible = [^on^,^on^,^on^];" & vbCrLf
4290 RichTextBox2.Text = RichTextBox2.Text & "a.x_label.font_size = 3;" & vbCrLf
4300 RichTextBox2.Text = RichTextBox2.Text & "a.x_label.text =^" & "Test 1" & "^;" & vbCrLf
4310 RichTextBox2.Text = RichTextBox2.Text & "a.y_label.font_size = 3;" & vbCrLf
4320 RichTextBox2.Text = RichTextBox2.Text & "a.y_label.text =^" & "Test 2" & " ^" & vbCrLf
4330 RichTextBox2.Text = RichTextBox2.Text & "a.z_label.font_size = 3;" & vbCrLf
4340 RichTextBox2.Text = RichTextBox2.Text & "a.z_label.text =^^;" & vbCrLf
4350 RichTextBox2.Text = RichTextBox2.Text & "a.title.font_size = 3;" & vbCrLf
4360 RichTextBox2.Text = RichTextBox2.Text & "a.title.text = ^Data Distribution^;" & vbCrLf
4370 RichTextBox2.Text = RichTextBox2.Text & "a.rotation_angles =[50,-30];" & vbCrLf
4380 RichTextBox2.Text = RichTextBox2.Text & "a.children(1, 1).color_mode = 12;" & vbCrLf
4390 RichTextBox2.Text = RichTextBox2.Text & "a.children(1, 1).hiddencolor = 9;" & vbCrLf
4400 RichTextBox2.Text = RichTextBox2.Text & "a.children(2, 1).color_mode = 5;" & vbCrLf
4410 RichTextBox2.Text = RichTextBox2.Text & "a.children(2, 1).hiddencolor = 21;" & vbCrLf
```

```
4420 RichTextBox2.Text = RichTextBox2.Text & "a.axes_reverse = [^off^,^off^,^off^];" & vbCrLf
4430 ' 3D hazırlayalım
4440 RichTextBox2.Text = RichTextBox2.Text & "scf;" & vbCrLf
4450 RichTextBox2.Text = RichTextBox2.Text & " mesh(X, Y, Specificity);" & vbCrLf
4460 RichTextBox2.Text = RichTextBox2.Text & "mesh(X, Y, Sensitivity);" & vbCrLf
4470 RichTextBox2.Text = RichTextBox2.Text & "a = gca();" & vbCrLf
4480 RichTextBox2.Text = RichTextBox2.Text & "a.thickness = 3;" & vbCrLf
4490 RichTextBox2.Text = RichTextBox2.Text & "a.tight_limits = [^on^,^on^,^on^];" & vbCrLf
4500 RichTextBox2.Text = RichTextBox2.Text & "a.isoview =^on^;" & vbCrLf
4510 RichTextBox2.Text = RichTextBox2.Text & "a.axes_visible = [^on^,^on^,^on^];" & vbCrLf
4520 RichTextBox2.Text = RichTextBox2.Text & "a.x_label.font_size = 3;" & vbCrLf
4530 RichTextBox2.Text = RichTextBox2.Text & "a.x_label.text =^" & "Test 1" & "^;" & vbCrLf
4540 RichTextBox2.Text = RichTextBox2.Text & "a.y_label.font_size = 3;" & vbCrLf
4550 RichTextBox2.Text = RichTextBox2.Text & "a.y_label.text =^" & "Test 2" & " ^" & vbCrLf
4560 RichTextBox2.Text = RichTextBox2.Text & "a.z_label.font_size = 3;" & vbCrLf
4570 RichTextBox2.Text = RichTextBox2.Text & "a.z_label.text =^%^;" & vbCrLf
4580 RichTextBox2.Text = RichTextBox2.Text & "a.title.font_size = 3;" & vbCrLf
4590 RichTextBox2.Text = RichTextBox2.Text & "a.title.text =^"&ComboBox2.Text&" Se & Sp^;"&vbCrLf
4600 RichTextBox2.Text = RichTextBox2.Text & "a.rotation_angles =[50,-30];" & vbCrLf
4610 RichTextBox2.Text = RichTextBox2.Text & "a.children(1, 1).color_mode = 12;" & vbCrLf
4620 RichTextBox2.Text = RichTextBox2.Text & "a.children(1, 1).hiddencolor = 9;" & vbCrLf
4630 RichTextBox2.Text = RichTextBox2.Text & "a.children(2, 1).color_mode = 5;" & vbCrLf
4640 RichTextBox2.Text = RichTextBox2.Text & "a.children(2, 1).hiddencolor = 21;" & vbCrLf
4650 RichTextBox2.Text = RichTextBox2.Text & "a.axes_reverse = [^off^,^off^,^off^];" & vbCrLf
4660 '' 2D hazırlayalım
4670 ' 3D Youden
4680 RichTextBox2.Text = RichTextBox2.Text & "scf;" & vbCrLf
4690 RichTextBox2.Text = RichTextBox2.Text & " mesh(X, Y, Youden);" & vbCrLf
4700 RichTextBox2.Text = RichTextBox2.Text & "a = gca();" & vbCrLf
4710 RichTextBox2.Text = RichTextBox2.Text & "a.thickness = 3;" & vbCrLf
4720 RichTextBox2.Text = RichTextBox2.Text & "a.tight_limits = [^on^,^on^,^on^];" & vbCrLf
4730 RichTextBox2.Text = RichTextBox2.Text & "a.isoview =^on^;" & vbCrLf
4740 RichTextBox2.Text = RichTextBox2.Text & "a.axes_visible = [^on^,^on^,^on^];" & vbCrLf
4750 RichTextBox2.Text = RichTextBox2.Text & "a.x_label.font_size = 3;" & vbCrLf
4760 RichTextBox2.Text = RichTextBox2.Text & "a.x_label.text =^" & "Test 1" & "^;" & vbCrLf
4770 RichTextBox2.Text = RichTextBox2.Text & "a.y_label.font_size = 3;" & vbCrLf
4780 RichTextBox2.Text = RichTextBox2.Text & "a.y_label.text =^" & "Test 2" & " ^" & vbCrLf
4790 RichTextBox2.Text = RichTextBox2.Text & "a.z_label.font_size = 3;" & vbCrLf
4800 RichTextBox2.Text = RichTextBox2.Text & "a.z_label.text =^%^;" & vbCrLf
4810 RichTextBox2.Text = RichTextBox2.Text & "a.title.font_size = 3;" & vbCrLf
4820 RichTextBox2.Text = RichTextBox2.Text & "a.title.text =^"&ComboBox2.Text&" - Youden^;"&vbCrLf
4830 RichTextBox2.Text = RichTextBox2.Text & "a.rotation_angles =[50,-30];" & vbCrLf
4840 RichTextBox2.Text = RichTextBox2.Text & "a.children(1, 1).color_mode = 12;" & vbCrLf
4850 RichTextBox2.Text = RichTextBox2.Text & "a.children(1, 1).hiddencolor = 9;" & vbCrLf
4860 RichTextBox2.Text = RichTextBox2.Text & "a.axes_reverse = [^off^,^off^,^off^];" & vbCrLf
4870 '' 3D Classifier Data1
4880 '' 3D Classifier Data2
4890 ' 3D Classifier Data
4900 RichTextBox2.Text = RichTextBox2.Text & "scf;" & vbCrLf
4910 RichTextBox2.Text = RichTextBox2.Text & " mesh(X, Y, ClassifierData);" & vbCrLf
4920 RichTextBox2.Text = RichTextBox2.Text & "a = gca();" & vbCrLf
4930 RichTextBox2.Text = RichTextBox2.Text & "a.thickness = 3;" & vbCrLf
4940 RichTextBox2.Text = RichTextBox2.Text & "a.tight_limits = [^on^,^on^,^on^];" & vbCrLf
4950 RichTextBox2.Text = RichTextBox2.Text & "a.isoview =^on^;" & vbCrLf
4960 RichTextBox2.Text = RichTextBox2.Text & "a.axes_visible = [^on^,^on^,^on^];" & vbCrLf
4970 RichTextBox2.Text = RichTextBox2.Text & "a.x_label.font_size = 3;" & vbCrLf
4980 RichTextBox2.Text = RichTextBox2.Text & "a.x_label.text =^" & "Test 1" & "^;" & vbCrLf
```

```
4990 RichTextBox2.Text = RichTextBox2.Text & "a.y_label.font_size = 3;" & vbCrLf
5000 RichTextBox2.Text = RichTextBox2.Text & "a.y_label.text =^" & "Test 2" & " ^" & vbCrLf
5010 RichTextBox2.Text = RichTextBox2.Text & "a.z_label.font_size = 3;" & vbCrLf
5020 RichTextBox2.Text = RichTextBox2.Text & "a.z_label.text =^%^;" & vbCrLf
5030 RichTextBox2.Text = RichTextBox2.Text & "a.title.font_size = 3;" & vbCrLf
5040 RichTextBox2.Text = RichTextBox2.Text & "a.title.text =^" & ComboBox2.Text & _
5045     " - Classifier^;" & vbCrLf
5050 RichTextBox2.Text = RichTextBox2.Text & "a.rotation_angles =[50,-30];" & vbCrLf
5060 RichTextBox2.Text = RichTextBox2.Text & "a.children(1, 1).color_mode = 12;" & vbCrLf
5070 RichTextBox2.Text = RichTextBox2.Text & "a.children(1, 1).hiddencolor = 9;" & vbCrLf
5080 RichTextBox2.Text = RichTextBox2.Text & "a.axes_reverse = [^off^,^off^,^off^];" & vbCrLf
5090 ' 2d classfier
5100 RichTextBox2.Text = RichTextBox2.Text & "scf;" & vbCrLf
5110 RichTextBox2.Text = RichTextBox2.Text & " mesh(X, Y, ClassifierData);" & vbCrLf
5120 RichTextBox2.Text = RichTextBox2.Text & " mesh(X, Y, ClassifierDataBaz);" & vbCrLf
5130 RichTextBox2.Text = RichTextBox2.Text & "a = gca();" & vbCrLf
5140 RichTextBox2.Text = RichTextBox2.Text & "a.thickness = 3;" & vbCrLf
5150 RichTextBox2.Text = RichTextBox2.Text & "a.tight_limits = [^on^,^on^,^on^];" & vbCrLf
5160 RichTextBox2.Text = RichTextBox2.Text & "a.isoview =^on^;" & vbCrLf
5170 RichTextBox2.Text = RichTextBox2.Text & "a.axes_visible = [^on^,^on^,^on^];" & vbCrLf
5180 RichTextBox2.Text = RichTextBox2.Text & "a.x_label.font_size = 3;" & vbCrLf
5190 RichTextBox2.Text = RichTextBox2.Text & "a.x_label.text =^" & "Test 1" & "^;" & vbCrLf
5200 RichTextBox2.Text = RichTextBox2.Text & "a.y_label.font_size = 3;" & vbCrLf
5210 RichTextBox2.Text = RichTextBox2.Text & "a.y_label.text =^" & "Test 2" & " ^" & vbCrLf
5220 RichTextBox2.Text = RichTextBox2.Text & "a.z_label.font_size = 3;" & vbCrLf
5230 RichTextBox2.Text = RichTextBox2.Text & "a.z_label.text =^%^;" & vbCrLf
5240 RichTextBox2.Text = RichTextBox2.Text & "a.title.font_size = 3;" & vbCrLf
5250 RichTextBox2.Text = RichTextBox2.Text & "a.title.text =^" & ComboBox2.Text & _
5255     " - Classifier^;" & vbCrLf
5260 RichTextBox2.Text = RichTextBox2.Text & "a.rotation_angles =[50,-30];" & vbCrLf
5270 RichTextBox2.Text = RichTextBox2.Text & "a.children(1, 1).color_mode = 12;" & vbCrLf
5280 RichTextBox2.Text = RichTextBox2.Text & "a.children(1, 1).hiddencolor = 9;" & vbCrLf
5290 RichTextBox2.Text = RichTextBox2.Text & "a.children(2, 1).color_mode = 5;" & vbCrLf
5300 RichTextBox2.Text = RichTextBox2.Text & "a.children(2, 1).hiddencolor = 21;" & vbCrLf
5310 RichTextBox2.Text = RichTextBox2.Text & "a.view = ^2d^;" & vbCrLf
5320 RichTextBox2.Text = RichTextBox2.Text & "a.axes_reverse = [^off^,^off^,^off^];" & vbCrLf
5330 RichTextBox2.Text = RichTextBox2.Text.Replace("^", """")
5340 End If
5350 Label3.Text = Math.Round((1 - TPR) * 100, 2) & "%"
5360 Label11.Text = TNNew
5370 Label12.Text = FPnew
5380 Label13.Text = FNNew
5390 Label14.Text = TPNew
5400 Label15.Text = Excluded
5410 s = ComboBox1.Text & vbTab & ComboBox4.Text & vbTab & _
5411 ComboBox5.Text & vbTab & ComboBox2.Text & vbTab & _
5420 TNNew & vbTab & FPnew & vbTab & FNNew & vbTab & _
5421 TPNew & vbTab & Excluded & vbTab & Math.Round((1 - TPR) * 100, 2) & "%"
5430 RichTextBox3.Text = RichTextBox3.Text & vbLf & s
5440 End Sub
5450 Sub IslemiYap()
5460 Panel2.Visible = False
5470 DataSifirla()
5480 DataOku()
5490 HesaplariYap()
5500 hesabi_goster()
5510 Panel2.Visible = True
```

```
5520 End Sub
5530 Private Sub Button2_Click(sender As Object, e As EventArgs) Handles Button2.Click
5540 batchprocess = False
5550 RichTextBox2.Clear()
5560 IslemiYap()
5570 End Sub
5580 Private Sub Baslik_Al_Click(sender As Object, e As EventArgs) Handles Button1.Click
5590 Dim txt As String = RichTextBox1.Text
5600 txt = txt.Replace(vbCrLf, vbLf)
5610 txt = txt.Replace(vbCr, vbLf)
5620 Dim str As String
5630 str = txt.Split(vbLf)(0)
5640 ComboBox4.Items.Clear()
5650 ComboBox5.Items.Clear()
5660 ComboBox6.Items.Clear()
5670 For i = 0 To str.Split(vbTab).Count - 1
5680 ComboBox4.Items.Add(str.Split(vbTab)(i))
5690 ComboBox5.Items.Add(str.Split(vbTab)(i))
5700 ComboBox6.Items.Add(str.Split(vbTab)(i))
5710 Next
5720 ComboBox4.SelectedIndex = 3
5730 ComboBox5.SelectedIndex = 10
5740 ComboBox6.SelectedIndex = 1
5750 ComboBox2.SelectedIndex = 0
5760 ComboBox1.SelectedIndex = 0
5770 RichTextBox3.Text = "Adım" & vbTab & "Test 1" & vbTab & "Test 2" _
5771 & vbTab & "Kombinasyon" _
5780 & vbTab & "TN" & vbTab & "FP" & vbTab & "FN" & vbTab & _
5781 "TP" & vbTab & "Excluded" & vbTab & "CCR%"
5790 End Sub
5800 Private Sub Button3_Click(sender As Object, e As EventArgs) Handles Button3.Click
5810 batchprocess = True
5820 RichTextBox2.Clear()
5830 Dim n As Integer
5840 n = ComboBox4.Items.Count * ComboBox5.Items.Count * ComboBox2.Items.Count
5850 ProgressBar2.Maximum = n + 1
5860 ProgressBar2.Value = 0
5870 For i = 3 To 9
5880 For j = 10 To 44
5890 For k = 0 To ComboBox2.Items.Count - 1
5900 ComboBox4.SelectedIndex = i
5910 ComboBox5.SelectedIndex = j
5920 ComboBox2.SelectedIndex = k
5930 IslemiYap()
5940 ProgressBar2.Value = ProgressBar2.Value + 1
5950 Next
5960 Next
5970 Next
5980 End Sub
5990 End Class
```

APPENDIX B. HP4284A DATASHEET

HP4284A can measure at 8610 distinct frequencies between 20 Hz to 1 MHz, with ±0.01% accuracy [206]. HP4284A has built in "zero open" calibration feature for eliminating measurement errors caused by the parasitic stray impedance. Similarly "zero short" calibration functionality, can be used to eliminating measurement errors caused by the residual impedance. The measurement accuracy of HP4284A is ≈ 0.05% between 1 kHz to 100 kHz, and increases with the frequency of the measurement as

$$Accuracy(\%) = 0.05 + 5 * 10^{-5} * f \tag{B.1}$$

where f is the measurement frequency. The measurement accuracy changing with the frequency can be plot as in Figure B.1 [206].

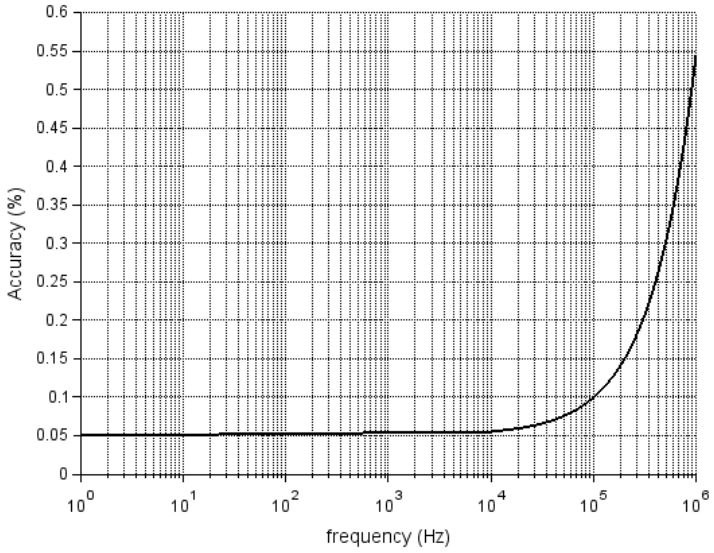

Figure B.1 Measurement accuracy of HP4284 changes when measurement frequency is changed.

HP4284A can be programmed to list sweep at 10 different measurement frequencies at a time. Therefore, for measuring more than 10 frequencies by a control program, the measurement should be start list sweep for maximum of 10 frequencies, read the results and start list sweep for the next 10 frequencies.

APPENDIX C. IMPEDIMED SFB7 USER MANUAL

Imp SFB7
Instructions For Use

ImpediMed Limited
ABN 65 089 705 144
Unit 1
50 Parker Court
Pinkenba Qld 4008
Australia

Phone: + 61 7 3860 3700
Fax: + 61 7 3260 1225
Email: enquiries@impedimed.com
Website: http://www.impedimed.com\

EC	REP

MediMark Europe Sarl
11 rue Emile ZOLA,
B.P. 2332, 38033 Grenoble Cedex 2
France

CE 0120

For patent(s) and/or patent application(s) see: www.impedimed.com.au/products/patents

Contents

Notes on Safety

The warning signs and the symbols below are listed in order for you to use this product safely and correctly as well as to prevent risk and injury to you and others.

The meanings of the signs are as follows:

Symbol	Definition
Warning	Indicates matters in which the possibility of death or serious injury may arise as a result of incorrect handling.
Caution	Indicates matters in which bodily harm or material damage or incorrect measurements may arise as a result of incorrect handling.
	What you should NOT do.
	An action that must be followed.
	Follow instructions for use

Warning

Only use the power adaptor that is supplied with this device. The use of any other power adaptor may expose the patient to the risk of electrocution.

Caution

Do not use or operate the device in the presence of strong electromagnetic fields.

This Medical Device may interfere with other Medical Devices in its vicinity.

Run a calibration check with the test cell prior to using on a patient.

For EU Customers: All products at the end of their life may be returned to ImpediMed for recycling.

There are no user adjustable parts in the device, do not disassemble unit.

This device is rated BF as per IEC60601-1.
This device meets the standard IEC60601-1-2.

Description of Features

Bioimpedance analysers offer rapid, non-invasive, inexpensive determination of body composition by measuring fat-free mass, fat mass, intra and extra cellular fluid. The instruments also enable long-term patient monitoring and provide reports to support clinical and research practices.

The SFB7 is a portable battery powered device. It takes 6 hours to charge the fully depleted battery, with 4 to 8 hours of operating time before recharging is needed.

Note Imp SFB7 is supplied with fully depleted battery. It should be charged for 6 to 8 hours before using the device.

The device has a tetra-polar set of leads, which are attached to self-adhesive skin electrodes by means of alligator clips.

The SFB7 has two operating modules: Bioimpedance Spectroscopy (BIS) and Selected Frequencies bioimpedance.

Caution

Imp SFB7 is designed to be used on battery during the measurement process. This process combined with the advanced noise reduction engineering will ensure the high precision in each measurement by reducing the background noise. Running the device from the mains during the measurement process can cause noise in the measurements. The Imp SFB7 should be unplugged from the recharging unit before use to avoid this possible noise contamination of the measurement.

BIS Mode (Bioimpedance Spectroscopy)

BIS mode measures bioimpedance parameters over a frequency range of 4 - 1000 kHz with 256 data points defining the BIS mode as a true bioimpedance spectroscopy. On-screen graphs display the measured data in the form of a Cole plot, resistance vs. frequency and reactance vs. frequency. In addition the characteristic frequency for the subject is determined as well as total cell membrane capacitance. These estimates are then used in algorithms to give body water and fat free mass.

The SFB7 will store more than 1000 data records which can be analysed on the device or downloaded via an Ethernet connection to the supplied BioImp BIS software running on a Windows PC.

Selected Frequencies Mode (SFBI)

Selected Frequencies Mode BioImpedance mode measures bioimpedance parameters over a frequency range of 4 – 1000 kHz. There are 8 selectable frequencies, of which 5 are fixed and three are user definable. The five fixed frequencies are 5, 10, 50, 100 and 500 kHz, and the 3 user definable frequencies may be any in the range of available frequencies. Results for all 8 frequencies are presented on the LCD.

A user may also specify the number of measurements to be taken, with a specified Measurement Interval.

The SFBI function is included to allow a user to compute and present estimates of Body Composition using published algorithms.

Caution

Please read all these instructions completely before use.

User Information

Intended Use

The ImpediMed Imp SFB7 is a medical device, intended to be operated by users who have read this manual, for use on healthy patients for the purpose of Body Composition Analysis.

Contraindications

Warning

Do not connect the Imp SFB7 device to:

- Patients with active implanted medical devices, e.g. cardiac pacemakers, defibrillators or patients connected to electronic life support devices
- Patients undergoing external defibrillation

Caution

- Pregnant patients

  While the use of bioimpedance technology in pregnant patients has been shown to have had no adverse effects[1][2][3], the Imp SFB7 has yet to be clinically validated for use with that population group.

[1] Ritsuko Y *et al.* Bioelectrical impedance analysis in the clinical management of preclamptic women with edema. *J Perinat.Med* 31 (2003) 275 - 280

[2] Valensise H *et al* Multifrequency bioelectrical impedance analysis in women with a normal and hypertensive pregnancy. *Am J Clin Nutr* 72 (2000) 780 - 783

[3] Larciprete *et al.*, Body composition during normal pregnancy: reference ranges. *Acta Diabetol* 40 (2003) S225 – S232

Components of the Imp SFB7 System

ImpediMed Imp SFB7 is supplied with following accessories

- Single use BIA electrodes (1)
- Lead set (2)
- Four alligator clips (3)
- Test cell for calibration check (4)
- Power module for recharging the battery (5)
- Mains power Cable (Region specific)
- Crossover network cable (7)
- Carry case*
- CD-ROMs containing (8):

Disk 1: Imp SFB7 - Instructions for Use
BioImp Body Composition Analysis Software
BioImp Body Composition Analysis Software Instructions For Use
Network Setup Guide
Electrode Placement Chart

- Stylus pen(9)
- Microfibre cloth (10)
- Alcohol swabs*
- Notepad*
- Warranty card*
- Ethernet network adaptor*

* Not shown in above photograph

Main Display and Control Functions

Front Panel

Imp SFB7 front panel has a On / Off button, measure button and touch screen. Always use the ImpediMed supplied rubber end of stylus pen to operate the touch screen.

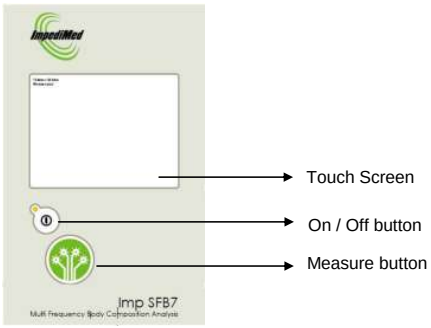

Caution

Do not use any sharp or metal objects to operate the touch screen. Use the stylus end (rubber tip) of the ImpediMed supplied pen. Avoid excessive force as this may damage the screen.

Start-up Screen

Turn the unit on by pressing the On/Off button on the front panel of the unit. After a couple of seconds, the unit will display the ImpediMed logo. The unit will then undertake several self-diagnostic tests before displaying the opening screen, as shown below:

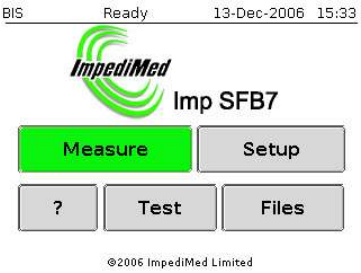

The Imp SFB7 will automatically switch OFF if there is no activity after the set amount of time. (Power options refer to page 14).

Caution

Before use, check the battery status on the display. If the battery level is low, the red LED on the device flashes and device turns off, preventing from taking the measurements.

Measure

Touching the “Measure” button brings up the loaded module’s “Measurement Setup” screen, as described in the appropriate module section of this manual.

Setup

Touching the “Setup” button brings up the “System Setup” screen, as described in the “Setup” section. Refer to Setup page 12.

Files

When the BIS module is loaded, touching the “Files” button will provide access to the list of saved measurement files on the device. From this list, measurement files can be viewed and/or deleted as described in the BIS Measurement Data Files section.

Help

Help is available on most screens by touching the “?” button.

Status Bar

The status bar is displayed at the top of the screen in all menu screens.

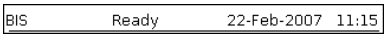

Loaded Module Indicator

The text on the left side of the status bar shows the currently loaded module of the device: BIS (Spectroscopy) or SFBI (Selected Frequencies). The loaded module may be changed in the Module Selection screen (see Module Selection section below), accessible via the System setup screen (see Device Setup section below).

Status Indicator

Next to the loaded module indicator is a status indicator. In most cases, this will display “Ready”, to indicate that the device is ready to receive commands. This status indicator will change while the device is busy or waiting.

Date and Time

Next to the status indicator is the current date and time. The date and time can be set in the device screen.

Keypad Screen

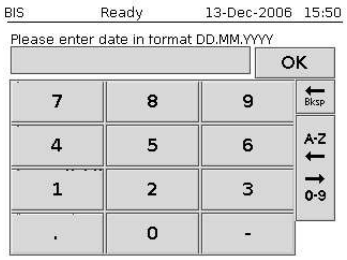

The keypad screen appears when text or numerical input is required. The Prompt will indicate what information is required. Touch the keys to type in the "Entered text" edit box. Touch the "OK" button to save the entered text.

Note Touch "0-9" toggle button to access and use numerical inputs, and touch "A-Z" toggle button to access and use alphabets for text entry.

Setup

Touching the “Setup” button on the opening screen opens the “System Setup” screen as shown below:

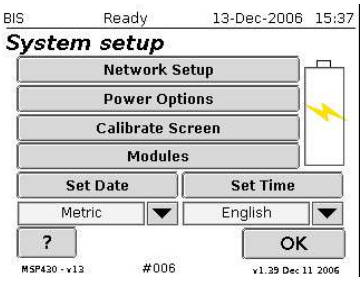

Network Setup

The addresses used for intranet data communication can be set by touching the “Network setup” button, which opens the following screen:

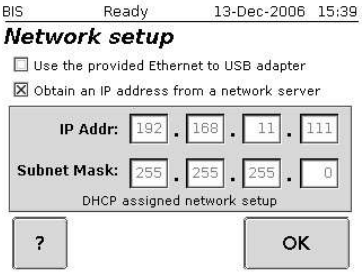

Note See Network Setup Guide supplied with the device for detailed information

The device can be setup to have it obtain an IP address from a DHCP server on the connected network or default to the IP address for the supplied Ethernet to USB adapter. Touch the “OK” button to save the selections and return to the system setup screen.

Note Before connecting the device to a network please contact your network administrator

Power Options

Depending on the user requirements, battery power saving options “Idle Shutdown” and “Screen saver” can be set on this.

By enabling and setting the “Idle Shutdown” time, the device will automatically shut itself down if no actions are performed on the device in the set time limit. By enabling and setting the “Screen saver” time, the device displays a screen saver if no actions are performed on the device in the set time limit.

Calibrate touch screen

The touch screen can be recalibrated by touching the “Calibrate screen” button and following instructions. Once the calibration is complete, press the “OK” button on the calibration confirmation screen before the timer times out.

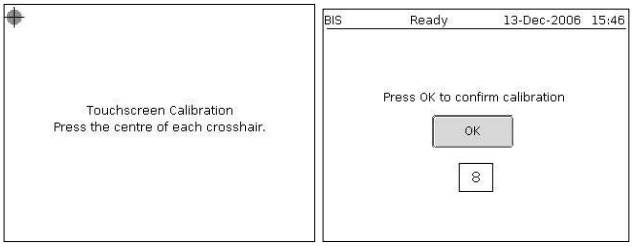

If a mistake is made while calibrating, continue to follow instructions and then allow the device to timeout before repeating the calibration.

Module Selection

Touching the “Modules” button on the “System Setup” screen opens the “Module Selection” screen, as shown below.

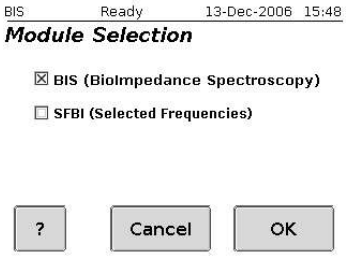

To activate a module, click the appropriate button. The currently loaded module is shown in the left corner of the status bar at the top of the screen.

Setting date, time, units of measurement and language

The date and time should be factory set and displayed at the top of the LCD display. If, however, they are incorrect they can be selected by touching the “Set date” or “Set time” buttons. A keypad, as described above, will be displayed and the date or time can be edited, as instructed on the screen. Please note that a “full stop” must separate day, month and year, or hours, minutes and seconds.

Units of measurement (either metric or imperial) can be selected by touching the arrow next to the units of measurement selection box.

One of the five languages (English, French, German, Italian and Spanish) can be selected by touching the arrow next to the language selection box. Touch the OK button to initiate the selected language.

Calibration Date

The date of last calibration is displayed in the device setup screen.

Battery Status Indicator

The LED indicator on the Imp SFB7 indicates the status of the internally installed rechargeable Lithium-ion. The colour of the LED behaviour is defined as below:

LED Colour	LED behaviour	Description
None	Off	- Unit is turned off - No external power is present
Green	Off, flicking on at 1 second intervals.	- Unit is turned off - External power is present - Batteries are charging
Green	On	- Unit is operational - External power is present - Batteries are fully charged
Green	On, flicking off at 1 second intervals.	- Unit is operational - External Power is present - Batteries are charging.
Green	1 second on, 1 second off	- Unit is operational - No external power is present - Unit is running off batteries
Orange	On	- Unit is operational - Batteries are near flat
Red	Off, flicking on at 1 second intervals.	- Unit is operational - Batteries are flat - Unit will shut down after four seconds.
Red	Off, flicking on twice at 1 second intervals	- Battery Charger Fault
Red, Orange	Off, flicking on twice – once red, once orange – at 1 second intervals	- Battery Voltage Detection Fault

Note Imp SFB7 should be unplugged from the recharging unit before use to avoid possible noise contamination of the measurement.

Note The colour of LED indicator on the power adaptor indicates the level of current that the Imp SFB7 is drawing to recharge its built in battery. Red indicates higher current is being drawn because the internal battery is flat, yellow indicates moderate current is being used, and green indicates trickle current is being used to charge the battery.

Preparing For Measurements

Patient selection

Certain situations are known to affect body water concentration:

- Just prior, during, just after menstruation
- Use of diuretics
- Renal or heart failure
- Excessive exercise 2 hours prior to bioimpedance analysis (BIA)
- Consumption of excessive alcohol within 12 hours prior to BIA

For patients whose hydration status is affected by these conditions, use of the algorithm(s) to estimate total body water, intracellular fluid, extracellular fluid, fat-free mass, or fat mass may lead to results that do not reflect the individual's normal state[4]

Patient preparation

Prior to analysis the patient should:

1. Remove all jewellery (rings on fingers may be left on)
2. Remove stockings / pantyhose or socks
3. Have an empty bladder
4. Be accurately measured, for height (to the nearest 0.5cm) and weight (to the nearest 0.1kg)
5. Lie on their back in a fully supine position on the examination table
6. Extend their arms by their side, hands resting next to their body, palms down, with their legs slightly apart

Note It is preferable if the measurements are undertaken under similar conditions, e.g. time of day, activity levels, and food and fluid intake and the analysis is completed within 10 minutes of the patient assuming the supine position.

[4] Bioelectrical Impedance Analysis in Body Composition Measurement, National Institutes of Health Technology Assessment Conference Statement, December 12-14, 1994, p 13

Placing the electrodes on the patient

1. Shave electrode sites if necessary to gain good skin contact. Thoroughly clean the areas and allow to dry
2. Tear open sealed foil pouch
3. Slowly and carefully remove electrodes from backing sheet
4. Apply each electrode adhesive side to the skin, at one of the standard placement sites (as shown below) so that the tab faces outward from the body
5. To ensure good electrode contact, start from the outer edge and run your finger around the electrode several times, working toward the centre
6. Place all four electrodes on the patient before connecting any alligator clips
7. Reseal pouch after opening, to prevent electrode gel on unused electrodes from dehydrating

Caution

Only use ImpediMed Electrodes

Avoid placing an electrode on an irritated skin site

If skin irritation occurs seek professional advice

Allow skin to dry thoroughly before placing electrodes on skin

Do not connect alligator clips to patient's skin

Do not mix single use and reusable or different brands of electrodes

Do not cut the electrode, use whole electrode only

Do not use extra electrode gel with solid gel electrodes

Do not leave the electrodes attached to the skin for longer than 1 hour

Standard placement sites for the electrodes in BIS and SFBI Modes

Note Measurements can be done on either the right hand side or the left hand side. However it is a good clinical practice to always use the same side for BIA measurements to ensure longitudinal stability over repeated measurements.

RIGHT HAND

On the right hand wrist between the two protruding bones

Ensure that the two electrodes on the hand are 5cm apart

RIGHT FOOT

On the right foot, on the ankle at the level of and between the medial and lateral malleoli (the large protruding bones on the side of the ankle)

Ensure that the two electrodes are 5cm apart

Plug leads into the Device

The device includes four (blue, black, yellow, red) colour coded locking socket connectors designed to accept a single-lead patient cable on each connector.

Align the groove on the connector lead (female insert) to locking socket (male insert) head on the device.

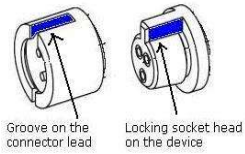

Press firmly to attach each colour coded lead plug to the similar colour locking socket on the Imp SFB7 one by one.

Caution

Hold the locking socket plug on the connector lead firmly one at a time, and pull the lead off straight to avoid any damage to the leads.

Caution

Use only the cable leads supplied by ImpediMed Limited with the Imp SFB7. The use of non ImpediMed leads can cause damage to the device or give an incorrect reading.

Apply lead wires according to the colour code shown above. Use an alligator clip to connect each lead to the tab portion of an electrode.

Warning

Do not plug SFB7 leads to any mains power outlet/point.

Ensure that the metallic part of the clip is in direct contact with the conductor side (underside) of the electrode tab and that the clips are aligned to the centres of the electrode tabs.

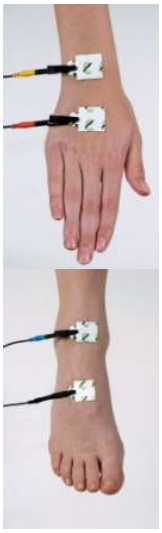

Yellow (Sense lead)

The **yellow** lead end is attached to the electrode on the right hand, on the wrist next to the ulnar head (wrist joint)

Red (Current source lead)

The **red** lead end is attached to the electrode on the dorsal surface of the right hand

Blue (Sense lead)

The **blue** lead end is attached to the electrode on the dorsal surface of the right foot, on the ankle at the level of medial and lateral malleoli (large protruding bones on the side of the ankle)

Black (Current sink lead)

The **black** lead end is attached to the electrode on the dorsal surface of the right foot

Ensure that the patient's limbs are not crossed (so the electrical path is not short-circuited) and that their legs are completely separated

For patients who cannot effectively separate their inner thighs, it may be necessary to place insulating material (e.g. dry clothes) between them.

Note Hanging up the leads vertically for storage greatly mitigates tangling

Typical final set-up ready for measurement

Taking a Measurement in BIS Mode (Bioimpedance Spectroscopy)

Measurement setup

Touching the “Measure” on the opening screen opens the “Measurement Setup” screen as shown below:

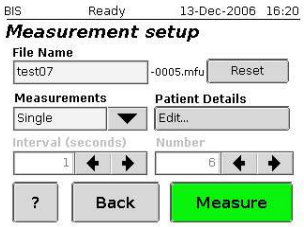

File Name

Touching the “File Name” edit box brings up the keypad as described in the Start up Screen section.

A filename may be specified for saving the measurement data for later analysis. When measurement data is saved, an incrementing number is attached to the specified filename. If no filename is specified, measurement data will not be saved.

Patient Details

Touching the Patient Details “Edit…” button gives access to the BIS Patient Details screen, where the patient parameters required for the TBW calculations may be entered.

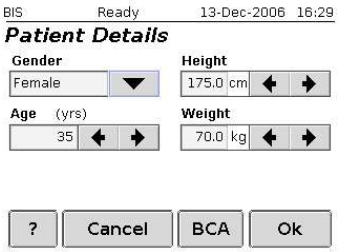

Touching the arrow button next to the “Gender” selection box toggles the selection of gender. Touching the arrow buttons next to the “Height”, “Age” and “Weight” edit box allows the selection of the height, age and weight respectively. The values can also be entered using the keypad (see Start up Screen section) that is selected by touching the appropriate edit box itself.

Note Maximum height is 250cm, maximum weight is 350kg, and maximum age is 110 years.

Touch the “OK” button to return to the previous screen.

Additional information relating to the calculation of body composition parameters can be set up by touching the “BCA” button, which opens the following screen:

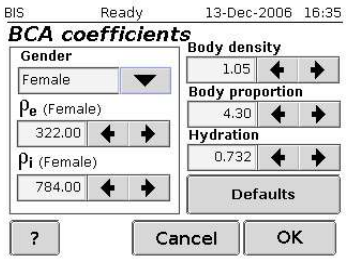

As with the previous screen, the values of each parameter can be selected by touching the arrow buttons adjacent to the parameter edit box or by using the keypad that is selected by touching the appropriate edit box itself. Touch the “OK” or “Cancel” button to return to the “Patient Details” screen.

Measurements setting (and interval and number of measurements)

Touching the arrow button next to the “Measurements” selection box allows the selection of single or continuous measurements, or several measurements made spaced at a selected interval of time. In continuous mode, another measurement is commenced immediately after the previous measurement has been completed. In interval mode, another sequential measurement is made after the interval of time selected (in seconds).

For Interval measurement setting, the interval between measurements can be selected by touching the arrow buttons next to the “Interval” edit box or by using the keypad (see Start up Screen section) that is selected by touching the “Interval” edit box.

For Interval and Continuous measurement settings, the number of measurements can be selected by touching the arrow buttons next to the “Number” edit box or by using the keypad (see Start up screen section) that is selected by touching the “Number” edit box.

The “Number” and “Interval” edit box are greyed out and inaccessible when they are not applicable to the current “Measurements” setting.

Making a Measurement

Touch the “Measure” button on the Measurement Setup screen or press the large green button on the device front panel to enter the Begin Measurement screen.

Begin Measurement

Touching the “Measure” button on the opening screen, or pressing the large green button on the front panel of the device, opens the “Begin measurement” screen as shown below. The screen shows a summary of the measurement setup for confirmation.

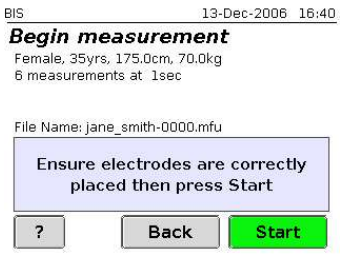

Caution

If the combination of the file name specified in the "Measurement setup" screen and the current increment number already exists in the device file memory, a warning message will appear in the "Begin measurement" screen: "One or more files already exist. Press start to overwrite". Touching the "Start" button overwrites the existing files with new measurement data and touching the "Back" button displays the "Measurement setup" page for editing the file name.

Note If the grey box in "Begin measurement" screen displays a message "Not Calibrated", please contact ImpediMed or an authorised agent for device calibration.

Making a measurement

A measurement is made by touching the "Start" button on the "Begin measurement" screen, or by pressing the large green button on the front panel of the device when in the "Begin Measurement" screen. The device will take a measurement, and then bring up the Measurement Results screens as described in Measurement Results section immediately below.

Measurement Results

The first results screen displays the measurement analysis results

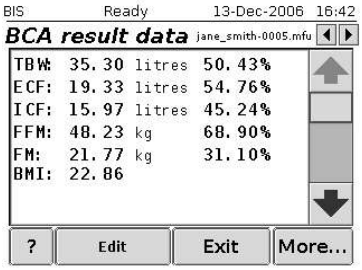

Touch the up and down arrow buttons or the scroll bar to show the full results. The patient settings may be modified, and the results recalculated, by touching the "Setup" button, which brings up the "Patient Details" screens, as described in "BIS patient settings" above.

The file navigation arrows are greyed out and inaccessible. These are only accessible when viewing files from the file list.

Touching the "More…" button will display a Cole plot (Reactance vs. Resistance).

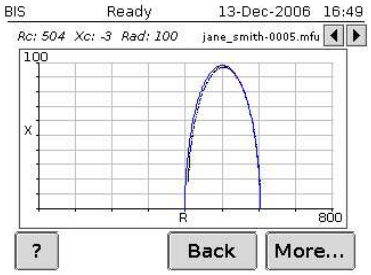

The Cole plot gives a visual representation of the measurement and is used to indicate a valid measurement has been taken. The absence of scattered data points and well fit Cole plot signifies noise free data and that a valid measurement has been performed.

The file navigation arrows are greyed out and inaccessible. These are only accessible when viewing files from the file list.

Touching the “More…” button will display resistance and reactance plots as below:

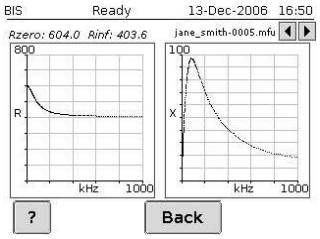

Resistance vs. frequency plot and reactance vs. frequency plots are visual representation of the measured bioimpedance data.

The file navigation arrows are greyed out and inaccessible. These are only accessible when viewing files from the file list.

Taking a Measurement in Selected Frequencies Mode (SFBI)

Measurement setup

Touching the “Measure” on the opening screen opens the “Measurement Setup” screen as shown below:

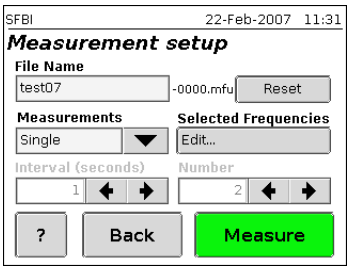

File Name

Touching the “File Name” edit box brings up the keypad as described in “Keypad Screen” under Main Display and Control Functions above.

A filename may be specified for saving the measurement data for later analysis. When measurement data is saved, an incrementing number is attached to the specified filename. If no filename is specified, measurement data will not be saved.

Selected Frequencies

Touching the Selected Frequencies “Edit…” edit box gives access to the “Frequency Selection” screen where the frequencies to be used in measurements may be entered. This screen is described in “SFBI Selected Frequencies” section below.

Measurements setting (and interval and number of measurements)

Touching the arrow button next to the “Measurements” selection box allows the selection of single or continuous measurements, or several measurements made spaced at a selected interval of time. In continuous mode, another measurement is commenced immediately after the previous measurement has been completed. In interval mode, another sequential measurement is made after the interval of time selected (in seconds).

For Interval measurement setting, the interval between measurements can be selected by touching the arrow buttons next to the “Interval” edit box by using the keypad (see “Keypad Screen” under Main Display and Control Functions above) that is selected by touching the “Interval” edit box.

For Interval and Continuous measurement settings, the number of measurements can be selected by touching the arrow buttons next to the “Number” edit box or by using the keypad (see “Keypad Screen” under Main Display and Control Functions above) that is selected by touching the “Number” edit box.

The “Number” and “Interval” edit boxes are greyed out and inaccessible when they are not applicable to the current “Measurements” setting.

Making a Measurement

Touch the “Measure” button on the Measurement Setup screen or press the large green button on the device front panel to enter the Begin Measurement screen.

Selected Frequencies (SFBI)

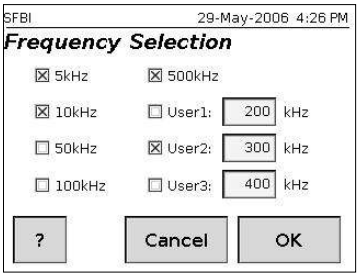

Up to eight single frequency measurements can be taken for a single SFBI measurement by selecting the tick boxes for each of the frequency values. Five of the frequency values are preset to set values (5 kHz, 10 kHz, 50 kHz, 100 kHz, 500 kHz). The other three frequency values are user definable with in the range of 4 – 1000 kHz, and can be entered using the keypad that is selected by touching the appropriate text box (see “Keypad Screen” under Main Display and Control Functions above).

Touch the “OK” button to return to the previous screen.

Begin Measurement

Touching the “Measure” button on the “Measurement Setup” screen, or pressing the large green button on the front panel of the device, opens the “Begin measurement” screen as shown below. The screen shows a summary of the measurement setup for confirmation.

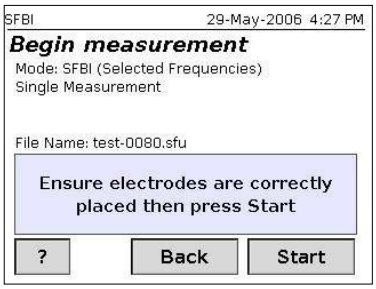

Caution

If the combination of the file name specified in the “Measurement setup” screen and the current increment number already exists in the device file memory, a warning message will appear in the “Begin measurement” screen: “One or more files already exist. Press start to overwrite”. Touching the “Start” button overwrites the existing files with new measurement data and touching the “Back” button displays the “Measurement setup” page for editing the file name.

Note If the grey box in “Begin measurement” screen displays a message “Not Calibrated”, please contact ImpediMed or an authorised agent for device calibration.

Making a measurement

A measurement is made by touching the “Start” button on the “Begin measurement” screen, or by pressing the large green button on the front panel of the device when in the “Begin Measurement” screen. The device will take a measurement, and then bring up the Measurement Results screens as described in Measurement Results section immediately below.

Measurement Results

The SFBI results screen lists the resistance and reactance values for each the selected frequencies.

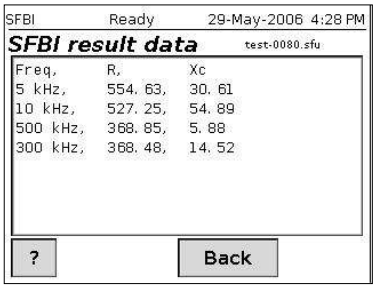

Measurement results may be affected by

- Placing a mobile phone in close proximity to the device during operation
- Metal implants, clips or other types of artificial limbs or implants in the patient
- Patients touching a metal surface during the measurement process
- Using the device when the patient is connected to other medical devices (due to the effect of electrical interference)
- Incorrect height and/or weight values entered into the device
- Incorrect electrode placement
- Using non ImpediMed electrodes
- Using electrodes which are past their use by date
- Re-using disposable electrodes
- Using a part of the full electrode tab
- Using extra electrode gel with solid gel electrodes
- Taking measurements while the device is connected to main power for recharging the battery

BIS Measurement Data Files

Stored files of previous BIS measurements can be deleted or viewed by touching the “Files” button on the opening screen when the BIS module is loaded. Touching the “Files” button opens the “File listing” screen, similar to that shown below:

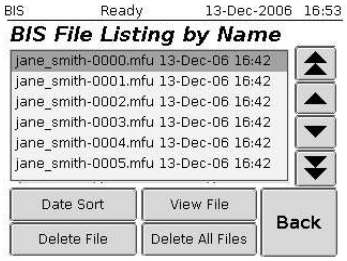

Touching the “Back” button returns to the opening screen.

Navigating the file list

The arrow buttons navigate the file list. The single arrows moves the selection bar at a time, the double arrows move one page at a time. Keeping an arrow button touched will move through the list quickly. The selected file is shown with a darker background. A file can also be selected by touching the appropriate file detail line.

Sort stored files

The stored files can be sorted either by name or by date and time, by touching the lower left hand button titled either “Name sort” or “Date sort”.

Viewing files

The selected file can be viewed by touching the “View File” button. This brings up the BCA result data screen. Touching the “More…” button will display a Cole plot (Reactance vs. Resistance). In addition, the file BCA result data screen and Cole plot screen allows the use of the file navigation tool, allowing the user to move through the file list from the result data screen and plot screen.

Deleting files

Select the desired file using the arrow buttons or by touching the device detail line (the selected file will be shown in reverse video). The selected file can be deleted by touching the “Delete File” button, at which time a confirmation message will be displayed, as below:

Confirm or cancel the action by touching the appropriate button.

Caution

Use with caution. Deleted files cannot be retrieved

Deleting all files

The whole file list can be deleted by touching the “Delete All Files” button, at which time a confirmation message will be displayed, as below:

Confirm or cancel the action by touching the appropriate button.

Caution

Use with caution. Deleted files cannot be retrieved.

SFBI Measurement Data Files

Stored files of previous SFBI measurements can be deleted or viewed by touching the "Files" button on the opening screen when the SFBI module is loaded. Touching the "Files" button opens the "File listing" screen, similar to that shown below:

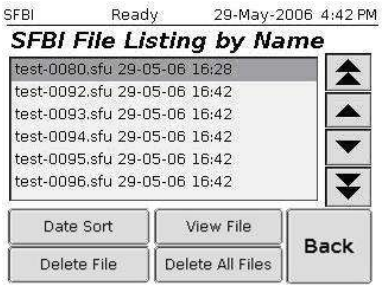

Touching the "Back" button returns to the opening screen.

Navigating the file list

The arrow buttons navigate the file list. The single arrows move one file at a time, the double arrows move one page at a time. Keeping an arrow button touched will move through the list quickly. The selected file is shown with a darker background. A file can also be selected by touching the appropriate file detail line.

Sort stored files

The stored files can be sorted either by name or by date and time, by touching the lower left hand button titled either "Name sort" or "Date sort".

Viewing files

The selected file can be viewed by touching the "View File" button. This brings up the SFBI result screen as in the measurement process.

Deleting files

Select the desired file using the arrow buttons or by touching the device detail line (the selected file will be shown in reverse video). The Selected file can be deleted by touching the “Delete File” button, at which time a confirmation message will be displayed, as below:

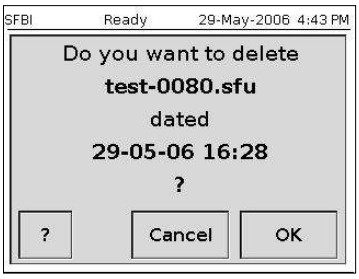

Confirm or cancel the action by touching the appropriate button.

Caution

Use with caution. Deleted files cannot be retrieved

Deleting all files

The whole file list can be deleted by touching the “Delete All Files” button, at which time a confirmation message will be displayed, as below:

Confirm or cancel the action by touching the appropriate button.

Caution

Use with caution. Deleted files cannot be retrieved

File Storage

In BIS or Selected Frequencies mode, when the file storage memory on the device is full, the device stops taking measurements and displays the “File system full remove files to make space” screen.

In order to continue taking measurements, transfer the files on to a PC loaded with BioImp Body Composition Analysis software or delete the files which are not required.

If the user tries to make measurements when the file system is full, it will show the error message in the grey box of “Begin measurement” screen that “No file space left! Remove old files”, and the start button on the “Begin measurement” screen become grey preventing the user to make any measurements.

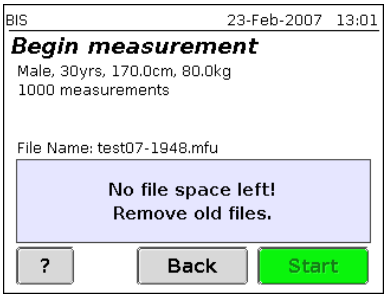

Data Transfer to Analysis Software

Ethernet (BIS or SFBI Module)

Follow the instructions in the BioImp Analysis Software Instructions For Use to connect to the device and retrieve the stored BIS measurement data.

Note BIS and SFBI measurement data is stored on board, but only BIS measurement data is retrievable via Ethernet.

If battery runs flat during data/file upload from the Imp SFB7 via an ethernet, the data/file will be saved on the device.

Note Uploaded files are automatically deleted from the Imp SFB7. Sophisticated file transfer ensures that each file is transferred, confirmed as received, before deletion.

Calibration Check Instructions

There are no user-adjustable parts in the SFB7. Calibration may, however, be checked for quality assurance purposes with the test cell provided. Remove clips and connect the leads to the test cell according to the colour-coding. Select the BIS module on the device. After making a measurement, the following values should be displayed:

Ro: 604 ohms (± 7ohms)

Rinf: 403 ohms (± 5 ohms)

If the readings are not within the specified limits, contact ImpediMed for recalibration of the unit.

For consistently accurate readings we recommend calibration checks be performed at the start of each day of use using the test cell.

Self test patient lead function

The SFB7 is equipped with a function enabling the user to perform a quick test on the patient lead set prior to use. This allows the user to perform a degree of self diagnosis on the device to check the device is performing within specification. From the Main Screen press the “Test” button to bring up the screen below, then remove clips and connect the leads to the test cell according to the colour-coding. Select the BIS module on the device. Press the “Start” button to make a test reading.

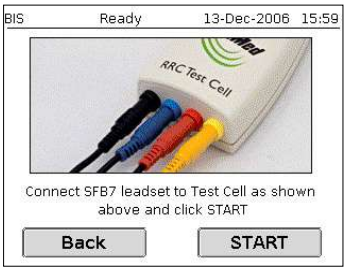

The SFB7 will make a reading while presenting a “Calculating” screen, after which the result of the test will be shown. A “Passed” screen signifies the patient leads are in a serviceable condition.

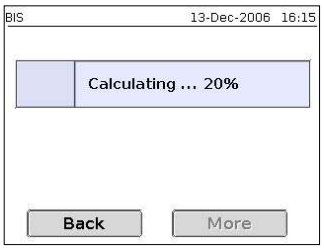

The Cole plot, reactance and resistance plots are also available by pressing the “More” button.

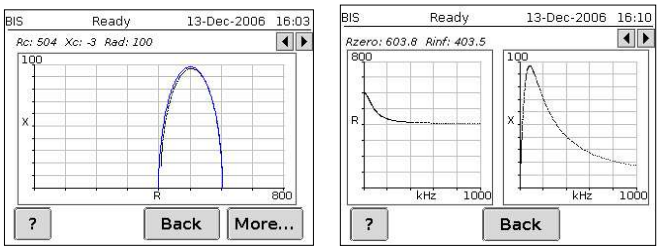

If the patient lead set fails the test, a “Failed” screen with a corresponding error code will be shown. In this case, contact ImpediMed, your distributor or an authorised service centre, quoting the error code, to arrange for service or repair of the patient leads and/or device.

Care and Maintenance

Care of the product

When not in use always keep the SFB7 in the carry case.
Clean the SFB7 with a dry, clean cloth only.
Avoid exposure to water, impact and excessive heat (direct exposure to sunlight).

Caution

Imp SFB7 should not be subjected to ingress of liquid or liquid spillage, impact and excessive heat (direct exposure to sunlight). This can cause damage to the device or harm to the patient or give an incorrect reading. Imp SFB7 should be used in a dry environment. Contact ImpediMed or an authorised agent for repair.

Care of the leads

Clean the leads with a damp cloth if required.

Wherever possible leads should remain connected to the device.

Unnecessary removal of the leads from the device may reduce lead life.

Ensure that the lid of the case does not close on the leads.

Do not wind the leads tightly, crinkle, or twist the leads, as this may cause the fine wires inside to break.

If the leads appear to be damaged, contact ImpediMed or a licensed distributor for replacements.

Leads are consumables. So, handle them carefully.

Care of the electrodes

The electrodes are for single use. Please discard after use.

Reseal the electrode pouch after use.

Unused electrodes should remain in the supplied pouch and in a cool dry place to prevent electrode gel from dehydrating.


Use by expiry date


Single use only

Refer to the expiration date that is printed on each package.

Do not use an electrode IF the conductive adhesive is dry and no longer pliable or sticky. This may result in inaccurate measurements.

Care of the Touch Screen

Always use the stylus pen provided to operate the touch screen.

Note The stylus included in the Imp SFB7 kit is a dual purpose stylus pen. Use the rubber end of the stylus pen to operate Imp SFB7 touch screen

If necessary clean the touch screen with a soft damp cloth, and do not use any liquids directly.

Do not use any sharp or metal objects to operate the touch screen. Use the stylus end (rubber tip) of the ImpediMed supplied pen. Avoid excessive force as this may damage the screen.

Fragile

Battery Replacement and Disposal

The batteries in the SFB7 are rechargeable Lithium Ion batteries and cannot be replaced by the user. Please contact ImpediMed for instructions on the replacement of these batteries by qualified technical personnel.

Repairs

There are no-user repairable electronic parts within the SFB7. Please contact ImpediMed or an authorised agent should service or repair of the Imp SFB7 be required.

Technical Support

Phone: + 61 7 3860 3700

Fax: + 61 7 3260 1225

Email: technicalsupport@impedimed.com

Accessories

The following accessories and consumables are available from ImpediMed.

Description	Part Number
Electrodes (pack of 100)	292-STE
Test cell	292-BISTC
Lead set	292-BISLD
Alligator Clips	292-ALLCP
CD-ROM containing BioImp Analysis Software, BioImp Instructions For Use and the SFB7 Instructions For Use	299-SFB7

Troubleshooting

Problem	*Possible cause*	*Solution*
No display when SFB7 is switched ON.	• Battery power is low.	• Attach external power pack and try again.
	• No external power.	• If external power pack is attached, check that power pack is plugged in and switched on (light on power pack will be on).
The message “Out of Range Check Leads and Electrodes” is displayed on the screen. or The reading is obviously incorrect.	• The device is not correctly set up.	• Ensure the leads have been correctly fitted according to the colour coding (see section “Plug lead in to the device”). • Ensure the leads are inserted properly into the lead sockets. • Ensure the leads are not damaged or tangled. • Ensure the leads are properly inserted into the alligator clips. • Ensure the alligator clips are securely attached to the electrodes. • Ensure the electrodes are fresh. • Perform the calibration check (see section “Calibration Check Instructions”) to determine if the device is faulty. • If performing the calibration check, ensure the colour coding is correct and the leads are pushed snugly into the test cell.
The device stops responding to touch screen commands.	• Internal software fault.	• Power the device off. Power the device on. • Report the fault to ImpediMed.
Power light is blinking. Or Power light is red. Or Power light is orange.	• Normal behaviour	• Refer to section “Battery Status Indicator”.

Product Specifications

Drive AC current	200μA RMS at a variable frequency of 4 kHz to1000 kHz.
Frequency Scan	Range: 4 to 1000 kHz (256 frequencies) Scan speed: <700ms
Battery Charging	12V DC, 2.5A
Impedance	10 to 1100Ω Resolution: 0.1Ω Accuracy: ±1.0% 50Ω to 1100Ω ±5.0% <50Ω
Phase	Range: -90° to +90°, only positive phases displayed Resolution: 0.1° Accuracy: ±0.5° 50 to 1100Ω ±0.5° <50Ω, <315kHz ±5.0° <50Ω, 315 to 1000kHz
Dimensions	L=190mm, W=130mm, D=110mm
Weight	1 kg
Display	320x240 pixel ¼-VGA LCD display
Data displayed	Total body water (TBW), % Total body water Intracellular fluid (ICF), % Intracellular fluid Extracellular fluid (ECF), % Extracellular fluid Fat-free mass (FFM), % Fat-free mass, Fat mass (FM), % Fat mass, BMI Raw data : X centre, R centre, Radius, SEE, R_0, R_∞, Re, Ri, Z char, f char, Membrane capacitance Graphs : Cole plot, Frequency-Resistance plot, Frequency-Reactance plot
Environmental transport, and storage conditions	+10° to +40°C temperature 5% to 95% relative humidity
Environmental operating conditions	+10°C to +40°C 5% to 95% relative humidity
Electrode leads	1.5m lengths with tetra polar electrodes. (Patient circuit is d.c. isolated.)
Device (IEC 60601-1) electrical classification	Type BF 

Electromagnetic Compatibility	Meets the requirements of IEC 60601-1-2.

Glossary

BIA	bioimpedance analysis
ECF	extracellular fluid
FFM	fat-free mass
FM	fat mass
ICF	intracellular fluid
P	phase
R	resistance
TBW	total body water
Xc	reactance
Z	Impedance
SFBI	Selected frequency bioimpedance
BIS	Multi frequency bioimpedance analysis

Notes

REFERENCES

1. Christodoulou, C., and C. Cooper, "What is osteoporosis?," *Postgraduate Medical Journal*, Vol. 79, no. 929, pp. 133–138, 2003.

2. Kanis, J. A., "Diagnosis of osteoporosis and assessment of fracture risk," *The Lancet*, Vol. 359, no. 9321, pp. 1929–1936, 2002.

3. Marcus, R., D. Feldman, D. Nelson, and C. Rosen, *Fundamentals of Osteoporosis*, Academic Press, 2009.

4. Drinkwater, L., R. S. Goldsmith, C. C. Johnston Jr, R. Lindsay, T. M. Mack, P. J. Meunier, B. C. Nordin, and A. M. Parfitt, "Consensus development conference: prophylaxis and treatment of," *British Medical Journal*, Vol. 295, p. 10, 1987.

5. Warming, L., C. Hassager, and C. Christiansen, "Changes in bone mineral density with age in men and women: a longitudinal study," *Osteoporosis International*, Vol. 13, no. 2, pp. 105–112, 2002.

6. Barrett-Connor, E., E. S. Siris, L. E. Wehren, P. D. Miller, T. A. Abbott, M. L. Berger, A. C. Santora, and L. M. Sherwood, "Osteoporosis and fracture risk in women of different ethnic groups," *Journal of Bone and Mineral Research*, Vol. 20, no. 2, pp. 185–194, 2005.

7. Rosen, C. J., and M. L. Bouxsein, "Mechanisms of disease: is osteoporosis the obesity of bone?," *Nature Clinical Practice Rheumatology*, Vol. 2, no. 1, pp. 35–43, 2006.

8. Sharma, S., V. R. Tandon, S. Mahajan, V. Mahajan, and A. Mahajan, "Obesity: Friend or foe for osteoporosis," *Journal of Mid-life Health*, Vol. 5, no. 1, p. 6, 2014.

9. Morcov, C., C. Vulpoi, and D. Branisteanu, "Correlation between adiponectin, leptin, insulin growth factor-1 and bone mineral density in pre and postmenopausal women," *Revista Medico-Chirurgicala a Societatii de Medici si Naturalisti din Iasi*, Vol. 116, no. 3, pp. 785–9, 2012.

10. Baert, A., *Radiology of Osteoporosis*, Springer, 2008.

11. Li, N., D. Cornelissen, S. Silverman, D. Pinto, L. Si, I. Kremer, S. Bours, R. de Bot, A. Boonen, S. Evers, *et al.*, "An updated systematic review of cost-effectiveness analyses of drugs for osteoporosis," *PharmacoEconomics*, pp. 1–29, 2020.

12. Johnell, O., and J. Kanis, "An estimate of the worldwide prevalence and disability associated with osteoporotic fractures," *Osteoporosis International*, Vol. 17, no. 12, pp. 1726–1733, 2006.

13. Parthan, A., M. Kruse, N. Yurgin, J. Huang, H. N. Viswanathan, and D. Taylor, "Cost effectiveness of denosumab versus oral bisphosphonates for postmenopausal osteoporosis in the us," *Applied Health Economics and Health Policy*, Vol. 11, no. 5, pp. 485–497, 2013.

14. Hernlund, E., A. Svedbom, M. Ivergård, J. Compston, C. Cooper, J. Stenmark, E. V. McCloskey, B. Jönsson, and J. A. Kanis, "Osteoporosis in the european union: medical management, epidemiology and economic burden," *Archives of Osteoporosis*, Vol. 8, no. 1, pp. 1–115, 2013.

15. Kanis, J. A., C. Cooper, R. Rizzoli, and J.-Y. Reginster, "Executive summary of the european guidance for the diagnosis and management of osteoporosis in postmenopausal women," *Calcified Tissue International*, Vol. 104, no. 3, pp. 235–238, 2019.

16. Sözen, T., L. Özışık, and N. Ç. Başaran, "An overview and management of osteoporosis," *European Journal of Rheumatology*, Vol. 4, no. 1, p. 46, 2017.

17. Tuzun, S., N. Eskiyurt, U. Akarirmak, M. Saridogan, M. Senocak, H. Johansson, and J. A. Kanis, "Incidence of hip fracture and prevalence of osteoporosis in turkey: the fracturk study," *Osteoporosis International*, Vol. 23, no. 3, pp. 949–955, 2012.

18. Aziziyeh, R., J. G. Perlaza, N. Saleem, Y. Kirazlı, E. Akalın, R. K. McTavish, C. Duperrouzel, and C. Cameron, "The burden of osteoporosis in turkey: a scorecard and economic model," *Archives of Osteoporosis*, Vol. 15, no. 1, pp. 1–9, 2020.

19. Carey, J. J., and M. F. Delaney, "T-scores and z-scores," *Clinical Reviews in Bone and Mineral Metabolism*, Vol. 8, no. 3, pp. 113–121, 2010.

20. Nayak, S., M. S. Roberts, and S. L. Greenspan, "Factors associated with osteoporosis screening and recommendations for osteoporosis screening in older adults," *Journal of General Internal Medicine*, Vol. 24, no. 5, pp. 585–591, 2009.

21. Altin, E., B. Karadeniz, F. Türkyön, F. Baldan, N. Akkaya, N. Atalay, and F. Şahin, "The comparison of knowledge level and awareness of osteoporosis between women and men," *Denizli Pamukkale University*, 2014.

22. Fırat, K., and İ. ÖZTÜRK, "Birinci basamak sağlık hizmetlerinin karşılaştırmalı analizi (benchmarking): Türkiye ve ispanya örneği," *Batı Karadeniz Tıp Dergisi*, Vol. 5, no. 1, pp. 19–26, 2021.

23. Gao, S. S., M. J. Y. Yon, K. J. Chen, D. Duangthip, E. C. M. Lo, and C. H. Chu, "Utilization of a mobile dental vehicle for oral healthcare in rural areas," *International Journal of Environmental Research and Public Health*, Vol. 16, no. 7, p. 1234, 2019.

24. Grossi, M., and B. Riccò, "Electrical impedance spectroscopy (eis) for biological analysis and food characterization: A review," *Journal of Sensors and Sensor Systems*, Vol. 6, no. 2, pp. 303–325, 2017.

25. Grimnes, S., and O. G. Martinsen, *Bioimpedance and Bioelectricity Basics*, Academic press, 2011.

26. Williams, P. A., and S. Saha, "The electrical and dielectric properties of human bone tissue and their relationship with density and bone mineral content," *Annals of Biomedical Engineering*, Vol. 24, no. 2, pp. 222–233, 1996.

27. lJ Frick, H., "A mathematical treatment of the electrical conductivity and capacity of disperse systems," *I: Hysj. cs Review*, no. 25, p. 361, 1925.

28. Damez, J.-L., S. Clerjon, S. Abouelkaram, and J. Lepetit, "Dielectric behavior of beef meat in the 1–1500 khz range: Simulation with the fricke/cole–cole model," *Meat Science*, Vol. 77, no. 4, pp. 512–519, 2007.

29. Ülgen, Y., and M. Sezdi, "Physiological quality assessment of stored whole blood by means of electrical measurements," *Medical & Biological Engineering & Computing*, Vol. 45, no. 7, pp. 653–660, 2007.

30. Matur, F., N. Ozturk, and Y. Ulgen, "Prediction of bone mineral density in menopaused women by using bioimpedance parameters," in *EMBEC & NBC 2017*, pp. 807–810, Springer, 2017.

31. Albright, F., E. C. Reifenstein, *et al.*, "The parathyriod glands and metabolic bone disease," *The Parathyriod Glands and Metabolic Bone Disease*, 1948.

32. Riggs, B., H. Wahner, E. Seeman, K. Offord, W. Dunn, R. Mazess, K. Johnson, L. Melton, *et al.*, "Changes in bone mineral density of the proximal femur and spine with aging: differences between the postmenopausal and senile osteoporosis syndromes," *The Journal of Clinical Investigation*, Vol. 70, no. 4, pp. 716–723, 1982.

33. Appelboom, T., and J.-J. Body, "The antiquity of osteoporosis: more questions than answers," *Calcified Tissue International*, Vol. 53, no. 6, pp. 367–369, 1993.

34. Bonakdarpour, A., W. R. Reinus, and J. S. Khurana, *Diagnostic Imaging of Musculoskeletal Diseases: a Systematic Approach*, Springer Science & Business Media, 2010.

35. Wolff, J., *The Law of Bone Remodelling*, Springer Science & Business Media, 2012.

36. Koch, J. C., "The laws of bone architecture," *American Journal of Anatomy*, Vol. 21, no. 2, pp. 177–298, 1917.

37. Kaplan, F., W. Hayes, T. Keaveny, A. Boskey, T. Einhorn, and J. Iannotti, "Form and function of bone," *Orthopaedic Basic Science*, Vol. 4, pp. 131–133, 1994.

38. Clarke, B., "Normal bone anatomy and physiology," *Clinical Journal of the American Society of Nephrology*, Vol. 3, no. Supplement 3, pp. S131–S139, 2008.

39. Dresing, K., and B. Lumpp, "Bone anatomy and healing," *Airbeitsgemeinschaft fur Osteosynthesefragen Trauma ORP*, Vol. 5, no. 45, pp. 1–10, 2015.

40. Weiss, L., *et al.*, *Cell and Tissue Biology*, Urban & Schwarzenberg, 1988.

41. Wall, A., and T. Board, "The compressive behavior of bone as a two-phase porous structure," in *Classic Papers in Orthopaedics*, pp. 457–460, Springer, 2014.

42. Morgan, E. F., and T. M. Keaveny, "Dependence of yield strain of human trabecular bone on anatomic site," *Journal of Biomechanics*, Vol. 34, no. 5, pp. 569–577, 2001.

43. Eriksen, E. F., "Cellular mechanisms of bone remodeling," *Reviews in Endocrine and Metabolic Disorders*, Vol. 11, no. 4, pp. 219–227, 2010.

44. Parfitt, A., "Bone remodeling," *Henry Ford Hospital Medical Journal*, Vol. 36, no. 3, pp. 143–144, 1988.

45. Parfitt, A., "The cellular basis of bone remodeling: the quantum concept reexamined in light of recent advances in the cell biology of bone," *Calcified Tissue International*, Vol. 36, no. 1, pp. S37–S45, 1984.

46. Robling, A. G., A. B. Castillo, and C. H. Turner, "Biomechanical and molecular regulation of bone remodeling," *Annual Review of Biomedical Engineering*, Vol. 8, pp. 455–498, 2006.

47. Turan, S., "Endocrine disrupting chemicals and bone," *Best Practice & Research Clinical Endocrinology & Metabolism*, p. 101495, 2021.

48. De Faria, M. L., *Magnetic scaffolds for bone regeneration.* PhD thesis, Faculty of Engineering of the University of Porto, University of Porto, 2020.

49. Sahm, F., J. Ziebart, A. Jonitz-Heincke, D. Hansmann, T. Dauben, and R. Bader, "Alternating electric fields modify the function of human osteoblasts growing on and in the surroundings of titanium electrodes," *International Journal of Molecular Sciences*, Vol. 21, no. 18, p. 6944, 2020.

50. Wada, T., T. Nakashima, N. Hiroshi, and J. M. Penninger, "Rankl–rank signaling in osteoclastogenesis and bone disease," *Trends in Molecular Medicine*, Vol. 12, no. 1, pp. 17–25, 2006.

51. Sims, N. A., and J. H. Gooi, "Bone remodeling: Multiple cellular interactions required for coupling of bone formation and resorption," in *Seminars in Cell & Developmental Biology*, Vol. 19, pp. 444–451, Elsevier, 2008.

52. Baim, S., "The future of fracture risk assessment in the management of osteoporosis," *Journal of Clinical Densitometry*, Vol. 20, no. 3, pp. 451–457, 2017.

53. Cundy, T., "Paget's disease of bone," *Metabolism*, Vol. 80, pp. 5–14, 2018.

54. Princy, B. A., S. T. Chacko, A. Lucas, M. N. Deepa, R. K. Dharshini, *et al.*, "Stone bone–is osteopetrosis as hard as it can be???," *Indian Journal of Continuing Nursing Education*, Vol. 21, no. 1, p. 20, 2020.

55. Almeida Paz, I., and L. Bruno, "Bone mineral density," *Brazilian Journal of Poultry Science*, Vol. 8, no. 2, pp. 69–73, 2006.

56. Hui, S. L., S. Gao, X.-H. Zhou, C. C. Johnston Jr, Y. Lu, C. C. Glüer, S. Grampp, and H. Genant, "Universal standardization of bone density measurements: a method with optimal properties for calibration among several instruments," *Journal of Bone and Mineral Research*, Vol. 12, no. 9, pp. 1463–1470, 1997.

57. Strid, K.-G., and P. Kälebo, "Bone mass determination from microradiographs by computer-assisted videodensitometry: I. methodology," *Acta Radiologica*, Vol. 29, no. 4, pp. 465–472, 1988.

58. Carricart-Ganivet, J. P., and D. J. Barnes, "Densitometry from digitized images of x-radiographs: methodology for measurement of coral skeletal density," *Journal of Experimental Marine Biology and Ecology*, Vol. 344, no. 1, pp. 67–72, 2007.

59. Zhang, B., and C. N. Coon, "The relationship of various tibia bone measurements in hens," *Poultry Science*, Vol. 76, no. 12, pp. 1698–1701, 1997.

60. Seedor, J. G., H. A. Quartuccio, and D. D. Thompson, "The bisphosphonate alendronate (mk-217) inhibits bone loss due to ovariectomy in rats," *Journal of Bone and Mineral Research*, Vol. 6, no. 4, pp. 339–346, 1991.

61. Shapurian, T., P. D. Damoulis, G. M. Reiser, T. J. Griffin, and W. M. Rand, "Quantitative evaluation of bone density using the hounsfield index," *International Journal of Oral & Maxillofacial Implants*, Vol. 21, no. 2, 2006.

62. Johansson, C., D. Black, O. Johnell, A. Oden, and D. Mellström, "Bone mineral density is a predictor of survival," *Calcified Tissue International*, Vol. 63, no. 3, pp. 190–196, 1998.

63. World Health Organization and others, *Assessment of Fracture Risk and Its Application to Screening for Postmenopausal Osteoporosis: Report of a WHO Study Group [Meeting Held in Rome from 22 to 25 June 1992]*, World Health Organization, 1994.

64. Rizzoli, R., J.-P. Bonjour, and T. Chevalley, "Dietary protein intakes and bone growth," in *International Congress Series*, Vol. 1297, pp. 50–59, Elsevier, 2007.

65. Wilkin, L. D., M. C. Jackson, T. D. Sims, and B. L. Haddock, "Racial/ethnic differences in bone mineral density of young adults," *International Journal of Exercise Science*, Vol. 3, no. 4, p. 197, 2010.

66. Schönau, E., "The peak bone mass concept: is it still relevant?," *Pediatric Nephrology*, Vol. 19, no. 8, pp. 825–831, 2004.

67. Dallaire, F., J.-L. Bigras, M. Prsa, and N. Dahdah, "Bias related to body mass index in pediatric echocardiographic z scores," *Pediatric Cardiology*, Vol. 36, no. 3, pp. 667–676, 2015.

68. Curtis, A. E., T. A. Smith, B. A. Ziganshin, and J. A. Elefteriades, "The mystery of the z-score," *AORTA Journal*, Vol. 4, no. 4, p. 124, 2016.

69. McKiernan, F., R. Berg, and J. Linneman, "The utility of bmd z-score diagnostic thresholds for secondary causes of osteoporosis," *Osteoporosis International*, Vol. 22, no. 4, pp. 1069–1077, 2011.

70. Dibley, M. J., N. Staehling, P. Nieburg, and F. L. Trowbridge, "Interpretation of z-score anthropometric indicators derived from the international growth reference," *The American Journal of Clinical Nutrition*, Vol. 46, no. 5, pp. 749–762, 1987.

71. Kanis, J. A., L. J. Melton III, C. Christiansen, C. C. Johnston, and N. Khaltaev, "The diagnosis of osteoporosis," *Journal of Bone and Mineral Research*, Vol. 9, no. 8, pp. 1137–1141, 1994.

72. Kanis, J., and C.-C. Glüer, "An update on the diagnosis and assessment of osteoporosis with densitometry," *Osteoporosis International*, Vol. 11, no. 3, pp. 192–202, 2000.

73. Glorieux, F. H., and C. Munns, "Juvenile osteoporosis," *Primer on the Metabolic Bone Diseases and Disorders of Mineral Metabolism*, p. 419, 2018.

74. Melton, L., "Biomechanical aspects of fractures," *Osteoporosis: Etiology, Diagnosis, and Management*, pp. 111–131, 1988.

75. Gallagher, J., "The pathogenesis of osteoporosis," *Bone and Mineral*, Vol. 9, no. 3, pp. 215–227, 1990.

76. Mosekilde, L., "Sex differences in age-related loss of vertebral trabecular bone mass and structure—biomechanical consequences," *Bone*, Vol. 10, no. 6, pp. 425–432, 1989.

77. Ding, M., A. Odgaard, F. Linde, and I. Hvid, "Age-related variations in the microstructure of human tibial cancellous bone," *Journal of Orthopaedic Research*, Vol. 20, no. 3, pp. 615–621, 2002.

78. Heidari, B., R. Hosseini, Y. Javadian, A. Bijani, M. H. Sateri, and H. G. Nouroddini, "Factors affecting bone mineral density in postmenopausal women," *Archives of Osteoporosis*, Vol. 10, no. 1, pp. 1–7, 2015.

79. Demir, B., A. Haberal, P. Geyik, B. Baskan, E. Ozturkoglu, O. Karacay, and S. Deveci, "Identification of the risk factors for osteoporosis among postmenopausal women," *Maturitas*, Vol. 60, no. 3-4, pp. 253–256, 2008.

80. Slemenda, C. W., S. L. Hui, C. Longcope, and C. C. Johnston Jr, "Cigarette smoking, obesity, and bone mass," *Journal of Bone and Mineral Research*, Vol. 4, no. 5, pp. 737–741, 1989.

81. Ghadimi, R., S. R. Hosseini, S. Asefi, A. Bijani, B. Heidari, and M. Babaei, "Influence of smoking on bone mineral density in elderly men," *International Journal of Preventive Medicine*, Vol. 9, 2018.

82. Lorentzon, M., D. Mellstroḿ, E. Haug, and C. Ohlsson, "Smoking is associated with lower bone mineral density and reduced cortical thickness in young men," *The Journal of Clinical Endocrinology & Metabolism*, Vol. 92, no. 2, pp. 497–503, 2007.

83. Mazess, R. B., and H. S. Barden, "Bone density in premenopausal women: effects of age, dietary intake, physical activity, smoking, and birth-control pills," *The American Journal of Clinical Nutrition*, Vol. 53, no. 1, pp. 132–142, 1991.

84. Law, M., and A. Hackshaw, "A meta-analysis of cigarette smoking, bone mineral density and risk of hip fracture: recognition of a major effect," *British Medical Journal*, Vol. 315, no. 7112, pp. 841–846, 1997.

85. Yu, P.-A., W.-H. Hsu, W.-B. Hsu, L.-T. Kuo, Z.-R. Lin, W.-J. Shen, and R. W.-W. Hsu, "The effects of high impact exercise intervention on bone mineral density, physical fitness, and quality of life in postmenopausal women with osteopenia: A retrospective cohort study," *Medicine*, Vol. 98, no. 11, 2019.

86. Huuskonen, J., S. Väisänen, H. Kröger, J. Jurvelin, E. Alhava, and R. Rauramaa, "Regular physical exercise and bone mineral density: a four-year controlled randomized trial in middle-aged men. the dnasco study," *Osteoporosis International*, Vol. 12, no. 5, pp. 349–355, 2001.

87. Maggi, S., M. Noale, S. Giannini, S. Adami, D. Defeo, G. Isaia, L. Sinigaglia, P. Filipponi, and G. Crepaldi, "Quantitative heel ultrasound in a population-based study in italy and its relationship with fracture history: the esopo study," *Osteoporosis International*, Vol. 17, no. 2, pp. 237–244, 2006.

88. De Martinis, M., M. M. Sirufo, M. Polsinelli, G. Placidi, D. Di Silvestre, and L. Ginaldi, "Gender differences in osteoporosis: A single-center observational study," *The World Journal of Men's Health*, Vol. 38, 2020.

89. Curry, S. J., A. H. Krist, D. K. Owens, M. J. Barry, A. B. Caughey, K. W. Davidson, C. A. Doubeni, J. W. Epling, A. R. Kemper, M. Kubik, *et al.*, "Screening for osteoporosis to prevent fractures: Us preventive services task force recommendation statement," *The Journal of the American Medical Association*, Vol. 319, no. 24, pp. 2521–2531, 2018.

90. Bliuc, D., D. Alarkawi, T. V. Nguyen, J. A. Eisman, and J. R. Center, "Risk of subsequent fractures and mortality in elderly women and men with fragility fractures with and without osteoporotic bone density: the dubbo osteoporosis epidemiology study," *Journal of Bone and Mineral Research*, Vol. 30, no. 4, pp. 637–646, 2015.

91. Bor, A., M. Matuz, N. Gyimesi, Z. Biczók, G. Soós, and P. Doró, "Gender inequalities in the treatment of osteoporosis," *Maturitas*, Vol. 80, no. 2, pp. 162–169, 2015.

92. Prince, R. L., A. Devine, S. S. Dhaliwal, and I. M. Dick, "Effects of calcium supplementation on clinical fracture and bone structure: results of a 5-year, double-blind, placebo-controlled trial in elderly women," *Archives of Internal Medicine*, Vol. 166, no. 8, pp. 869–875, 2006.

93. Finkelstein, J. S., M.-L. T. Lee, M. Sowers, B. Ettinger, R. M. Neer, J. L. Kelsey, J. A. Cauley, M.-H. Huang, and G. A. Greendale, "Ethnic variation in bone density in premenopausal and early perimenopausal women: effects of anthropometric and lifestyle factors," *The Journal of Clinical Endocrinology & Metabolism*, Vol. 87, no. 7, pp. 3057–3067, 2002.

94. Morton, D. J., E. Barrett-Connor, D. Kritz-Silverstein, D. L. Wingard, and D. L. Schneider, "Bone mineral density in postmenopausal caucasian, filipina, and hispanic women," *International Journal of Epidemiology*, Vol. 32, no. 1, pp. 150–156, 2003.

95. Ross, P., Y.-F. He, A. Yates, C. Coupland, P. Ravn, M. McClung, D. Thompson, R. W. for the EPIC Study Group, *et al.*, "Body size accounts for most differences in bone density between asian and caucasian women," *Calcified Tissue International*, Vol. 59, no. 5, pp. 339–343, 1996.

96. Davis, J., R. Novotny, P. Ross, and R. Wasnich, "The peak bone mass of hawaiian, filipino, japanese, and white women living in hawaii," *Calcified Tissue International*, Vol. 55, no. 4, pp. 249–252, 1994.

97. Huang, C., P. Ross, S. Fujiwara, J. Davis, R. Epstein, K. Kodama, and R. Wasnich, "Determinants of vertebral fracture prevalence among native japanese women and women of japanese descent living in hawaii," *Bone*, Vol. 18, no. 5, pp. 437–442, 1996.

98. Manisalı, M., D. Özaksoy, E. Yilmaz, Ö. Şenocak, H. Tatari, Ö. Baran, and H. Havıtçıoğlu, "Bone mineral density reference values in the normal female and male population of izmir, turkey," *European Radiology*, Vol. 13, no. 1, pp. 157–162, 2003.

99. Tüzün, Ş., İ. Karacan, N. Selim, and F. Tüzün, "Bone mineral density in a normal turkish female population," *Türkiye Fiziksel Tıp ve Rehabilitasyon Dergisi*, Vol. 50, no. 1, pp. 10–16, 2004.

100. Gürlek, A., M. Bayraktar, and M. Ariyürek, "Inappropriate reference range for peak bone mineral density in dual-energy x-ray absorptiometry: implications for the interpretation of t-scores," *Osteoporosis International*, Vol. 11, no. 9, pp. 809–813, 2000.

101. Elffors, I., E. Allander, J. Kanis, B. Gullberg, O. Johnell, J. Dequeker, G. Dilsen, C. Gennari, A. L. Vaz, G. Lyritis, *et al.*, "The variable incidence of hip fracture in southern europe: the medos study," *Osteoporosis International*, Vol. 4, no. 5, pp. 253–263, 1994.

102. Morizio, P., J. I. Burkhart, and S. Ozawa, "Denosumab: a unique perspective on adherence and cost-effectiveness compared with oral bisphosphonates in osteoporosis patients," *Annals of Pharmacotherapy*, Vol. 52, no. 10, pp. 1031–1041, 2018.

103. McCloskey, E., J. Rathi, S. Heijmans, M. Blagden, B. Cortet, E. Czerwinski, P. Hadji, J. Payer, K. Palmer, R. Stad, *et al.*, "The osteoporosis treatment gap in patients at risk of fracture in european primary care: a multi-country cross-sectional observational study," *Osteoporosis International*, Vol. 32, no. 2, pp. 251–259, 2021.

104. Cipriani, C., J. Pepe, S. Minisola, and E. M. Lewiecki, "Adverse effects of media reports on the treatment of osteoporosis," *Journal of Endocrinological Investigation*, Vol. 41, no. 12, pp. 1359–1364, 2018.

105. Açıksöz, S., G. Kurt, and M. Seyfi, "Evaluation of health beliefs and knowledge status of nursing students related to osteoporosis," *Tepecik Egit. ve Arast. Hast. Dergisi*, no. 30, pp. 203–11, 2020.

106. Chun, K. J., "Bone densitometry," in *Seminars in Nuclear Medicine*, Vol. 41, pp. 220–228, Elsevier, 2011.

107. Koot, V., S. Kesselaer, G. J. Clevers, P. De Hooge, T. Weits, and C. van der Werken, "Evaluation of the singh index for measuring osteoporosis," *The Journal of Bone and Joint Surgery. British Volume*, Vol. 78, no. 5, pp. 831–834, 1996.

108. Singh, M., A. Nagrath, and P. S. Maini, "Changes in trabecular pattern of the upper end of the femur as an index of osteoporosis," *The Journal of Bone and Joint Surgery*, Vol. 52, no. 3, pp. 457–467, 1970.

109. Griffiths, H. J., and P. Virtama, "Cortical thickness and trabecular pattern of the femoral neck as a measure of osteopenia," *Investigative Radiology*, Vol. 25, no. 10, pp. 1116–1119, 1990.

110. Peacock, M., C. Turner, G. Liu, A. Manatunga, L. Timmerman, and C. Johnston, "Better discrimination of hip fracture using bone density, geometry and architecture," *Osteoporosis International*, Vol. 5, no. 3, pp. 167–173, 1995.

111. Kalla, A., O. Meyers, N. Parkyn, and T. v. W. Kotze, "Osteoporosis screening—radiogrammetry revisited," *Rheumatology*, Vol. 28, no. 6, pp. 511–517, 1989.

112. Bouxsein, M., L. Palermo, C. Yeung, and D. Black, "Digital x-ray radiogrammetry predicts hip, wrist and vertebral fracture risk in elderly women: a prospective analysis from the study of osteoporotic fractures," *Osteoporosis International*, Vol. 13, no. 5, pp. 358–365, 2002.

113. Marcus, R., D. Feldman, D. W. Dempster, M. Luckey, and J. A. Cauley, "Chapter 64 - imaging of osteoporosis," in *Osteoporosis (Fourth Edition)*, pp. 1505–1534, San Diego: Academic Press, fourth edition ed., 2013.

114. Albright, F., P. H. Smith, and A. M. Richardson, "Postmenopausal osteoporosis: its clinical features," *Journal of the American Medical Association*, Vol. 116, no. 22, pp. 2465–2474, 1941.

115. Heuck, F., and E. Schmidt, "Die quantitative bestimmung des mineralgehaltes der knochen aus dem röntgenbild," in *RöFo-Fortschritte auf dem Gebiet der Röntgenstrahlen und der Bildgebenden Verfahren*, Vol. 93, pp. 523–554, © Georg Thieme Verlag KG Stuttgart· New York, 1960.

116. Looker, A., H. Wahner, W. Dunn, M. Calvo, T. Harris, S. Heyse, C. Johnston Jr, and R. Lindsay, "Updated data on proximal femur bone mineral levels of us adults," *Osteoporosis International*, Vol. 8, no. 5, pp. 468–490, 1998.

117. Bonnick, S. L., C. C. Johnston Jr, M. Kleerekoper, R. Lindsay, P. Miller, L. Sherwood, and E. Siris, "Importance of precision in bone density measurements," *Journal of Clinical Densitometry*, Vol. 4, no. 2, pp. 105–110, 2001.

118. Forsén, L., G. K. R. Berntsen, H. E. Meyer, G. S. Tell, and V. Fønnebø, "Differences in precision in bone mineral density measured by sxa and dxa: the norepos study," *European Journal of Epidemiology*, Vol. 23, no. 9, pp. 615–624, 2008.

119. Celenk, C., and P. Celenk, "Bone density measurement using computed tomography," *Computed Tomography - Clinical Applications*, pp. 123–136, 2012.

120. Hans, D. B., J. A. Shepherd, E. N. Schwartz, D. M. Reid, G. M. Blake, J. N. Fordham, T. Fuerst, P. Hadji, A. Itabashi, M.-A. Krieg, *et al.*, "Peripheral dual-energy x-ray absorptiometry in the management of osteoporosis: the 2007 iscd official positions," *Journal of Clinical Densitometry*, Vol. 11, no. 1, pp. 188–206, 2008.

121. Berntsen, G. K. R., V. Fønnebø, A. Tollan, A. J. Søgaard, R. M. Joakimsen, and J. H. Magnus, "The tromsø study: Determinants of precision in bone densitometry," *Journal of Clinical Epidemiology*, Vol. 53, no. 11, pp. 1104–1112, 2000.

122. Adams, J., "Single-and dual-energy: X-ray absorptiometry," *Bone Densitometry and Osteoporosis*, pp. 305–334, 1998.

123. Cosman, F., B. Herrington, S. Himmelstein, and R. Lindsay, "Radiographic absorptiometry: a simple method for determination of bone mass," *Osteoporosis International*, Vol. 2, no. 1, pp. 34–38, 1991.

124. Yates, A. J., P. D. Ross, E. Lydick, and R. S. Epstein, "Radiographic absorptiometry in the diagnosis of osteoporosis," *The American Journal of Medicine*, Vol. 98, no. 2, pp. 41S–47S, 1995.

125. Yang, S.-O., S. Hagiwara, K. Engelke, M. S. Dhillon, G. Guglielmi, E. J. Bendavid, O. Soejima, D. L. Nelson, and H. K. Genant, "Radiographic absorptiometry for bone mineral measurement of the phalanges: precision and accuracy study," *Radiology*, Vol. 192, no. 3, pp. 857–859, 1994.

126. Genant, H. K., K. Engelke, T. Fuerst, C.-C. Glüer, S. Grampp, S. T. Harris, M. Jergas, T. Lang, Y. Lu, S. Majumdar, *et al.*, "Noninvasive assessment of bone mineral and structure: state of the art," *Journal of Bone and Mineral Research*, Vol. 11, no. 6, pp. 707–730, 1996.

127. Huang, C., P. Ross, A. Yates, R. Walker, K. Imose, K. Emi, and R. Wasnich, "Prediction of fracture risk by radiographic absorptiometry and quantitative ultrasound: a prospective study," *Calcified Tissue International*, Vol. 63, no. 5, pp. 380–384, 1998.

128. Gulam, M., M. M. Thornton, A. B. Hodsman, and D. W. Holdsworth, "Bone mineral measurement of phalanges: comparison of radiographic absorptiometry and area dual x-ray absorptiometry," *Radiology*, Vol. 216, no. 2, pp. 586–591, 2000.

129. Cameron, J. R., and J. Sorenson, "Measurement of bone mineral in vivo: an improved method," *Salud Pública de México*, Vol. 51, pp. s126–s131, 2009.

130. Goodwin, P. N., "Methodologies for the measurement of bone density and their precision and accuracy," in *Seminars in Nuclear Medicine*, Vol. 17, pp. 293–304, Elsevier, 1987.

131. Valkema, R., H. Prpic, J. Blokland, J. Camps, S. Papapoulos, O. Bijvoet, and E. Pauwels, "Dual photon absorptiometry for bone mineral measurements using a gamma camera," *Acta Radiologica*, Vol. 35, no. 1, pp. 45–52, 1994.

132. Genant, H. K., and D. Boyd, "Quantitative bone mineral analysis using dual energy computed tomography," *Investigative Radiology*, Vol. 12, no. 6, pp. 545–551, 1977.

133. Blake, G. M., and I. Fogelman, "Technical principles of dual energy x-ray absorptiometry," in *Seminars in Nuclear Medicine*, Vol. 27, pp. 210–228, Elsevier, 1997.

134. Krølner, B., and S. P. Ntelsen, "Measurement of bone mineral content (bmc) of the lumbar spine, i. theory and application of a new two-dimensional dual-photon attenuation method," *Scandinavian Journal of Clinical and Laboratory Investigation*, Vol. 40, no. 7, pp. 653–663, 1980.

135. Baroncelli, G. I., "Quantitative ultrasound methods to assess bone mineral status in children: technical characteristics, performance, and clinical application," *Pediatric Research*, Vol. 63, no. 3, pp. 220–228, 2008.

136. Njeh, C., C. Boivin, and C. Langton, "The role of ultrasound in the assessment of osteoporosis: a review," *Osteoporosis International*, Vol. 7, no. 1, pp. 7–22, 1997.

137. Gregg, E. W., A. M. Kriska, L. M. Salamone, M. M. Roberts, S. Aderson, R. E. Ferrell, L. H. Kuller, and J. A. Cauley, "The epidemiology of quantitative ultrasound: a review of the relationships with bone mass, osteoporosis and fracture risk," *Osteoporosis International*, Vol. 7, no. 2, pp. 89–99, 1997.

138. Pluskiewicz, W., A. Pyrkosz, B. Drozdzowska, and Z. Halaba, "Quantitative ultrasound of the hand phalanges in patients with genetic disorders: a pilot case-control study," *Osteoporosis International*, Vol. 14, no. 10, pp. 787–792, 2003.

139. Vignolo, M., E. Di Battista, A. Parodi, C. Torrisi, F. De Terlizzi, and G. Aicardi, "Bone quality assessed by phalangeal quantitative ultrasonography in children and adolescents with isolated idiopathic growth hormone deficiency," *Journal of Endocrinological Investigation*, Vol. 30, no. 6, pp. 445–450, 2007.

140. Raju, T. N., "The nobel chronicles," *The Lancet*, Vol. 353, no. 9168, p. 1981, 1999.

141. Brooks, R. A., "A quantitative theory of the hounsfield unit and its application to dual energy scanning," *Journal of Computer Assisted Tomography*, Vol. 1, no. 4, pp. 487–493, 1977.

142. Reinbold, W., H. Genant, U. Reiser, S. Harris, and B. Ettinger, "Bone mineral content in early-postmenopausal and postmenopausal osteoporotic women: comparison of measurement methods," *Radiology*, Vol. 160, no. 2, pp. 469–478, 1986.

143. Wehrli, F. W., J. A. Hopkins, S. N. Hwang, H. K. Song, P. J. Snyder, and J. G. Haddad, "Cross-sectional study of osteopenia with quantitative mr imaging and bone densitometry," *Radiology*, Vol. 217, no. 2, pp. 527–538, 2000.

144. Romano, J. D., and R. H. Price, "The conical resistor conundrum: a potential solution," *American Journal of Physics*, Vol. 64, no. 9, pp. 1150–1153, 1996.

145. Schwan, H. P., "Electrical properties of tissue and cell suspensions," in *Advances in Biological and Medical Physics*, Vol. 5, pp. 147–209, Elsevier, 1957.

146. Pethig, R., and D. B. Kell, "The passive electrical properties of biological systems: their significance in physiology, biophysics and biotechnology," *Physics in Medicine & Biology*, Vol. 32, no. 8, p. 933, 1987.

147. Hanai, T., "Theory of the dielectric dispersion due to the interfacial polarization and its application to emulsions," *Kolloid-Zeitschrift*, Vol. 171, no. 1, pp. 23–31, 1960.

148. Cole, K. S., and R. H. Cole, "Dispersion and absorption in dielectrics i. alternating current characteristics," *The Journal of Chemical Physics*, Vol. 9, no. 4, pp. 341–351, 1941.

149. Da Silva, J. E., J. M. De Sá, and J. Jossinet, "Classification of breast tissue by electrical impedance spectroscopy," *Medical and Biological Engineering and Computing*, Vol. 38, no. 1, pp. 26–30, 2000.

150. Grimnes, S., and O. G. Martinsen, "Cole electrical impedance model-a critique and an alternative," *IEEE Transactions on Biomedical Engineering*, Vol. 52, no. 1, pp. 132–135, 2004.

151. Cole, K. S., "Electric impedance of suspensions of spheres," *The Journal of General Physiology*, Vol. 12, no. 1, pp. 29–36, 1928.

152. Teunissen, P., "Nonlinear least squares," *Manuscripta Geodaetica*, Vol. 15, pp. 137–150, 1990.

153. Coope, I. D., "Circle fitting by linear and nonlinear least squares," *Journal of Optimization Theory and Applications*, Vol. 76, no. 2, pp. 381–388, 1993.

154. Cornish, B., B. Thomas, and L. Ward, "Improved prediction of extracellular and total body water using impedance loci generated by multiple frequency bioelectrical impedance analysis," *Physics in Medicine & Biology*, Vol. 38, no. 3, p. 337, 1993.

155. Ayllon, D., F. Seoane, and R. Gil-Pita, "Cole equation and parameter estimation from electrical bioimpedance spectroscopy measurements-a comparative study," in *2009 Annual International Conference of the IEEE Engineering in Medicine and Biology Society*, pp. 3779–3782, IEEE, 2009.

156. Kun, S., and R. A. Peura, "Selection of measurement frequencies for optimal extraction of tissue impedance model parameters," *Medical & Biological Engineering & Computing*, Vol. 37, no. 6, pp. 699–703, 1999.

157. Donawa, M. E., "European medical device usability requirements," *European Medical Device Technology*, Vol. 2, no. 6, pp. 12–14, 2011.

158. Gomez Abad, D., "Development of a capacitive bioimpedance measurement system," Master's thesis, Universitat Politècnica de Catalunya, 2009.

159. Boukamp, B. A., "A linear kronig-kramers transform test for immittance data validation," *Journal of the Electrochemical Society*, Vol. 142, no. 6, p. 1885, 1995.

160. Schwan, H., "Physical techniques in biological research," *Electrophysiological Methods*, Vol. 6, no. pt B, 1963.

161. Grimnes, S., and Ø. G. Martinsen, "Sources of error in tetrapolar impedance measurements on biomaterials and other ionic conductors," *Journal of Physics D: Applied Physics*, Vol. 40, no. 1, p. 9, 2006.

162. Roy, A., S. Bhattacharjee, S. Podder, and A. Ghosh, "Measurement of bioimpedance and application of cole model to study the effect of moisturizing cream on human skin," *AIMS Biophysics*, Vol. 7, no. 4, pp. 362–379, 2020.

163. Oh, S., L. Leung, D. Bommannan, R. Guy, and R. Potts, "Effect of current, ionic strength and temperature on the electrical properties of skin," *Journal of Controlled Release*, Vol. 27, no. 2, pp. 115–125, 1993.

164. Lorraine, M., *et al.*, "Electrical properties of human stratum corneum and transdermal drug transport," *Journal of the Chemical Society, Faraday Transactions*, Vol. 89, no. 15, pp. 2839–2845, 1993.

165. Cornish, B., B. Thomas, and L. Ward, "Effect of temperature and sweating on bioimpedance measurements," *Applied Radiation and Isotopes*, Vol. 49, no. 5-6, pp. 475–476, 1998.

166. Maw, G., I. Mackenzie, and N. Taylor, "Redistribution of body fluids during postural manipulations," *Acta Physiologica Scandinavica*, Vol. 155, no. 2, pp. 157–163, 1995.

167. Zhu, F., D. Schneditz, E. Wang, and N. W. Levin, "Dynamics of segmental extracellular volumes during changes in body position by bioimpedance analysis," *Journal of Applied Physiology*, Vol. 85, no. 2, pp. 497–504, 1998.

168. De Laet, C., J. Kanis, A. Odén, H. Johanson, O. Johnell, P. Delmas, J. Eisman, H. Kroger, S. Fujiwara, P. Garnero, *et al.*, "Body mass index as a predictor of fracture risk: a meta-analysis," *Osteoporosis International*, Vol. 16, no. 11, pp. 1330–1338, 2005.

169. Reid, I. R., R. Ames, M. C. Evans, S. Sharpe, G. Gamble, J. T. France, T. Lim, and T. Cundy, "Determinants of total body and regional bone mineral density in normal postmenopausal women–a key role for fat mass," *The Journal of Clinical Endocrinology & Metabolism*, Vol. 75, no. 1, pp. 45–51, 1992.

170. Reid, I. R., L. D. Plank, and M. C. Evans, "Fat mass is an important determinant of whole body bone density in premenopausal women but not in men," *The Journal of Clinical Endocrinology & Metabolism*, Vol. 75, no. 3, pp. 779–782, 1992.

171. Lukaski, H. C., P. E. Johnson, W. W. Bolonchuk, and G. I. Lykken, "Assessment of fat-free mass using bioelectrical impedance measurements of the human body," *The American Journal of Clinical Nutrition*, Vol. 41, no. 4, pp. 810–817, 1985.

172. Newby, M. J., N. L. Keim, and D. L. Brown, "Body composition of adult cystic fibrosis patients and control subjects as determined by densitometry, bioelectrical impedance, total-body electrical conductivity, skinfold measurements, and deuterium oxide dilution," *The American Journal of Clinical Nutrition*, Vol. 52, no. 2, pp. 209–213, 1990.

173. Biggs, J., K. Cha, and K. Horch, "Electrical resistivity of the upper arm and leg yields good estimates of whole body fat," *Physiological Measurement*, Vol. 22, no. 2, p. 365, 2001.

174. Brožek, J., F. Grande, J. T. Anderson, and A. Keys, "Densitometric analysis of body composition: revision of some quantitative assumptions," *Annals of the New York Academy of Sciences*, Vol. 110, no. 1, pp. 113–140, 1963.

175. Thomas, W. B., A. Juan, S. Andreas, and B. Philippe, "In-vivo measurement of bone electric properties," *Proceedings of the 2nd World Congress on Electrical Engineering and Computer Systems and Science (EECSS'16) Budapest*, August 16-17 2016.

176. Davidović Cvetko, E., I. Drenjančević, N. Nešić, and J. MILAS AHIĆ, "Possibilities of use bioelectrical impedance analysis as measuring technique in prevention of osteoporosis," *Periodicum Biologorum*, Vol. 116, no. 1, pp. 65–70, 2014.

177. Ngai, H. H., C.-L. Cheung, T.-J. Yao, and A. W. Kung, "Bioimpedance: can its addition to simple clinical criteria enhance the diagnosis of osteoporosis?," *Journal of Bone and Mineral Metabolism*, Vol. 27, no. 3, pp. 372–378, 2009.

178. Lukaski, H., and W. Bolonchuk, "Theory and validation of the tetrapolar bioelectrical impedance method to assess human body composition," in *In Vivo Body Composition Studies; Proceedings of an International Symposium Held at Brookhaven National Laboratory*, London: The Institute of Physical Sciences in Medicine, 1987. IPSM; 3, 1987.

179. Lohman, T. G., "Skinfolds and body density and their relation to body fatness: a review," *Human Biology*, pp. 181–225, 1981.

180. Baumgartner, R. N., P. M. Stauber, K. M. Koehler, L. Romero, and P. J. Garry, "Associations of fat and muscle masses with bone mineral in elderly men and women," *The American Journal of Clinical Nutrition*, Vol. 63, no. 3, pp. 365–372, 1996.

181. Bracco, D., D. Thiebaud, R. L. Chiolero, M. Landry, P. Burckhardt, and Y. Schutz, "Segmental body composition assessed by bioelectrical impedance analysis and dexa in humans," *Journal of Applied Physiology*, Vol. 81, no. 6, pp. 2580–2587, 1996.

182. Morale, M., E. Rathbun, E. Robert, Q. Smith, and N. Paces, "Studies o n body composition: Ii. theoretical considerations regarding the majo r body tissue components, with suggestions for application to man," *Journal of Biological Chemistry*, Vol. 158, pp. 677–684, 1945.

183. Siri, W. E., "Body composition from fluid spaces and density: analysis of methods," *Washington, DC: National Academy of Sciences*, p. 223–44, 1956.

184. Wagner, D. R., and V. H. Heyward, "Measures of body composition in blacks and whites: a comparative review," *The American Journal of Clinical Nutrition*, Vol. 71, no. 6, pp. 1392–1402, 2000.

185. Dempster, W. T., and G. R. Gaughran, "Properties of body segments based on size and weight," *American Journal of Anatomy*, Vol. 120, no. 1, pp. 33–54, 1967.

186. Wang, Z., P. Deurenberg, S. S. Guo, A. Pietrobelli, J. Wang, R. Pierson Jr, and S. B. Heymsfield, "Six-compartment body composition model: inter-method comparisons of total body fat measurement," *International Journal of Obesity*, Vol. 22, no. 4, pp. 329–337, 1998.

187. Manual, M., "Medcalc for windows," *Statistics for Biomedical Research. Software Manual. Bélgica*, 1993.

188. Rayat, C. S., "Variance-ratio test and analysis of variance (anova)," in *Statistical Methods in Medical Research*, pp. 95–109, Springer, 2018.

189. Altman, D. G., *Practical Statistics for Medical Research*, CRC press, 1990.

190. Obuchowski, N. A., "Receiver operating characteristic curves and their use in radiology," *Radiology*, Vol. 229, no. 1, pp. 3–8, 2003.

191. Gönen, M., *et al.*, "Receiver operating characteristic (roc) curves," *SAS Users Group International (SUGI)*, Vol. 31, pp. 210–231, 2006.

192. Perkins, N. J., and E. F. Schisterman, "The youden index and the optimal cut-point corrected for measurement error," *Biometrical Journal: Journal of Mathematical Methods in Biosciences*, Vol. 47, no. 4, pp. 428–441, 2005.

193. Dancey, C., and J. Reidy, "Variables and research design," *Statistics without Maths for Psychology: Using SPSS for Windows*, pp. 1–33, 2004.

194. Yiannoutsos, C. T., C. T. Nakas, B. A. Navia, P. M. Consortium, *et al.*, "Assessing multiple-group diagnostic problems with multi-dimensional receiver operating characteristic surfaces: application to proton mr spectroscopy (mrs) in hiv-related neurological injury," *Neuroimage*, Vol. 40, no. 1, pp. 248–255, 2008.

195. Li, J., and X.-H. Zhou, "Nonparametric and semiparametric estimation of the three way receiver operating characteristic surface," *Journal of Statistical Planning and Inference*, Vol. 139, no. 12, pp. 4133–4142, 2009.

196. Matur, F., and Y. Ülgen, "2d-roc: a receiver operating surface and its illustrative application in clinical diagnostics," *Physiological Measurement*, Vol. 40, no. 7, p. 075004, 2019.

197. Fluss, R., D. Faraggi, and B. Reiser, "Estimation of the youden index and its associated cutoff point," *Biometrical Journal: Journal of Mathematical Methods in Biosciences*, Vol. 47, no. 4, pp. 458–472, 2005.

198. Benoit, K., "Linear regression models with logarithmic transformations," *London School of Economics, London*, Vol. 22, no. 1, pp. 23–36, 2011.

199. Babai, M. A., P. Arasteh, M. Hadibarhaghtalab, M. M. Naghizadeh, A. Salehi, A. Askari, and R. Homayounfar, "Defining a bmi cut-off point for the iranian population: the shiraz heart study," *The Public Library of Science One*, Vol. 11, no. 8, p. e0160639, 2016.

200. General Assembly of the World Medical Association and others, "World medical association declaration of helsinki: ethical principles for medical research involving human subjects," *The Journal of the American College of Dentists*, Vol. 81, no. 3, pp. 14–18, 2014.

201. Lukaski, H. C., W. W. Bolonchuk, C. B. Hall, and W. A. Siders, "Validation of tetrapolar bioelectrical impedance method to assess human body composition," *Journal of Applied Physiology*, Vol. 60, no. 4, pp. 1327–1332, 1986.

202. Impedimed Limited, *ImpediMed SFB7 Multi-Frequency Analysis.* Impedimed Limited, Unit 1, 50 Parker Court Pinkenba, QLD 4008 Australia, 2012.

203. Sezdi, M., *Electrical impedance spectroscopy of human blood.* PhD thesis, PhD thesis, Bogazici University, 1998.

204. Leski, J. M., "Robust weighted averaging [of biomedical signals]," *IEEE Transactions on Biomedical Engineering*, Vol. 49, no. 8, pp. 796–804, 2002.

205. Hassan, U., and M. S. Anwar, "Reducing noise by repetition: introduction to signal averaging," *European Journal of Physics*, Vol. 31, no. 3, p. 453, 2010.

206. Agilent Technologies, *HP4284A Precision LCR-Meter Operation Manual HP4284A Precision LCR-Meter Operation Manual*, Agilent Technologies, 1990.

207. Sheskin, D. J., *Handbook of Parametric and Nonparametric Statistical Procedures*, crc Press, 2020.

208. Chatfield, C., "Exploratory data analysis," *European Journal of Operational Research*, Vol. 23, no. 1, pp. 5–13, 1986.

209. DeLong, E. R., D. M. DeLong, and D. L. Clarke-Pearson, "Comparing the areas under two or more correlated receiver operating characteristic curves: a nonparametric approach," *Biometrics*, pp. 837–845, 1988.

210. Efron, B., "Better bootstrap confidence intervals," *Journal of the American Statistical Association*, Vol. 82, no. 397, pp. 171–185, 1987.

211. Efron, B., and R. J. Tibshirani, *An Introduction to the Bootstrap*, CRC press, 1994.

212. Park, Y.-W., S. Zhu, L. Palaniappan, S. Heshka, M. R. Carnethon, and S. B. Heymsfield, "The metabolic syndrome: prevalence and associated risk factor findings in the us population from the third national health and nutrition examination survey, 1988-1994," *Archives of Internal Medicine*, Vol. 163, no. 4, pp. 427–436, 2003.